Expansion after Inflation and Reheating with a Charged Inflaton

Kaloian Dimitrov Lozanov

Trinity College & Institute of Astronomy
University of Cambridge

Under the supervision of
Dr Mustafa Amin & Dr Anthony Challinor

This dissertation is submitted for the degree of
Doctor of Philosophy

October 5, 2017
Cambridge, United Kingdom

Expansion after Inflation and Reheating with a Charged Inflaton

Kaloian Lozanov

Summary

Within the inflationary paradigm, our patch of the universe near the end of inflation is highly homogeneous and isotropic as necessitated by cosmic microwave background observations. This patch, however, is also in a cold and non-thermal state. A successful model of an inflationary primordial universe should account for how the universe transitioned from an inflationary to a radiation-dominated, hot, thermal phase required for the production of light elements via big-bang nucleosynthesis. It is desirable for such a model also to include a mechanism for the generation of the observed matter-antimatter asymmetry and perhaps a primordial mechanism for the generation of cosmic magnetic fields.

The transition from an inflationary to a radiation-dominated, thermal phase (reheating) is likely to be phenomenologically rich. Reheating could include explosive particle production and various other non-perturbative, non-linear and non-equilibrium phenomena. Reheating can leave its own observational signatures in the form of gravitational waves and non-Gaussianities. Importantly, reheating can also affect the observational predictions of the preceding phase of inflation. Reheating remains an active field of research, with significant gaps in our understanding of the process. This thesis is an attempt to improve our understanding of the period following inflation, including reheating, through an exploration and analysis of realistic post-inflationary models with the aid of detailed numerical simulations. The focus of the studies is on aspects of the models with potential observational implications.

In Part I of this thesis, we provide an overview of inflation and its end, concentrating on our current understanding of reheating and the challenges we face in trying to constrain reheating observationally.

In Part II, we consider the post-inflationary expansion history in a broad class of observationally-favoured single-field models of inflation. In general, the ambiguity in the expansion history of reheating can cause significant uncertainty in predictions for inflationary observables such as the spectral index, $n_{\rm s}$, and the tensor-to-scalar ratio, r. The work in this part considers the full non-linear evolution of the inflaton during the initial stages of reheating and places bounds on the post-inflationary expansion history when perturbative couplings of the inflaton to other relativistic fields are included.

In Part III, we investigate non-perturbative particle production and non-linear dynamics after inflation in models where the inflaton is charged under global and local symmetries. We first explore the effects of the non-linear inflaton dynamics for the generation of matter-antimatter asymmetry in the case where a global $U(1)$ symmetry of the inflaton is weakly broken. We find a parameter range in which the model successfully predicts the observed baryon-to-photon ratio. We then consider the particle production during and after inflation in models with a charged inflaton under Abelian, $U(1)$, and non-Abelian, $SU(2)$ and $U(1)\times SU(2)$, gauge symmetries (at the linearized level). We find the magnitude of the generated magnetic fields and charge perturbations on large scales to be below the current observational bounds. Finally, we present a novel algorithm for evolving the full set of coupled, non-linear equations of motion for the $U(1)$ charged inflaton and accompanying gauge fields on a lattice in an expanding universe. The novel feature here is that the gauge constraints are satisfied to machine precision when the gravitational dynamics are self-consistently included at the background level, and there are no restrictions on the order of the time-integrators.

In Part IV, we present the conclusions and future prospects.

To Elena and my big loving family

Declaration

This dissertation is the result of my own work and includes nothing which is the outcome of work done in collaboration except as declared in the Preface and specified in the text. It is not substantially the same as any that I have submitted, or, is being concurrently submitted for a degree or diploma or other qualification at the University of Cambridge or any other University or similar institution except as declared in the Preface and specified in the text. I further state that no substantial part of my dissertation has already been submitted, or, is being concurrently submitted for any such degree, diploma or other qualification at the University of Cambridge or any other University of similar institution except as declared in the Preface and specified in the text. The choice to write this dissertation in the first-person-plural point of view conveys my stylistic preference.

The chapters of this dissertation based on collaborative, published or submitted work are as follows:

- Chapter 6

  The Equation of State and Duration to Radiation Domination After Inflation,

  K. D. Lozanov and M. A. Amin, Phys. Rev. Lett. 119, 061301 (2017)

  Self-resonance after inflation: oscillons, transients and radiation domination,

  K. D. Lozanov and M. A. Amin (in preparation)

- Chapter 7

  End of inflation, oscillons and matter-antimatter asymmetry,

  K. D. Lozanov and M. A. Amin, Phys. Rev. D 90, 083528 (2014)

- Chapter 8

  The charged inflaton and its gauge fields: preheating and initial conditions for reheating,

  K. D. Lozanov and M. A. Amin, JCAP 1606, 032 (2016)

This dissertation is less than 60000 words in length, including footnotes, captions and bibliography.

Acknowledgements

I would like to express my deepest gratitude to Mustafa Amin for his guidance, patience, support and tutelage for the past three years. I would also like to thank Anthony Challinor for introducing me to and supporting my first steps in the field of cosmology. Without them this thesis would have not been possible.

Throughout my PhD at University of Cambridge, I have benefited much from discussions on various topics in physics and cosmology with Daniel Baumann, David Daverio, George Efstathiou, Andrew Fabian, Jonathan Gair, Martin Haehnelt, David Khmelnitskii, Paul Shellard and Debora Sijacki, as well as fellow PhD students, in particular Sarah Bosman, Sebastian Cespedes, Johnathan Hung, Patricia Larsen, Deyan Mihailov and Bjoern Soergel. I am grateful to Debora Sijacki for her generosity regarding the use of her computational resources under the Cambridge COSMOS Consortium.

I also thank all of my friends, for showing me that life in Cambridge is not only about work, but also about unforgettable experiences, including Alex, Angel, Deyan, Dimitur, Ivan, Jordan, Katya, Martin, Momchil, Nenko, Richard, Rumen, Stanislav, Victor and all of the members of CantaBG.

This would not be a proper acknowledgement without thanking my first science teacher Mrs Maria Vurbanova, who instilled in me the love of physics from a very young age, and of course Mr Teodosii Teodosiev, whose dedication to his students knows no bounds and whose brilliance has inspired many.

Finally, last but not least, I am immensely thankful to Elena for staying beside me all these years and continuing to support unconditionally all my endeavours – I cannot imagine a life without her encouragement; and to my dear parents, siblings, grandparents, aunt, uncles and cousins for putting up with my extended absences, and their limitless love and support.

Notation

We use natural units in which $\hbar = c = k_{\rm B} = \epsilon_0 = 1$. In these units, the reduced Planck mass is given by $m_{\rm Pl} = 1/\sqrt{8\pi G}$.

Greek indices μ, ν and so on go over the four space-time coordinates $x^\mu = [x^0,\, x^1,\, x^2,\, x^3]^T$ with x^0 for the time coordinate.

Minkowski metric is given by $\eta_{\mu\nu} = \text{diag}[1, -1, -1, -1]$.

Latin labels i, j, k and so on go over the three spatial coordinates.

Spatial vectors are written in boldface.

Summation over repeated indeces is assumed unless otherwise stated.

The spatial Fourier transform of a field $f(\mathbf{x})$ is $f_{\mathbf{k}} = \int f(\mathbf{x}) \mathrm{e}^{-i\mathbf{k}\cdot\mathbf{x}} \mathrm{d}^3\mathbf{x}/(2\pi)^3$ and the inverse transform is $f(\mathbf{x}) = \int f_{\mathbf{k}} \mathrm{e}^{i\mathbf{k}\cdot\mathbf{x}} \mathrm{d}^3\mathbf{k}$.

Contents

Part I

Introduction

Over the past decades, the understanding of our cosmic history has improved spectacularly. Precise measurements of the temperature anisotropies in the cosmic microwave background (CMB) [1, 2] have revealed a homogeneous and isotropic universe on large scales with tiny (if any) spatial curvature, Ω_K, and nearly scale-invariant primordial curvature perturbations. The observations provide compelling evidence for an inflationary phase in the early universe [3–8], implying a connection between gravity and quantum mechanics. Measurements of the relative abundances of light-elements are also in excellent agreement with our expectations [9]. The predictions of big-bang nucleosynthesis (BBN), based on the well-understood physics of nuclear reactions, point towards a hot and dense universe, in local thermal equilibrium at late times. They tell us that the first light-elements started forming at cosmic time $t_{\rm BBN} \gtrsim 1\,{\rm s}$ at equilibrium temperature $T_{\rm BBN} \sim E_{\rm BBN} \sim 1\,{\rm MeV}$.

Connecting these two remarkable epochs, however, could be challenging. Since the energy scale at the end of inflation can be as high as $E_{\rm inf} \sim 10^{16}\,{\rm GeV}$, with the duration of inflation corresponding to $\Delta t_{\rm inf} \gtrsim 10^{-36}\,{\rm s}$, there is a huge range of energy (and time) scales which is poorly understood and poorly observationally constrained. Current cosmological experiments cannot probe the period between inflation and BBN. This is because typically the effects from the interesting post-inflationary dynamics are on subhorizon scales due to causality and are washed out by the later non-linear evolution of structure. The thermal state of the universe, required for BBN, also hides information about earlier times. Collider experiments can shed light on some intermediate-energy phenomena, e.g., the electro-weak symmetry breaking and QCD phase transitions, $E_{\rm EW} \sim 10^2\,{\rm GeV}$ and $E_{\rm QCD} \sim 10^2\,{\rm MeV}$, respectively, but they will not be able to cover the entire energy range in the foreseeable future.

Nevertheless, it is crucial that we try to understand the period between inflation and BBN better, for both theoretical and observational reasons. In the standard lore, the universe at the end of inflation is cold and dark, virtually empty of particles and dominated by the approximately homogeneous inflaton field. The energy of the inflaton that drove inflation, must be somehow transferred to other species of matter, eventually populating all relevant degrees of freedom of the Standard Model, leaving a hot, thermal, radiation-dominated universe, setting the scene for BBN. Importantly, this reheating process explains not only the cosmic origin of the matter that we are made of, but it also accounts for the production of cosmic relics such as photons and neutrinos, and perhaps dark matter and gravitational waves, as well as the generation of the observed matter-antimatter asymmetry in our universe (baryogenesis). Any unified theory of high-energy physics must include a complete understanding of inflation, reheating and the later evolution of the universe.

Given the current and planned advances in observational cosmology and the improvement of constraints on inflation, reheating will be an integral part of research in the coming years. Arguably, one of the most important observational implications of the post-inflationary dynamics is its effect on the expansion history of the universe between inflation and BBN. It determines how we map perturbation modes from their exiting the Hubble horizon during inflation to horizon re-entry at late times. Thereby, the poorly constrained and understood post-inflationary expansion history influences directly the predictions for cosmological observables of specific models of inflation. For instance, it leads to significant uncertainties in the predictions for the spectral index, n_s, and the tensor-to-scalar ratio, r, in different models. It is critical that we understand these uncertainties better, if we wish to narrow the range of the observationally-allowed models of inflation. Works on reheating have also shown the possibility of formation of relics such as solitons and cosmic defects, helping us further constrain the variety of scenarios.

The initial stage of reheating, also known as preheating, can involve highly non-perturbative processes, during which the universe gets populated via parametric resonances. They cannot be described with

the usual perturbative expansions in coupling constants, even if the couplings are weak [10–17]. Such resonances arise as the inflaton condensate (or generally any light scalar, that has attained a non-zero vacuum expectation value during inflation) begins to oscillate about the origin, soon after inflation. The oscillations induce an effective time-dependence in the couplings of the inflaton to the other species of matter. While the background inflaton field dominates the energy budget of the system, the evolution of the remaining fields it is coupled to can be linearised. As the effective frequencies of the individual Fourier modes of the daughter fields change non-adiabatically every time the inflaton crosses the origin, we observe 'explosive' (or resonant) particle production. This can be quite efficient, since it involves the collective decay of many inflatons from the condensate. When the energy of the newly-populated degrees of freedom becomes comparable to the background, back-reaction effects become important. Typically, the condensate fragments and the subsequent evolution is non-linear. It can be studied in the classical approximation, using classical lattice simulations, since all relevant modes have large occupancies and hence quantum effects are negligible.[1] The non-linear dynamics can lead to many interesting phenomena, e.g., the production of solitons that can delay the thermalisation required as an initial condition for BBN, field configurations evolving self-similarly in a turbulent manner [18, 19], non-thermal phase transitions and the production of cosmic defects [20–22].

Research in the field of reheating has been divided into three main areas. On the theoretical side, there is a need to consider more realistic high-energy physics models [23–32], including fermions and gauge bosons, in addition to the more traditional scalars, in the quest for a unified description of our cosmic history. Another direction for future work concerns the phenomenology of the many stages of reheating: from the non-perturbative particle production during preheating and the following non-linear classical evolution, to the late-time approach to a radiation-dominated period of expansion in local thermal equilibrium [32–41]. A lot of effort has been dedicated to observational signatures of reheating [22, 27, 42–44], as well as their important implications for inflationary observables [34, 45–51]. These three areas have also formed the common thread of our research.

The first part of this thesis is meant to serve as a generic introduction to the field of reheating after inflation, starting with a brief summary of the inflationary paradigm (Chapter 1), followed by a review of the different preheating mechanisms (Chapter 2) and the ensuing non-linear evolution (Chapter 3), and finally considering some high-energy physics (Chapter 4) and observational (Chapter 5) aspects of reheating. The rest of the thesis (Chapters 6 - 9) is based on our original research.

We begin in Chapter 6 with a calculation of the equation of state parameter, w, soon after inflation in the simplest and most natural models of inflation favoured by observations. After a careful study of the non-linear dynamics following self-resonance during preheating, we arrive at a rather simple and general result for the expansion history: unless the inflaton has a substantial bare mass (much greater than the Hubble parameter), the universe reaches radiation-dominated expansion at sufficiently late times. We also derive analytical estimates for the relevant time-scales, taking into account the interactions of the inflaton with other species of matter. This improved understanding of the post-inflationary expansion history leads to a reduction in the uncertainty in the predictions of many inflationary models. The case of a more common massive inflaton is also discussed.

Chapters 7 and 8 are based on our work on preheating with a charged inflaton, published as Refs.

[1] However, since the universe at the beginning of BBN is in local thermal equilibrium, late-stage reheating analysis should eventually include a full quantum mechanical computation of the approach of all relevant degrees of freedom to states with maximal local entropy such as Bose-Einstein or Fermi-Dirac distributions [18, 19].

[52] and [32], respectively. The main motivation is to consider the observational and phenomenological consequences of more realistic embeddings of reheating. In Chapter 7 we study a scenario in which the inflaton is responsible for both the generation of primordial curvature perturbations and the observed matter-antimatter asymmetry in the universe. This model of reheating baryogenesis assumes a charged inflaton under a global symmetry that is broken dynamically for a short period of time after inflation. This allows for the post-inflationary non-linear dynamics to generate an asymmetry between the number of inflatons and anti-inflatons which can be eventually transferred into ordinary matter if we allow for the inflatons to decay into baryons. Through semi-analytical and numerical means, we show that the non-linear dynamics on small scales, after inflation in observationally-consistent models, can affect predictions for global observables such as the baryon-to-photon ratio, η. In Chapter 8 we turn our attention to the case of a charged inflaton under local (gauged) symmetries. These models are particularly interesting, since such interactions appear in the Standard Model and its extensions. We carry out the linear calculation of the evolution of Abelian and non-Abelian gauge fields during inflation and preheating, taking into account the gauge constraints and the quantum nature of the fields, as well as metric perturbations. We show for the first time that not only the transverse, but also the longitudinal modes of the vector bosons can be resonantly produced during preheating, clarifying contradicting claims in the literature. We also discuss observational aspects such as the generation of primordial magnetic fields and gravitational waves. The generated charge fluctuations on cosmological scales are within the observational bounds, so the possibility of an electrically charged inflaton is not ruled out. However, the magnetic fields are found to be very small and cannot account for the observed extragalactic ones [53]. Initial conditions for the subsequent non-linear stage of reheating and estimates for the time when it ensues are also provided.

Finally, in Chapter 9 we propose a new algorithm, based on symplectic integration techniques, for studying the non-linear dynamics in models with a charged inflaton under a local symmetry. It can be used to simulate the classical dynamics of Abelian-Higgs systems on a co-moving lattice. The expansion rate is calculated self-consistently, whereas the appropriately discretized gauge constraints are conserved exactly (i.e., to machine-precision) regardless of the order of the time integrator. To the best of our knowledge, this is the only existing numerical scheme that works to arbitrary order of the time integrator. Another advantage of the numerical method is that, unlike conventional integrators based on Lattice Field Theory [22, 54], it is second-order accurate in space, but can be higher order in time (up to 8-th order is practical). This allows for machine-precision energy conservation with reasonable time steps. Symplectic integrators do not require additional storage of intermediate results (unlike the more common Runge-Kutta schemes), which can be also crucial for large 3d lattice simulations. Our scheme is particularly well-suited for reheating studies. We can study the post-inflationary expansion history in models with gauge fields, to understand the important uncertainties in predictions for inflationary observables due to the formation of non-linear objects such as defects (e.g., cosmic strings) and solitons (e.g., gauged oscillons and Q-balls). Other applications are discussed in Chapter 9.

Chapter 1

Inflation and initial conditions for reheating

'With the new cosmology the universe must have been started off in some very simple way. What, then, becomes of the initial conditions required by dynamical theory? Plainly there cannot be any, or they must be trivial. We are left in a situation which would be untenable with the old mechanics. If the universe were simply the motion which follows from a given scheme of equations of motion with trivial initial conditions, it could not contain the complexity we observe. Quantum mechanics provides an escape from the difficulty. It enables us to ascribe the complexity to the quantum jumps, lying outside the scheme of equations of motion. The quantum jumps now form the uncalculable part of natural phenomena, to replace the initial conditions of the old mechanistic view.'

P. A. M. Dirac (1939)

1.1 Standard cosmology, its puzzles and why we need inflation

Standard cosmology is based on the empirical observation that the universe is homogeneous and isotropic on large scales [1]. In the context of General Relativity, it means that the space-time metric takes the Friedmann-Robertson-Walker (FRW) form

$$ds^2 = dt^2 - a(t)^2 \left(\frac{dr^2}{1 - Kr^2} + r^2 d\theta^2 + r^2 \sin^2\theta d\phi^2 \right) , \tag{1.1}$$

where t is the cosmic time and $a(t)$ is the Robertson-Walker scale factor. The term in brackets represents the line element of the three-dimensional homogeneous and isotropic space. For positive, zero and negative K this hypersurface can be considered as a 3-dimensional sphere embedded in a 4-dimensional Euclidean space, a 3-dimensional Euclidean space and a 3-dimensional hypersphere embedded in a 4-dimensional pseudo-Euclidean space, respectively [55]. The positive, zero and negative cases are better known as the closed, flat and open universes, respectively.

The evolution of $a(t)$ is determined by the Einstein equations

$$R_{\mu\nu} - \frac{1}{2} g_{\mu\nu} R = \frac{T_{\mu\nu}}{m_{\rm Pl}^2} + g_{\mu\nu}\Lambda \, . \tag{1.2}$$

Here Λ is the cosmological constant, introduced by Einstein to make the universe static. Henceforth, we set $\Lambda = 0$[1]. Near the origin of locally Cartesian co-moving coordinates, the components of the energy-momentum tensor, $T^{\mu\nu}$, in a homogeneous universe are functions of t only. Isotropy also imposes the additional constraints $T^{i0} = 0$ and $T^{ij} \propto \delta^{ij}$. Conventionally, the energy density, ρ, and the pressure, p, of the perfect fluid filling the homogeneous and isotropic universe are defined locally as

$$T^{00} = \rho(t)\,, \qquad T^{ij} = -a(t)^{-2}\delta^{ij}p(t)\,. \tag{1.3}$$

Then only the 00 and the ii Einstein equations, eq. (1.2), do not vanish

$$\begin{aligned} H^2 &= \frac{\rho}{3m_{\rm Pl}^2} - \frac{K}{a^2}\,, \\ \frac{\ddot{a}}{a} &= -\frac{\rho + 3p}{6m_{\rm Pl}^2}\,, \end{aligned} \tag{1.4}$$

and are known as the Friedmann and Raychaudhuri equations, respectively. The Einstein equations, eq. (1.2), also imply the conservation of the energy-momentum tensor $T^{\nu\mu}{}_{;\mu} = 0$. Due to isotropy the momentum-conservation law $T^{i\mu}{}_{;\mu} = 0$ is automatically satisfied. The energy-conservation $T^{0\mu}{}_{;\mu} = 0$ yields

$$\dot{\rho} + 3H(\rho + p) = 0\,. \tag{1.5}$$

This expression could be derived from a combination of the Friedmann and Raychaudhuri equations, eq. (1.4). For an equation of state of the form $p = w\rho$, the energy-conservation law implies $\rho \propto a^{-3-3w}$. Using this result in eq. (1.4) we find the power-law solution

$$a(t) \propto t^{2/(3+3w)}\,. \tag{1.6}$$

In standard cosmology the typical sources of gravity are non-relativistic matter (dust) and relativistic matter (radiation). If one of these components is dominant, then

$$\begin{aligned} \text{for dust:} \quad & a \propto t^{2/3}\,, \quad & \rho \propto a^{-3}\,, \quad & w = 0\,, \\ \text{for radiation:} \quad & a \propto t^{1/2}\,, \quad & \rho \propto a^{-4}\,, \quad & w = 1/3\,. \end{aligned} \tag{1.7}$$

The second column also applies for individual species, even if subdominant, provided they are self-interacting only. Note that the universe always decelerates, $\ddot{a} < 0$.

The Friedmann equation, eq. (1.4), can be rewritten as

$$\Omega - 1 = \frac{K}{a^2H^2}\,, \tag{1.8}$$

where the energy density makes up a fraction $\Omega = \rho/\rho_{\rm c}$ of the critical energy density, $\rho_{\rm c} = 3m_{\rm Pl}^2H^2$. Similarly, one often writes the spatial curvature term as $\Omega_K = -K/(a^2H^2)$. Cosmological observations give very tight constraints on this quantity, consistent with zero. The 95% limit, from the most recent

[1]Observations favor a small, but non-zero value of Λ, unjustifiable by Quantum Field Theory (QFT) if interpreted as the energy of the vacuum. This drawback of standard cosmology and QFT is known as the *Cosmological constant problem*. The contribution of the Λ term to the energy budget of the universe (known as dark energy) becomes significant only at very late times, at a redshift of about 1, so it is safe to ignore Λ at earlier epochs.

measurement of the anisotropies in the CMB [1], on the spatial curvature today is $|\Omega_{K,0}| < 0.005$. This small value leads to one of the fine-tuning problems in standard cosmology. Since $\ddot{a} < 0$, $aH = \dot{a}$ increases when going backwards in time. Hence, Ω_K becomes even smaller at earlier times, or in other words, the energy density tends to the critical one, $\Omega \to 1$, with unnaturally high precision. To get some rough idea about the degree of fine-tuning in the initial condition for Ω at some early time, $t_{\rm early}$, required by current measurements, consider the ratio

$$\left|\frac{\Omega_{\rm early}-1}{\Omega_0-1}\right| = \left(\frac{a_0H_0}{a_{\rm early}H_{\rm early}}\right)^2 = \left(\frac{a_0H_0}{a_{\rm eq}H_{\rm eq}}\right)^2\left(\frac{a_{\rm eq}H_{\rm eq}}{a_{\rm early}H_{\rm early}}\right)^2 \sim \frac{1+z_{\rm eq}}{(1+z_{\rm early})^2}\,. \tag{1.9}$$

We assume the universe to be radiation dominated at early times, $t_{\rm early} < t < t_{\rm eq}$, and matter dominated after the epoch of radiation-matter equality $t_{\rm eq} < t < t_0$. For $t_{\rm early} \sim t_{\rm BBN}$, $|\Omega_{\rm BBN}-1| \ll 10^{-17}$, assuming $T_{\rm BBN} \sim 1\,{\rm MeV}$ and $z_{\rm eq} \sim 10^3$. At the GUT epoch, $T_{\rm GUT} \sim 10^{16}\,{\rm GeV}$, $|\Omega_{\rm GUT}-1| \ll 10^{-55}$. Unless the initial conditions are set very precisely, the universe either collapses too quickly or expands too fast before large-scale structure can form. This is known as the *flatness problem*.

The deceleration of the scale factor in standard cosmology also leads to contradictions with measurements of the causal structure of the observable universe. The physical length, $l_{\rm phys} = al$, of a given co-moving length-scale l, increases as the universe expands. On the other hand, its ratio with the Hubble radius $l_{\rm phys}/H^{-1} = \dot{a}l$ decreases with time, since $\ddot{a} < 0$. Hence, any co-moving length-scale becomes much greater than the Hubble scale at sufficiently early times. This implies that the causally-connected region in the universe today should lie deep inside the Hubble volume. We can easily calculate the expected size of this region at the epoch of recombination. Ignoring spatial curvature, the physical size of the region at recombination is equal to the particle horizon $d_{\rm rec} = a_{\rm rec}\int_{t_{\rm early}}^{t_{\rm rec}} dt/a(t)$. For $a \sim t^n$, $0 < n < 1$ and $t_{\rm rec} \gg t_{\rm early}$ the upper bound of the integral determines its value. For dust or radiation or any mixture of the two, $d_{\rm rec} \sim H_{\rm rec}^{-1}$. We also have $d_{\rm rec} = a_{\rm rec}r_{\rm rec}\Delta\theta$, where the co-moving distance to the CMB is $r_{\rm rec} = \int_{t_{\rm rec}}^{t_0} dt/a(t) \sim 1/(a_0H_0)$ and $\Delta\theta$ is the angular size of the causal region. Assuming matter domination between recombination and today, $\Delta\theta \sim (1+z_{\rm rec})^{-1/2}$, which corresponds to about $1^{\rm o}$ for $z_{\rm rec} \sim 10^3$. This is in conflict with observations of the microwave sky, showing the same temperature to high accuracy in all directions [1]. Within standard cosmology this isotropy of the CMB cannot be accounted for, since there is no way for points separated by more than a degree to be in thermal equilibrium (and in causal contact) before the epoch of last-scattering. This constitutes the *horizon problem*.

The tiny anisotropies measured in the CMB have a nearly scale-invariant power-spectrum, even on large, causally disconnected at the time of last-scattering, scales [1]. They reflect small variations in the matter density at the epoch of recombination. Later on, these density fluctuations act as seeds for the formation of large-scale structure. Hence, standard cosmology also fails to explain the deviations from the FRW metric.

High-energy physics theories take the view that the physical laws look simpler at higher energies. This implies that gauge symmetries inevitably get broken during the evolution of the early universe, leaving behind them topological defects such as monopoles. The density of monopoles is bounded from below, due to the existence of a maximal correlation length determined by the causal length, i.e., the particle horizon, during the phase transition. This presents a serious problem for standard cosmology. If these relics do not annihilate efficiently, their abundance on sub-horizon scales can become large after the phase transition. Furthermore, these massive relics behave as dust. Their energy density can become the dominant component at dangerously early times, e.g., before or around BBN, since it decays more slowly with $a(t)$ than that of

radiation. This is known as the *monopole problem*[2].

All of the above problems can be shown to have the same origin – the expansion with time of the co-moving Hubble sphere, $(aH)^{-1} = \dot{a}^{-1}$, following from $\ddot{a} < 0$. One can resolve all of these puzzles by postulating the existence of an earlier stage of inflation, during which the universe undergoes accelerated expansion and the co-moving Hubble sphere shrinks [3–5]. The most common expansion history of inflation is the quasi-exponential one, i.e., $a \sim \exp(Ht)$, with H varying very slowly with time. Another possibility is power-law inflation, $a \sim t^n$, $n > 1$. For $n \gg 1$, H again varies very slowly with time.

The measured tiny value of $|\Omega_{K,0}|$ is in fact a prediction of inflation. If we assume that $|\Omega_{K,\mathrm{init}}|$ at the beginning of inflation is of order unity then from eq. (1.8) follows

$$\left|\frac{\Omega_{\mathrm{init}} - 1}{\Omega_0 - 1}\right| > 1\,. \tag{1.10}$$

For a constant expansion rate during inflation, H_{inf}, the number of e-folds of expansion until the end of inflation, $N = \ln(a_{\mathrm{end}}/a_{\mathrm{init}})$, is bounded to be

$$e^N > \frac{a_{\mathrm{end}} H_{\mathrm{inf}}}{a_0 H_0}. \tag{1.11}$$

Making the tentative assumption of $t_{\mathrm{end}} \sim t_{\mathrm{early}}$, see eq. (1.9), i.e., of the universe becoming radiation dominated immediately after the end of inflation, we find that for $t_{\mathrm{early}} \sim t_{\mathrm{BBN}}$ we need at least about 40 e-folds to resolve the flatness problem, whereas for $t_{\mathrm{early}} \sim t_{\mathrm{GUT}}$, N has to be over 60.

To account for the isotropy of the CMB, we need to make sure that the co-moving particle horizon at recombination is greater than the co-moving distance photons travel after recombination until today, i.e.,

$$\int_{t_{\mathrm{init}}}^{t_{\mathrm{rec}}} \frac{dt}{a(t)} > \int_{t_{\mathrm{rec}}}^{t_0} \frac{dt}{a(t)}\,. \tag{1.12}$$

Note that $\int dt/a(t) = \int d\ln a/\dot{a}$. Hence, each integral is dominated by the smallest $\dot{a}$, i.e., the moment when the co-moving Hubble sphere is the largest. It implies for the right-hand side of eq. (1.12) a value $\sim 1/(a_0 H_0)$ as already shown above and $\sim 1/(a_{\mathrm{init}} H_{\mathrm{inf}})$ for the left-hand side. Thus, the condition in eq. (1.11) also applies to the horizon problem.

The scale-invariance of the power-spectrum of the small density fluctuations, imprinted on the CMB as tiny anisotropies, is also a consequence of the accelerated expansion during inflation. At the beginning of inflation, small-scale perturbations, lying deep inside the Hubble radius, are generated by Minkowski space-time quantum fluctuations (since the space-time curvature can be neglected). As the universe undergoes accelerated expansion, perturbations of fixed co-moving wavelength cross outside the shrinking co-moving Hubble sphere. As they become superhorizon, the Hubble friction term starts to dominate and they become over-damped. Since H is approximately constant during inflation and is the only scale determining the evolution of perturbations after Hubble exit, the perturbations which leave the Hubble sphere during inflation have an almost scale-invariant power-spectrum. As the co-moving Hubble radius begins to increase after inflation, perturbations of a given co-moving wavelength start to re-enter the horizon, accounting for the observed approximate scale-invariance of density perturbations over a range of different scales. By letting the Hubble sphere shrink during inflation and then begin to expand as the universe becomes

[2]This issue plagues all theories featuring massive relics, e.g., gravitinos, Kaluza-Klein particles and moduli fields.

radiation and then matter dominated we provide a causal mechanism for producing seemingly-acausal correlations in the density perturbations. Basically, inflation opens up the past light cones for fundamental observers (those who are stationary with respect to the cosmic grid).

Inflation also provides a straightforward solution to the monopole problem. If the phase transition occurs during or before inflation, we need to make sure that there is sufficient number of e-folds of accelerated expansion after the transition to dilute the concentration of the relics. If the gauge symmetry is broken after inflation, the correlation length at the phase transition, equal to the particle horizon, is substantially increased in comparison to standard cosmology and we can again put a lower bound on the duration of inflation. For instance, let us consider the generation of monopoles after spontaneous symmetry breaking at the GUT scale, $E_{\rm GUT} = 10^{16}\,{\rm GeV}$, immediately after the end of inflation. The number density of monopoles is determined by the correlation length of the scalar fields, which is set by the particle horizon and is $\sim a_{\rm end}/(a_{\rm init}H_{\rm inf}) = e^N/H_{\rm inf}$. On the other hand, $H_{\rm inf} \sim E_{\rm GUT}^2/m_{\rm Pl}$. Hence, there is roughly one monopole per $E_{\rm GUT}^{-6}m_{\rm Pl}^3 e^{3N}$. Assuming the universe becomes radiation dominated and reaches local thermal equilibrium soon after the formation of monopoles, the number density of photons at that time is $\sim E_{\rm GUT}^3$. Ignoring subsequent processes that can change the number of photons and annihilation of monopoles, the ratio of the number densities of monopoles and photons remains constant, since each $\propto a^{-3}$. Thus, $n_0^{\rm mon}/n_0^\gamma \sim e^{3N}E_{\rm GUT}^3/m_{\rm Pl}^3 = 10^{-9}e^{3N}$. For less than 10^{-39} monopoles per photon [55], as suggested by terrestrial experiments, $N > 23$. An identical bound is obtained if GUT scale monopoles are generated during or before inflation. A possibility that cannot be resolved by inflation is the production of massive particles during the reheating process after inflation. If the reheating temperature is low enough, thermal particle production of dangerous massive relics, that can ruin the successful BBN in standard cosmology, can be evaded. On the other hand, non-thermal production has to be dealt with on a case-by-case basis.

1.2 Dynamics of inflation and setting the scene for reheating

The semi-classical theory of inflation provides not only a solution to the horizon, flatness and monopole problems, but more importantly predicts the generation of density perturbations exhibiting a nearly scale-invariant power-spectrum. These act as seeds for the large-scale structure in the late universe.

The inflationary paradigm can be interpreted in at least two different ways. We could think of it as an approximate description (some sort of a parametrisation), which does not capture the actual physical laws, due to its semi-classical nature. We could also argue that the universe genuinely underwent a stage of accelerated expansion, driven by a scalar condensate whose origin can be traced back to any of the high-energy models going beyond the Standard Model of Particle Physics. This way of thinking makes inflation the link between quantum gravity or/and extensions of the Standard Model, and the well-understood physics of BBN in standard cosmology.

In this work, we consider the most common (and consistent with observations [2]) models of inflation, in which a single scalar field ϕ, called the inflaton, sources the accelerated expansion of the universe, with action

$$S = \int d^4x\sqrt{-g}\left[-\frac{m_{\rm Pl}^2}{2}R + \frac{1}{2}\nabla_\mu\phi\nabla^\mu\phi - V(\phi)\right] + S_{\rm matter}\,. \tag{1.13}$$

We limit ourselves to models, minimally coupled to gravity, with canonical kinetic terms[3]. The matter action

[3]There are examples of non-minimal and non-canonical models in which a conformal transformation or a field redefinition can reduce the action to the form given in eq. (1.13).

term, $S_{\rm matter}$, contains the entire information regarding the other constituents of the matter sector, including the Standard Model Lagrangian as well as the terms describing the couplings of the inflaton to other fields.

1.2.1 Homogeneous dynamics of inflation

Isotropy and homogeneity require that the dominant component of the scalar field depends on t only, $\bar{\phi}(t)$. This scalar condensate provides the classical background configuration during inflation (and the initial stages of reheating). The energy density and the pressure of the isotropic and homogeneous scalar fluid are simply

$$\rho_{\bar{\phi}} = \frac{1}{2}\dot{\bar{\phi}}^2 + V(\bar{\phi})\,, \qquad p_{\bar{\phi}} = \frac{1}{2}\dot{\bar{\phi}}^2 - V(\bar{\phi})\,. \tag{1.14}$$

To have acceleration, $\ddot{a} > 0$, the Raychaudhuri equation, eq. (1.4), demands $\rho_{\bar{\phi}} + 3p_{\bar{\phi}} < 0$. This means that inflation occurs as long as $\dot{\bar{\phi}}^2 < V(\bar{\phi})$. The Friedmann equation, eq. (1.4), and the Euler-Lagrange equation for $\bar{\phi}$ following from the action in eq. (1.13) are

$$H^2 = \frac{1}{3m_{\rm Pl}^2}\left[\frac{1}{2}\dot{\bar{\phi}}^2 + V(\bar{\phi})\right]\,, \qquad \ddot{\bar{\phi}} + 3H\dot{\bar{\phi}} + \partial_{\bar{\phi}}V(\bar{\phi}) = 0\,. \tag{1.15}$$

1.2.2 Slow-roll inflation

Having derived the equations of motion and shown that accelerated expansion is possible, we need to find what conditions V has to satisfy to have enough number of *e*-folds of inflation to solve the horizon and flatness problems. Note that $\ddot{a} = a(\dot{H} + H^2)$, hence

$$\epsilon_H \equiv -\frac{\dot{H}}{H^2} < 1\,, \tag{1.16}$$

has to hold to have $\ddot{a} > 0$. Inflation ends when $\epsilon_H = 1$, corresponding to $\ddot{a} = 0$. Since H^{-1} is the characteristic time-scale for one *e*-fold of expansion (recall $dN = d\ln a = Hdt$), known as the Hubble time, $\epsilon_H = -d\ln H/dN < 1$ implies that the time-scale over which the fractional decrease in H is significant is greater than a Hubble time. Or in other words the rate of decrease of H must be slower than the rate of expansion of the universe in order to have inflation. To achieve sufficiently many *e*-folds (at least 40 up to 60, see Section 1.1) of inflation we need ϵ_H to be much less than 1 for a long enough period, implying that for most of the time $\epsilon_H \ll 1$. The parameter quantifying the rate of change of ϵ_H is

$$\eta_H \equiv \frac{\dot{\epsilon}_H}{H\epsilon_H} = \frac{d\ln\epsilon_H}{dN}\,. \tag{1.17}$$

For ϵ_H to increase slowly, over many Hubble times, $|\eta_H|$ has to be less than unity. But because of the large number of *e*-folds required by observations, $|\eta_H| \ll 1$ has to hold[4]. All of this basically means that $H \approx \text{const}$ for most of inflation, and that the scale factor increases quasi-exponentially. That is why this period is also called quasi-de Sitter expansion. Current observational constraints are roughly $\epsilon_H < 0.01$ and $\eta_H \approx 0.03 \pm 0.01$ [2] and are in support of this picture.

[4]If $\eta_H \sim \mathcal{O}(1)$, inflation still takes place for roughly $\Delta N \sim \ln(1/\epsilon_H)$. If ϵ_H is several orders of magnitude less than unity, the number of *e*-folds of inflation is much less than the one required by observations.

Using the Friedmann equation, eq. (1.4), the energy conservation equation, eq. (1.5), and the expressions for the energy density and pressure of the inflaton condensate, eq. (1.14), we find that $\epsilon_H = 3\dot{\bar{\phi}}^2/(2\rho_{\bar{\phi}})$. Thus, $\epsilon_H \ll 1$ implies a negligible contribution of the kinetic energy density to the total energy density of the condensate, which also means that $\dot{\bar{\phi}}^2/2 \ll V(\bar{\phi})$ during inflation, consistent with our comments under eq. (1.14). Hence, V has to be very flat, for $\bar{\phi}$ to roll sufficiently slowly. This is called *slow-roll inflation*. For slow-roll inflation to last long enough, we need the kinetic energy density to remain small. This means that the fractional change in $\dot{\bar{\phi}}$ during one expansion time H^{-1}, $|\ddot{\bar{\phi}}/\dot{\bar{\phi}}|H^{-1}$, has to be much less than 1. It implies, given $\epsilon_H \ll 1$, that $|\eta_H| \ll 1$, since one can show that $\eta_H = 2\epsilon_H + 2\ddot{\bar{\phi}}/(\dot{\bar{\phi}}H)$.

Finally, we are in a position to put constraints on the form of V that can support inflation for sufficiently long periods. Applying $\dot{\bar{\phi}}^2/2 \ll V(\bar{\phi})$ to the first expression in eq. (1.15), yields $H^2 \approx V/3m_{\rm Pl}^2$, whereas substituting $|\ddot{\bar{\phi}}/\dot{\bar{\phi}}|H^{-1} \ll 1$ in the second expression in eq. (1.15) gives $3H\dot{\bar{\phi}} \approx -\partial_{\bar{\phi}}V(\bar{\phi})$. Hence, $\epsilon_H \approx (m_{\rm Pl}^2/2)(\partial_{\bar{\phi}}V/V)^2$. Taking the time derivative of $3H\dot{\bar{\phi}} \approx -\partial_{\bar{\phi}}V(\bar{\phi})$ yields $\epsilon_H - \ddot{\bar{\phi}}/(\dot{\bar{\phi}}H) \approx m_{\rm Pl}^2\partial_{\bar{\phi}}^2 V/V$. These two ratios of V and its derivatives are conventionally denoted as

$$\epsilon_V \equiv \frac{m_{\rm Pl}^2}{2}\left(\frac{\partial_{\bar{\phi}}V(\bar{\phi})}{V}\right)^2, \qquad \eta_V \equiv m_{\rm Pl}^2\frac{\partial_{\bar{\phi}}^2 V(\bar{\phi})}{V}, \tag{1.18}$$

and are known as the potential slow-roll parameters (similarly, ϵ_H and η_H are known as the Hubble slow-roll parameters). ϵ_H and $|\eta_H| \ll 1$ is equivalent to ϵ_V and $|\eta_V| \ll 1$.

To see that within the slow-roll approximation, the expansion during inflation can be exponentially large consider[5]

$$\begin{aligned} e^N \equiv \frac{a_{\rm end}}{a_{\rm init}} = \exp\left[\int_{t_{\rm init}}^{t_{\rm end}} H(t)dt\right] &= \exp\left[\int_{\bar{\phi}_{\rm init}}^{\bar{\phi}_{\rm end}} H(\bar{\phi})\frac{d\bar{\phi}}{\dot{\bar{\phi}}}\right] \\ &\approx \exp\left[-m_{\rm Pl}^{-2}\int_{\bar{\phi}_{\rm init}}^{\bar{\phi}_{\rm end}} \frac{V(\bar{\phi})}{\partial_{\bar{\phi}}V(\bar{\phi})}d\bar{\phi}\right], \end{aligned} \tag{1.19}$$

where we assume $0 < V(\bar{\phi}_{\rm end}) < V(\bar{\phi}_{\rm init})$ and $\Delta\bar{\phi} \equiv \bar{\phi}_{\rm init} - \bar{\phi}_{\rm end} > 0$, implying a positive argument in the last exponential. The slow-roll condition $\epsilon_V \ll 1$ leads to $N \gg \Delta\bar{\phi}/m_{\rm Pl}$. If the value of the inflaton changes by $\sim m_{\rm Pl}$, we definitely get a huge number of *e*-foldings. Note that such large field values do not mean that the quantum nature of gravity becomes important. For this to happen the energy density of the condensate must be $\sim m_{\rm Pl}^4$. This can be easily avoided, even for $\bar{\phi} \gtrsim m_{\rm Pl}$, if $V(\bar{\phi})$ is proportional to a sufficiently small coupling constant. None of the potential slow-roll parameters, eq. (1.18), depends on it.

We can find the approximate trajectory of the inflaton during inflation. Since, during slow-roll $\epsilon_H \approx \epsilon_V \ll 1$, $\dot{\bar{\phi}} \approx -m_{\rm Pl}\partial_{\bar{\phi}}V/\sqrt{3V}$. As a test case, we consider the simplest form for the inflaton potential, i.e., $V(\bar{\phi}) = m^2\bar{\phi}^2/2$. In general, all monomial potentials satisfy the slow-roll conditions, eq. (1.18), for some $\Delta\bar{\phi} \gtrsim m_{\rm Pl}$. These models belong to the class of Chaotic inflation [56, 57]. It encompasses all models having V that supports slow-roll inflation for $\Delta\bar{\phi} \sim \mathcal{O}(m_{\rm Pl})$ or smaller. In this thesis, we will concentrate on Chaotic inflation models[6]. For the quadratic potential the slow-roll trajectory and the expansion law take

[5]The total number of *e*-folds of inflation is defined as the first integral with $\epsilon_H(t_{\rm init}) = \epsilon_H(t_{\rm end}) = 1$ and $\epsilon_H(t) < 1$ for $t_{\rm init} < t < t_{\rm end}$.

[6]Examples of single-field models that do not belong to Chaotic inflation include Small-field models in which necessarily $\Delta\bar{\phi} \ll m_{\rm Pl}$, models in which higher-order kinetic terms or higher-order curvature terms, instead of V, drive inflation and models in which phase transitions stop or trigger inflation, e.g., Old and New inflation, respectively.

the simple approximate analytic form ($t_{\rm init} = 0$)

$$\dot{\bar{\phi}} \approx -\sqrt{\frac{2}{3}} m_{\rm Pl} m \,, \qquad a \approx a_{\rm init} \exp\left[\frac{mt}{\sqrt{6} m_{\rm Pl}} \left(\bar{\phi}_{\rm init} - \frac{m_{\rm Pl} m}{\sqrt{6}} t\right)\right] . \tag{1.20}$$

It breaks down towards the end of inflation, $\bar{\phi}_{\rm end} \approx m_{\rm Pl}$ for which the slow-roll conditions in eq. (1.18) are violated. This solution is also known as the attractor solution, since one can show that for a broad range of $\bar{\phi}_{\rm init}$ [58, 59], even for large $\dot{\bar{\phi}}_{\rm init}$ such that $\epsilon_H(t_{\rm init}) > 1$, the field velocity decays very rapidly and $\bar{\phi}(t)$ and $a(t)$ quickly approach eq. (1.20). This goes to show how broad the set of initial conditions is that can lead to an inflationary stage in chaotic models.

Speaking of initial conditions, the term 'chaotic' derives from the possibility of having initially a scalar field varying randomly with position, i.e., having almost arbitrary initial conditions for the inflaton, and still getting slow-roll inflation after that. Even if the value of the inflaton varies from one spatial region to another, there should be a patch of space in which the inflaton looks uniform enough and has a value for which the slow-roll conditions in eq. (1.18) are satisfied, e.g., a super-Planckian value for monomial potentials [58]. One can easily show that the initial physical size of the homogeneous patch, $L_{\rm init} = a_{\rm init} l$, has to obey $H_{\rm init} L_{\rm init} \gg \dot{\bar{\phi}}_{\rm init}/m_{\rm Pl}$ for the gradients to be negligible. For monomial potentials, this implies that a sufficiently large uniform patch has to be super-Hubble initially[7] (and super-Planckian after imposing the condition of sub-Planckian $V_{\rm init}$).

1.2.3 End of slow-roll inflation

For inflation to be successful it must feature a graceful exit into the deceleration stage of standard cosmology; otherwise the homogeneity and isotropy of the universe are destroyed. A famous example of non-graceful exit is Alan Guth's Old inflation [3] in which the inflaton is initially trapped in a false vacuum. As the inflaton leaks through the potential barrier and forms bubbles of true vacuum, the energy released in the transition ends up concentrated within the bubble walls. If the bubbles are able to merge, a homogeneous and isotropic universe emerges. However, the bubbles never collide, since the background false-vacuum space in which they formed, never stops inflating. Hence, for an observer located inside a bubble the universe would appear highly anisotropic and inhomogeneous, since structure has to grow out of the energy concentrated in the bubble walls. The graceful exit problem is naturally avoided in Chaotic inflation. For power-law potentials, the homogeneous inflaton background simply begins to oscillate about the potential minimum. One can easily determine the oscillatory attractor solution for a quadratic minimum. We put $\bar{\phi} = \sqrt{6} H (m_{\rm Pl}/m) \cos\theta$ and $\dot{\bar{\phi}} = \sqrt{6} H m_{\rm Pl} \sin\theta$ to satisfy the first expression in eq. (1.15). After differentiating it with respect to time and using the second expression in eq. (1.15) we find $\dot{H} = -3H^2 \sin^2\theta$. This implies that H decays during the oscillatory stage as t^{-1}. Taking the time derivative of the new definition of $\bar{\phi}$ in terms of θ and using the definition of $\dot{\bar{\phi}}$ in terms of θ we find $\dot{\theta} = -m - (3/2) H \sin(2\theta)$. The second term on the right decays with time, so $\theta \approx mt$ up to a constant for $mt \gg 1$. We can use this result in the expression for $\dot{H}$. After integration we find

$$H \approx \frac{2}{3t}\left(1 + \frac{\sin(2mt)}{2mt}\right) , \qquad \text{and} \qquad \bar{\phi} \approx \frac{2\sqrt{2} m_{\rm Pl} \cos(mt)}{\sqrt{3} mt}\left(1 + \frac{\sin(2mt)}{2mt}\right) . \tag{1.21}$$

[7] Which is interpreted as a requirement for fine-tuning of the initial conditions for inflation by some authors [60, 61].

This decaying scalar field condensate provides the classical background during the reheating phase. Note that $a \propto t^{2/3}$ up to subdominant decaying oscillating terms, which implies that the universe is in a dust-dominated state of expansion. Ultimately, the universe has to reheat itself to reach eventually a radiation-like state of expansion, with the inflaton energy transferred into radiation, baryons and leptons. Also note that even if the oscillating terms are very small, they can play an important role for the space-time curvature (neglecting the spatial curvature for simplicity)

$$R = -6\left(\frac{\ddot{a}}{a^2} + \frac{\dot{a}^2}{a^2}\right) \approx -\frac{4}{3t^2}\left(1 + 3\cos(2mt)\right) . \tag{1.22}$$

Before moving forward, we should point out that the state of expansion of a universe dominated by a homogeneous oscillating scalar, about the minimum of its potential, depends on the form of V. For simple power-laws, $V \propto |\phi|^{2n}$, where n need not be an integer, one can easily determine the temporal mean equation of state during the oscillatory phase. Ignoring expansion, since H decays with time after inflation, and multiplying by $\bar{\phi}$ the second expression in eq. (1.15), we find $\langle \bar{\phi}\partial_{\bar{\phi}} V\rangle = -\langle \bar{\phi}\ddot{\bar{\phi}}\rangle = \langle \dot{\bar{\phi}}^2\rangle$. The angle brackets represent time averaging over many oscillations. The last equality follows from virialization, i.e., $0 = \langle d(\bar{\phi}\dot{\bar{\phi}})/dt\rangle = \langle \dot{\bar{\phi}}^2\rangle + \langle \bar{\phi}\ddot{\bar{\phi}}\rangle$. Thus, assuming $\langle p_{\bar{\phi}}/\rho_{\bar{\phi}}\rangle \approx \langle p_{\bar{\phi}}\rangle/\langle \rho_{\bar{\phi}}\rangle$, we find [62]

$$\langle w\rangle \approx \frac{\langle \dot{\bar{\phi}}^2\rangle/2 - \langle V\rangle}{\langle \dot{\bar{\phi}}^2\rangle/2 + \langle V\rangle} = \frac{\langle \bar{\phi}\partial_{\bar{\phi}} V\rangle/2 - \langle V\rangle}{\langle \bar{\phi}\partial_{\bar{\phi}} V\rangle/2 + \langle V\rangle} = \frac{n-1}{n+1} . \tag{1.23}$$

For quadratic potentials, $n = 1$, we have the expected $w = 0$ matter-like equation of state, whereas for quartic potentials, $n = 2$, we have a radiation-like equation of state, $w = 1/3$. When $n \leq 1/2$, $w \leq -1/3$, and eq. (1.6) tells us that $\ddot{a} > 0$ – the universe inflates. However, consistency requires that the inflaton oscillates around a potential that has a non-singular first derivative at its minimum, for the equation of motion to be well-defined for all field values, implying the condition $n > 1/2$, i.e., the potential has to be steeper than linear at the minimum. Oscillations about such minima always lead to a decelerating stage of expansion with $w > -1/3$.

1.2.4 Cosmological perturbations from inflation

Having described what the homogeneous and isotropic universe looks like at the end of inflation, we now consider the small deviations from the FRW approximation. After all, these small departures enable us to distinguish between different models. As mentioned above, the tiny anisotropies measured in the CMB, as well as the seeds for Large Scale Structure (LSS) can be explained within the inflationary paradigm, as being microscopic quantum fluctuations, stretched to cosmic sizes during inflation. As we will see in later sections, they also laid down the seeds for particle production during reheating. To understand the initial conditions for this process, we need to consider their evolution during inflation.

We expand the metric and the energy momentum tensor about their background values [63]

$$g_{\mu\nu}(x^\alpha) = \bar{g}_{\mu\nu}(t) + \delta g_{\mu\nu}(x^\alpha) , \qquad T_{\mu\nu}(x^\alpha) = \bar{T}_{\mu\nu}(t) + \delta T_{\mu\nu}(x^\alpha) , \tag{1.24}$$

where $\bar{g}_{\mu\nu}(t)$ is given in eq. (1.1) and we set the spatial curvature, K, to zero, since during inflation it quickly becomes negligible. While we know the non-zero components of $\bar{T}_{\mu\nu}(t)$, see eq. (1.3), it is easier to work with a co-variant form for the tensor. Since the FRW universe is filled with a perfect homogeneous

fluid, i.e., a fluid that looks the same in all directions for all co-moving observers at equal cosmic times, the rank-2 tensor $\bar{T}_{\mu\nu}(t)$ has to be a linear combination of $\bar{\rho}(t)\bar{g}_{\mu\nu}(t)$, $\bar{p}(t)\bar{g}_{\mu\nu}(t)$, $\bar{\rho}(t)\bar{u}_\mu(t)\bar{u}_\nu(t)$ and $\bar{p}(t)\bar{u}_\mu(t)\bar{u}_\nu(t)$, where $\bar{u}_\mu(t)$ is the 4-velocity of a co-moving observer. The only linear combination that respects homogeneity and isotropy is $\bar{T}_{\mu\nu}(t) = (\bar{\rho}+\bar{p})\bar{u}_\mu\bar{u}_\nu - \bar{g}_{\mu\nu}\bar{p}$, where we used $[1,0,0,0]^T$ for $\bar{u}^\mu(t)$. More generally, in an arbitrary gravitational field, a perfect fluid is a medium, with energy momentum tensor

$$T_{\mu\nu}(x^\alpha) = [\rho(x^\alpha) + p(x^\alpha)]\, u_\mu(x^\alpha)u_\nu(x^\alpha) - g_{\mu\nu}(x^\alpha)p(x^\alpha)\,. \tag{1.25}$$

We now write the actual forms of the perturbations $\delta g_{\mu\nu}(x^\alpha)$ and $\delta T_{\mu\nu}(x^\alpha)$. We use the conformal time, $d\tau \equiv dt/a(t)$, which simplifies the background metric, $\bar{g}_{\mu\nu}(\tau) = a^2(\tau)\eta_{\mu\nu}$. The most general metric perturbations are

$$\begin{aligned} ds^2 &= (\bar{g}_{\mu\nu} + \delta g_{\mu\nu})dx^\mu dx^\nu \\ &= (1+2\varphi)\, a^2(\tau)d\tau^2 + 2\left(\partial_i\mathcal{B} + \mathcal{S}_i\right) a^2(\tau)dx^i d\tau \\ &\quad - \left[\,(1-2\psi)\,\delta_{ij} - 2\partial_i\partial_j\mathcal{E} - \partial_j\mathcal{K}_i - \partial_i\mathcal{K}_j - \tilde{h}_{ij}\right] a^2(\tau)dx^i dx^j\,, \end{aligned} \tag{1.26}$$

where $\varphi(x^\sigma)$, $\mathcal{B}(x^\sigma)$, $\psi(x^\sigma)$, $\mathcal{E}(x^\sigma)$ are scalar perturbations, $\mathcal{S}_i(x^\sigma)$, $\mathcal{K}_i(x^\sigma)$ are divergence-free 3-vector perturbations, and $\tilde{h}_{ij}(x^\sigma)$ is a traceless transverse 3-tensor perturbation. Consistency requires the energy density, pressure and 4-velocity fields to be also perturbed

$$\rho(x^\alpha) = \bar{\rho}(t) + \delta\rho(x^\alpha)\,, \qquad p(x^\alpha) = \bar{p}(t) + \delta p(x^\alpha)\,, \qquad u_\mu(x^\alpha) = \bar{u}_\mu(t) + \delta u_\mu(x^\alpha)\,, \tag{1.27}$$

where $\bar{u}_\mu = [a,0,0,0]^T$, $\delta u_\mu \equiv [\delta u_0, \partial_i\delta u^\parallel + \delta u_i^\perp]^T$ and $\partial_i u_i^\perp = 0$. Since the 4-velocity of an observer is normalized, i.e., $\bar{g}_{\mu\nu}\bar{u}^\mu\bar{u}^\nu = 1$ and $g_{\mu\nu}u^\mu u^\nu = 1$ one can show to linear order that $\delta u_0 = a\varphi$. In deriving this expression, we have used $\delta g^{\mu\nu} = -\bar{g}^{\mu\alpha}\delta g_{\alpha\beta}\bar{g}^{\beta\nu}$, which also holds to linear order for $\bar{g}_{\mu\nu}\bar{g}^{\nu\alpha} = \delta^\alpha_\mu$ and $g_{\mu\nu}g^{\nu\alpha} = \delta^\alpha_\mu$. This also implies $u^\mu = a^{-1}[1-\varphi, -a^{-1}\partial_i\delta u^\parallel - a^{-1}\delta u_i^\perp - \partial_i\mathcal{B} - \mathcal{S}_i]^T$, to first order in perturbations. The perturbations in the energy momentum tensor then take the form

$$\begin{aligned} &\delta T^\mu{}_\nu = (\delta\rho + \delta p)\bar{u}^\mu\bar{u}^\nu - \delta p\delta^\mu_\nu - (\bar{\rho}+\bar{p})\bar{u}^\mu\delta u_\nu - (\bar{\rho}+\bar{p})\delta u^\mu\bar{u}_\nu\,, \\ &\delta T^0{}_0 = \delta\rho\,, \qquad \delta T^0{}_i = -(\bar{\rho}+\bar{p})a^{-1}(\partial_i\delta u^\parallel + \delta u_i^\perp)\,, \\ &\delta T^i{}_j = -\delta p\delta_{ij}\,, \qquad \delta T^i{}_0 = (\bar{\rho}+\bar{p})a^{-1}(a^{-1}\partial_i\delta u^\parallel + a^{-1}\delta u_i^\perp + \partial_i\mathcal{B} + \mathcal{S}_i)\,. \end{aligned} \tag{1.28}$$

Decomposing perturbations into scalars, divergence-free vectors and traceless transverse tensors, also known as the scalar-vector-tensor decomposition, is very useful since the Einstein equations decouple the three kinds of modes to linear order. This is a consequence of the symmetries of the FRW background. The Einstein equations are also invariant under diffeomorphisms, i.e., space-time coordinate transformations

$$x^\mu \to x'^\mu = x^\mu + \xi^\mu(x^\alpha). \tag{1.29}$$

We assume $\xi^\mu = [\xi^0, \partial_i\xi^\parallel + \xi_i^\perp]^T$ to be small, of the order of the metric and energy momentum tensor perturbations. Since the metric transforms as

$$g'_{\mu\nu}(x'^\alpha) = \frac{\partial x^\beta}{\partial x'^\mu}\frac{\partial x^\gamma}{\partial x'^\nu}g_{\beta\gamma}(x^\alpha)\,, \tag{1.30}$$

the metric perturbations at x^α transform, to linear order, as[8]

$$\begin{aligned}\Delta\delta g_{\mu\nu}(x^\alpha) = g'_{\mu\nu}(x^\alpha) - g_{\mu\nu}(x^\alpha) &\approx g'_{\mu\nu}(x'^\alpha) - \frac{\partial g_{\mu\nu}}{\partial x^\beta}\xi^\beta - g_{\mu\nu}(x^\alpha) \\ &\approx -\bar{g}_{\beta\nu}(x^\alpha)\frac{\partial \xi^\beta}{\partial x^\mu} - \bar{g}_{\mu\beta}(x^\alpha)\frac{\partial \xi^\beta}{\partial x^\nu} - \frac{\partial \bar{g}_{\mu\nu}(x^\alpha)}{\partial x^\beta}\xi^\beta\,.\end{aligned} \tag{1.31}$$

Similarly,

$$\Delta\delta T^\mu{}_\nu(x^\alpha) \approx \bar{T}^\beta{}_\nu(x^\alpha)\frac{\partial \xi^\mu}{\partial x^\beta} - \bar{T}^\mu{}_\beta(x^\alpha)\frac{\partial \xi^\beta}{\partial x^\nu} - \frac{\partial \bar{T}^\mu{}_\nu(x^\alpha)}{\partial x^\beta}\xi^\beta\,. \tag{1.32}$$

From this follows that perturbations depend on our choice of space-time coordinates, e.g.,

$$\Delta\psi = \mathcal{H}\xi^0\,, \qquad \Delta\delta u^\parallel = -a\xi^0\,. \tag{1.33}$$

This issue can be resolved by working in diffeomorphism invariant quantities that take the same values for all choices of coordinates, i.e., in all gauges. For instance, the quantity

$$\mathcal{R} = \psi + \frac{\mathcal{H}}{a}\delta u^\parallel\,, \tag{1.34}$$

is gauge invariant. It is known as the co-moving curvature perturbation. We can construct other gauge-invariant quantities, e.g.,

$$\begin{aligned}\Phi &= \varphi - \frac{1}{a}\partial_\tau\left[a\left(\mathcal{B} - \partial_\tau\mathcal{E}\right)\right]\,, \\ \Psi &= \psi + \mathcal{H}\left(\mathcal{B} - \partial_\tau\mathcal{E}\right)\,,\end{aligned} \tag{1.35}$$

known as Bardeen variables. We can either calculate such quantities directly, by solving their equations of motion, or we can fix the gauge first by imposing conditions on the gauge dependent perturbations and then solve for the metric and energy momentum tensor perturbations. No matter what gauge we choose in the latter case, the gauge-invariant quantities always have the same values.

To make further progress, we need to specify the energy momentum tensor. In single-field inflation, see eq. (1.13), the contribution from the matter action term to the energy momentum tensor vanishes at linear order. Hence, the scalar metric perturbations are coupled to linear order only to the perturbation in the inflaton

$$\phi(x^\alpha) = \bar{\phi}(t) + \delta\phi(x^\alpha)\,. \tag{1.36}$$

The unperturbed energy momentum tensor is

$$T_{\mu\nu} = \nabla_\mu\phi\nabla_\nu\phi - g_{\mu\nu}\left[\frac{1}{2}\nabla^\alpha\phi\nabla_\alpha\phi - V\right], \tag{1.37}$$

from which follows that

$$\delta T^0{}_i = \frac{\partial_\tau\bar{\phi}}{a^2}\partial_i\delta\phi\,. \tag{1.38}$$

Given the expressions for the background pressure and energy density in eq. (1.14), the scalar velocity perturbation can be found directly by using eq. (1.28) to be

$$\delta u^\parallel = \frac{a\delta\phi}{\partial_\tau\bar{\phi}}, \tag{1.39}$$

[8]It is understood that $\bar{g}_{\mu\nu}(x^\alpha) = \bar{g}'_{\mu\nu}(x^\alpha)$, i.e., eq. (1.29) yields $\delta g_{\mu\nu}(x^\alpha) \to \delta g'_{\mu\nu}(x^\alpha) = \delta g_{\mu\nu}(x^\alpha) + \Delta\delta g_{\mu\nu}(x^\alpha)$.

implying $\mathcal{R} = \psi + \mathcal{H}\delta\phi/\partial_\tau\bar{\phi}$. We can calculate this quantity during inflation, working in the slow-roll approximation. The most suitable gauge for analytical analysis is the spatially-flat gauge defined as $\psi = \mathcal{E} = 0$ (fixing the two scalar perturbations removes the gauge freedom due to ξ^0 and $\xi^\parallel$). This implies that the scalar modes in δg_{ij} vanish. The second order terms in the action in eq. (1.13) which couple the non-zero scalar metric perturbations, δg_{00} and δg_{0i}, to the inflaton perturbations, coming from the $g_{\mu\nu}\partial^\mu\phi\partial^\nu\phi/2$ term are proportional to $\dot{\bar{\phi}}$, whereas those coming from $\sqrt{-g}V$ are $\sim \partial_{\bar{\phi}}V$. This means that all couplings between metric perturbations and inflaton perturbations are slow-roll suppressed and can be ignored during inflation. The effective mass term due to the inflaton potential also vanishes in the slow-roll limit, $\partial^2_{\bar{\phi}}V \sim \eta_V H^2$. Thus, the second order action for the Fourier components of the inflaton perturbations, without the slow-roll suppressed terms, reduces to

$$\begin{aligned} S^{(2)}_{\rm sr} &= \int \mathrm{d}\tau L^{(2)}_{\rm sr}(\tau) = \int d\tau \int d^3k\; b_{\rm sr}(k,\tau)\left[\frac{1}{2}|\partial_\tau\delta\phi_{\mathbf{k}}|^2 - \frac{1}{2}\omega^2_{\rm sr}(k,\tau)|\delta\phi_{\mathbf{k}}|^2\right], \\ b_{\rm sr}(k,\tau) &= a^2\,, \qquad \omega^2_{\rm sr}(k,\tau) = k^2\,. \end{aligned} \tag{1.40}$$

Note that the due to the $b_{\rm sr}$ pre-factor the kinetic term in the action is not canonically-normalized. If one wishes, $b_{\rm sr}$ can absorbed into a field re-definition which makes the kinetic term canonical.

Having derived the second order action for the inflaton fluctuations, we can now quantize them. First we need the conjugate momentum density

$$\pi^{\rm sr}_{\mathbf{k}}(\tau) = \frac{\delta\left(L^{(2)}_{\rm sr}(\tau)\right)}{\delta\left(\partial_\tau\delta\phi_{-\mathbf{k}}\right)} = b_{\rm sr}\partial_\tau\delta\phi_{\mathbf{k}}\,, \tag{1.41}$$

where we have taken the functional derivative of the Lagrangian and made use of the reality of the inflaton fluctuations, i.e., $\delta\phi^*_{\mathbf{k}} = \delta\phi_{-\mathbf{k}}$. In the Heisenberg picture, the field operators $\delta\hat{\phi}^I_{\mathbf{k}}$ and their conjugate momenta operators $\hat{\pi}^{\rm sr}_{\mathbf{k}}$ satisfy the equal time commutators:

$$\left[\delta\hat{\phi}_{\mathbf{k}}(\tau), \delta\hat{\phi}_{\mathbf{q}}(\tau)\right] = 0\,, \quad \left[\hat{\pi}^{\rm sr}_{\mathbf{k}}(\tau), \hat{\pi}^{\rm sr}_{\mathbf{q}}(\tau)\right] = 0\,, \quad \left[\delta\hat{\phi}_{\mathbf{k}}(\tau), \hat{\pi}^{\rm sr}_{\mathbf{q}}(\tau)\right] = i\,(2\pi)^{-3}\,\delta(\mathbf{k}+\mathbf{q})\,. \tag{1.42}$$

The only non-vanishing commutator and the expression for the conjugate momentum in eq. (1.41) yield

$$\left[\delta\hat{\phi}_{\mathbf{k}}(\tau), \partial_\tau\delta\hat{\phi}_{\mathbf{q}}(\tau)\right] = i\,(2\pi)^{-3}\,(b_{\rm sr}(k,\tau))^{-1}\,\delta(\mathbf{k}+\mathbf{q})\,. \tag{1.43}$$

The quantized perturbations $\delta\hat{\phi}_{\mathbf{k}}$ can be written in terms of operators $\hat{a}_{\mathbf{k}}$ and mode functions $u_k(\tau)$ as

$$\delta\hat{\phi}_{\mathbf{k}}(\tau) = \hat{a}_{\mathbf{k}}u_k(\tau) + \hat{a}^\dagger_{-\mathbf{k}}u^*_k(\tau)\,. \tag{1.44}$$

The two mode functions, $u_k(\tau)$ and its complex conjugate, span the space of solutions to the classical equation of motion for $\delta\phi_{\mathbf{k}}$ obtained by varying the action in eq. (1.40), i.e.,

$$\partial^2_\tau u_k + (\partial_\tau \ln b_{\rm sr})\,\partial_\tau u_k + \omega^2_{\rm sr}u_k = 0\,. \tag{1.45}$$

Given a set of initial conditions for the mode functions, we can evolve them forwards in time. To calculate $\delta\hat{\phi}$ and ultimately $\hat{\mathcal{R}}_{\mathbf{k}}$ we need to know not only the initial conditions for the mode functions, but also the commutators for $\hat{a}_{\mathbf{k}}$ and $\hat{a}^\dagger_{\mathbf{k}}$. Since, during inflation the co-moving Hubble sphere shrinks,

observationally-relevant co-moving modes lie inside the sphere at early times and cross out of it at some point before the end of inflation. Hence, at very early times, the physical wavelength of these modes is much shorter than the Hubble radius, and they are not affected by the space-time curvature. At these early times, the mode functions should resemble those of free fields in flat space-time, while the $\hat{a}_{\mathbf{k}}$ and $\hat{a}^{\dagger}_{\mathbf{k}}$ operators should be interpreted as creation and annihilation operators. Note that the latter are time-independent, meaning their commutation relations remain the same even after Hubble exit. We can show all of this rigorously.

Consider eq. (1.45). Since we work in the slow-roll approximation, we can set $H = \partial_\tau a(\tau)/a^2 = \text{const}$, implying $a(\tau) = -1/(H\tau)$. We can then find the general solution exactly

$$u_k = c_{k1}\tau\left(1 - \frac{i}{k\tau}\right)e^{-ik\tau} + c_{k2}\tau\left(1 + \frac{i}{k\tau}\right)e^{ik\tau}\,. \tag{1.46}$$

The two constant coefficients, c_{k1} and c_{k2}, can be found by imposing that at early times, when modes are still sub-Hubble, $k/aH = -k\tau \gg 1$, $\delta\hat{\phi}$ behaves as a free, massless[9] scalar with creation and annihilation operators satisfying

$$[\hat{a}_{\mathbf{k}}, \hat{a}_{-\mathbf{q}}] = 0\,, \qquad \left[\hat{a}_{\mathbf{k}}, \hat{a}^{\dagger}_{-\mathbf{q}}\right] = \delta(\mathbf{k}+\mathbf{q})\,. \tag{1.47}$$

Using eq. (1.43), we find $c_{k1} = -(2\pi)^{-3/2}H/\sqrt{2k}$ and $c_{k2} = 0$. This means that mode functions of co-moving modes that are still sub-Hubble are of the form $e^{-ik\tau}/a$, i.e., plane waves with a decaying amplitude, scaling inversely with $a(\tau)$. The scale factor is simply a consequence of the non-canonical kinetic term in the action in eq. (1.40). One can easily check that the rescaled field $a\delta\phi$ has a canonically-normalized action and the equation of motion for its mode functions is of the form given in eq. (1.45), with $b_{\rm sr} = 1$ and $\omega^2_{\rm sr} = k^2 - \partial^2_\tau a/a$. The plane wave factor can also be checked to enforce the vacuum state that is annihilated by $\hat{a}_{\mathbf{k}}$, $|0\rangle$, as the ground state of the second order Hamiltonian. This state is known as the Bunch-Davies vacuum. Conventionally, it is assumed that observationally-relevant modes started in the Bunch-Davies vacuum while lying deep inside the Hubble sphere during inflation. As the universe expands these modes become super-Hubble and according to eq. (1.46), for $k/aH = -k\tau \to 0$, $u_k \approx i(2\pi k)^{-3/2}H/\sqrt{2}$, i.e., the inflaton perturbations freeze. The canonically-normalized field, $a\delta\hat{\phi}$, then simply grows linearly with scale factor, whereas its conjugate momentum is equal to $a\mathcal{H}\delta\hat{\phi}$, and therefore the two effectively commute. Hence, the superhorizon inflaton perturbations behave classically, and can be treated as a classical stochastic field. The quantum expectation value with respect to the Bunch-Davies vacuum translates into the classical ensemble average over field realizations drawn from a Gaussian probability distribution. Since we work in the spatially-flat gauge, the curvature perturbation, $\hat{\mathcal{R}} = H\delta\hat{\phi}/\dot{\bar{\phi}}$, on super-Hubble scales is Gaussian, too. Its power-spectrum, $\Delta^2_{\mathcal{R}}$, is defined as follows

$$\begin{aligned}\langle 0|\mathcal{R}(\tau,\mathbf{x})\mathcal{R}(\tau,\mathbf{x})|0\rangle &= \int 4\pi k^2 dk \frac{H^2}{\dot{\bar{\phi}}^2}|u_k(\tau)|^2\,,\\ &\equiv \int d\ln k \Delta^2_{\mathcal{R}}(k,\tau)\,.\end{aligned} \tag{1.48}$$

Note that the expressions on the right do not depend on the arbitrary space coordinate $\mathbf{x}$. It can be understood in terms of the isotropy and homogeneity of the universe. On super-Hubble scales during inflation the

[9] During slow-roll $\partial^2_{\bar{\phi}} V \ll H^2$.

power-spectrum is scale-invariant, i.e., independent of k, $\Delta^2_{\mathcal{R}} \approx H^2/(8\pi^2 m_{\rm pl}^2 \epsilon_H)$ and constant in time if we assume $\eta_H = \dot{\epsilon}_H/H\epsilon_H = 0$. This result was derived in the de Sitter approximation in which H is approximated to be constant. The conservation of the co-moving curvature on super-Hubble scales can be proven to hold more generally, independently of the assumption of de Sitter expansion. We will discuss it further below. However, it is important to note that since H and ϵ_H vary slowly with time during inflation, the conserved value for $\Delta^2_{\mathcal{R}}$ is slightly different for different k. Essentially, the value of the conserved power-spectrum is determined by the value of H and ϵ_H at horizon exit, $k = aH$. This introduces a weak scale-dependence. The power-spectrum of the co-moving curvature perturbation generated during slow-roll inflation is

$$\Delta^2_{\mathcal{R}}(k) \approx \frac{H^2}{8\pi^2 m_{\rm pl}^2 \epsilon_H}\Big|_{k=aH} . \tag{1.49}$$

This result is obtained in the spatially-flat gauge, ignoring interactions of the inflaton perturbations with those in the metric due to slow-roll suppression. The approximation breaks down towards the end of inflation, when the slow-roll coefficients become of order unity. However, this does not affect eq. (1.49) for observationally-relevant modes, since the expression is evaluated at the time of Hubble horizon exit, when the slow-roll approximation still holds.

One can derive the above results by working in gauge-invariant variables only. Under the diffeomorphism given in eq. (1.29), the inflaton perturbation transforms as $\Delta\delta\phi = -\partial_\tau\bar{\phi}\xi^0$. We then define the gauge-invariant inflaton perturbation

$$\delta\tilde{\phi} = \delta\phi - \left(\partial_\tau\bar{\phi}\right)\left(\mathcal{B} - \partial_\tau\mathcal{E}\right) . \tag{1.50}$$

The gauge-invariant co-moving curvature perturbation can be then expressed only in terms of gauge-invariant quantities, $\mathcal{R} = \Psi + H\delta\tilde{\phi}/\dot{\bar{\phi}}$; see eq. (1.35). The linearised equation of motion for the gauge-invariant field perturbation is

$$\partial_\tau^2\delta\tilde{\phi}_{\mathbf{k}} + 2\mathcal{H}\partial_\tau\delta\tilde{\phi}_{\mathbf{k}} + k^2\delta\tilde{\phi}_{\mathbf{k}} + a^2\frac{\partial^2 V}{\partial\bar{\phi}^2}\delta\tilde{\phi}_{\mathbf{k}} - \partial_\tau\bar{\phi}\left(3\partial_\tau\Psi_{\mathbf{k}} + \partial_\tau\Phi_{\mathbf{k}}\right) + 2a^2\frac{\partial V}{\partial\bar{\phi}}\Phi_{\mathbf{k}} = 0 , \tag{1.51}$$

and the linearised Einstein equations yield

$$\begin{aligned}
&\Phi_{\mathbf{k}} = \Psi_{\mathbf{k}} , \\
&\left(\partial_\tau\mathcal{H} - \mathcal{H}^2 + k^2\right)\Psi_{\mathbf{k}} = \frac{1}{2m_{\rm pl}^2}\left[-\partial_\tau\bar{\phi}\left(\partial_\tau\delta\tilde{\phi}_{\mathbf{k}} + \mathcal{H}\delta\tilde{\phi}_{\mathbf{k}}\right) + \delta\tilde{\phi}_{\mathbf{k}}\partial_\tau^2\bar{\phi}\right] , \\
&\partial_\tau\Psi_{\mathbf{k}} + \mathcal{H}\Psi_{\mathbf{k}} = \frac{1}{2m_{\rm pl}^2}\delta\tilde{\phi}_{\mathbf{k}}\partial_\tau\bar{\phi} .
\end{aligned} \tag{1.52}$$

These equations can be most easily derived in the Newtonian gauge, $\mathcal{B} = \mathcal{E} = 0$, in which the only non-zero scalar metric perturbations φ and ψ are equal to Φ and Ψ, respectively, whereas $\delta\phi = \delta\tilde{\phi}$ and therefore, the gauge-invariant quantities should obey the same equations of motion as the perturbations in the Newtonian gauge. In the equation of motion for the gauge-invariant inflaton perturbation, eq. (1.51), the couplings to the Bardeen variables are slow-roll suppressed. Similarly, the source terms involving the inflaton perturbation in the Einstein equations, eq. (1.52), are also slow-roll suppressed (they also vanish in the limit $k/aH \gg 1$). Thus, the evolution of the gauge-invariant $\delta\tilde{\phi}$ is identical to the one of $\delta\phi$ in the spatially-flat gauge. Furthermore, since the source terms for Ψ vanish during slow-roll inflation and the

contribution of $\delta\tilde{\phi}$ to $\mathcal{R}$ dominates due to division by $\sqrt{\epsilon_H}$, we find the same value for $\Delta^2_{\mathcal{R}}(k)$ as in eq. (1.49), but this time using gauge-invariant variables. We should also point out that Ψ (as well as Φ) plays the role of an auxiliary field. One can see this most easily by substituting for the scalar metric perturbations in eq. (1.51), using eq. (1.52)

$$\partial_\tau^2\delta\tilde{\phi}_{\mathbf{k}} + 2\mathcal{H}\partial_\tau\delta\tilde{\phi}_{\mathbf{k}} + k^2\delta\tilde{\phi}_{\mathbf{k}} + a^2\frac{\partial^2 V}{\partial\bar{\phi}^2}\delta\tilde{\phi}_{\mathbf{k}} + \frac{2}{m_{\rm Pl}^2}\left[\left(\mathcal{H}\partial_\tau\bar{\phi} + \frac{a^2}{2}\frac{\partial V}{\partial\bar{\phi}}\right)\frac{\delta\tilde{\phi}_{\mathbf{k}}\partial_\tau^2\bar{\phi} - \partial_\tau\bar{\phi}\left(\partial_\tau\delta\tilde{\phi}_{\mathbf{k}} + \mathcal{H}\delta\tilde{\phi}_{\mathbf{k}}\right)}{\partial_\tau\mathcal{H} - \mathcal{H}^2 + k^2} - \left(\partial_\tau\bar{\phi}\right)^2\delta\tilde{\phi}_{\mathbf{k}}\right] = 0\,. \tag{1.53}$$

This is a second-order ordinary differential equation for $\delta\tilde{\phi}$. Its quantized solution is of the form given in eq. (1.44). This means that the scalar metric perturbations do not have their own creation and annihilation operators. They can be expressed in terms of $\delta\tilde{\phi}$ according to eq. (1.52) and do not represent gravitational radiation. It is also obvious that during slow-roll, only the first three terms in eq. (1.53) are important, as expected, so the same considerations as before apply to the initial conditions for the mode functions and ultimately the expression in eq. (1.49) can be shown to hold.

So far we have shown that $\mathcal{R}$ is conserved on super-Hubble scales during single-field slow-roll inflation. Using eqs. (1.51) and (1.52), we can obtain the equation of motion for the co-moving curvature perturbation

$$a^{-4}\epsilon_H^{-1}\partial_\tau\left(a^2\epsilon_H\partial_\tau\mathcal{R}_{\mathbf{k}}\right) + \frac{k^2}{a^2}\mathcal{R}_{\mathbf{k}} = 0\,. \tag{1.54}$$

This equation, often rearranged in a different form, is referred to as the Mukhanov-Sasaki equation. In the limit of $k/aH \ll 1$ it has a constant solution and a decaying solution going like $\int d\tau/(a^2\epsilon_H)$. The constant solution is the relevant one for observations. It remains constant even after the end of slow-roll of inflation.

In fact, a theorem due to Weinberg [55] states that no matter what the constituents of the universe are, for scalar and tensor perturbations about an FRW background, in the limit $k/aH \ll 1$ there always exist two *adiabatic solutions*, one constant and one decaying. Adiabatic solutions have the same ratio $\delta s/\dot{\bar{s}}$ for any 4-scalar, s.[10] In single-field inflation, there is only one degree of freedom, $\delta\tilde{\phi}$ (the scalar metric perturbations are auxiliary fields), which implies that there are two solutions to its second-order differential equation. Since there are only two solutions, they must approach the adiabatic limit for $k/aH \ll 1$ according to Weinberg. One can check this by considering the gauge-invariant quantity known as the non-adiabatic pressure, $\delta p_{\rm nad} = \delta p - \delta\rho\dot{\bar{p}}/\dot{\bar{\rho}}$. In single-field models, it can be shown to vanish on super-Hubble scales. However, in multi-field models, the non-adiabatic pressure does not vanish necessarily. When it does not, the equation of motion for $\mathcal{R}$ has an additional source term, due to the non-adiabatic (entropy) perturbations. There are more than two solutions for $\mathcal{R}$, implying that $\mathcal{R}$ is not generally conserved in these cases.

The tensor metric perturbations given in eq. (1.26), $\tilde{h}_{ij}$, are gauge invariant and evolve independently of the matter instabilities. The $\tilde{h}_{ij}$ represent gravitational waves. There are no constraint equations on them and they represent the gravitational degrees of freedom. Since the 3-tensor $\tilde{h}_{ij}$ is traceless and transverse, it has two degrees of freedom only. They are frequently denoted as $h^+ = \tilde{h}_{11}/\sqrt{2} = -\tilde{h}_{22}/\sqrt{2}$ and $h^\times = \tilde{h}_{21}/\sqrt{2} = \tilde{h}_{12}/\sqrt{2}$ and referred to as the $+$ and $\times$ polarizations, respectively. In this notation $h_{3i} = h_{i3} = 0$

[10] This can occur if the universe is in thermal equilibrium even when perturbed, so that $\delta p(T) = \bar{p}'(T)\delta T$ and $\delta\rho(T) = \bar{\rho}'(T)\delta T$ from which follows $\delta\rho/\dot{\bar{p}} = \delta p/\dot{\bar{p}} = \delta T/\dot{\bar{T}}$, hence the name.

(the transverse plane waves are propagating along the z-direction). Perturbing the Einstein-Hilbert term in the action in eq. (1.13), one can show that the second order action governing each polarization state is of the form given in eq. (1.40) with $b = m_{\rm Pl}^2 a^2$ and $\omega^2 = k^2$. Note that in deriving the gravitational waves action we do not make the slow-roll assumption. We can then follow the standard quantization procedure, eq. (1.41–1.45), separately for each polarization state. The equation of motion governing the mode functions reduces to

$$\partial_\tau^2 u_k^{(+,\times)} + 2\mathcal{H}\partial_\tau u_k^{(+,\times)} + k^2 u_k^{(+,\times)} = 0\,, \tag{1.55}$$

manifesting the free nature of the tensor perturbations. The calculation of the mode function evolution during inflation is then identical to the one in the spatially-flat gauge for the scalar perturbations after ignoring slow-roll suppressed terms. At early times, for modes lying deep inside the Hubble sphere, one can show that $u_k^{(+,\times)} = (2\pi)^{-3/2} e^{-ik\tau}/(a\sqrt{2k} m_{\rm Pl})$, corresponding to the ground state of the Hamiltonian calculated in the Bunch-Davies vacuum $|0\rangle$, annihilated by $\hat{a}_{\mathbf{k}}^{(+,\times)}$. Later on, as $k/aH = -k\tau \ll 1$, the mode function freezes to a constant $u_k^{(+,\times)} \approx i(2\pi)^{-3/2} H/(\sqrt{2} m_{\rm Pl})$. Like in the scalar perturbations case, one can again show that on superhorizon scales the canonically-normalized tensor perturbation operators $\hat{h}_c^{(+,\times)} = a m_{\rm Pl} \hat{h}^{(+,\times)}$ become proportional to their conjugate momenta. Hence, the gravitational waves become classical and Gaussian. Their total power is then given by

$$\begin{aligned}\langle 0|4h^+(\tau,\mathbf{x})h^+(\tau,\mathbf{x}) + 4h^\times(\tau,\mathbf{x})h^\times(\tau,\mathbf{x})|0\rangle &= \int 4\pi k^2 dk \left(4|u_k^+(\tau)|^2 + 4|u_k^\times(\tau)|^2\right)\,, \\ &\equiv \int d\ln k \Delta_{\rm t}^2(k,\tau)\,,\end{aligned} \tag{1.56}$$

where in the last line we define the tensor power-spectrum. Similarly to the power-spectrum of the co-moving curvature perturbation, see eq. (1.49), the tensor power-spectrum generated during slow-roll inflation is

$$\Delta_{\rm t}^2(k) \approx \frac{2H^2}{\pi^2 m_{\rm Pl}^2}\Big|_{k=aH}\,. \tag{1.57}$$

The tensor perturbations are generally conserved in the limit $k/(aH) \ll 1$, just like the co-moving curvature perturbation. One can see that most easily from eq. (1.55), which shows that the mode functions become overdamped in the super-Hubble limit. Hence, again there is a constant and a decaying solution.

The weak scale-dependences in $\Delta_{\mathcal{R}}^2(k)$ and $\Delta_t^2(k)$ are characterised by their logarithmic derivatives

$$n_{\rm s} - 1 \equiv \frac{d\ln\Delta_{\mathcal{R}}^2}{d\ln k}\,, \qquad n_{\rm t} \equiv \frac{d\ln\Delta_{\rm t}^2}{d\ln k}\,. \tag{1.58}$$

In other words, one can approximate the scale-dependences by simple power-laws

$$\Delta_{\mathcal{R}}^2 \approx A_{\rm s}\left(\frac{k}{k_\star}\right)^{n_{\rm s}-1}\,, \qquad \Delta_{\rm t}^2 \approx A_{\rm t}\left(\frac{k}{k_\star}\right)^{n_{\rm t}}\,. \tag{1.59}$$

The quantities $n_{\rm s}$ and $n_{\rm t}$ are known as the scalar and tensor spectral indices, respectively, $k_\star$ is the pivot scale, and $A_{\rm s}$ and $A_{\rm t}$ are the amplitudes of the scalar and tensor power-spectra, respectively. Normally, the tensor amplitude is normalized by the scalar amplitude

$$r = \frac{A_{\rm t}}{A_{\rm s}}\,. \tag{1.60}$$

The quantity is known as the tensor-to-scalar ratio.

Slow-roll inflation predicts small values for the logarithmic derivatives in eq. (1.58), $n_{\rm s}-1 = -2\epsilon_H - \eta_H$ and $n_{\rm t} = -2\epsilon_H$. All slow-roll parameters are evaluated at Hubble exit of the pivot scale, $k_\star = aH$, during inflation. In deriving these expressions, we have made use of the identity $d/d\ln k|_{k=aH} \approx H^{-1}d/dt|_{k=aH}$, which follows from the assumption that during slow-roll inflation $d\ln a/d\ln k|_{k=aH} \approx 1$ as $H \approx$ const. The scalar and tensor amplitudes can be also written in terms of the Hubble slow-roll parameters during inflation, $A_{\rm s} = H^2/(8\pi^2 m_{\rm Pl}^2\epsilon_H)$, $A_{\rm t} = 2H^2/(\pi^2 m_{\rm Pl}^2)$ and $r = 16\epsilon_H$ with again all quantities evaluated at $k_\star = aH$. Note that $r = -8n_{\rm t}$ and is known as the consistency relation for slow-roll inflation. To connect with the shape of the inflaton potential in models of single-field slow-roll inflation, we recall that $\eta_H/2 + \eta_V = 2\epsilon_H \approx 2\epsilon_V$ and $H^2 \approx V/(3m_{\rm Pl}^2)$, implying

$$n_{\rm s} - 1 \approx -6\epsilon_V + 2\eta_V\,, \qquad r = -8n_{\rm t} \approx 16\epsilon_V\,, \qquad A_{\rm s} \approx \frac{V}{24\pi^2 m_{\rm Pl}^4\epsilon_V}\,, \tag{1.61}$$

with all potential and potential derivative terms evaluated at $\bar\phi = \bar\phi_\star$, corresponding to the inflaton value at the Hubble exit of the pivot scale. CMB observations [2] yield $A_{\rm s} = 2.2\times10^{-9}$, $n_{\rm s} = 0.968 \pm 0.006$ and the constraint $r < 0.11$ at $95\,\%$ confidence level. They are consistent with adiabatic primordial fluctuations, as predicted by single-field inflation.

In the above analysis of cosmological perturbations, we made several approximations. We ignored the contribution to $\delta T^\mu{}_\nu$ due to anisotropic stresses, $\Pi^\mu{}_\nu$. They are a complimentary source of perturbations to the isotropic pressure term, i.e., $\Pi^0{}_0 = \Pi^0{}_i = \Pi^i{}_i = 0$, while $\Pi^i{}_j \neq 0$ for $i \neq j$. The anisotropic stress in single-field inflation is zero at linear order. Multi-field models involving scalar fields only, also have $\Pi^i{}_j = 0$ at the linear level. More complicated models with vector fields in some homogeneous and isotropic background configuration for instance, can feature a non-negligible $\Pi^i{}_j$. Even in the presence of anisotropic stresses, according to the Weinberg theorem, there always exist a constant and a decaying solution for the scalar and tensor perturbations on super-Hubble scales. We have also not talked about the vector metric perturbations. The reason is that according to Einstein equations, the vector metric perturbations are always redshifted away in the absence of sources.

The aim of this section was to show that inflation can make the universe homogeneous and isotropic at the level required by observations. However, this comes at a price. At the end of inflation, the universe is in a cold and non-thermal state. On the other hand the successful theory of big-bang nucleosynthesis calls for a universe very close to thermal equilibrium at temperatures at least around $1\,\mathrm{MeV}$. That is why reheating is an integral part of inflationary cosmology. Any successful theory of inflation must give an account of the production of Standard Model matter out of the energy stored overwhelmingly in the oscillating inflaton condensate at the end of the period of accelerated expansion. Reheating should also include baryogenesis and perhaps the production of dark matter. In the remaining chapters in this part of the thesis we review our current understanding of reheating. The early transfer of energy, from the inflaton condensate to the fields it is coupled to, is the subject of the next chapter. The main focus is on preheating – the exponential particle production due to non-perturbative resonances and tachyonic instabilities. Chapter 3 discusses the non-linear dynamics ensuing after the fragmentation of the inflaton condensate, and the approach to thermalization. Chapters 4 and 5 connect phenomenological models of reheating with High-Energy Physics models and cosmological observations. We should point out that the details of the reheating process depend on the underlying particle physics theory beyond the Standard Model. Since there are so many possible

extensions of the Standard Model, it makes more sense to begin by studying simple toy models inspired by High-Energy Physics to clarify the relative importance of different reheating mechanisms. Many toy models of reheating allow for a thermal universe at the epoch of big-bang nucleosynthesis. To some this is disappointing, since it shows that the current precision of observations does not let us distinguish between different models of inflation and reheating, but to others it is encouraging, since it advocates the inflationary scenario.

Chapter 2

Preheating: the decay of the inflaton condensate

'The career of a young theoretical physicist consists of treating the harmonic oscillator in ever-increasing levels of abstraction.'

Sidney Coleman

Around the end of inflation, $\epsilon_H = 1$, the homogeneous inflaton begins to oscillate about the minimum of its potential. The inflaton condensate must decay into other forms of matter and radiation, eventually giving the particle content of the Standard Model and perhaps dark matter. These more familiar forms of matter and radiation must eventually reach thermal equilibrium at temperatures greater than $1\,\mathrm{MeV}$ in order to recover the successful big-bang nucleosynthesis scenario. The transition of the universe from the supercooled state at the end of inflation to the hot, thermal, radiation dominated state required for big-bang nucleosynthesis is called reheating. The subject of this chapter is the early transfer of energy from the inflaton condensate to the fields it is coupled to. We begin with the perturbative theory of reheating – historically, the process was first treated this way. We then show the importance of non-perturbative effects arising from the coherent nature of the inflaton condensate. They include parametric resonances and tachyonic instabilities, all of which lead to exponential growth in the occupation numbers of the fields the inflaton decays to (i.e., the decay products). These kinds of rapid decay are called preheating, with the decay products in a highly non-thermal state. Finally, we discuss the implications from coupling these decay products to additional matter fields for the energy transfer from the inflaton condensate.

2.1 Perturbative treatment of reheating

Originally, reheating was studied as a perturbative process [64] in which individual inflaton particles were assumed to decay independently of each other. Interaction rates and decay rates were calculated in the usual manner, using perturbative coupling expansions. For illustrative purposes we consider inflaton interactions of the form $S_{\mathrm{matter}} \supset \int d^4x\sqrt{-g}(-\sigma\phi\chi^2 - h\phi\bar{\psi}\psi)$, where χ and ψ are some scalar and fermion decay products. These sort of couplings arise in gauge theories with spontaneously broken symmetries. We avoid tachyonic instabilities in χ by assuming that its mass, m_χ, is greater than $\sqrt{\sigma|\phi|}$. The inflaton potential is assumed to be $V = m^2\phi^2/2$. To tree-level order, for decay products much lighter than the inflaton quanta,

the decay rates are [65]

$$\Gamma_{\phi\to\chi\chi} = \frac{\sigma^2}{8\pi m}\,, \qquad \Gamma_{\phi\to\bar{\psi}\psi} = \frac{h^2 m}{8\pi}\,. \tag{2.1}$$

The total width, $\Gamma_{\rm tot} \equiv \Gamma_{\phi\to\chi\chi} + \Gamma_{\phi\to\bar{\psi}\psi}$, is supposed to determine the decay rate of the number of inflaton quanta in a fixed co-moving volume

$$\frac{d\left(a^3 n_{\bar{\phi}}\right)}{dt} = -\Gamma_{\rm tot} a^3 n_{\bar{\phi}}\,, \tag{2.2}$$

where $n_{\bar{\phi}} = \rho_{\bar{\phi}}/m$ is the number density of inflaton particles in the condensate. Hence, $a^3(t) n_{\bar{\phi}}(t) \sim \exp(-\Gamma_{\rm tot} t)$. Since after inflation $m \gg H \sim t^{-1}$, the homogeneous inflaton undergoes many oscillations during one Hubble time. If $\Gamma_{\rm tot}^{-1} \gg m^{-1}$, then we can approximate $\bar{\phi} \approx \bar{\Phi}(t)\cos(mt)$, where $\bar{\Phi}(t)$ varies much more slowly than the phase. Using eq. (1.14), we then find that $n_{\bar{\phi}} \approx m\bar{\Phi}^2/2$. Thus, $\bar{\Phi}(t) \sim a^{-3/2}(t)\exp(-\Gamma_{\rm tot} t/2)$, which agrees with eq. (1.21) to leading order up to an extra exponential factor. We can check that this additional exponential decrease due to particle production can be roughly taken into account by including a friction term into the background equation of motion

$$\ddot{\bar{\phi}} + (3H + \Gamma_{\rm tot})\dot{\bar{\phi}} + m^2\bar{\phi} = 0\,. \tag{2.3}$$

Having $m \gg H \sim \Gamma_{\rm tot}$, one can write the WKB ansatz $\bar{\phi} \approx \bar{\Phi}(t)\cos(mt)$ assuming the phase varies much faster than the amplitude. Neglecting $\ddot{\bar{\Phi}}$ and $H\dot{\bar{\Phi}}$ terms, we then find that $2\dot{\bar{\Phi}} + (3H + \Gamma_{\rm tot})\bar{\Phi} = 0$ as required. Even if $m \gg H \gg \Gamma_{\rm tot}$ one can still show that the second order WKB solution is $a^{-3/2}(t)\exp(-\Gamma_{\rm tot} t/2)\cos(mt)$.

For small coupling constants, as required for radiative corrections to not spoil the flatness of the potential during inflation, typically $\Gamma_{\rm tot} \ll H$. At the beginning of the oscillatory phase, the inflaton condensate mainly loses energy due to the expansion of space. Once the Hubble rate has decreased to $H \lesssim \Gamma_{\rm tot}$, the particle production becomes effective. Thus, the energy density transferred into decay products is $\sim 3m_{\rm Pl}^2\Gamma_{\rm tot}^2$. Note that $H \lesssim \Gamma_{\rm tot}$ is one of the conditions for establishing thermal equilibrium between the inflaton particles and (at least one of) the decay products. Setting the decay rates into individual species to be comparable to each other, i.e., $\Gamma_{\phi\to\chi\chi} \sim \Gamma_{\phi\to\bar{\psi}\psi}$, all decay products can be in thermal equilibrium provided they have sufficiently high concentrations. Thereby, we can find an upper bound on the reheating temperature. It is safe to assume that most of the energy has been transferred into the light (with respect to m) decay products. Assuming they are relativistic as well, the energy density of the universe is $\pi^2 g_* T^4/30$, where g_* is the number of relativistic degrees of freedom, of order 10^2 for the Standard Model. The maximal reheating temperature is

$$T_{\rm reh} \sim \left(\frac{90}{g_*\pi^2}\right)^{1/4}\sqrt{m_{\rm Pl}\Gamma_{\rm tot}}\,. \tag{2.4}$$

Recalling eq. (1.49) and the CMB bound on the tensor-to-scalar ratio we find that $T_{\rm reh} < 10^{15}\,{\rm GeV}$, implying that the GUT symmetries cannot be restored after inflation and the solution to the monopole problem is not in danger. However, this does not rule out the production of other dangerous massive relics such as gravitinos. They could ruin the predictions of the successful big-bang nucleosynthesis by leading to an unwanted matter dominated state of expansion at the beginning of the epoch or by releasing excessive amounts of entropy close to it. One needs to make sure that in this sort of models, the reheating temperature is low enough to avoid the thermal production of such relics.

We should point out that since each Γ is proportional to the square of the small coupling constants, the perturbative decay is actually quite slow and can take many e-folds of expansion after inflation before the Hubble rate becomes small enough for perturbative particle production to become efficient.

2.1.1 Limitations

There are many issues with the above perturbative analysis. The heuristic equation of motion in eq. (2.3), while capturing the qualitative behaviour, does not provide a consistent description of even the perturbative decay of the condensate. It violates the fluctuation dissipation theorem which states that dissipation inevitably leads to fluctuations within the system at hand. The effects of these fluctuations on the effective mass of the inflaton condensate are not included in eq. (2.3) [14].

Another problem with the above perturbative approximation is that it does not account for the Bose condensation effects. Even if the couplings of the inflaton to bosons, e.g., to χ, are small enough to allow for a perturbative coupling expansion, if the phase space of bosonic decay products, e.g., of χ particles, is densely populated Bose condensation effects can greatly enhance the decay rate. We discuss this situation in Section 2.1.2.

Most importantly, for larger couplings (but still small enough for radiative corrections to be negligible) the perturbative methods fail. Particle production has to be treated as a non-perturbative effect. The inflaton condensate is a coherent oscillating homogeneous field, implying that particle production has to be treated as a collective process in which many inflaton particles decay simultaneously, not independently of each other. Due to the large occupation number, we can treat the condensate classically. However, the decay products have to be described quantum mechanically, since they have vanishing occupation numbers at the end of inflation (due to the enormous dilution of space during the accelerated expansion). It is justified to use their vacuum state as an initial condition for the ensuing quantum mechanical particle production in the classical inflaton background. The periodic time-dependence of the effective masses of the decay products in the classical oscillating background can have a powerful effect on their production rates in the form of a parametric resonance, which will be the subject of Section 2.2.

Despite all of these problems, the perturbative analysis in this section can be applied to the late stages of reheating, e.g., to the decay of remnant inflaton particles after most of the energy has been transferred into relativistic species. Note that such decay channels are crucial to include, so that the energy transfer can be completed. Otherwise, we can face another relic problem.

2.1.2 Bose condensation of decay products in the perturbative limit

We finish this section with a short discussion of the Bose condensation effects in the perturbative limit, $\sigma \ll m^2/\bar{\Phi}$. By a perturbative limit, we mean that the tree-level order Feynman diagram gives the dominant contribution to the decay of the condensate into χ particles. Higher-order Feynman diagrams are subdominant. They can describe the simultaneous decay of more than one inflaton particles from the condensate and are negligible in the perturbative limit to leading order. To avoid significant radiative corrections to the Lagrangian we also put $\sigma \ll m$. Taking into account that the condensate is comprised of particles at rest with large occupation number $n_{\mathbf{0}}^{\phi}$, the decay rate to a pair of χ particles at tree-level order is proportional to

$$|\langle n_{\mathbf{0}}^{\phi}-1, n_{\mathbf{k}}^{\chi}+1, n_{-\mathbf{k}}^{\chi}+1| \left(\hat{a}_{\mathbf{k}}^{\chi}\right)^{\dagger} \left(\hat{a}_{-\mathbf{k}}^{\chi}\right)^{\dagger} \hat{a}_{\mathbf{0}}^{\phi} |n_{\mathbf{0}}^{\phi}, n_{\mathbf{k}}^{\chi}, n_{-\mathbf{k}}^{\chi}\rangle|^2 = (n_{\mathbf{k}}^{\chi}+1)(n_{-\mathbf{k}}^{\chi}+1) n_{\mathbf{0}}^{\phi}\,, \tag{2.5}$$

whereas the rate of the inverse process is proportional to

$$|\langle n^{\phi}_{\mathbf{0}}+1, n^{\chi}_{\mathbf{k}}-1, n^{\chi}_{-\mathbf{k}}-1|\left(\hat{a}^{\phi}_{\mathbf{0}}\right)^{\dagger}\hat{a}^{\chi}_{\mathbf{k}}\hat{a}^{\chi}_{-\mathbf{k}}|n^{\phi}_{\mathbf{0}}, n^{\chi}_{\mathbf{k}}, n^{\chi}_{-\mathbf{k}}\rangle|^2 = n^{\chi}_{\mathbf{k}}n^{\chi}_{-\mathbf{k}}(n^{\phi}_{\mathbf{0}}+1)\,. \tag{2.6}$$

Note that the occupation number is the number of occupied states per $(2\pi)^3$ phase space volume. The only exception is the inflaton condensate for which $n^{\phi}_{\mathbf{0}}/V_{\rm com} = n_{\bar{\phi}} = m\bar{\Phi}^2/2$, whereas for the χ particles the number density, n_χ, is related to the occupation number in the standard way $n_\chi = \int d^3k\, n^{\chi}_{\mathbf{k}}/(2\pi)^3$. Note that $n^{\chi}_{\mathbf{k}} = n^{\chi}_{-\mathbf{k}}$ and are independent of the direction of $\mathbf{k}$. From now on we put them to be equal to n^{χ}_{k}. Roughly speaking, due to energy and momentum conservation, a stationary inflaton particle decays into a pair of χ particles, each of which has energy $m/2$ and momentum $[m^2/4 - m_\chi^2 - 2\sigma\bar{\phi}(t)]^{1/2}$. Since $m \gg m_\chi > \sigma\bar{\Phi}$, all particles are produced within a thin spherical momentum shell in phase space, centred near $m/2$ and of width $4\sigma\bar{\Phi}/m$. Hence, $n^{\chi}_{k=m/2} = n_\chi/[4\pi(m/2)^2(4\sigma\bar{\Phi}/m)/(2\pi)^3] = (\pi^2\bar{\Phi}/\sigma)(n_\chi/n_{\bar{\phi}})$. Then the rate of change of χ particles within a given co-moving volume is

$$\begin{aligned}\frac{d\left(a^3 n_\chi\right)}{dt} &= \frac{2a^3}{V_{\rm com}}\Gamma_{\phi\to\chi\chi}\left[(n^{\chi}_{\mathbf{k}}+1)(n^{\chi}_{-\mathbf{k}}+1)n^{\phi}_{\mathbf{0}} - n^{\chi}_{\mathbf{k}}n^{\chi}_{-\mathbf{k}}(n^{\phi}_{\mathbf{0}}+1)\right] \\ &\approx 2a^3\Gamma_{\phi\to\chi\chi}n_{\bar{\phi}}\left[1+2n^{\chi}_{k}\right] \approx 2a^3\Gamma_{\phi\to\chi\chi}n_{\bar{\phi}}\left[1+\frac{2\pi^2\bar{\Phi}}{\sigma}\frac{n_\chi}{n_{\bar{\phi}}}\right]\,.\end{aligned} \tag{2.7}$$

where $n^{\phi}_{\mathbf{0}} \gg \{n^{\chi}_{k}, 1\}$ and $|\mathbf{k}| = m/2$. For $n^{\chi}_{k} > 1$, i.e, $n_\chi > \sigma n_{\bar{\phi}}/(\pi^2\bar{\Phi})$, the second term inside the brackets in the last line in eq. (2.7) becomes important, which is a manifestation of Bose condensation effects becoming relevant. Since $\rho_\chi/n_\chi \sim m = \rho_{\bar{\phi}}/n_{\bar{\phi}}$, Bose effects should be considered for fractions of energy stored in the decay product satisfying $\rho_\chi/\rho_{\bar{\phi}} > \sigma/\bar{\Phi}$. For small coupling constants and large amplitudes, the right-hand side can be much less than unity and the equality can be satisfied shortly after inflation. Bose effects become important and the perturbative treatment presented in the beginning of this section breaks down. For high occupancies, $n^{\chi}_{k} \gg 1$, after ignoring the expansion of space, and using eq. (2.1) we can integrate eq. (2.7) to get

$$n_\chi \sim \exp\left(\frac{\pi\sigma\bar{\Phi}t}{2m}\right)\,. \tag{2.8}$$

Bose effects lead to an exponential increase of the decay efficiency. We have shown it for small enough couplings which allow for a perturbative treatment. When couplings are increased, non-perturbative effects become important, but the exponential increase in the decay efficiency remains. This is shown in the next two sections. A discussion of the effects on the particle production rate due to the expansion of the universe is also included.

2.2 Parametric resonance

As shown at the end of the previous section, Bose condensation effects can exponentially enhance the rate at which energy is transferred from the oscillating inflaton condensate to the bosonic fields it is coupled to. We worked in the perturbative limit in which the coupling is small, e.g., $\sigma\bar{\Phi} \ll m^2$ in the trilinear interaction model $V(\phi,\chi) = m^2\phi^2/2 + m_\chi^2\chi^2/2 + \sigma\phi\chi^2$, with $m \gg m_\chi > \sqrt{\sigma\bar{\Phi}}$. In this limit a perturbative coupling expansion makes sense. If the amplitude of inflaton oscillations and/or the coupling constant become large, e.g., $\sigma\bar{\Phi} > m^2$ in the trilinear case, high-order Feynman diagrams give comparable predictions to the

lowest-order ones and the problem has to be approached non-perturbatively. Note that simultaneous decays of more than one inflaton particles from the condensate are described by high-order diagrams. Such decays are a consequence of the coherent nature of the oscillating condensate and the non-perturbative calculation presented below captures them, unlike the perturbative one in the previous section. It turns out that Bose effects still exponentially enhance the rate of energy transfer. It is more efficient than in the perturbative limit, due to contributions from the simultaneous decays of more than one inflaton particle. The phenomenon can be understood most easily in the language of parametric resonance. Of course, the method can be applied to the perturbative case as well.

At the end of inflation, matter fields can be treated as fluctuations on top of the oscillating homogeneous inflaton background. Typically, they start in the vacuum state, since inflation has diluted the corresponding particle densities to vanishing values. Ignoring the expansion of space for now, the linearised equations of motion take the form

$$\ddot{\hat{\chi}}_{\mathbf{k}} + \omega^2(k,t)\hat{\chi}_{\mathbf{k}}(t) = 0\,, \tag{2.9}$$

where the angular frequency is periodic, i.e., $\omega^2(k,t) = \omega(k,t+T)^2$; T is the period of oscillations of the condensate. In the trilinear model, $\omega^2(k,t) = k^2 + m_\chi^2 + 2\sigma\bar{\Phi}\cos(mt)$ and $T = 2\pi/m$. Unlike the previous section, here we do not assume anything about the relative values of m, m_χ and $\sqrt{\sigma\bar{\Phi}}$. The equation of the form given in eq. (2.9) with ω a periodic function of time is known as the Hill's equation [66, 67]. In the triliniear case ω evolves harmonically and the equation can be reduced to the Mathieu equation form

$$\frac{d^2}{dz^2}\hat{\chi}_{\mathbf{k}} + \left[A_k + 2q\cos(2z)\right]\hat{\chi}_{\mathbf{k}}(z) = 0\,, \tag{2.10}$$

with A_k, q and z dimensionless and determined by the form of ω. In the trilinear model, $A_k = 4(k^2 + m_\chi^2)/m^2$, $q = 4\sigma\bar{\Phi}/m^2$ and $z = mt/2$.[1]

2.2.1 Floquet theory

The action leading to the Hill's equation, eq. (2.9), is that of a harmonic oscillator with a periodic angular frequency

$$S_\chi^{(2)} = \int dt d^3x \left[\frac{|\dot{\chi}_{\mathbf{k}}|^2}{2} - \omega^2(k,t)\frac{|\chi_{\mathbf{k}}|^2}{2}\right]. \tag{2.11}$$

We can follow the quantization procedure outlined after eq. (1.40). Now the mode functions of $\hat{\chi}_{\mathbf{k}}$ obey the Hill's equation

$$\ddot{u}_k + \omega^2(k,t)u_k(t) = 0\,. \tag{2.12}$$

The Floquet theorem [66] states that the most general solution of the Hill's equation is given by

$$u_k(t) = e^{\mu_k t}\mathcal{P}_{k+}(t) + e^{-\mu_k t}\mathcal{P}_{k-}(t)\,, \tag{2.13}$$

where μ_k is called the Floquet exponent and $\mathcal{P}_{k\pm}(t) = \mathcal{P}_{k\pm}(t+T)$. If $\Re(\mu_k) \neq 0$ one of the two terms increases exponentially with time. This is called parametric resonance. Let's prove eq. (2.13) [17, 68] and show how to find numerically μ_k [17, 69], knowing the form of $\omega(k,t)$.

[1] Another popular model that can be described with the Mathieu equation is $V(\phi,\chi) = m^2\phi^2/2 + g^2\chi^2\phi^2/2 + m_\chi^2\chi^2/2$ [14], for which $z = mt$, $A_k = (k^2 + m_\chi^2)/m^2 + 2q$, $2q = g^2\bar{\Phi}^2/(2m^2)$.

If $u_k(t)$ is a solution to eq. (2.12), then so must be $u_k(t+T)$. Hence, if $u_{k1}(t)$ and $u_{k2}(t)$ are two linearly independent solutions, their time-shifted counterparts must be linear combinations of them, i.e., $u_{ki}(t+T) = \sum_{j=1}^{2} B_{ij} u_{kj}(t)$ with B_{ij} a constant 2×2 invertible matrix. We can diagonalize the expression to get $v_{ki}(t+T) = \sum_{j=1}^{2} \lambda_i^B \delta_{ij} v_{kj}(t)$ where λ_i^B are the two eigenvalues of B_{ij} and $v_{ki}(t)$ are independent linear combinations of $u_{ki}(t)$. From this follows that $v_{ki}(t+T) = \lambda_i^B v_{ki}(t)$, i.e., a time sift $t \to t+T$ leads to a rescaling by an eigenvalue. The most general solutions having this property are $v_{ki}(t) = (\lambda_i^B)^{t/T} P_{ki}(t)$, where $P_{ki}(t+T) = P_{ki}(t)$. Since the Wronskian, $W[u_{k1}, u_{k2}] \equiv u_{k1}\dot{u}_{k2} - \dot{u}_{k1}u_{k2}$, of the Hill's equation, eq. (2.12), is constant, $\dot{W}[u_{k1}, u_{k2}] = 0$, so must be $\dot{W}[v_{k1}, v_{k2}] = 0$. On the other hand, $W[v_{k1}, v_{k2}](t+T) = \lambda_1^B \lambda_2^B W[v_{k1}, v_{k2}](t)$, implying $\lambda_1^B = 1/\lambda_2^B \equiv \lambda^B$. This completes the proof of eq. (2.13). The Floquet exponent is simply $\mu_k = \ln(\lambda^B)/T$, whereas each of the periodic functions $\mathcal{P}_{k\pm}(t)$ is some linear combination of $P_{k1,2}(t)$.

To find the Floquet exponent, we just need to calculate the eigenvalues of B_{ij}, which, as we just showed, has a unit determinant. To do that we choose two orthogonal initial conditions $\{u_{k1}(t_0), \dot{u}_{k1}(t_0)\} = \{1, 0\}$ and $\{u_{k2}(t_0), \dot{u}_{k2}(t_0)\} = \{0, 1\}$ at some initial time t_0. This implies that $\{B_{i1}, B_{i2}\} = \{u_{ki}(t_0 + T), \dot{u}_{ki}(t_0 + T)\}$. Hence, after evolving the Hill's equation forward for one period T for the two sets of initial conditions we can find the eigenvalues

$$\lambda_{1,2}^B = \frac{1}{2}\left\{u_{k1}(t_0+T) + \dot{u}_{k2}(t_0+T) \pm \sqrt{[u_{k1}(t_0+T) - \dot{u}_{k2}(t_0+T)]^2 + 4\dot{u}_{k1}(t_0+T)u_{k2}(t_0+T)}\right\}. \tag{2.14}$$

Using the fact that for our choice of initial conditions $W[u_{k1}, u_{k2}](t_0) = 1$ and that $W[u_{k1}, u_{k2}](t_0 + T) = \lambda_1^B \lambda_2^B W[u_{k1}, u_{k2}](t_0)$, one can easily show that this expression is consistent with B_{ij} having a unit determinant.

The initial conditions are relevant for the efficiency of the parametric resonance. Essentially, if both the initial field and field velocities are zero, parametric resonance does not lead to any growth. We can see this most easily by re-writing eq. (2.13) as a linear combination of the linearly independent $v_{k1,2}(t) = \exp(\pm\mu_k t) P_{k1,2}(t)$, i.e., $u_k(t) = c_1 v_{k1}(t) + c_2 v_{k2}(t)$. If both $u_k(t_0)$ and $\dot{u}_k(t_0)$ are zero, then the only possibility for the constant pre-factors is $c_1 = c_2 = 0$. Hence, unlike ordinary resonance where the forcing term leads to a rapid growth even if initially the field displacement and velocity are zero, parametric resonance does not allow for any resonant excitations if no energy is stored in the fluctuations initially. That is why vacuum fluctuations, albeit small, play a crucial role for particle production after inflation as seeds for parametric resonance.

2.2.2 Narrow resonance

As an exercise, we can now calculate the dimensionless Floquet exponent, $\tilde{\mu}_k$, of the Mathieu equation eq. (2.10). The magnitude of the real part of $\tilde{\mu}_k$ is plotted in Fig. 2.1 as a function of the parameters A_k and q. We call plots of this type instability charts. There is a series of regions of stability in which $\Re(\tilde{\mu}_k) = 0$. They are surrounded by 'unstable' regions in which $\Re(\tilde{\mu}_k) > 0$. For $|q| \ll 1$ and $A_k > 0$, the regions of instability become narrow and approach $A_k^{(n)} = n^2$ as $q \to 0$ (n is an integer). In the first narrow band the peak value of the Floquet exponent is $\Re\,(\tilde{\mu}_k)_{\max}^{(1)} \approx |q|/2$, while $A_k^{(1)} \approx 1 \pm |q|$ [66]. For the triliniear model, this corresponds to resonant production of χ particles with momentum in the range $m/2 \pm \sigma\bar{\Phi}/m$ (assuming $m_\chi = 0$) and mode functions growing as $\exp(\sigma\bar{\Phi}t/m)$ (see also Fig. 2.2). Since the χ particles are described with the action of a time-dependent simple harmonic oscillator, eq. (2.11), the energy stored

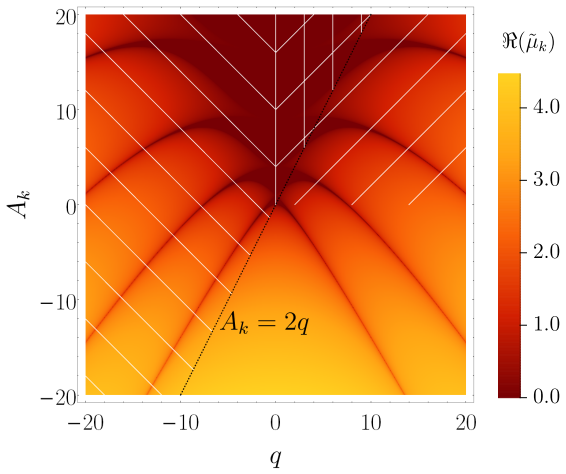

Figure 2.1: The instability chart of the Mathieu equation, eq. (2.10). The dark areas correspond to vanishing real part of the Floquet exponent and are regions of stability. Narrow parametric resonance occurs for $A_k = n^2$ and $|q| \to 0$ (n is an integer) and broad resonance takes place when $A_k < 2|q|$ as well as $A_k - 2|q| \ll |q|^{1/2}$. Resonant decay of the inflaton condensate into χ particles in the trilinear model, $V(\phi,\chi) = m^2\phi^2/2 + m_\chi^2\chi^2/2 + \sigma\phi\chi^2$, can be understood in terms of the Mathieu equation – the equation of motion for χ_k (after ignoring the expansion of space) can be mapped onto the Mathieu equation with $A_k \geq 0$ and $q \geq 0$, i.e., the square region with northeast white lines (see also Fig. 2.2). Resonant production of χ particles in another common toy model, $V(\phi,\chi) = m^2\phi^2/2 + m_\chi^2\chi^2/2 + g^2\phi^2\chi^2/2$, can be also mapped onto this chart – for $g^2 > 0$, the wedge-shaped region with vertical white lines, whereas for $g^2 < 0$ the region with northwest white lines, cover the relevant ranges of A_k and q (see also Figs. 2.3 and 2.4).

in a given $\mathbf{k}$ mode is simply

$$E^\chi_{\mathbf{k}} = \frac{1}{(2\pi)^3}\left(n^\chi_{\mathbf{k}} + \frac{1}{2}\right)\omega(k,t) = \frac{|\dot{u}_k|^2}{2} + \omega^2(k,t)\frac{|u_k|^2}{2}\,, \tag{2.15}$$

where $n^\chi_{\mathbf{k}}$ can be interpreted as the mean occupation number (mean, because it is evaluated by taking the expectation value of the Hamiltonian with respect to the Bunch-Davies vacuum). Hence, for $q = 4\sigma\bar{\Phi}/m^2 \ll 1$, modes lying near the peak in the first narrow instability band have occupation numbers growing as $n^\chi_{|\mathbf{k}|\approx m/2} \propto \exp(2\sigma\bar{\Phi}t/m)$. This is in good agreement with the perturbative treatment of Bose condensation from the previous section, see, e.g., eq. (2.8). Thus, in the perturbative limit, $\sigma\bar{\Phi}/m^2 \ll 1$, the Bose effects, due to the population of χ modes, in the leading order $\phi \to \chi\chi$ Feynman diagram can be described as a parametric resonance due to the first, $n = 1$, narrow, $q \ll 1$, instability band. Higher order, $n > 1$, narrow bands lead to production of particles with momentum in the range $k^{(n)} = nm/2 \geq m$. They correspond to higher order Feynman diagrams describing the simultaneous decay of n ϕ particles from the condensate into a pair of χs, taking into account the Bose effects due to the dense populations of the χ modes, $n^\chi_{|\mathbf{k}|=nm/2} > 1$. Since this happens in the perturbative limit, one should be able to describe it using the methods from the previous section, leading to eq. (2.8). In summary, resonance from the narrow bands, $|q| \ll 1$, describes perturbative decays of particles from the inflaton condensate in the trilinear model, taking into account the occupation of χ modes. This type of parametric resonance is known as narrow resonance. It corresponds to $|q| \ll 1$ for the Mathieu equation, but for the general Hill's equation it corresponds to the parametric resonance in some region of parameter space which features a narrow instability band.

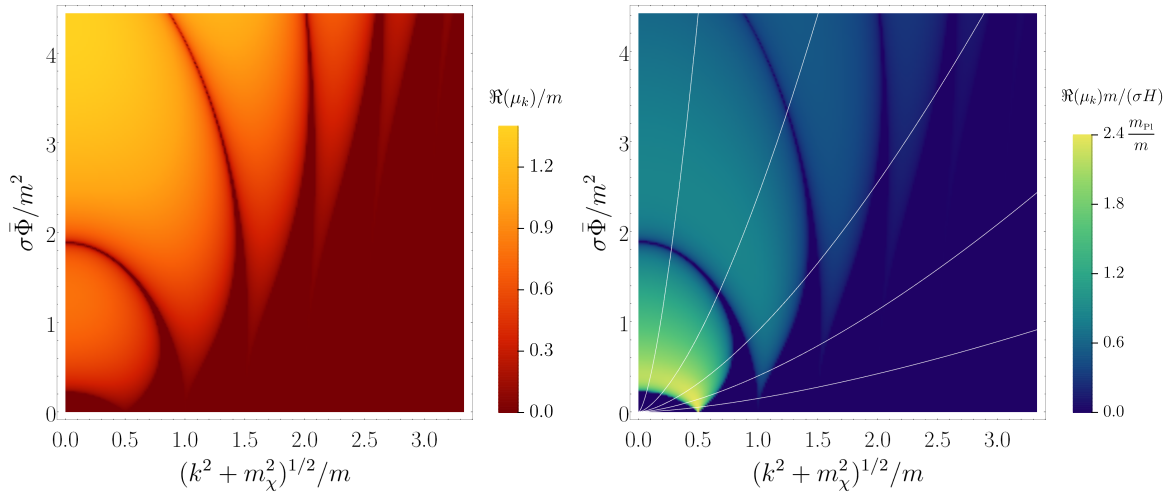

Figure 2.2: The instability chart featuring the real part of the Floquet exponent normalized by the inflaton mass (left) and the Hubble rate (right), characterizing the χ particle production rate in the trilinear model, $V(\phi,\chi) = m^2\phi^2/2 + m_\chi^2\chi^2/2 + \sigma\phi\chi^2$. The equation of motion for χ_k can be reduced to the Mathieu equation, eq. (2.10), with $A_k = 4(k^2+m_\chi^2)^{1/2}/m$, $q = 4\sigma\bar{\Phi}/m^2$, where $\bar{\Phi}$ is the amplitude of inflaton oscillations (see also Fig. 2.1). In FRW space-time $\bar{\Phi} \propto a^{-3/2}$ and $k \propto a^{-1}$, implying that a given co-moving mode flows towards the bottom left corner of the chart as the universe expands as indicated with the white lines in the second chart (drawn for $m_\chi = 0$ for simplicity). Note that resonance is efficient if $\Re(\mu_k)/H \sim \sigma m_{\rm Pl}/m^2 \gg 1$.

2.2.3 Broad resonance

Similarly, the term broad resonance is used to describe parametric resonance in broad instability bands in parameter space. For instance, it occurs if $|q| \gtrsim 1$ for the Mathieu equation, see Fig. 2.1. This corresponds to the non-perturbative limit in the trilinear model. In this limit, the only means for calculating the particle production is by solving the mode equation, eq. (2.12), and a very intuitive way of describing its solutions is the Floquet analysis we have developed. Broad resonance is much more efficient than narrow resonance since a broad, continuous range of k modes is excited. The typical rate of excitation is comparable to the background oscillation rate, $|\Re(\mu_k)| \sim T^{-1}$, and is much greater than in narrow resonance. The reason why the period of inflaton oscillations is the characteristic time-scale for particle production can be understood from the fact that in broad resonance, particles are produced in bursts, rather than smoothly as in the narrow resonance. Those bursts are separated in time by $\sim T$. They occur every time the adiabadicity condition

$$\frac{\dot{\omega}(k,t)}{\omega^2(k,t)} \ll 1\,, \tag{2.16}$$

is violated. Since broad resonance occurs in the non-perturbative regime, where interactions with the inflaton background determine $\omega(k,t)$, and since their magnitude varies with period T, the adiabadicity condition is violated each time the background value of the inflaton is such that the interaction terms vanish – then $\dot{\omega}(k,t) \gg \omega^2(k,t)$. For an oscillating field, this happens twice a period, implying a rate of particle production comparable to T. Note that in the narrow resonance the adiabadicity condition is always satisfied, since interactions are weak (they can be treated perturbatively) and $\omega^2(k,t) \approx k^2 = \text{const}$ always. The only reason for resonance there is the dense occupation of χ modes, which leads to a smooth exponential increase

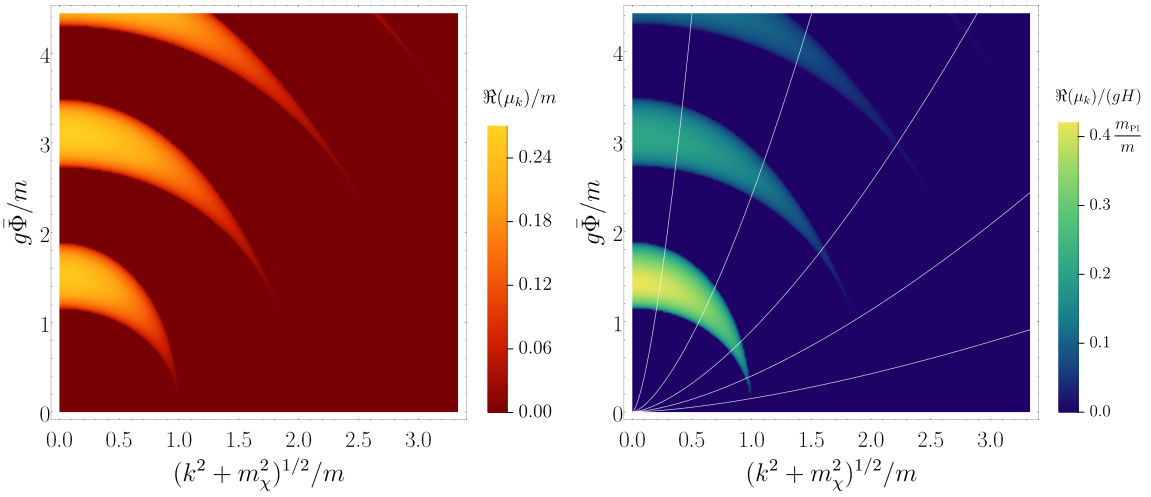

Figure 2.3: Same as Fig. 2.2, but for $V(\phi,\chi)=m^2\phi^2/2+m_\chi^2\chi^2/2+g^2\phi^2\chi^2/2$, for which $A_k=(k^2+m_\chi^2)/m^2+2q$, $2q=g^2\bar{\Phi}^2/(2m^2)$. The charts are for $g^2>0$, see Fig. 2.1. Broad resonance occurs only for $A_k-2q\ll q^{1/2}$, i.e., for low-momentum modes $(k^2+m_\chi^2)/m^2\ll g\bar{\Phi}/m$, for specific ranges of $g\bar{\Phi}/m$.

in the occupation numbers of particular modes. The reason why the case of broad resonance is different can be understood qualitatively by considering the mode functions in the adiabatic and non-adiabatic regimes. In the adiabatic limit, the WKB solutions to eq. (2.12) are

$$u_k(t)=\frac{1}{(2\pi)^{3/2}}\left[\frac{\alpha_k}{\sqrt{2\omega(k,t)}}e^{-i\int\omega(k,t)dt}+\frac{\beta_k}{\sqrt{2\omega(k,t)}}e^{i\int\omega(k,t)dt}\right]. \tag{2.17}$$

The vacuum state mode functions which minimize the Hamiltonian corresponding to the action in eq. (2.11) and which are such that the commutators in eqs. (1.42) and (1.47) are satisfied for $\hat{\chi}_{\mathbf{k}}$ and $\hat{\pi}^\chi_{\mathbf{k}}$, and $a^\chi_{\mathbf{k}}$ and $a^{\chi\dagger}_{\mathbf{k}}$, respectively, have $|\alpha_k|=1$ and $\beta_k=0$ [70]. More generally, mode functions satisfying the field-momentum commutator in eq. (1.42), given eq. (1.47), correspond to $|\alpha_k|^2-|\beta_k|^2=1$. One can show that this expression is consistent with the constancy of the Wronskian, since $W[u_k,u_k^*]=i(|\alpha_k|^2-|\beta_k|^2)/(2\pi)^3$ and is equal to $i/(2\pi)^3$ if we start in the vacuum. The mean occupation number, see eq. (2.15), is simply $n^\chi_{\mathbf{k}}=|\beta_k|^2$, i.e., an adiabatic invariant and equal to zero in the vacuum state. We should note that for $|\beta_k|>0$, the Bunch-Davies vacuum is no longer an eigenstate of the Hamiltonian.

For instance, the adiabaticity condition, eq. (2.16), for the Mathieu equation reduces to

$$\frac{2q\sin(2z)}{(A_k+2q\cos(2z))^{3/2}}\ll 1\,, \tag{2.18}$$

implying that if $A_k\lesssim 2|q|$, the inequality is not satisfied near $z_j=\pi/4,3\pi/4,...$ and the WKB solution, see eq. (2.17), does not hold. Away from these z_j, the WKB solution is a good approximation. If $A_k\gtrsim 2q>0$, adiabadicity can be also violated for $A_k-2q\ll q^{1/2}$ near $z_j=\pi/2,3\pi/2,...$ (similar expressions hold for $A_k\gtrsim -2q>0$; this provides a qualitative explanation of the broad bands in Figs. 2.1, 2.2, 2.3, 2.4). In general, since $|\alpha_k^j|^2-|\beta_k^j|^2=|\alpha_k^{j+1}|^2-|\beta_k^{j+1}|^2=1$, where the superscript j labels the coefficients between the jth and $(j+1)$th violation of adiabadicity, etc., the connection between these Bogolyubov type

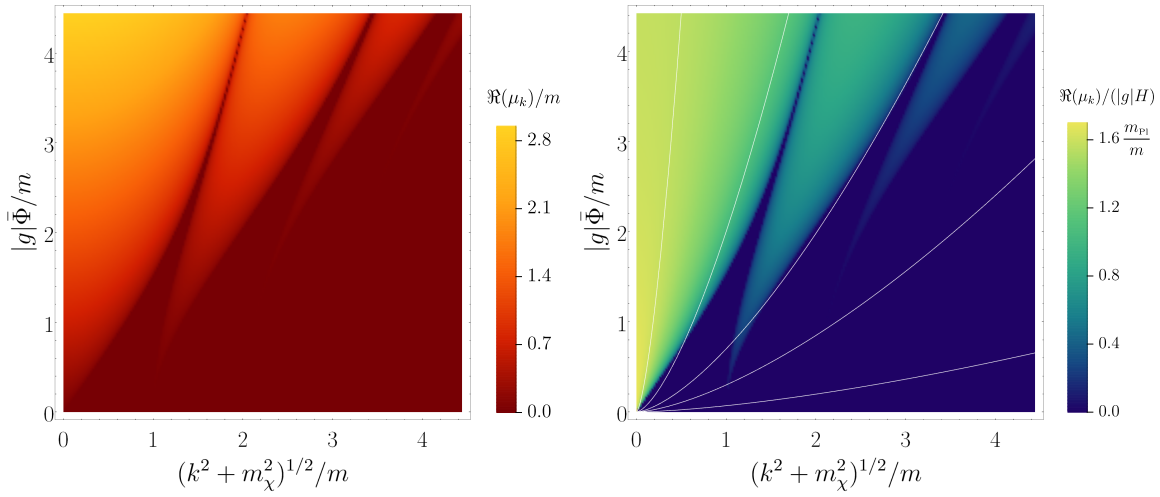

Figure 2.4: Same as Fig. 2.3, but for $g^2 < 0$, (see also Fig. 2.1). Note the prominent broad resonance bands, corresponding to $A_k \lesssim 2q < 0$, not present in the instability chart given in Fig. 2.3 for $g^2 > 0$.

coefficients is

$$\begin{pmatrix} \alpha_k^{j+1} e^{-i\theta_k^j} \\ \beta_k^{j+1} e^{i\theta_k^j} \end{pmatrix} = \begin{pmatrix} 1/D_k^j & R_k^{j*}/D_k^{j*} \\ R_k^j/D_k^j & 1/D_k^{j*} \end{pmatrix} \begin{pmatrix} \alpha_k^j e^{-i\theta_k^j} \\ \beta_k^j e^{i\theta_k^j} \end{pmatrix} , \tag{2.19}$$

where $\theta_k^j = \int_{t_0}^{t_j} \omega(k,t)dt$ is the accumulated phase until the jth violation of adiabadicity, and the reflection and transmission coefficients must obey $|R_k^j|^2 + |D_k^j|^2 = 1$, to preserve the Bogolyubov nature of the αs and the βs. The calculation of the reflection and transmission coefficients is tedious – one has to derive connection formulae for the WKB solution on both sides of the non-adiabatic region [71] for a given form of $\omega(k,t)$. Nevertheless, one can use the general expression in eq. (2.19) to study particle production. If we assume that we start in the vacuum state, i.e., $\beta_k^{j=0} = 0$, there will be particle production after the first violation of adiabadicity – $n_{\mathbf{k}}^{\chi,j=1} = |\beta_k^{j=1}|^2 = |R_k^{j=1}/D_k^{j=1}|^2$. In general,

$$n_{\mathbf{k}}^{\chi,j+1} = \left|\frac{R_k^j}{D_k^j}\right|^2 (n_{\mathbf{k}}^{\chi,j}+1) + \left|\frac{1}{D_k^j}\right|^2 n_{\mathbf{k}}^{\chi,j} + 2\left|\frac{R_k^j}{D_k^j D_k^{j*}}\right| \sqrt{n_{\mathbf{k}}^{\chi,j}(n_{\mathbf{k}}^{\chi,j}+1)}\cos(\theta_k^j + \Delta\theta_k^j) , \tag{2.20}$$

where $\Delta\theta_k^j = \arg(R_k^j \alpha_k^j \beta_k^{j*})$. In the limit $n_{\mathbf{k}}^{\chi,j} \gg 1$, we can write $n_{\mathbf{k}}^{\chi,j+1} = e^{2\mu_k^j} n_{\mathbf{k}}^{\chi,j}$, where

$$\mu_k^j = \ln\left|\frac{1+|R_k^j|e^{i(\theta_k^j+\Delta\theta_k^j)}}{\sqrt{1-\left|R_k^j\right|^2}}\right| . \tag{2.21}$$

The argument of the logarithm can take values greater or smaller than unity. $\mu_k^j > 0$ corresponds to non-adiabatic particle production at event j. We note that violation of adiabaticity is a necessary, but not sufficient condition for particle production. The actual form of $\omega(k,t)$ must be such that R_k^j and $\theta_k^j + \Delta\theta_k^j$ allow for $\mu_k^j > 0$, at least on average. That is why regions in parameter space in which the adiabatic

condition is not satisfied can still contain stability bands, e.g., see the narrow regions of stability for $A_k \lesssim 2q$ in Fig. 2.1 for the Mathieu equation.

2.2.4 Classical limit

The last point we wish to make for parametric resonance after inflation and preheating in general, is that the exponentially amplified modes can be treated classically. Intuitively, this can be understood from the large occupation numbers of these modes. Quantitatively, we can see it by considering the field-momentum commutator

$$\hat{\chi}_{\mathbf{k}}(t)\hat{\pi}_{\mathbf{q}}(t) = \hat{\pi}_{\mathbf{q}}(t)\hat{\chi}_{\mathbf{k}}(t) + i(2\pi)^{-3}\delta(\mathbf{k}+\mathbf{q})\,. \tag{2.22}$$

The expectation values of the operator products on the left and right hand sides of the expression grow as $e^{2|\Re(\mu_k)|t}$ and can become much greater than unity. Their difference, however, remains small and constant. It is equal to the delta-function term. We can check this by evaluating the commutator explicitly

$$[\hat{\chi}_{\mathbf{k}}(t), \hat{\pi}_{\mathbf{q}}(t)] = W[u_k(t), u_k^*(t)] \times [a_{\mathbf{k}}, a^\dagger_{-\mathbf{q}}] = W[u_k(t), u_k^*(t)]\delta(\mathbf{k}+\mathbf{q})\,. \tag{2.23}$$

Since the Wronskian $W[u_k(t), u_k^*(t)] = \text{const}$ for any equation of the form given in eq. (2.12), and since we start with vacuum fluctuations ($\beta_k = 0$) $W[u_k(t), u_k^*(t)] = i/(2\pi)^3$ always, even if each of the terms has grown exponentially. This proves that even though the commutation relation is respected, the quantum correction delta-function term affects the expectation value of $\hat{\chi}_{\mathbf{k}}(t)\hat{\pi}_{\mathbf{q}}(t)$ negligibly for the resonantly amplified $\mathbf{k}$. Hence, the quantum expectation value with respect to the Bunch-Davies vacuum of any function of the densely populated $\hat{\chi}_{\mathbf{k}}$ mode can be treated as a classical ensemble average over field realizations drawn from a Gaussian probability distribution. The variance of a (zero-mean) field in the WKB regime at some time t is

$$\begin{aligned}\langle\chi^2(t,\mathbf{x})\rangle_{\text{ens}} &= \int d^3k d^3q \langle\chi_{\mathbf{k}}(t)\chi_{\mathbf{q}}(t)\rangle_{\text{ens}} e^{i(\mathbf{k}+\mathbf{q})\cdot\mathbf{x}} \\ &\approx \langle 0|\hat{\chi}^2(t,\mathbf{x})|0\rangle = \int d^3k d^3q \delta(\mathbf{k}+\mathbf{q}) u_k^*(t) u_q(t) e^{i(\mathbf{k}+\mathbf{q})\cdot\mathbf{x}}\,,\end{aligned} \tag{2.24}$$

where $(2\pi)^3|u_k(t)|^2 = [1 + 2n^\chi_{\mathbf{k}} + 2\sqrt{n^\chi_{\mathbf{k}}(n^\chi_{\mathbf{k}}+1)}\cos(\gamma_k)]/(2\omega(k,t)) \approx 2n^\chi_{\mathbf{k}}\cos^2(\gamma_k/2)/\omega(k,t)$ for $n^\chi_{\mathbf{k}} \gg 1$, where $\gamma_k = \arg(\alpha_k\beta_k^*)$. Similar considerations apply to more complicated functions which depend on time derivatives of $\hat{\chi}_{\mathbf{k}}(t)$ as well.

In the following section we discuss how gravity and additional oscillating background fields can affect the resonant particle production described here.

2.3 Stochastic resonance

In the previous section we showed that parametric resonance can play an important role in the preheating phase. We considered the growth of matter fields, represented as fluctuations in an oscillating background, by applying Floquet analysis to the linear equations of motion with periodic coefficients. In doing so, we made several simplifying assumptions. In this section we re-introduce some of the ignored effects and show that they lead to a phenomenon known as stochastic resonance.

Neglecting gravity and assuming that the inflaton is the only field that has a background value allows for the possibility of having strictly periodic linear equations of motion, with exponentially growing solutions. One expects that any extension beyond this set-up can spoil the exact periodicity and, in general, counteract the growth of perturbations.

2.3.1 Metric fluctuations

Actually, incorporating gravity is not difficult. The metric perturbations remain negligible while particle production takes place. One can see that from the generalized Poisson equation (which follows from a combination of the Einstein equations)

$$\frac{\Delta\Psi}{a^2} = \frac{\delta\rho_{\rm m}}{2m_{\rm Pl}^2}\,, \tag{2.25}$$

where, Ψ, is the Bardeen potential, see eq. (1.35), and $\delta\rho_{\rm m} \equiv \delta\rho + [\bar{\rho}'(\tau)/a(\tau)]\delta u^{\parallel}$ is the co-moving, gauge-invariant, density perturbation.[2] After defining the co-moving overdensity field $\delta_{\rm m} = \delta\rho_{\rm m}/\bar{\rho}$, we can say that the linearized equations of motion governing the perturbations hold for small $\delta_{\rm m} \ll 1$. The Fourier transform of eq. (2.25) is $\Psi_{\mathbf{k}} = (3/2)(aH/k)^2\delta_{\rm m\mathbf{k}}$, implying $\Psi_{\mathbf{k}} \to 0$ as $aH/k \ll 1$ for small $\delta_{\rm m\mathbf{k}}$. Hence, metric perturbations remain vanishingly small on sub-Hubble scales during the preheating phase. During this phase, the super-horizon metric perturbations also do not grow in single-field models of inflation according to Weinberg's adiabatic theorem [55].

2.3.2 Expansion of space

Unlike the metric perturbations, the background space-time curvature cannot be easily neglected during preheating. The FRW expansion of space causes the amplitude of inflaton oscillations to decay, while co-moving wave-numbers are red-shifted to smaller physical values. Going back to our parametric resonance approach, we can see that the equation of motion for the scalar matter fields, eq. (2.9), can still be reduced to the form of a simple harmonic oscillator with a time varying frequency. Using the canonically-normalized field $\hat{\chi}_c(t) = a(t)^{3/2}\hat{\chi}(t)$, where t is cosmic time, we obtain

$$\ddot{\hat{\chi}}_{c\mathbf{k}} + \omega^2(k,t)\hat{\chi}_{c\mathbf{k}}(t) = 0\,. \tag{2.26}$$

In the trilinear model, see Sections 2.1 and 2.2, $\omega^2(k,t) = (k/a)^2 + m_\chi^2 + 2\sigma^2\bar{\Phi}(t)\cos(mt) - (3H/2)^2 - (3/2)\dot{H}$, implying that this is not the Hill's equation any more. Nevertheless, one can depict qualitatively the effects from FRW expansion on particle production by adding flow lines to the Floquet chart, tracing the evolution of particular co-moving modes. Since, in $m^2\phi^2/2$, $\bar{\Phi}(t) \sim a(t)^{-3/2}$ and $3H^2 \approx -2\dot{H}$ a given co-moving mode k flows exactly along $\bar{\Phi} \sim k_{\rm phys}^{3/2} \equiv (k/a)^{3/2}$ curve in the $k_{\rm phys} - \bar{\Phi}$ plane, see right panel in Fig. 2.2 (see also Figs. 2.3, 2.4 for other models). Empirically, a condition for parametric resonance (both narrow and broad) to result in significant particle production is

$$\frac{|\Re(\mu_k)|}{H} \gg 1\,, \tag{2.27}$$

for sufficiently long times. This is another way of saying that particle production occurs only in those bands in which the resonant growth is rapid on the Hubble time-scale. Using the heuristic picture of Floquet

[2] Under a diffeomorphism, eq. (1.29), $\delta u^{\parallel}$ transforms according to eq. (1.33), while from eq. (1.32) follows $\Delta\delta\rho = \bar{\rho}'(\tau)\xi_0$

theory, we can conclude that depending on the model, broad resonance can be enhanced or shut off by the expansion of space. When more and more co-moving modes are redshifted towards a broad instability band, we observe a temporary increase in the net particle production, see bottom left corner of right panel in Fig. 2.2, but as they eventually leave the instability regions the resonance gets completely shut-off.

As we showed in the previous section, broad resonance can be described as a series of particle creation events in which the adiabaticity condition, eq. (2.16), is violated. Taking into account the effects of the expansion of space, implies that the quantities appearing in eq. (2.21) will be time-dependent. The reflection coefficient, R_k^j, should have some model dependent and usually monotonic time-dependence, whereas the phase, $\theta_k^j + \Delta\theta_k^j$, can be assumed to vary randomly in the interval $[0, 2\pi)$. The fact that the Floquet index μ_k^j in eq. (2.21) can change stochastically between successive particle creation events is the reason why broad resonance in an expanding space is called *stochastic resonance*. On average $\mu_k^j \approx (1/2)\ln[(1+|R_k^j|^2)/(1-|R_k^j|^2)] > 0$, implying an increasing number of particles, in agreement with entropic arguments. Note that due to the randomness of the phase, μ_k^j on average can be smaller than in the Minkowski space-time limit. This is a curious feature of stochastic resonance, where particle production occurs on time-scales much shorter than the Hubble time, but still the expansion of space affects the final result.

On the other hand, the efficiency of narrow resonance is severely degraded by the FRW expansion. As one can see in the Floquet charts in Figs. 2.2, 2.3, 2.4, co-moving modes cross the narrow instability bands much faster than in the broad resonance regime. Thus, expansion takes particles out of the thin resonance layers and the occupation numbers boosting the Bose condensation effect become smaller than in the Minkowski limit. If the rate of escape of particles is greater than the rate of their production, i.e., eq. (2.27) does not hold, then Bose effects play no role. The efficiency of narrow resonance is sensitive to other suppressing effects such as the re-scattering of the newly created particles out of the resonance layer, as well as the shift of the resonance region from its original location due to the change of the inflaton effective mass as a consequence of particle production.

We also note that after including the expansion of space we are still allowed to treat the heavily populated modes classically. In particular, the analysis after eq. (2.22) still holds for the canonically-normalized field $\hat{\chi}_c(t)$.

2.3.3 Multi-field preheating

The periodicity of the time-dependent background can be violated also if there are several oscillating homogeneous fields. Even without expansion of space, unless the motion at the background level in the multi-field space occurs along special trajectories such as Lissajous curves or effectively one-dimensional oscillatory trajectories, the time-dependent coefficients in the linear equations of motion governing the fluctuations are not exactly periodic. This can again lead to stochastic resonance if the adiabaticity condition, eq. (2.16), is violated [72]. Note that this time both the reflection coefficient, R_k^j, and the phase, $\theta_k^j + \Delta\theta_k^j$, can be assumed to vary randomly between successive non-adiabatic events. Even the length of the time intervals separating such events can vary randomly. Nevertheless, just like in the case of an expanding space, we could approximate the motion in field space at the background level as being periodic to check if substantial instability (both broad and narrow) bands exist.

We should point out that there is an alternative description of resonant particle production when the number of oscillating homogeneous fields is much greater than one. In this case the effective masses of the daughter fields evolve with a random component to a very good approximation. This reduces the efficiency of the particle production, but resonance still takes place. It occurs at all wavenumbers, not

only within particular resonance bands. The alternative way to see why this happens is to note that there is a duality between the equation of motion of daughter fields, see eq. (2.26), and the time-independent one-dimensional Schrodinger equation. The duality interchanges time and space, the mode-function with the wavefunction, the time-dependent effective mass squared with the space-dependent one-dimensional potential energy and k^2 with the eigenenergy. Then recalling the celebrated condensed matter phenomenon of Anderson localization, in which small random impurities make eigenfunctions exponentially localized in space, we expect that in the case of preheating, time-dependent masses with random components give rise to exponentially growing modes at all wavelengths; for more details on the condensed matter analogue and the random resonance see [72].

We have shown that realising a strictly periodic motion at the end of inflation is difficult. The FRW expansion and the possibility of having more than one oscillating homogeneous fields can lead to a quasi-periodic motion at the background level. This can lead to stochastic resonance if the adiabaticity condition, eq. (2.16), is not respected. Even if it is, there could be still some particle production due to perturbative decays. However, as opposed to the strictly periodic case, the Bose enhancement of decays into scalar fields is normally not significant. Despite all that, Floquet analysis remains an important first step towards understanding the instabilities in the evolution of matter fields during preheating.

2.4 Tachyonic decay

So far we have assumed that the effective frequency, $\omega^2(k,t)$, of the matter fields, χ_c, changes (quasi) periodically with time due to the inflaton oscillations. This need not be the case always. For instance, towards the end of Hybrid inflation [73], $V(\phi,\chi) = \lambda_\chi(\chi^2 - v^2)^2 + g^2\phi^2\chi^2 + V_{\rm infl}(\phi)$, as the inflaton becomes smaller than a critical value, $\phi^2 < \lambda_\chi v^2/g^2$, but is not oscillating, the sign of $\omega^2(k,t)$ changes from positive to negative for long-wavelength modes and can remain such for an extended period of time. Since one of the two imaginary frequency solutions to eq. (2.26) is exponentially growing with time, $\chi_c \propto e^{|\omega|t}$, we again have exponential particle production. A negative squared frequency, $\omega^2(k,t) = (k/a)^2 + m^2_{\chi\rm eff} < 0$, implies an imaginary effective mass, $m^2_{\chi\rm eff} < -(k/a)^2 < 0$. That is why this mechanism for particle production is dubbed tachyonic preheating. Importantly, all modes whose momenta are less than the magnitude of the imaginary effective mass are unstable, and in the limit $k \to 0$ the exponential index approaches the maximal value of $|m_{\chi,\rm eff}|$. Tachyonic instabilities in fluctuations always occur in symmetry breaking models for small background field values, e.g., in Hybrid inflation for small enough ϕ. Tachyonic instabilities can be also observed in the fluctuations of the inflaton field itself, e.g., when it has a symmetry breaking self-interaction potential or in field ranges where the self-interaction potential is shallower than quadratic.

Just like in the case of resonant particle production, to have efficient tachyonic decay of the inflaton condensate,

$$\frac{|m_{\chi,\rm eff}|}{H} \gg 1 \tag{2.28}$$

must hold for a sufficiently long time. Otherwise, the expansion of space drives $m^2_{\chi,\rm eff}$ to its equilibrium, positive value (implying positive $\omega^2(k,t)$) before substantial energy can be transferred from the condensate to fluctuations.

In general, tachyonic instabilities can be achieved in models with negative couplings. For instance, in the trilinear model in Sections 2.1 and 2.2, the interaction term $\sigma\phi\chi^2$ implies that even if the inflaton is oscillating, half of the period small k modes will be tachyonic. This corresponds to the $0 < A_k < 2q$ region in the Mathieu instability chart in Fig. 2.1, and explains why there the stability bands are so narrow (see also Fig. 2.2). They correspond to the small parameter region in which effectively only the exponentially decaying imaginary frequency solution is excited. Note that the expansion of space blurs the boundaries between different regions in the Floquet chart and the narrow stability bands in the tachyonic region go away. Another example of negative coupling resonance is the models with a $g^2\phi^2\chi^2/2$ interaction, where $g^2 < 0$, see Fig. 2.4. This implies $q < 0$ in the notation of the Mathieu equation, see Fig. 2.1. Note that in models like this, where interaction terms are always negative to ensure stability we should add higher order positive potential terms. In this case, we can add quartic potential terms, that dominate at large field values, but are unimportant during preheating. In terms of the Mathieu instability chart the tachyonic region corresponds to $2|q| \geq A_k \geq 2q$, where the latter bound comes from the q-dependence of A_k in this model, see Figs. 2.1, 2.4. Compared with the standard resonant preheating scenario ($g^2 > 0$) where $\mu_k^{\max} \lesssim m$, see Fig. 2.3, tachyonic preheating can be much more efficient, with maximal exponential index $\sim |g|\bar{\Phi}$. Even if the couplings are small, $|g| \ll 1$, to ensure negligible radiative corrections, we can still have $|g|\bar{\Phi} \gg m$ at the end of inflation. Typically, $\bar{\Phi} \sim m_{\rm Pl}$, and even with small couplings it can take less than one oscillation of the condensate for the tachyonic growth of the long-wavelength modes to lead to interesting non-linear dynamics.

2.5 Instant preheating

The time-dependent nature of the effective mass of fluctuations can give rise to another preheating mechanism. Normally, for a coupling of χ to some fermion ψ of the Yukawa form, $h_\chi\chi\bar{\psi}\psi$, the decay $\chi \to \bar{\psi}\psi$ is kinematically forbidden if the corresponding bare masses are such that $m_\chi < 2m_\psi$. However, if the scalar is coupled to the inflaton via $g^2\phi^2\chi^2/2$ (assume $g^2 > 0$) then the effective mass, $m^2_{\chi\rm eff} = m_\chi^2 + g^2\phi^2$, can become significantly bigger. And even for a scalar of vanishing bare mass, the decay can be kinematically allowed. For an oscillating inflaton with large enough amplitude, $\bar{\Phi} > 2m_\psi/g$, the decay rate, see also eq. (2.1),

$$\Gamma_{\chi\to\bar{\psi}\psi} = \frac{h_\chi^2 g|\bar{\phi}|}{8\pi}\,, \tag{2.29}$$

vanishes when $\bar{\phi} \approx 0$, and is maximal as the oscillating inflaton reaches its maximal value $|\bar{\phi}| = \bar{\Phi}$. In the large coupling limit, $\sqrt{q} = g\bar{\Phi}/m \gg 1$, we have broad resonance, or in other words non-adiabatic particle production every time the non-adiabaticity condition given in eq. (2.16) is violated. This happens when $\bar{\phi} \approx 0$, implying that $\Gamma_{\chi\to\bar{\psi}\psi}$ is maximal half-way between two consecutive particle production events. Hence, even if a significant amount of χ particles are produced at each creation event, they can all decay into fermions before the next one. This mechanism is called instant preheating. In it, the back-reaction of χ particles on the ϕ condensate is slowed down and the efficiency of the resonance maintained for very long times. Furthermore, for $g \sim 10^{-2}$ and $\bar{\Phi} \sim m_{\rm Pl}$ the light inflaton, $m \sim 10^{-6}m_{\rm Pl}$, can decay to heavier scalars and fermions, as heavy as the GUT scale $\sim 10^{16}\,\mathrm{GeV}$. The return of the GUT scale into play obviously presents a threat to inflationary models. Far-from-equilibrium production of topological defects can take place, thus allowing cosmological observations to place bounds on different preheating scenarios.

Chapter 3

Non-linear reheating

'The world is richer than it is possible to express in any single language.'
Ilya Prigogine

As inflation ends, non-perturbative phenomena such as stochastic resonances and tachyonic preheating can amplify quantum fluctuations of the matter fields, creating particles in a far-from-equilibrium state. The instabilities grow exponentially fast on cosmological time-scales. Such exponential growth cannot proceed forever. Eventually, the produced particles back-react on the preheating process. Mode-mode couplings and non-linear interactions become important. Soon the inflaton condensate fragments and non-linear dynamics takes over. The subsequent evolution of the bosonic fields can be rather non-trivial and a lot of interesting things can happen. Towards the end of this out-of-equilibrium evolution, the fields must thermalize, marking the end of reheating and setting the scene for big-bang nucleosynthesis.

This chapter begins with a discussion of the end of preheating. We talk about the various places back-reaction can arise in and terminate preheating. We then focus on the non-linear dynamics following the initial burst of particle production and the fragmentation of the inflaton condensate. We survey the different numerical techniques available for tackling the non-linear evolution, and also review the various non-trivial structures that have been studied. We finish with a discussion of the approach to thermalization which can include the turbulent evolution of scalar fields.

3.1 Back-reaction: the end of preheating

Resonant particle production and tachyonic instabilities can be terminated in various ways. If the expansion of space does not intercept the non-perturbative particle production, then the back-reaction of the produced particles eventually shuts it off. Back-reaction effects are associated with higher order in field fluctuations correction terms to the equations of motion in the approximate picture of preheating in which the inflaton condensate is treated as a time-dependent classical background with quantum field fluctuations on top of it.

3.1.1 Back-reaction at the background level

The equation of motion describing the evolution of the classical inflaton background, eq. (1.15), can have corrections due to non-vanishing spatial averages of interaction terms. For instance, in the $V(\phi,\chi) = m^2\phi^2/2 + g^2\phi^2\chi^2/2$ model, the presence of χ particles alters the effective squared mass of the inflaton

condensate oscillations by $\Delta m_{\bar{\phi}}^2 = g^2\langle\chi^2\rangle$. The angle brackets represent a volume average of the classical χ (classical in the sense described at the end of Section 2.2). From now on, when discussing back-reaction and non-linear dynamics, we shall treat all bosonic fields classically and drop their hats. If there are exponentially unstable modes, then

$$\langle\chi^2\rangle = \int \frac{d\ln k}{2\pi^2} k^3 |\chi_k|^2 \propto e^{2\mu t}\,, \tag{3.1}$$

where μ is some effective growth index, close to the maximal one $\mu_k^{\max}$. [1] The coefficient of proportionality varies slowly with time (apart from an oscillating modulation, it decays monotonically due to the expansion of space). Hence, back-reaction effects become important, $\Delta m_{\bar{\phi}}^2 \sim m^2$, within, up to logarithmic factors,

$$\Delta t_{\rm br} \sim \mu^{-1}\,, \tag{3.2}$$

from the beginning of particle production. For broad resonance, $\mu \sim m \gg H$, and so $\Delta t_{\rm br}$ is very short in comparison to the Hubble expansion time-scale. Physically, the effect on the condensate from the increase in its effective mass is that its amplitude of oscillations, $\bar{\Phi}$, decreases whereas its frequency increases. In the Mathieu equation notation, the resonance parameter $q = g^2\bar{\Phi}^2/m_{\bar{\phi}}^2$ rapidly decreases and soon it is difficult for the resonant production of χ particles to continue further.

3.1.2 Re-scattering and non-linearity

The equations of motion describing the field fluctuations are also affected by the particle production. Working in the mean-field/Hartree approximation in which different modes and fields evolve independently (are uncorrelated in time), i.e., $\langle\chi^*_{\mathbf{k}-\mathbf{q}}\chi_{\mathbf{k}}\rangle_{\rm time} \approx 0$ if $\mathbf{q} \neq \mathbf{0}$, $\langle\delta\phi^*_{\mathbf{k}-\mathbf{q}}\chi_{\mathbf{k}}\rangle_{\rm time} \approx 0$ for all $\mathbf{q}$, etc.,[2] there are only correction mass terms, $\Delta m_\chi^2 = g^2\langle\delta\phi^2\rangle$ and $\Delta m_{\delta\phi}^2 = g^2\langle\chi^2\rangle$, for χ and the inflaton fluctuations, respectively. They may change the evolution of the field fluctuations slightly, e.g., shift χ particles out of resonance bands. However, as the number of particles increases, the mean-field/Hartree approximation stops being a good description. The coupling between different Fourier modes becomes important, heralding the true beginning of the non-linear stage. The mode-mode coupling between different momentum modes is called *re-scattering* and is what actually leads to the fragmentation of the inflaton condensate. For instance, there is an additional non-vanishing source term in the equation of motion for the inflaton fluctuations $\sim g^2\Phi\int \mathbf{d}^3\mathbf{k}\langle\chi^*_{\mathbf{k}-\mathbf{q}}\chi_{\mathbf{k}}\rangle_{\rm time} \propto e^{2\mu t}$. Having an inhomogeneous equation with exponentially growing source term, implies that its particular solution also grows exponentially, i.e., $\delta\phi_q \propto e^{2\mu t}$. Thus, due to the interactions of pairs of χ particles with particles in the condensate, inflaton fluctuations grow twice as fast. The growth is a manifestation of inflaton particles being scattered out of the inflaton condensate. They are low-momentum excitations, predominantly. When $\langle\delta\phi^2\rangle \gtrsim \Phi^2$, we say that the condensate is substantially fragmented and if $\Phi \approx 0$ we say that it is completely fragmented or destroyed. Re-scattering also re-distributes the energy stored in the χ particles. Parametric resonance leads to the excitation of χ momentum modes lying in instability bands. The re-scattering transfers energy from the amplified modes to modes with momenta lying in the stability regions. This may slow down the resonant particle production.

[1] Note that according to the Ergodic theorem [55], the spatial average of χ^2 is also equal to the ensemble average over realizations of the stochastic field. This is what the vacuum expectation value of the quantum field tends to, since $\langle 0|\hat{\chi}(t)^2|0\rangle = \int k^3|u_k(t)|^2 d\ln k/(2\pi^2) \propto e^{2\mu t}$, where we integrate mode function.

[2] The time average is taken over several oscillations of the more slowly oscillating Fourier transform.

Even if it completely shuts off the resonance, re-scattering becoming important is a sign of the ensuing non-linear evolution and fragmentation of the inflaton condensate.

We should point out that having a fragmented inflaton condensate, $\langle \delta\phi^2 \rangle \gtrsim \Phi^2$, does not necessarily imply that the energy stored in it is negligible. However, we can say with certainty that re-scattering and fragmentation kick in when the energy stored in interaction terms and/or fluctuations is comparable to the energy of the classical background. Hence, non-perturbative particle production ends and non-linear evolution begins with either most or at least a non-negligible fraction of the total energy being stored in field fluctuations.

Before moving forward to different approaches for studying the non-linear stage, we consider the possibility of having a second field that has a small, but non-vanishing background value, e.g., $\Phi \gg |\bar{\chi}| > 0$. While the back-reaction mechanisms remain largely unchanged, the preceding linear evolution during preheating can exhibit novel behaviour. Essentially, there are additional mixing terms, $\sim g^2\Phi\bar{\chi}\delta\phi_k$ and $\sim g^2\Phi\bar{\chi}\chi_k$, in the equations for χ_k and the inflaton fluctuations, respectively. They lead to chaotic evolution of the field fluctuations. The strong dependence on the initial value of $\bar{\chi}$ can give rise to observational signatures of preheating, as we will discuss in Section 5.3.

We now proceed with the non-linear stage of reheating, following the back-reaction of the produced particles on the inflaton condensate and the breakdown of the linear analysis.

3.2 Non-linear evolution

Preheating ends when the occupation numbers of excited bosonic field modes become large and back-reaction effects render the linearized approximation not applicable. The inflaton and the fields it is coupled to start evolving as a combined system. Non-linear interactions lead to the transfer of power between different wavenumbers. This non-linear phase is dynamically rich and can be studied numerically.

3.2.1 Numerical approach

The standard approach in numerical analysis is to solve the classical evolution equations, e.g.,

$$\Box\phi + \partial_\phi V(\phi,\chi) = 0\,, \qquad \Box\chi + \partial_\chi V(\phi,\chi) = 0\,, \qquad R_{\mu\nu} - \frac{1}{2}g_{\mu\nu}R = \frac{T_{\mu\nu}}{m_{\rm Pl}^2}\,. \tag{3.3}$$

There are several publicly available codes created for this purpose. Most of them use a finite-difference method for solving the equations. The fields are discretized on a cubic co-moving spatial grid, with periodic boundary conditions. The time evolution is then a matter of evolving forward a system of coupled ordinary differential equations. For numerical integration in time LATTICEEASY [74] uses the simplest symplectic integrator – the leapfrog scheme, which is fast (no need for storage of field and field time derivatives simultaneously during a time step) and second order accurate in time. DEFROST [75] and HLATTICE [76] use higher order symplectic integrators. GABE [77] uses a second order Runge-Kutta method which stores field and field time derivatives on the same time slices, unlike symplectic integrators. Although, this requires more time to run the simulations and more physical memory, it allows for non-canonical kinetic terms. CUDAEASY [78] and PYCOOL [79] are GPU-accelerated codes based on DEFROST. A pseudo-spectral code, PSpectre [80], is also available, which evolves the Fourier transforms of the fields. In it, unlike

in finite-difference codes, Laplace terms are dealt with straightforwardly. Each contributes a single term, e.g., $k^2\phi_{\mathbf{k}}$, to the Fourier transformed equations of motion with no computational cost, whereas $\Delta_{\mathbf{x}}\phi(\mathbf{x})$ in finite-difference codes is more costly, since one has to compute the differences with neighbouring points for each lattice site. However, non-linear interaction terms in the equations of motion, e.g., $g^2\phi^2(\mathbf{x})\chi(\mathbf{x})$, are easy to deal with in finite-difference codes, whereas for pseudo-spectral codes they present a problem, since there one has to calculate multidimensional integrals.

We should also point out that most publicly available codes do not include metric perturbations, i.e., they evolve the fields in pure FRW space-time. In addition to the Klein-Gordan equations, they solve one equation for the evolution of the scale factor, $a(t)$. Note that the Einstein equations yield two equations for the evolution of $a(t)$, namely the Friedmann and Raychaudhuri equations given in eq. (1.4), with $\rho(t) = \langle\rho\rangle$ and $p(t) = \langle p\rangle$ averaged over the simulation box. Programs typically evolve the Raychaudhuri equation and treat the Friedmann equation as a constraint that has to be satisfied after each time step. Violations of the Friedmann equation ≥ 0.1 % indicate poor energy conservation and render the simulations unreliable. Some studies simplify matters further, by assuming a fixed time-dependence of $a(t)$. This means that the expansion of space is not calculated self-consistently, e.g., by solving the Raychaudhuri. Common choices are $a \propto t^n$ with $n = 2/3,\ 1/2$ for matter and radiation-dominated backgrounds, respectively. But still the Friedmann equation is treated as a constraint that has to be checked after each time step. Approximating the space-time to be FRW is justified, since the lattice size of typical simulations is sub-horizon and just like during preheating, metric perturbations are suppressed on these scales and do not affect the non-linear evolution of the fields. The reason why sub-horizon scales are of main interest are the causal mechanisms which drive the non-linear evolution of the fields. Causally disconnected Hubble patches evolve independently and almost identically, implying that it is sufficient to capture one Hubble volume in numerical simulations. Otherwise, the only publicly available code that can include metric perturbations is HLATTICE.

Of course, the FRW approximation is non-viable if large sub-horizon inhomogeneities, that can lead to the formation of primordial black holes, are present during preheating. However, such inhomogeneities rarely form due to matter field instabilities [15, 69]. They either occur in models in which significant super-horizon inhomogeneities generated during inflation re-enter the horizon during preheating, or are induced by gravitational instabilities which become important long after the end of inflation.

We should also point out that all publicly available codes are written for scalar fields. The GABE code can be adapted for gauge field dynamics, but its ability to respect the gauge constraints has not been fully tested yet, especially with charged scalar fields. We should also note that DEFROST differs from the other finite-difference codes. In it, instead of directly discretizing the equations of motion, the Lagrangian is discretized and then the corresponding equations of motion are evolved numerically. We shall adopt this approach to study non-linear dynamics in the Abelian-Higgs system in Chapter 9.

3.2.2 Non-linear dynamics

Non-linear effects can become important even in the simplest models of reheating in which the interactions of the inflaton with other fields are negligible. If self-interaction terms, e.g., $\propto \phi^n$, $n \neq 2$, become important, the inflaton condensate can fragment after self-resonance. It can form non-trivial field configurations such as oscillons which can lead to long periods of matter-dominated state of expansion [36], or form Q-balls if the inflaton is a complex scalar [81]. Oscillons (as well as Q-balls) can also affect predictions in baryogenesis models with a complex inflaton [52], as we will show in Chapter 7. If the inflaton is very light, but self-interacting, it inevitably fragments and attains a radiation-like equation of state [34]. This

can have important observational consequences as will be shown in Chapter 6. Gravitational waves can also be generated due to fragmentation induced by self-interactions [44, 82]. Even if the inflaton is not self-interacting, the condensate inevitably fragments due to gravitational instabilities [83].

Coupling the inflaton to other fields can lead to very rich phenomenology. Interaction with scalar fields can lead to the formation of metastable bubble-wall-like configurations [84], whose size is not much smaller than H^{-1}. After they collide the density is transferred to much smaller scales. This could be interpreted as upscattering of modes to higher momenta due to non-linear interactions. Scalar field theories can also feature the formation of solitons and defects, such as domain walls and metastable global cosmic strings [20]. Models that include gauge fields lead to new phenomena as well [22]. Non-equilibrium phase transitions can lead to the formation of stable topological defects, whereas models with conformal couplings feature large-scale magnetic fields and a faster approach to a radiation dominated state of expansion [31, 37].

The reason why topological defects can be produced during preheating, in theories which allow them, is non-equilibrium restoration of broken symmetries [21, 85, 86]. Just like in phase transitions, a negative bare mass squared can receive significant positive contributions from large field variances leading to a positive effective mass squared and temporary restoration of a symmetry. This can happen either during back-reaction and re-scattering, or after the fields enter the full non-linear regime. Once the expansion of space dilutes the energy enough, the symmetry is re-broken and topological defects can be produced. For instance, in models allowing the formation of cosmic strings, one has to wait for the mean energy density to become less than the potential energy in the central unstable maximum, filling the ring at the bottom of the potential. This mechanism leads to the production of strings on both sub and super horizon scales [20]. The sub-horizon strings are transient – they evaporate due to the emission of classical radiation. In general, the density of topological defects arising in such non-equilibrium phase transitions is determined by the correlation length of the fields shortly before the symmetry is restored. For inhomogeneous configurations, the correlation length scale can be considerably smaller than the Hubble scale unlike in the Kibble mechanism. Thus, preheating provides a mechanism for copious production of dangerous topological defects, even at GUT scales, which can have implications for inflationary models.

3.3 Turbulent scaling

The early stage of the non-linear evolution, following back-reaction and re-scattering, in models with scalar fields is dynamically rich and chaotic. Various transient non-trivial field configurations can form, wiping out details on initial conditions from inflation and preheating. Unless long-lived objects form, e.g., oscillons, stable defects, black holes, etc., the state of the fields eventually enters a highly inhomogeneous phase which can persist for very long times, much longer than the preheating and transient phases. It is characterised by a slow, but steady transfer of energy to higher momenta. Essentially, straight after the transient stage the field occupation numbers in the infrared quickly saturate to a power-law, $n(k) \propto k^{-3/2}$, with a UV cut-off not much greater than the typical wavenumber of excited particles during preheating [18, 19]. The power-law is non-thermal – for a thermal distribution of relativistic weakly interacting bosons we expect $n(k) \propto k^{-1}$ in the infrared. It then slowly propagates towards higher momenta. Typically, the cascading of the distribution towards the UV can be characterized as turbulent scaling in which the occupation numbers evolve self-similarly, $n(k,\tau) = (\tau/\tau_0)^{-q_1} n_0(k\tau^{-q_2})$, where q_1 and q_2 are some positive powers, determined by the form of the interactions and τ_0 is the conformal time when the scaling regime begins. This slow fragmentation proceeds until the occupation numbers of the highest k-modes belonging to the power-law

distribution become of order unity. Then the classical description breaks down and quantum effects become important. Note that the energy density in a given mode is $\rho(k) \propto k^4 n(k)$, implying that the high-k modes belonging to the power-law dominate the energy budget. That is why, if present, their quantum behaviour cannot be neglected.

3.4 Thermalization

3.4.1 Two stages

None of the preheating mechanisms described in Section 2, nor the subsequent non-linear evolution yield a thermal spectrum of decay products. However, measurements of the anisotropies in the CMB and the relative abundances of light elements tell us that the Standard Model degrees of freedom were in thermal equilibrium at the beginning of the big-bang nucleosynthesis and that the universe at that time was in a radiation-dominated state [1]. The moment when the universe achieves thermal equilibrium for the first time after the end of inflation, at some reheating temperature, $T_{\rm reh} \geq T_{\rm BBN} \sim 1\,{\rm MeV}$, in a radiation-dominated state of expansion, $w \approx 1/3$, marks the end of thermalization and the reheating epoch. The value of $T_{\rm reh}$ can have an impact on the production of dangerous relics, such as gravitinos, or on the formation of topological defects from thermal phase transitions and the gravitational waves they generate. The expansion history of the universe during reheating, and in particular the moment when the equation of state approaches $1/3$ can have important implications for the uncertainties in predictions of inflationary models as will be shown in Chapter 6.

Thermalization can be a long process, much longer than the preceding preheating, transient and turbulent phases. In principle, the universe can attain a radiation-like equation of state during or shortly after the turbulent stage, i.e., it can satisfy one of the two criteria for thermalization quite early. However, reaching a state of Local Thermal Equilibrium (LTE) can take much longer and involve particle fusion and off-shell processes. We say that the universe is in a prethermalized state if $w \approx 1/3$, but LTE is not established yet. Prethermalization can be delayed by the formation of long-lived objects like oscillons and Q-balls. They behave as pressureless dust and therefore must decay into relativistic matter to achieve a radiation-like equation of state before BBN. Similar considerations apply to massive scalar field condensates. For instance, if there is some remnant inflaton condensate, even if subdominant in energy during thermalization, it can make the universe re-enter a matter-dominated state of expansion before BBN. To avoid this, one must ensure the complete decay of the condensate. Introducing perturbative decays through three-leg interactions like Yukawa couplings, $h\phi\bar{\psi}\psi$, proves to be a reliable way for the absolute removal of $\bar{\phi}$. That is why, albeit unimportant during the early non-perturbative stages of reheating, perturbative decays of $\bar{\phi}$ are vital for the late stage of thermalization.

In a state of LTE the local value of the entropy, i.e., the entropy per unit volume, s, is maximized. LTE is achieved by particle species which are both in kinetic and chemical equilibrium. This requires both the re-distribution of momentum and energy between different particles, as well as an increase in their total number. Hence, both number-conserving and number-violating (off-shell process, particle fusion) reactions are involved. Negligible interactions between different species lead to Bose-Einstein and Fermi-Dirac distributions for bosons and fermions, respectively, in kinetic equilibrium. Kinetic equilibrium entails efficient exchange of energy and momentum between particles, i.e., it is sufficient to have number-conserving interactions only. On the other hand, chemical equilibrium can be achieved only by changing the number of particles. If number-violating interactions are suppressed (this could occur if

the particles mediating the number-violating interactions acquire a large mass at early times) the state of kinetic equilibrium is also known as a quasi-thermal state. However, as number-violating processes become efficient and particles flow to lower chemical potentials until the sum of chemical potentials of reacting particles becomes equal to the sum of the chemical potentials of the products in every reaction, s can be truly maximized and full LTE reached.

3.4.2 Perturbative limit

If after the end of inflation Bose effects and non-adiabatic particle production are unimportant, i.e., the inflaton condensate undergoes perturbative decays as described at the beginning of Section 2.1, then the decay is completed when $\rho \sim \Gamma^2 m_{\rm Pl}^2$. In the trilinear model, $V(\phi,\chi) = m^2\phi^2/2 + \sigma\phi\chi^2$, the perturbative decay rate is $\Gamma = \Gamma_{\phi\to\chi\chi}$, see eq. (2.1), and to ensure no parametric resonance $q = \sigma\Phi/m^2 \lesssim \sigma m_{\rm Pl}/m^2 \ll 1$. Hence, $\rho \sim (\sigma^4/m^2)m_{\rm Pl}^2 \ll m^4(m/m_{\rm Pl})^2 \ll m^4$. The momentum of the massless χ particles will be $m/2$, implying a particle energy $\langle E\rangle = m/2 \gg \rho^{1/4}$. On the other hand, the χ particles number density is $n = \rho/\langle E\rangle \ll \rho^{3/4}$. Note that in LTE $\langle E\rangle_{\rm LTE} \sim T$ and $\rho_{\rm LTE} \sim T^4$, implying $n_{\rm LTE} = \rho_{\rm LTE}/\langle E\rangle_{\rm LTE} \sim T^3 \sim \rho_{\rm LTE}^{3/4}$. Thus, perturbative preheating leads to a non-equilibrium dilute universe containing very energetic particles. To ensure the completion of thermalization, we should now introduce number-conserving and number-violating interactions, which are efficient even in a dilute plasma. When the universe reaches a radiation-dominated state of expansion, and the rate of these interactions is $> H$, reheating is completed.

3.4.3 Non-perturbative effects

Resonant and/or tachyonic decays of the inflaton condensate are also highly non-thermal processes. They yield non-equilibrium spectra, with peaks lying in instability bands $n(k) \propto e^{2\mu_k t}$ at the end of preheating. After the phase of exponential growth is terminated by back-reaction and re-scattering, and after a brief period of chaotic evolution of inhomogeneous field configurations, the spectrum of a scalar field typically relaxes into a continuous band, $n(k) \propto k^{-1}$, going all the way to $k \to 0$ and having an increasing UV cut-off, $k_{\rm c}(\tau) = k_{\rm c0}(\tau_0)(\tau/\tau_0)^{q_2}$, as described in Section 3.3. After the front of the distribution, which dominates the energy budget of the universe, starts behaving quantum mechanically, $n(k_{\rm c}(\tau)) = \mathcal{O}(1)$, the matter spectra should relax into Bose-Einstein and Fermi-Dirac (for fermions weakly coupled to the scalars) distributions. We can then use the results obtained from the classical field theory analysis to put a lower bound on the duration of reheating. Assuming the radiation-dominated state of expansion begins soon after the end of inflation, $a(\tau)/a(\tau_0) = \tau/\tau_0 = \rho(\tau_0)^{1/4}/\rho(\tau)^{1/4}$ and putting $(k_{\rm c}(\tau_{\rm reh})/a(\tau_{\rm reh}))^4 \sim T_{\rm reh}^4$ (recall $n(k_{\rm c}(\tau_{\rm reh})) = \mathcal{O}(1)$ and $\rho(k) \sim (k/a)^4 n(k)$) and $k_{\rm c0}/a(\tau_0) \sim m$

$$\begin{aligned}\left(\frac{\tau_{\rm reh}}{\tau_0}\right)^{q_2} &= \frac{k_{\rm c}(\tau_{\rm reh})}{k_{\rm c}(\tau_0)} \sim \frac{T_{\rm reh}}{m}\frac{a(\tau_{\rm reh})}{a(\tau_0)} \sim \frac{\rho(\tau_0)^{1/4}}{m} \\ &= \left(\frac{a(\tau_{\rm reh})}{a(\tau_0)}\right)^{q_2} \sim \left(\frac{\rho(\tau_0)^{1/4}}{T_{\rm reh}}\right)^{q_2},\end{aligned} \tag{3.4}$$

we find that

$$T_{\rm reh} \sim \left(\frac{m}{\rho(\tau_0)^{1/4}}\right)^{1/q_2} \rho(\tau_0)^{1/4}\,. \tag{3.5}$$

Putting $m = 10^{-6} m_{\rm Pl}$ and $\rho(\tau_0)^{1/4} \sim 10^{15}\,\mathrm{GeV}$ and $q_2 = 1/7$ [18, 19] yields $T_{\rm reh} \sim 10^3\,\mathrm{eV}$. This estimate gives an unacceptably low reheating temperature, implying that additional interactions, e.g., decays into fermions, become important before the non-linear evolution of the scalar fields drives them into thermal equilibrium. The calculation of the reheating temperature in such models with highly inhomogeneous scalar field configurations remains an open challenge.

Chapter 4

Reheating and High-Energy Physics models

'Is the universe 'elegant', as Brian Greene tells us? Not as far as I can tell, not the usual laws of particle physics, anyway. I think I might find the universal principles of String Theory most elegant – if I only knew what they were.'

Leonard Susskind

Accelerator experiments such as the LHC have given us information about the governing particle theory up to $\mathcal{O}(10\,\mathrm{TeV})$. This is many orders of magnitude below the highest reheating scale allowed by observations. Measurements of the CMB anisotropies [2] constrain $r < 0.11$, implying that the energy scale at the end of inflation, see eq. (1.61), must be $V_{\mathrm{end}}^{1/4} < 10^{15}\,\mathrm{GeV}$. This is also the upper bound on T_{reh}. At such high energy scales we could ignore GUT-mass particles (approximately) and stringy states, but have to include all other degrees of freedom. Hence, there is a huge theoretical uncertainty regarding the actual model of reheating.

Since there is a great ambiguity regarding the degrees of freedom and their interactions at the high energy scales relevant to reheating we can just focus on the particle content of the Standard Model for simplicity. Ignoring the effects from extensions that account for baryogenesis and the generation of dark matter, one can study the evolution of the Standard Model degrees of freedom during preheating, assuming they were all spectator fields during inflation. Furthermore, coupling non-minimally the Standard Model Higgs field to gravity allows it to play the role of the inflaton field. This model is known as Higgs-inflation [87]. It is quite interesting since in it all couplings of the inflaton to the Standard Model degrees of freedom are known, allowing for a complete calculation of the thermal history of the visible universe. Studies of the non-perturbative preheating dynamics (in the linear approximation) [23, 24] have shown that non-linear effects become important soon after the end of Higgs-inflation and a further detailed numerical investigation is required for the calculation of T_{reh}.

The exploration of extensions of the Standard Model, motivated by e.g., supersymmetry and/or supergravity, can introduce many new degrees of freedom. Unfortunately, they come with new interactions and parameters, many of which are poorly constrained, if at all. The vast landscape of string theory is a good example of the level of theoretical uncertainty one has to deal with when building models of reheating. To make further progress in constraining the particle physics of reheating we should turn to observations. A determination of the exact model of inflation through observations of the CMB could give us some insight into the physical laws governing the dynamics of reheating. Another possibility is the detection of a reheating signal that cannot be mimicked by any inflationary model. The observational consequence of

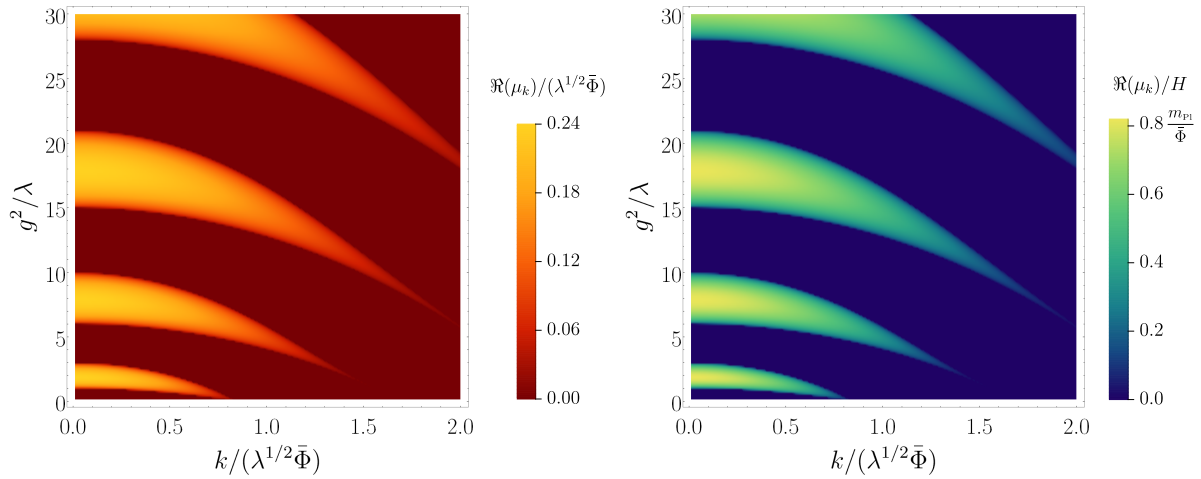

Figure 4.1: The instability chart featuring the real part of the Floquet exponent normalized by the effective inflaton mass (left) and the Hubble rate (right), characterizing the χ particle production rate in the Vanilla model of preheating, $V(\phi,\chi) = \lambda\phi^4/4 + g^2\phi^2\chi^2$, $g^2 > 0$ [88]. In FRW space-time $\bar{\Phi} \propto a^{-1}$ and $k \propto a^{-1}$, implying that co-moving modes do not flow across the chart as the universe expands unlike in Figs. 2.2, 2.3, 2.4. The resonance is virtually unaffected by the expansion of space.

reheating are the subject of the next chapter.

Despite the fact that we do not know the exact particle physics model describing reheating, it is safe to say that in any realistic scenario there will be a large number of scalar fields, fermions, vector fields, and perhaps non-minimal couplings to gravity and operators that are suppressed below some energy cut-off scale. In the rest of this chapter we briefly discuss their effects on various aspects of the non-perturbative linear dynamics of preheating by considering simple toy models. We also talk about some generic models of (p)reheating.

4.1 Scalar fields

Historically, non-perturbative effects during preheating were first studied in the context of scalar field dynamics [10–12, 14]. In Sections 2.2 and 2.3 we also used scalar fields to introduce the concept of resonant particle production. We showed that oscillations of the scalar condensate induce a time-dependence in the effective mass of the daughter scalar fields. Depending on the strength of the interactions, the occupation numbers of the decay products can grow either gradually in narrow momentum ranges for small couplings or in bursts in broad momentum ranges for large couplings, but in both regimes exponentially fast. We showed that this kind of particle production can be understood qualitatively using Floquet theory and, in particular, if the inflaton is massive – in terms of the instability chart of Mathieu equation. In this section we just wish to point out that although it is often enough to approximate the inflaton potential during the oscillatory phase of preheating by Taylor expanding around its minimum to quadratic order, there are models with massless inflatons that do not fall into this category. A famous example is the Vanilla model, $V(\phi,\chi) = \lambda\phi^4/4 + g^2\phi^2\chi^2$. The interesting thing about this model is that the Floquet analysis provides a virtually exact description of the resonant particle production [88]. Essentially, a certain choice of field

and time redefinitions can lead to the absorption of all terms containing the scale factor, $a(t)$, and higher order derivatives of it (provided we ignore the small oscillations in $a(t)$). The expansion of space can be transformed away, converting the equations of motion into Minkowski form. In this case the background equation is strictly periodic, whereas the equation for the field fluctuations is known as the Lame equation. The instability chart of the Lame equation, see Fig. 4.1, describes quite accurately the instabilities in the daughter fields and there is no need for the introduction of any flow lines, unlike the case of the Mathieu equation.

As we discussed in Section 2.3, stochastic resonance arises when we include the background expansion of space (apart from the Vanilla model). The effective masses of the daughter fields vary quasi-periodically with time and are modulated by powers of $a(t)$. The momentum range of unstable modes is increased, at the expense of decreasing the rate of particle production. The same phenomenon is observed if several scalar fields are oscillating at the background level. If any of the ratios of their frequencies is different from one the effective masses of the daughter fields rarely go to zero (non-adiabatic events are rare) and if the ratio is an irrational number, the motion is not periodic at all. When the number of the oscillating background fields is $\gg 1$, we still get resonant particle production, see Section 2.3.3. We note that it is quite natural for a large number of scalar fields to acquire VEVs during inflation in supersymmetric models.

4.2 Fermions

Interactions of the inflaton with fermion fields is a natural thing to consider. As already discussed at the end of Section 3.4, they can have important implications for the last stage of reheating. Interactions of, e.g., Yukawa form, are needed to ensure that any massive remnants of the inflaton decay into pairs of fermions and anti-fermions at late times, making it possible for the universe to become radiation-dominated.

We should point out that while the inflaton condensate oscillates, the fermions acquire a periodically varying mass and this can lead to fermionic preheating [89]. The resonance is not as efficient as in the case with daughter scalar fields, since the Pauli exclusion principle enforces the occupation number of a given mode to be ≤ 1. Nevertheless, the resonance can excite a broad range of modes, enhancing the decay rate in comparison with the standard perturbative estimate. In supergravity models, the gravitino can be non-perturbatively produced during reheating. Thermal production can take place after that as well. The danger of overproducing this massive relic can put constraints on its interactions and $T_{\rm reh}$ [90].

4.3 Gauge fields

Similar to scalars, gauge bosons can be resonantly amplified quite efficiently during preheating. If the inflaton is a gauge singlet, it can be coupled to gauge fields through conformal factors

$$S_{\rm matter} \supset \int d^4x\sqrt{-g}\left[-W_1(\phi)F_{\mu\nu}F^{\mu\nu} - W_2(\phi)\epsilon^{\mu\nu\eta\sigma}F_{\mu\nu}F_{\eta\sigma}\right] , \tag{4.1}$$

without violating the gauge invariance of the action. The first term can lead to very efficient resonant transfer of energy to the massless gauge fields [37] during preheating. The second term violates parity and can generate chiral gravitational waves [91]. The second term naturally arises in models where the inflaton is an axion, e.g., in Natural inflation, with $W_2(\phi) \propto \phi$. Axions are the Goldstone bosons, appearing whenever an axial symmetry is spontaneously broken. An axion possesses an almost exact shift symmetry,

so it naturally couples to total derivative terms such as $\epsilon^{\mu\nu\eta\sigma}F_{\mu\nu}F_{\eta\sigma}$ with $\epsilon^{\mu\nu\eta\sigma}$ the totally anti-symmetric tensor. Note that the mass dimension of both terms in eq. (4.1) is > 4 and they must be suppressed by some energy cut-off.

If the inflaton is charged under a gauge symmetry, the covariant derivative can give rise to novel types of interaction. For instance, if the inflaton is a complex scalar, charged under an Abelian $U(1)$ symmetry, the kinetic term in the action

$$S_{\rm matter} \supset \int d^4x\sqrt{-g}\, D_\mu\phi(D^\mu\phi)^* = \int d^4x\sqrt{-g}\left[\partial_\mu\phi\partial^\mu\phi^* + 2g_A\Im(\phi\partial_\mu\phi^*)A^\mu + g_A^2|\phi|^2A_\mu A^\mu\right] , \tag{4.2}$$

yields a term that couples the complex phase of the inflaton with the gauge fields, in addition to a $g^2\phi^2\chi^2$ type of term. It turns out that the two transverse components of the spatial part of the gauge field appear only in the final term and their evolution during preheating is identical to that of χ and has been studied extensively [28, 92–94]. However, the longitudinal spatial component of the gauge field, the complex phase of the inflaton and A_0 are all coupled through the $2g_A\Im(\phi\partial_\mu\phi^*)A^\mu$ term. Due to the complexity of the interaction, their evolution during preheating used to be approximated or ignored [28, 92–94] until very recently. Our paper [32] provided the first accurate treatment of the resonant particle production of these degrees of freedom, taking into account the redundancy introduced by the gauge freedom. It showed that all approximate treatments were insufficient for capturing the dynamics. The rigorous analysis will be presented in Chapter 8 and examples involving Abelain and non-Abelian gauge fields will be considered.

Preheating of a $U(1)$ gauge field can be applied to the generation of the observed large scale magnetic fields [53]. Conformal couplings like the ones in eq. (4.1) can generate strong magnetic fields soon after the end of inflation [95, 96]. They can act as primordial seeds for the galactic dynamo mechanism which can amplify them to the observed values today [53]. On the other hand, parametric resonance in models with an electrically charged inflaton fail to produce strong enough seed fields [32, 92–94]. It is worth pointing out that at the high energy scales relevant to preheating, the $U(1)$ symmetry of electromagnetism is unified with the weak force, making it necessary to consider the full electroweak gauge theory $SU(2)\times U(1)$ [32, 93]. This is included in Chapter 8.

4.4 Non-minimal couplings to gravity

The inflaton and the rest of the matter fields can have non-minimal couplings to gravity, which can become important at the high energies relevant to inflation and preheating. The simplest interaction one can consider is of the form $\xi\chi^2R$, where χ could be the inflaton or a daughter scalar field, R is the Ricci scalar and ξ is a dimensionless coupling constant. If it was the inflaton, than for field values $\gtrsim m_{\rm Pl}/\sqrt{\xi}$ the expansion of space will be affected by the interaction term, e.g., Higgs-inflation [87]. Otherwise, in general, since R oscillates during preheating, see eq. (1.22), this type of interaction provides a new way for amplifying scalar field fluctuations. If $|\xi R| \sim |\xi|H^2 \gtrsim$ the oscillating effective mass squared of field fluctuations (the mass induced by non-gravitational interactions), the parametric resonance could be affected. And if the gravitational interaction provides the dominant contribution to the effective mass, than it can induce resonant particle production on its own. We note that models with inflaton interaction terms that are linear in R can be studied in the Einstein frame, which is related to the original frame, also known as the Jordan frame, via a conformal transformation. The conformal transformation automatically makes coupling constants time-dependent during preheating. The resonant particle production in the Einstein frame has been studied in

[23, 24] for the Standard Model degrees of freedom, in [97–99] for scalar field fluctuations after multi-field inflation and in [100] for gauge fields.

4.5 Non-conventional interactions

We refer to all operators that have some cut-off scale, $\Lambda_{\rm UV}$, below which they are suppressed, as non-conventional. They can be important during preheating. For instance the non-minimal coupling to gravity discussed in Section 4.4 falls in this category and becomes negligible for field values $\ll m_{\rm Pl}/\sqrt{\xi} \equiv \Lambda_{\rm UV}$. All terms of higher than 4 mass dimension also have a cut-off scale, e.g., the terms in eq. (4.1). If the inflaton is an axion, we can write $W_2(\phi) = \phi/\Lambda_{\rm UV}$; $\Lambda_{\rm UV}$ should be associated with the Peccei-Quinn scale and the gauge fields with the gluons to resolve the Strong CP problem. Another example is the case of non-canonical kinetic terms, $f(\phi/\Lambda_{\rm UV})\partial_\mu\phi\partial^\mu\phi$, with $\lim_{x\to 0} f(x) = 1$. They automatically arise in models with non-minimal coupling to gravity, see Section 4.4, after transformation to the Einstein frame. Similar patterns are observed in models with non-local interactions where the Fourier transformed kinetic terms are non-canonical $f(k/k_{\rm UV})|\partial_\tau\phi_{\mathbf{k}}|^2$. The longitudinal component(s) of gauge field(s) in models with a charged inflaton have kinetic terms of this form with the role of the cut off played by the Compton wavenumber of the gauge field [32], as will be shown explicitly in Chapter 8. Another situation where suppression can occur is when high-derivative interactions are present $(\partial_\mu\phi\partial^\mu\phi)^{1+n}/\Lambda_{\rm UV}^n$, e.g., DBI inflation [101].

A common feature of all non-conventional interactions is that they modify the effective mass of the field fluctuations (after canonical normalization) above the cut off scale. This typically changes the resonance structure – it alters the shapes of the instability bands, but never degrades the efficiency of the resonant particle production. In fact non-conventional interactions can provide an alternative channel for resonant preheating.

4.6 Miscellaneous

Inflation and the subsequent stage of reheating allow for the testing of low energy models of particle physics (e.g., supersymmetric models), constrained by colliders. Even if all fields are negligibly coupled to the inflaton during inflation and reheating, they can still exhibit non-perturbative preheating dynamics or even lead to new phenomenology. Fields that have negligible interactions with the inflaton sector are known as spectator fields.

Light spectator scalar fields during inflation (having masses $\ll H$) develop an effective non-zero vacuum expectation value. Basically, the equation of motion for long-wavelength modes is overdamped during inflation. Once vacuum fluctuations cross outside the Hubble radius, they freeze and their amplitude is determined by the Hubble rate which is approximately constant, yielding a nearly scale-invariant power-spectrum

$$\Delta_\chi^2 \approx \left(\frac{H}{2\pi}\right)^2\Bigg|_{k=aH}. \tag{4.3}$$

The mechanism is similar to the one which generates the curvature perturbations. In fact, the fields evolve identically to the inflaton fluctuations in the spatially-flat gauge in the slow-roll approximation, see eq. (1.40).

As inflation ends the preheating dynamics of the spectator field χ is reminiscent of that of the inflaton. On small scales, comparable to or shorter than the Hubble radius at that time, the field can be approximately separated into background and inhomogeneous parts, i.e., $\chi(\mathbf{x}) = \bar{\chi}+\delta\chi(\mathbf{x})$, with $\bar{\chi}$ drawn from a Gaussian distribution with variance[1] Δ^2_χ, $\delta\chi(\mathbf{x})$ being vacuum sub-horizon fluctuations and $|\mathbf{x}| < H^{-1}$. This is known as the separate universe approach. The homogeneous value of the spectator, $\bar{\chi}$, does not evolve until the Hubble rate becomes smaller than its effective mass. Then it starts to oscillate about the bottom of its potential.

If χ is coupled to other fields, e.g., if it is the Standard Model Higgs, which is coupled to the charged leptons, W and Z bosons, its oscillations can lead to resonant particle production [28], followed by a non-linear period [26, 29], generating a stochastic gravitational wave background [27, 102]. More generally, a complex $\bar{\chi}$, embedded within, e.g., a supersymmetric model, can lead to baryogenesis, according to the Affleck-Dine mechanism [103], and the non-linear dynamics following the resonant stage can involve the formation of Q-balls [104, 105].

If $\bar{\chi}$ eventually comes to dominate the energy budget of the universe (e.g., if it oscillates about a quadratic minimum with its energy being redshifted as $\sim a^{-3}$), it has to decay into radiation to be in agreement with the big-bang nucleosynthesis scenario. If we assume that $\bar{\chi} \neq 0$ on cosmological length scales, than the radiation will have the inhomogeneities of the field imprinted on it. This is the essence of the curvaton scenario [106–108]. In it, the final primordial density fluctuations are generated after inflation and depend on the physics during reheating. Observations of the CMB give a constraint on the combination of the initial fluctuations from inflation and the post-inflationary ones coming from the decay of the curvaton field, χ.

Another possibility for a light spectator, χ, to lead to the generation of primordial curvature perturbations after inflation is if it affects the decay rate, Γ, of the inflaton into other fields. The fluctuations in χ will lead to a spatial variation in Γ. Hence, the final primordial curvature perturbation imprinted on the decay products is a consequence of the spatially varying couplings and any initial fluctuations generated during inflation. This mechanism is known as modulated reheating [109] and was first discussed in the context of Superstring theory models.

[1]Ignoring any scale-dependence in the inflationary power-spectrum due to departures from perfect de Sitter.

Chapter 5

Observational implications and signatures of reheating

'The recent developments in cosmology strongly suggest that the universe may be the ultimate free lunch.'

Alan Guth

Despite being a very important and phenomenologically rich period, reheating and the high-energy physics laws governing it are hard to constrain observationally. Just like inflation and all other epochs preceding recombination, reheating cannot be observed directly, since it is hidden by the opaque thermal baryonic plasma. Similarly to the case of inflation, one should look for observational signatures of reheating that survive thermalization and could be inferred from various cosmological measurements. Inflation predicts the stretch of microscopic quantum fluctuations to super Hubble scales, generating a superhorizon curvature perturbation, which is conserved and eventually imprinted on the CMB. Unfortunately, during the decelerating phase of reheating, co-moving modes re-enter the horizon and only the sub-horizon scales are affected by the non-linear dynamics. The length-scales on which the curvature perturbation is affected are so short, that the change is completely concealed by the later non-linear evolution of cosmic structure, making it impossible (for now) to be inferred from the CMB. Another reason why reheating is difficult to connect with observations is that by the time of BBN at the latest, all Standard Model species must be thermalized, hiding away the details of the earlier stages when they were produced.

Still, reheating can yield signatures, potentially observable in the future. These include the generation of relics and metric perturbations, which could be observed directly. In effect, the early universe takes the role of an accelerator for poor people, allowing us to probe roughly, yet freely, the fundamental physics at otherwise virtually inaccessible energy scales.

Indirect signatures are also possible. For instance, the mapping of co-moving modes between horizon exit during inflation and re-entry at later times depends on the entire expansion history between the two events. Thus, the confirmation of a particular model of inflation can give us information about reheating, e.g., constrain its expansion history. Or vice versa, a better understanding of reheating can reduce the uncertainties in predictions of simple inflationary models.

In the rest of this chapter we discuss different observational implications of reheating, starting with the indirect expansion history effect.

5.1 Expansion history of reheating and the CMB

The expansion history of reheating is largely uncertain. We only know that between the end of inflation and the time the universe thermalizated completely (i.e., achieved chemical and local thermal equilibrium), the mean equation of state is $\int_{t_{\rm end}}^{t_{\rm th}} dt\, w(t)/(t_{\rm th}-t_{\rm end}) \equiv \bar{w}_{\rm int} > -1/3$. This implies various possibilities for $N_\star$ – the number of *e*-folds of expansion before the end of inflation, when the pivot scale crossed outside the Hubble radius, $k_\star = a_\star H_\star$. $N_\star$ can take a range of different values, depending on the expansion history of reheating. Hence, the predictions of any model of inflation have an inherent uncertainty, due to the poorly constraint period of reheating. Before discussing inflationary observables in detail we consider the uncertainties in $N_\star$. Given a co-moving pivot scale that has re-entered the horizon at late times, having some fixed physical wavenumber today, say $k_{\star,{\rm phys0}} = k_\star/a_0$, we discuss how $N_\star$ depends on the details of the inflaton potential, $\bar{w}_{\rm int}$, $\rho_{\rm th}$ and $g_{\rm th}$ – the last two being the energy density and the number of relativistic degrees of freedom at thermalization.

We start with the free parameters

$$N_\star\,,\,\{q_i\}\,, \tag{5.1}$$

where $\{q_i\}$ are the parameters entering the inflaton potential, i.e., $V = V(\{q_i\},\phi)$. By definition

$$N_\star \equiv \ln\left(\frac{a_{\rm end}}{a_\star}\right) = \int_{a_\star}^{a_{\rm end}} d\ln a = \left|\int_{\phi_\star}^{\phi_{\rm end}} d\phi \frac{H}{\dot\phi}\right| \approx \left|\int_{\phi_\star}^{\phi_{\rm end}} \frac{d\phi}{m_{\rm Pl}}\frac{1}{\sqrt{2\epsilon_V}}\right|\,, \tag{5.2}$$

where the last expression follows from eq. (1.18) and the discussion above it. The value of the inflaton at the end of slow-roll inflation, $\phi_{\rm end}$, is to a very good approximation insensitive to the initial conditions and the inflationary dynamics, implying $\phi_{\rm end} = \phi_{\rm end}(\{q_i\})$.[1] Hence, $\phi_\star = \phi_\star(N_\star, \phi_{\rm end}, \{q_i - 1\}) = \phi_\star(N_\star, \{q_i\})$. This and eq. (1.61) imply that the measured magnitude of curvature perturbation $A_{\rm s} = A_{\rm s}(\{q_i\},\phi_\star) = A_{\rm s}(\{q_i\}, N_\star)$, from where we can determine one of the potential parameters, e.g., $q_1 = q_1(\{q_i - 1\}, N_\star, A_{\rm s})$. Given all that we can write

$$V_\star = V_\star(\{q_i\},\phi_\star) = V_\star(\{q_i - 1\}, N_\star, A_{\rm s})\,. \tag{5.3}$$

Note that for a single-parameter model, e.g., $V = m^2\phi^2/2$, this implies a one-to-one correspondence between $V_\star$ and $N_\star$ (and likewise for derivatives of $V_\star$), since $A_{\rm s}$ is known from observations. For a two-parameter model of inflation, e.g., $V = \Lambda^4 \tanh^2(\phi/M)$, there is a one-parameter set of solutions, etc.

To find $N_\star$ and $V_\star$ (given $\{q_i - 1\}$) we need to match the pivot scale today to the time it left the horizon, i.e., $k_\star/(a_0H_0) = (a_\star H_\star)/(a_0H_0)$. Taking the log of both sides of this equality, one can show that

$$N_\star = 66.89 - \ln\frac{k_\star}{a_0H_0} + \frac{1}{4}\ln\frac{V_\star^2}{m_{\rm Pl}^4\rho_{\rm end}} + \frac{1}{12}\ln\left[\frac{1}{g_{\rm th}}\left(\frac{\rho_{\rm th}}{\rho_{\rm end}}\right)^{\frac{1-3\bar{w}_{\rm int}}{1+\bar{w}_{\rm int}}}\right]\,, \tag{5.4}$$

making the only assumption that entropy, $s \sim gT^3$, is conserved, $sa^3 = {\rm const}$, after thermalization, $a > a_{\rm th}$. The derivation is given in Section 6.4.1. Since $\rho_{\rm end} = \rho_{\rm end}(\{q_i\})$, after substituting $V_\star$ from eq. (5.3)

[1] In fact, the end of inflation, $\ddot{a} = 0$, is near $\epsilon_V = 1$, implying that $\phi_{\rm end} \approx \phi_{\rm end}(\{q_i - 1\})$, i.e., the number of parameters is reduced by one due to the cancellation inside the squared brackets in eq. (1.18).

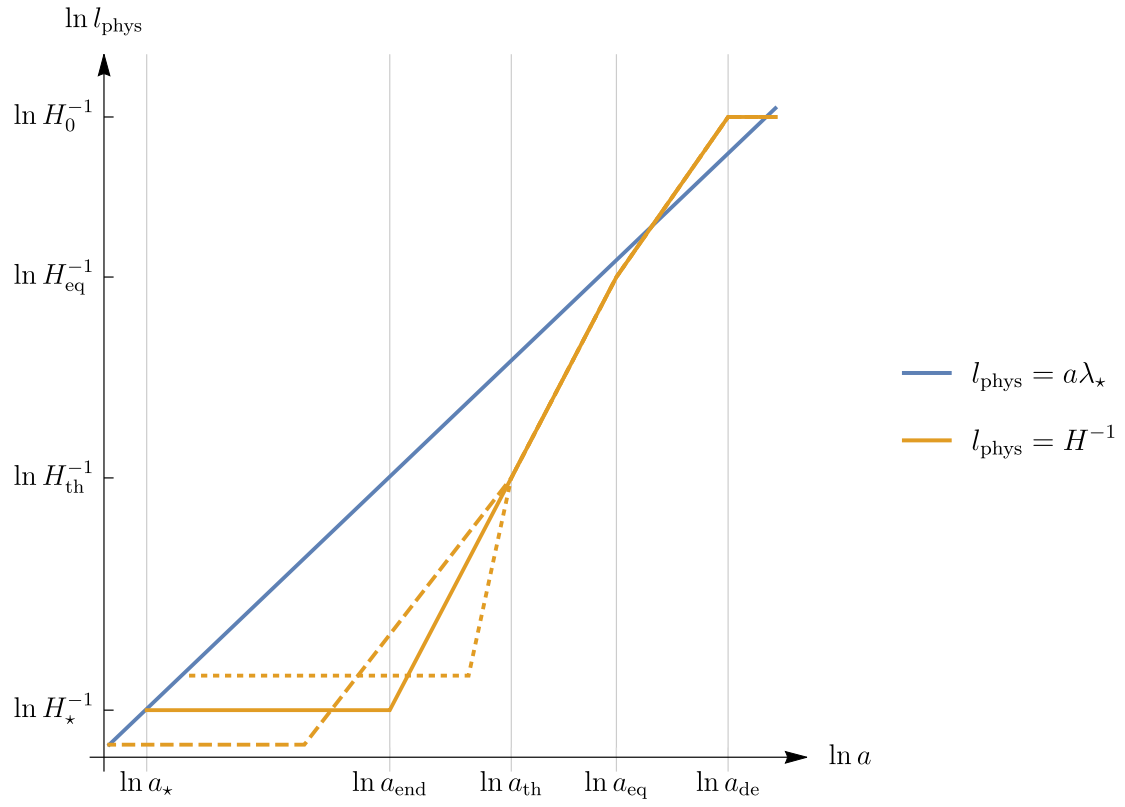

Figure 5.1: The figure illustrates how the uncertainty in the expansion history of reheating is translated on $N_\star = \ln(a_{\rm end}/a_\star)$ – the number of e-folds of expansion before the end of inflation when the pivot scale crossed outside the Hubble radius, H^{-1}. For simplicity we fix $\rho_{\rm th}$ and $a_{\rm th}$, and vary only the mean equation of state of reheating, $w = \bar{w}_{\rm int}$ (reheating takes place while $a_{\rm th} > a > a_{\rm end}$). We consider single-parameter models of inflation, e.g., $V = m^2\phi^2/2$, for which $N_\star = N_\star(\bar{w}_{\rm int})$ and $V_\star = V_\star(N_\star(\bar{w}_{\rm int})) = V_\star(\bar{w}_{\rm int})$. This implies that choosing an energy scale of inflation, $V_\star$, uniquely determines $N_\star$ and $\bar{w}_{\rm int}$, unlike in multi-parameter models of inflation where we have additional degrees of freedom, see Fig. 5.2. For plotting purposes, we have approximated the inflationary and the dark energy stages as de Sitter expansions, and the two periods preceding and following radiation-matter equality as radiation and matter dominated, respectively. None of the conclusions depend on these simplifications. Note that $\epsilon_H \equiv d(\ln H^{-1})/d(\ln a) = 3(1+w)/2$.

into eq. (5.4), we find that

$$N_\star = N_\star\left(\{q_i - 1\}, A_{\rm s}, \rho_{\rm th}^{\frac{1-3\bar{w}_{\rm int}}{1+\bar{w}_{\rm int}}}/g_{\rm th}\right) . \tag{5.5}$$

Reheating affects $N_\star$ only through the specific combination of quantities appearing in the last argument. Note that the $g_{\rm th}$ dependence contains the information about the time of thermaliztion, $a_{\rm th}$. Essentially, the conservation of entropy implies that $g_{\rm th} = ((\pi^2/30)g_0^{4/3}T_0^4/\rho_{\rm th})^3(a_{\rm th}/a_0)^{12}$, where $T_0 = 2.725\,{\rm K}$ and the effective number of relativistic degrees of freedom in entropy is $g_0 = 43/11$. In other words, $N_\star$ depends on a combination of the energy scale, $\rho_{\rm th}$, and the time, $a_{\rm th}$, of thermalization, as well as the mean equation of state, $\bar{w}_{\rm int}$, of reheating (holding for $a_{\rm th} > a > a_{\rm end}$). We depict this effect in Fig. 5.1 for a single-parameter model of inflation, e.g., $V(m,\phi) = m^2\phi^2/2$. For simplicity, we fix $\rho_{\rm th}$ and $a_{\rm th}$ (fixing these two quantities fixes $g_{\rm th}$) and vary only $\bar{w}_{\rm int}$. We plot the Hubble radius, H^{-1}, in orange and the

physical wavenumber corresponding to the pivot scale, $a\lambda_\star$, in blue. Both have some fixed values today, H_0^{-1} and $a_0\lambda_\star$, respectively. For plotting purposes, we approximate the dark energy dominated universe today and inflation as stages of de Sitter expansion, i.e, for $a > a_{\rm de}$ and $a < a_{\rm end}$, $H = H_0 = {\rm const}$ and $H = H_\star = \sqrt{V_\star/3}/m_{\rm Pl} = {\rm const}$, respectively. We also assume $w = 0$ between radiation-matter equality and dark energy domination, $a_{\rm de} > a > a_{\rm eq}$, and $w = 1/3$ between thermalization and radiation-matter equality $a_{\rm eq} > a > a_{\rm th}$. Note that for the single-parameter $m^2\phi^2/2$ inflation, $\{q_i - 1\} \in \varnothing$. Given that $A_{\rm s} = 2.2 \times 10^{-9}$, eq. (5.5) implies $N_\star = N_\star(\bar{w}_{\rm int})$. This is shown in the figure with the three orange solid, dashed and dotted lines corresponding to three different choices of $\bar{w}_{\rm int}$. Note that we also have $V_\star = V_\star(N_\star(\bar{w}_{\rm int})) = V_\star(\bar{w}_{\rm int})$, see eq. (5.3). Hence, in single-parameter models of inflation, $\bar{w}_{\rm int}$ uniquely defines $V_\star$ and $N_\star$ (provided $\rho_{\rm th}$ and $a_{\rm th}$ are fixed). This is a peculiar feature of single-parameter models. In multi-parameter models of inflaton there is a degeneracy, as we discuss below. Note that even in the single-parameter models of inflation, the uncertainty in the equation of state of reheating translates into an uncertainty in the energy scale of inflation. This could be turned the other way round – a possible confirmation of a single-parameter model of inflation with a given $V_\star$ uniquely determines $N_\star$ and hence $\bar{w}_{\rm int}$ if $\rho_{\rm th}$ and $a_{\rm th}$ are known (if they are not, it at least uniquely determines the combination of $\rho_{\rm th}$, $a_{\rm th}$ and $\bar{w}_{\rm int}$ on which $N_\star$ depends). So pinning down the model of inflation could give us information about reheating.

We now repeat the analysis for a two-parameter model of inflation, e.g., $V(M, \Lambda, \phi) = \Lambda^4 \tanh^2(\phi/M)$. This time, we have one additional degree of freedom, i.e., $\{q_i - 1\} = q_1$. For fixed $\rho_{\rm th}$ and $a_{\rm th}$ this implies $N_\star = N_\star(q_1, \bar{w}_{\rm int})$ and $V_\star = V_\star(q_1, N_\star(q_1, \bar{w}_{\rm int})) = V_\star(q_1, \bar{w}_{\rm int})$. The dependence is depicted in Fig. 5.2. As mentioned above, unlike the single-parameter models, multi-parameter models possess additional degeneracy due to the extra parameters. It explains the additional lines in Fig. 5.2. Essentially, there is not a one-to-one correspondence between $V_\star$ and $N_\star$, i.e., a particular $V_\star$ gives a range of $N_\star$. Note that in two-parameter models, having fixed $V_\star$ and $N_\star$, uniquely determines $\bar{w}_{\rm int}$. Conversely, one has to measure or calculate $V_\star$ and $\bar{w}_{\rm int}$ separately, to uniquely determine $N_\star$ in two-parameter models of inflation.

Hence, the uncertainty in the expansion history of reheating leads to an uncertainty in $N_\star$. This has consequences for spectral observables such as $n_{\rm s}$ and r, see eq. (1.61). The slow-roll potential parameters at the time of horizon exit are $\epsilon_{V\star} = \epsilon_{V\star}(\phi_\star, \{q_i - 1\})$ and $\eta_{V\star} = \eta_{V\star}(\phi_\star, \{q_i - 1\})$. The reason for having one fewer q_i is because we take ratios of the inflaton potential and corresponding derivatives in eq. (1.18). Substitution for $\phi_\star = \phi_\star(N_\star, \{q_i\})$ implies $\epsilon_{V\star} = \epsilon_{V\star}(N_\star, \{q_i\})$ and $\eta_{V\star} = \eta_{V\star}(N_\star, \{q_i\})$. However, the measured magnitude of curvature perturbation reduces the number of free parameters by one, e.g., $q_1 = q_1(\{q_i - 1\}, N_\star, A_{\rm s})$. The first two expressions in eq. (1.61) then imply

$$n_{\rm s} = n_{\rm s}(N_\star, \{q_i - 1\})\,, \qquad r = r(N_\star, \{q_i - 1\})\,. \tag{5.6}$$

In single-parameter models of inflation, $n_{\rm s}$ and r are only functions of $N_\star$. The reheating related uncertainty in $N_\star$ translates into a bar in the $n_{\rm s}$-r plane, as shown in Fig. 5.3 for $m^2\phi^2/2$ inflation. In two-parameter models of inflation, $n_{\rm s}$ and r are functions of $N_\star$ and an additional degree of freedom. This transforms the bars in the $n_{\rm s}$-r plane into bands as shown in Fig. 5.4 for $\Lambda^4 \tanh^2(\phi/M)$ inflation.

5.2 Relics

The out-of-equilibrium dynamics of reheating may lead to the generation of various relics. These include stable ones, e.g., topological defects, that have not been observed yet, tantalizing ones, e.g., dark matter and

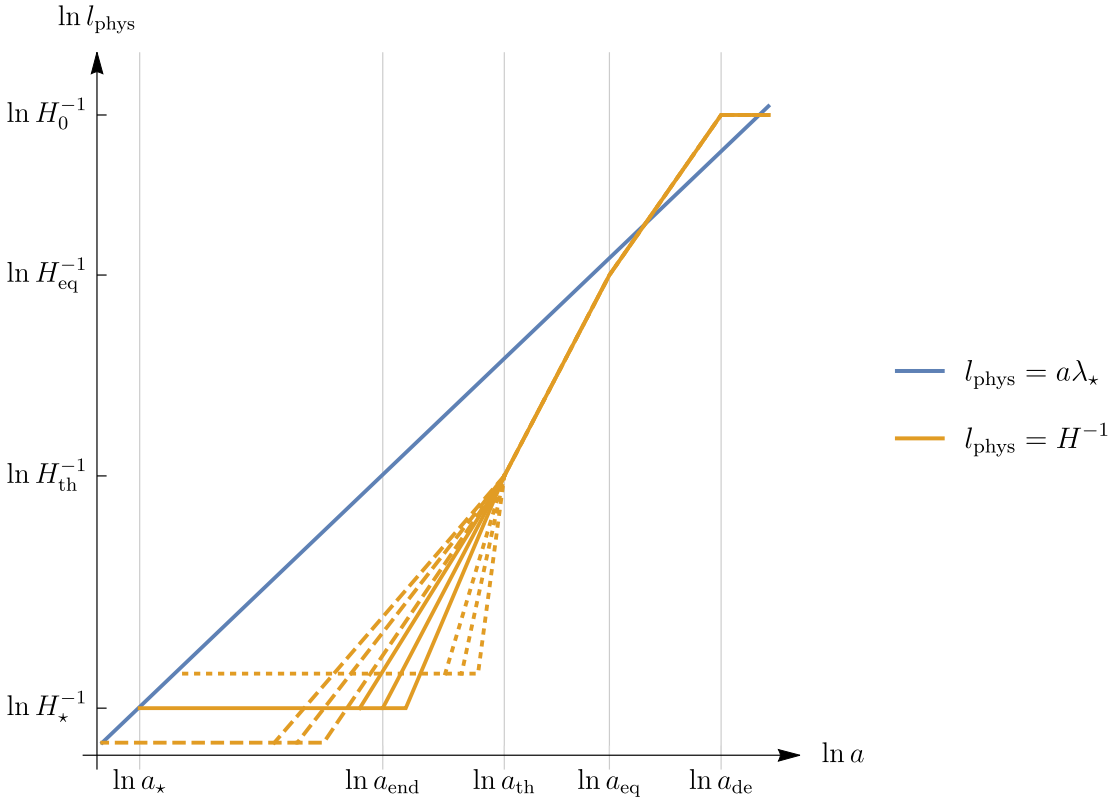

Figure 5.2: Same as Fig. 5.1, but for two-parameter models of inflation, e.g., $V = \Lambda \tanh^2(\phi/M)$. The extra parameter in the inflaton potential introduces an additional degree of freedom, $N_\star = N_\star(q_1, \bar{w}_{\rm int})$ and $V_\star = V_\star(q_1, N_\star(q_1, \bar{w}_{\rm int})) = V_\star(q_1, \bar{w}_{\rm int})$. This means that unlike in the single-parameter models of inflation, choosing an energy scale of inflation, $V_\star$, allows for a range of $N_\star$ and $\bar{w}_{\rm int}$.

primordial magnetic fields, for which there is some experimental evidence, and observed ones, such as the baryon asymmetry. In the following we briefly talk about each of these applications of reheating.

5.2.1 Baryon asymmetry

Models of baryogenesis try to explain the observed baryon-to-photon ratio

$$\eta \equiv \frac{n_b}{n_\gamma} \approx 6 \times 10^{-10}\,, \tag{5.7}$$

where $n_b = n_B - n_{\bar{B}}$ and n_γ are the (net) number densities of baryons and photons, respectively. There are many high-energy physics models that explain the value of η with some dynamical mechanism, none of which is singled out by observational tests. It is indeed very interesting to try to connect baryogenesis to reheating. We should point out that since the net number of baryons in the late universe, certainly after BBN, is conserved, then $n_b \propto a^{-3}$. Furthermore, since after the epoch of electron-positron annihilation, which also happened around BBN, $n_\gamma \propto a^{-3}$, this means that $\eta = \text{const}$. At earlier times η was still conserved, apart from the moments when a relativistic particle species went out of thermal equilibrium and

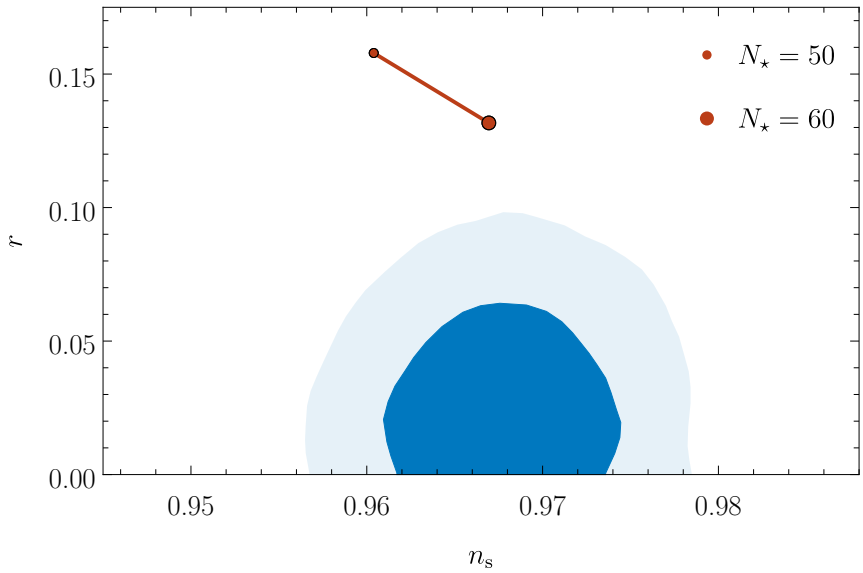

Figure 5.3: Red: the predictions for n_s and r in $V = m^2\phi^2/2$. Since this is a single-parameter model of inflation, $n_\mathrm{s} = n_\mathrm{s}(N_\star)$ and $r = r(N_\star)$, hence the bar-like prediction for $50 < N_\star < 60$. Here the inflaton mass is not a free parameter; instead $m = m(N_\star, A_\mathrm{s})$. Light and dark blue: the 68 % and 95 % confidence level regions for n_s and r from Planck and other data sets [2].

became non-relativistic – then it changed in a step-like manner by a factor that is determined by the ratio of the old and new number of relativistic degrees of freedom. However, what remained always constant in thermal equilibrium was the ratio n_b/s which is $\sim \eta_0$. The Standard Model of particle physics ensures the net conservation of baryons and cannot explain why there are so many photons (or so much entropy) per baryon today, assuming that the universe started in a natural state with no baryons $n_B = n_{\bar{B}} = 0$, or with no net baron number, $n_b = 0$. To explain the puzzling observed asymmetry in the amount of matter and antimatter, one has to invoke physics beyond the Standard Model. It must allow for physical processes that meet the following three criteria, known as Sakharov's conditions [110]: (i) non-conservation of the baryon number, b; (ii) violation of C and CP invariance; (iii) departure from thermal equilibrium. While condition (i) is obvious – to generate a net baryon number starting from $n_b = 0$ we need reactions that violate baryon number conservation – it is not enough. Condition (ii) is necessary to ensure different decay rates into baryons and anti-baryons. Consider a baryon number violating reaction $X \to Y + Z$. The violation of C invariance ensures that the rates of the reaction and its charge conjugated counterpart are different

$$\Gamma(X \to Y + Z) \neq \Gamma(\bar{X} \to \bar{Y} + \bar{Z})\,, \tag{5.8}$$

i.e., the b violating process that creates more baryons than anti-baryons is not counterbalanced by its conjugate that creates more anti-baryons than baryons. Taking into account the helicity of the baryons, e.g., a reaction of the form $X \to q_L + q_L$, CP violation ensures that $\Gamma(X \to q_L + q_L) \neq \Gamma(\bar{X} \to \bar{q}_R + \bar{q}_R)$ and $\Gamma(X \to q_R + q_R) \neq \Gamma(\bar{X} \to \bar{q}_L + \bar{q}_L)$. Otherwise, the amount of produced left-handed baryons equals the amount of produced right-handed anti-baryons and vice versa, implying that the net baryon number does

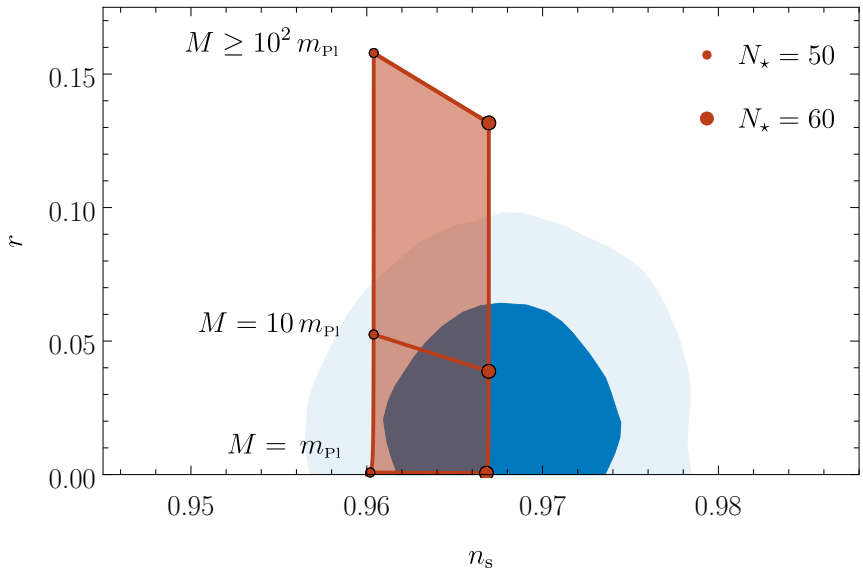

Figure 5.4: Same as Fig. 5.3, but the predictions for $n_{\rm s}$ and r are for $V = \Lambda^4 \tanh^2(\phi/M)$. Since this is a double-parameter model of inflation, we have an additional degree of freedom in comparison with single-parameter models, see Fig. 5.3. This means we can write $n_{\rm s} = n_{\rm s}(M, N_\star)$ and $r = r(M, N_\star)$, with M being a free parameter and $\Lambda = \Lambda(N_\star, A_{\rm s}, M)$. Hence, the wide band prediction for $50 < N_\star < 60$.

not change

$$\Gamma(X \to q_L + q_L) + \Gamma(X \to q_R + q_R) = \Gamma(\bar{X} \to \bar{q}_L + \bar{q}_L) + \Gamma(\bar{X} \to \bar{q}_R + \bar{q}_R)\,, \tag{5.9}$$

despite C invariance being violated and (i). The reason for condition (iii) is slightly less obvious. It comes from the fact that the equilibrium number densities of particles and anti-particles depend on their chemical potentials. In thermal equilibrium $\mu_{q_L} = -\mu_{\bar{q}_L}$, etc (recall that baryons and anti-baryons can annihilate into photons). However, since the baryon number is not conserved by the interactions, $\mu_{q_L} = \mu_{\bar{q}_L} = 0$. Hence, particles and anti-particles in thermal equilibrium have equal number densities despite conditions (i) and (ii).

Many high-energy physics models that satisfy the three criteria have been put forward to explain the observed baryon asymmetry. GUT-scale baryogenesis models rely on superheavy particles (with GUT-scale masses) decaying into baryons through C and CP violating reactions. As discussed in Section 2.5, such superheavy particles can be produced non-perturbatively after inflation, out of thermal equilibrium, making (p)reheating the ideal setting for these models. Leptogenesis, the generation of a number asymmetry, $n_l = n_L - n_{\bar{L}}$, between leptons and antileptons, can also account for the observed baryon-to-entropy ratio. The lepton number, l, can be converted into the baryon number via Standard Model sphalerons – transitions between degenerate topologically different $SU(2)$ electroweak gauge field configurations – they become suppressed at temperatures $< 300\,\text{GeV}$. Essentially, for sphaleron transitions (you can think of them as reactions) $b - l = \text{const}$, but $b \neq \text{const}$ and $l \neq \text{const}$. Thus, if one starts with $n_b = 0$, by the end of the transition it is converted into $n_b \sim n_{b-l}$. This is an example of electroweak baryogenesis

and preheating can provide a way for generating the initial lepton asymmetry. Another possibility is the Affleck-Dine baryogenesis mechanism. It involves a complex scalar field, X, that carries a baryon number and whose non-equilibrium dynamics does not conserve b. The field normally starts in a spatially homogeneous configuration in which invariance under C and CP may or may not be spontaneously broken. Then it evolves into a non-thermal configuration, in which the C and CP symmetries are spontaneously broken, with a final non-zero b, which is eventually converted into baryons. A version of this model where the inflaton plays the role of the scalar field is the subject of Chapter 7. There we show that the non-linear dynamics of reheating can play an important role for the prediction of η [52].

5.2.2 Magnetic fields

Magnetic fields are abundant in our universe [53]. They have been observed in galaxies $B_{10-10^2\,\mathrm{kpc}} \sim 10^{-5}\,\mathrm{G}$ and galaxy clusters $B_{0.1-1\,\mathrm{Mpc}} \sim 10^{-6}\,\mathrm{G}$. There is a (conservative) lower bound on the strength of magnetic fields with cosmic scale correlation lengths $B_{>1\,\mathrm{Mpc}} > 10^{-17}\,\mathrm{G}$. While galactic fields can be accounted for by the amplification of seed fields via the dynamo mechanism [111], the origin of those seeds, as well as the large-correlation-length fields that are unaffected by magnetohydrodynamic processes remains an open problem. It can be explained by a primordial magnetic field component. CMB observations have put upper bounds on it $B^{\mathrm{prim}}_{1\,\mathrm{Mpc}} < 10^{-9}\,\mathrm{G}$ [112], whereas the seed amplitude needed for the dynamo mechanism is model and scale-dependent.

It is difficult to connect the causal non-linear dynamics of reheating with the large scale magnetic fields. However, the linear stage of preheating can provide the perfect setting for magnetogenesis. Low momentum magnetic field modes can be resonantly amplified [92] or undergo tachyonic instabilities [95, 96]. The biggest challenge is to avoid back-reaction of small-scale modes before low-momentum modes have been sufficiently amplified [32, 113]. Tachyonic instability can be achieved quite easily. A conformal coupling of the form $\mathcal{L}_{\mathrm{Maxwell}} = -f(\tau)F_{\mu\nu}F^{\mu\nu}/4$ yields

$$\mathcal{A}_k^{T\prime\prime} + \left(k^2 - \frac{f''}{f}\right)\mathcal{A}_k^T(\tau) = 0\,, \tag{5.10}$$

where $\mathcal{A}_k^T(\tau) = a(\tau)f(\tau)A_k^T(\tau)$ are the canonically-normalized transverse (Fourier) modes. f tends to 1 at late times, but if it is $\propto \tau^\alpha$ earlier on, certain choices of α and the magnitude of f could lead to a successful magnetogenesis via tachyonic preheating [114].

5.2.3 Miscellaneous

In many dark matter models, the relic abundance is determined by the self-interactions of a thermalized dark matter sector. After the inflaton resonantly excites the Standard Model and dark matter degrees of freedom during preheating, the two sectors can attain different equilibrium temperatures – a phenomenon known as asymmetric reheating, which can be sensitive to the non-linear dynamics of reheating [115]. A detection of a temperature difference can put constraints on the inflaton mass and couplings [116].

The non-linear dynamics of reheating can lead to the formation of stable topological defects, see Section 3.2, for which there are no observational evidence [1]. Overproduction of such defects could overclose the universe or affect CMB anisotropies. In fact, CMB measurements provide the tightest constraints [1].

5.3 Metric fluctuations

Departures from the FRW universe described by matter and metric perturbations are at the heart of modern cosmology. Within current observational limits, an adiabatic curvature perturbation (a scalar mode) with Gaussian statistics can explain the measured CMB temperature anisotropies [1]. Furthermore, the detection of polarization B-modes generated by primordial tensor fluctuations in the metric (gravitational waves) is one of the main goals of the upcoming Stage-4 CMB experiments [117]. The linear and non-linear stages of reheating can give rise to gravitational waves, as well as entropic and non-Gaussian contributions to the curvature perturbation. Their non-detection constrains different reheating scenarios, as we discuss in the remainder of this section.

5.3.1 Gravitational waves

Shortly after it was appreciated that non-perturbative particle production during preheating can lead to the fragmentation of the inflaton condensate, it was shown that the non-linear dynamics can give rise to a stochastic gravitational wave background [118] in addition to the one generated during slow-roll inflation. Unlike the gravitational waves from inflation [119], whose origin is quantum mechanical and power-spectrum scale-invariant, the gravitational waves from reheating are sourced by the classical evolution of inhomogeneities on sub-horizon scales and their power-spectrum is strongly peaked around a single frequency. Typically, the frequency of the peak is determined by the fragmentation lengthscale, which can be estimated from the linear analysis of preheating. Taking into account the expansion of the universe between reheating and today, one can show, see Section 6.4.3 and [17],

$$f_0 \sim \beta^{-1}\sqrt{\frac{H_{\rm br}}{m_{\rm Pl}}} \times 4\times 10^{10}\,{\rm Hz}\,, \qquad \Omega_{\rm GW,0} \sim 10^{-6}\beta^2\,, \tag{5.11}$$

where f_0 and $\Omega_{\rm GW,0}$ are the peak frequency and gravitational energy density per logarithmic frequency interval normalized by the critical energy density, respectively. Both quantities are evaluated today. $H_{\rm br}$ is the Hubble rate at back-reaction – the time when most of the signal is generated, and $\beta H_{\rm br}^{-1}$ gives the physical wavelength of the excited mode causing the back-reaction on the condensate. Typically, $\beta = \mathcal{O}(10^{-2} - 10^{-3})$, thus for efficient preheating after GUT-scale inflation $f_0 \sim 10^{10} - 10^{11}\,{\rm Hz}$ and $\Omega_{\rm GW,0} \sim 10^{-10} - 10^{-12}$. These frequencies lie above the highest frequency ranges $10^3 - 10^4\,{\rm Hz}$ of planned gravitational wave detectors [120]. Decreasing the back-reaction energy scale drives the peak frequency towards the observable range, but the small amplitude of the signal is outside the reach of any of the upcoming gravitational wave observatories.

When the inflaton condensate fragments as a result of the resonant particle production of light scalar fields, the gravitational wave background can get tiny modulations on large scales [121, 122]. In addition to the prominent peak corresponding to the fragmentation (sub-horizon) lengthscale, the gravitational wave power-spectrum features a small component on low frequencies, too. The latter is a consequence of the superhorizon scale-invariant power-spectrum of light degrees of freedom developed during inflation, see eq. (4.3), which can be interpreted as the light fields having non-zero vevs that vary between different Hubble patches as discussed in Section 4.6 (recall that individual, causally disconnected, patches evolve independently of each other). The preheating and subsequent non-linear dynamics, including the amplitude of the generated gravitational waves, can be sensitive to these vevs, leading to a super-horizon modulation of the stochastic gravitational wave background. When a light scalar remains a spectator during inflation

and reheating, i.e., remains decoupled from the inflaton, similar effects are observed if it is allowed to decay non-perturbatively. This was shown for the gravitational waves produced out of the resonant decay of the Standard Model Higgs into W and Z bosons and their subsequent non-linear evolution [27], assuming no coupling between the inflaton and the Standard Model sector.

Stochastic gravitational wave backgrounds from reheating with additional features can be generated as a consequences of the formation of defects [123] and non-topological solitons [44, 81, 82]. Even if non-linear effects never become important during reheating, different expansion histories affect the spectrum of the gravitational wave background generated during inflation [124].

5.3.2 Non-Gaussianities

Scalar metric perturbations can also be generated during reheating. While the adiabatic curvature perturbations are unaffected by reheating, see eq. (1.54) and the subsequent discussion, the generation of an entropy (or isocurvature) perturbation, $\mathcal{S}$, during reheating could modify the total curvature perturbation, $\mathcal{R}$. A significant growth of super-Hubble modes of $\mathcal{R}$ occurs if on these scales $\Delta^2_{\mathcal{S}} \gtrsim \Delta^2_{\mathcal{R}}$ [16]. However, in models with interacting fields (prone to peheating), e.g., $V = \lambda\phi^4/4 + g^2\phi^2\chi^2/2$, the super-Hubble power-spectra at the end of slow-roll single-field inflation are $\Delta^2_{\mathcal{S}} \ll \Delta^2_{\mathcal{R}} \sim 10^{-9}$, where $\mathcal{S} = (H/\dot{\phi})\chi$ [15, 69]. Even if the entropy perturbation is resonantly amplified during preheating, back-reaction takes place while on super-Hubble scales $\Delta^2_{\mathcal{S}} \lesssim \Delta^2_{\mathcal{R}}$ [43] and the observationally-relevant part of the power-spectrum of $\mathcal{R}$ is affected weakly (at most).

On the other hand, important statistical properties of the curvature perturbation, such as the bispectrum of its non-Gaussianities [125, 126], can be affected significantly by the resonant entropy production during preheating and the subsequent non-linear dynamics. The same mechanism responsible for large-scale modulations in the gravitational wave spectrum from preheating (see the above discussion of gravitational waves) also leads to strong non-Gaussianities in the curvature perturbation [43]. Essentially, extreme sensitivity is shown to the vevs of light fields within individual Hubble patches by the expansion of these patches. The latter is equivalent to the curvature perturbation, implying, e.g.,

$$\mathcal{R}(\mathbf{x}) = \mathcal{R}_{\rm G}(\mathbf{x}) + F_{\rm NL}\left(\chi_{\rm G}(\mathbf{x})\right) , \tag{5.12}$$

where $\mathcal{R}_{\rm G}$ is the standard nearly Gaussian adiabatic mode from single-field slow-roll inflation and the last term comes from the back-reaction and non-linear dynamics following the resonant amplification of the nearly Gaussian and scale-invariant (at the end of inflation) $\chi_{\rm G}$, see eq. (4.3). As shown in [43], the transfer function $F_{\rm NL}$ is highly non-linear and describes non-Gaussianities very different from the standard (weak) local ones

$$\mathcal{R}(\mathbf{x}) = \mathcal{R}_{\rm G}(\mathbf{x}) + \frac{3}{5} f_{\rm NL}(\mathcal{R}^2_{\rm G}(\mathbf{x}) - \langle\mathcal{R}^2_{\rm G}(\mathbf{x})\rangle) . \tag{5.13}$$

The $F_{\rm NL}$ term can in principle lead to non-Gaussian components that could be observable in the CMB [43] and their non-detection [127] constrains preheating scenarios. Other reheating scenarios that lead to potentially observable levels of non-Gaussianity include curvaton reheating (where curvature perturbations are generated by the decay of a slightly inhomogeneous curvaton field after inflation) and modulated reheating (where curvature perturbations are generated due to the dependence of the decay rate of the inflaton on the local value of a spatially varying field). Evolution of non-Gaussianity during reheating after multi-field inflation was studied in [128, 129].

We should point out that the modification of large-scale curvature perturbations during preheating is consistent with causality, since it involves no transfer of energy across super-Hubble scales. Entropy perturbations are simply resonantly amplified and then converted into curvature perturbations.[2]

Even when the reheating dynamics is perturbative and no strong resonances take place, the local non-Gaussianity prediction in single-field inflationary scenarios [130]

$$f_{\rm NL} \sim \frac{n_{\rm s}-1}{4}\,, \tag{5.14}$$

depends on the expansion history of reheating, see eqs. (5.5) and (5.6).

[2]Conversely, if during reheating all particle species enter thermal equilibrium, having a common temperature and vanishing chemical potentials, the super-horizon curvature perturbations become purely adiabatic and no isocurvature perturbations are present at late times.

Part II

Expansion history after inflation

As discussed in Section 5.1, the post-inflationary expansion history can affect observational predictions of inflationary models. In this part of the thesis, we present a study of the post-inflaionary dynamics in a broad class of observationally favoured models of inflation aimed at reducing the model dependence in the reheating epoch and the uncertainty in inflationary and post-inflationary observables.

Chapter 6

Self-resonance after inflation: oscillons, transients and radiation domination

Abstract

Homogeneous oscillations of the inflaton after inflation can be unstable to small spatial perturbations even without coupling to other fields. We show that for inflaton potentials $\propto |\phi|^{2n}$ near $|\phi| = 0$ and flatter beyond some $|\phi| = M$, the inflaton condensate oscillations can lead to self-resonance, followed by its complete fragmentation. Using detailed numerical simulations, we find that for non-quadratic minima ($n > 1$), shortly after back-reaction, the equation of state parameter, $w \to 1/3$. If $M \ll m_{\rm Pl}$, radiation domination is established within less than an *e*-fold of expansion after the end of inflation. In this case self-resonance is efficient and the condensate fragments into transient, localised spherical objects which are unstable and decay, leaving behind them a virialized field with mean kinetic and gradient energies much greater than the potential energy. This end-state yields $w = 1/3$. When $M \sim m_{\rm Pl}$ we observe slow and steady, self-resonace that can last many *e*-folds before back-reaction eventually shuts it off, followed by fragmentation and $w \to 1/3$. We provide analytical estimates for the duration to $w \to 1/3$ after inflation, which can be used as an upper bound (under certain assumptions) on the duration of the transition between the inflationary and the radiation dominated states of expansion. This upper bound can reduce uncertainties in CMB observables such as the spectral tilt, $n_{\rm s}$, and the tensor-to-scalar ratio, r. For quadratic minima ($n = 1$), $w \to 0$ regardless of the value of M. This is because when $M \ll m_{\rm Pl}$, long-lived oscillons form within an e-fold after inflation, and collectively behave as pressureless dust thereafter. For $M \sim m_{\rm Pl}$, the self-resonance is inefficient and the condensate remains intact (ignoring long-term gravitational clustering) and keeps oscillating about the quadratic minimum, again implying $w = 0$. Finally, we discuss the likelihood of (primordial) black hole formation seeded by the oscillons and the unstable spherical objects, as well as the role of the fragmented condensate as a gravitational wave source.

6.1 Introduction

Inflationary cosmology [3, 4, 6, 131] provides a consistent framework for calculating the initial conditions responsible for the observed temperature fluctuations in the cosmic microwave background [2]. However, there is a gap in our understanding of how inflation ends and ultimately leads to a radiation-dominated, thermal universe before the production of light elements. The poorly constrained post-inflationary equation of state of the universe and the duration before radiation domination influence the interpretation of inflationary observables and the reheating temperature, $T_{\rm th}$, [45–47, 51, 132–142]; they affect predictions for baryogenesis and primordial relics [38, 143, 144].

In this chapter we calculate the equation of state parameter w soon after the end of inflation by accounting for the full non-linear dynamics of the inflaton field using 3+1 dimensional lattice simulations. Using our results, we can calculate an upper bound on the duration to radiation domination. Under the assumption of perturbative decay to other massless fields, this upper bound reduces the uncertainty in the interpretation and calculation of inflationary and post-inflationary observables such as $n_{\rm s}$ and r. Non-perturbative decay to light daughter fields is unlikely to change our results, though we cannot show this exhaustively.

The equation of state for oscillating *homogeneous* condensates in an expanding universe has been well understood since the 1980's [62]; however, general results for the cases where the scalar field undergoes significant fragmentation are not easily found in the literature. Detailed earlier works on the equation of state including non-linear dynamics certainly exist, e.g., [35], but are usually limited to quadratic and quartic inflaton potentials coupled to light fields. We allow for general shapes of the inflaton potential, ignore couplings to other light fields in our simulations, but include them in the bounds on the duration to radiation domination.

Our detailed studies of the nature of the self-resonance and the post-inflationary evolution of the inflaton reveal various behaviours in different regions in the parameter space. When $M \sim m_{\rm Pl}$, the amplitude of inflaton oscillations, $\bar{\phi}(t)$, is rapidly redshifted towards the $V \propto |\phi|^{2n}$ region. For $n > 1$ we observe slow and steady particle production from narrow resonance bands (similar to [18, 19, 145]), which eventually leads to the fragmentation of the condensate and the virialization of the inflaton. The $n = 1$ minimum does not lead to significant particle production – it describes a free scalar, hence the inflaton condensate remains intact and keeps oscillating about the quadratic minimum. The situation drastically changes as we decrease the scale $M \ll m_{\rm Pl}$. The universe expands slowly and $\bar{\phi}(t)$ spends many oscillations outside the power-law region, $|\phi| > M$. Particles are produced by a broad, low-momentum resonance band and the inflaton fragments in spherical localized objects. These are of transient nature for $n > 1$ – they decay away quickly leaving a completely virialized inflaton, whereas for $n = 1$ the objects are very stable and known as oscillons. To the best of our knowledge this is the first time the formation of transients in models with steeper than quadratic minima is reported. On the other hand, oscillons and their cosmological implications have been extensively studied in the literature [146, 147]. They can lead to long periods of matter dominated state of expansion [36, 146, 147] and stochastic gravitational wave backgrounds [44, 82]. Formation of light primordial black holes (PBHs) through collisions [148–150] and their evaporation through Hawking radiation can provide additional constraints on reheating or another channel for it [151]. The consequences of the fragmentation of the inflaton condensate for PBHs formation after inflation have been investigated in the context of interacting theories [152–157] but not in the self-resonating limit, where all, but the self-interactions of the inflaton field can be neglected and density fluctuations grow predominantly on subhorizon scales (however, cf. [158]). We find that it is very unlikely for transients and oscillons formed

after self-resonance to collapse into black holes.

The chapter is organized as follows. In Section 6.2 we briefly review the models we study and how observations constrain them. Then we move on to the particle production after the end of inflation. We start, in Section 6.3.1, with a linear stability analysis and show through semi-analytic means how the oscillating inflaton condensate can resonantly and non-perturbatively amplify its own inhomogeneities. This eventually leads to back-reaction and the subsequent evolution is non-linear. We present our lattice studies of the non-linear dynamics in Section 6.3.2, including the evolution of the equation of state and the likelihood of formation of PBHs. The implications of our investigations for CMB observables, the reheating temperature and stochastic gravitational wave backgrounds are given in Section 6.4. We conclude in Section 6.5, with a summary of our results and plans for future work.

6.2 Models

Our main focus will be on single-field models of inflation, minimally coupled to gravity, with inflaton potential that has an observationally favoured plateau region, see Fig. 6.1. We consider three different parametrizations: the α-attractor T-models [159, 160]

$$\begin{aligned} V(\phi) &= \Lambda^4 \tanh^{2n}\left(\frac{|\phi|}{M}\right) \\ &= \begin{cases} \Lambda^4 \left|\frac{\phi}{M}\right|^{2n} & |\phi| \ll M\,, \\ \Lambda^4 & |\phi| \gg M\,, \end{cases} \end{aligned} \tag{6.1}$$

the α-attractor E-models [159, 160]

$$\begin{aligned} V(\phi) &= \Lambda^4 \left|1 - \exp\left(-\frac{2\phi}{M}\right)\right|^{2n} \\ &= \begin{cases} \Lambda^4 \left|\frac{2\phi}{M}\right|^{2n} & |\phi| \ll M\,, \\ \Lambda^4 & \phi \gg M\,, \end{cases} \end{aligned} \tag{6.2}$$

and Monodromy type potentials [161, 162]

$$\begin{aligned} V(\phi) &= \Lambda^4 \left[\left(1 + \left|\frac{\phi}{M}\right|^{2n}\right)^{\frac{q}{2n}} - 1\right] \\ &= \begin{cases} \Lambda^4 \frac{q}{2n} \left|\frac{\phi}{M}\right|^{2n} & |\phi| \ll M\,, \\ \Lambda^4 \left|\frac{\phi}{M}\right|^{q} & |\phi| \gg M\,. \end{cases} \end{aligned} \tag{6.3}$$

We shall consider values of the parameter $n \geq 1$, for which $\partial_\phi V$ and $\partial_\phi^2 V$ are well-defined when $\phi = 0$, i.e., the elementary quanta of the inflaton always have well-defined mass[1]. The mass scale in eqs. (6.1,6.2) is related to the conventional α-parameter [159, 160, 164–173] through $M = \sqrt{6\alpha} m_{\rm Pl}$, whereas the

[1] See [163] for the stability analysis of some models with $n < 1$.

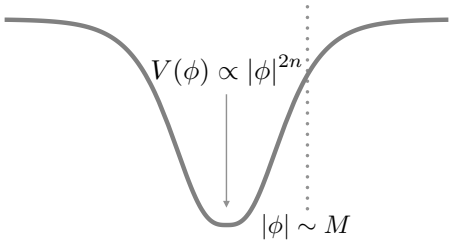

Figure 6.1: The generic profile of the inflaton potential, studied in this chapter. According to observations, slow-roll inflation is realised while the inflaton condensate is in one of the flat regions, rolling slowly towards the minimum.

additional parameter in eq. (6.3), q, should not exceed 1 to be consistent with CMB measurements [2]. As usual, inflation takes place while the inflaton condensate is rolling slowly down the shallow region of V, $\bar{\phi}(t) \gg M$. Using the slow-roll approximation and the measured amplitude of scalar fluctuations, we find a connection between the two dimensionful parameters in our potentials, Λ and M, cf. eqs. (1.61) and (5.2):

$$A_{\rm s} \approx \begin{cases} \frac{N_\star^2 m_{\rm Pl}^2}{3\pi^2 M^2}\left(\frac{\Lambda}{m_{\rm Pl}}\right)^4 & \text{T and E}\,, \\ \frac{1}{12\pi^2}\frac{\Lambda^4 M^2}{q^2 m_{\rm Pl}^6}\left(2qN_\star\frac{m_{\rm Pl}^2}{M^2}\right)^{\frac{q}{2}+1} & \text{Mon}\,, \end{cases} \qquad (6.4)$$
$$\approx 2.2\times 10^{-9}\,,$$

where $N_\star$ is the number of e-folds of accelerated expansion between the horizon crossing and end of inflation of the largest scales observed in the CMB. It is assumed to lie in the range $50 < N_\star < 60$, to resolve the horizon and flatness problems. Note also that eq. (6.4) holds for all n. This is a consequence of the slow-roll approximations we adopt. From now on, we shall treat M, n and q as free parameters, and Λ will be determined from eq. (6.4) for a given $N_\star$. The most recent constraints on the tensor-to-scalar ratio, $r_{0.002} < 0.11$ [2], bound M from above, $M < 10 m_{\rm Pl}$. The embedding in Supergravity of the T and E models has stability issues for $M < \sqrt{2} m_{\rm Pl}$ [166], which in principle narrows the parameter space significantly. However, we shall ignore this lower bound and consider inflation with V as given in eqs. (6.1, 6.2, 6.3) at the phenomenological level, and take $M < 10 m_{\rm Pl}$ only.

The fact that we have the same expression for the T and E models in eq. (6.4) explains why we have chosen to include the additional factor of 2 in the parametrization in eq. (6.2). This way, for a given M we get the same slow-roll parameters for the T and E models[2]. However, the behaviour after the end of slow-roll inflation is affected by this parametrization – it depends on the transition scale in the potential which is M for the T and $M/2$ for the E models.

6.3 Particle production

6.3.1 Linear analysis

After inflation $\bar{\phi}(t)$ begins to oscillate around the minimum of V. This may lead to non-adiabatic production of inflaton particles of definite co-moving momentum, i.e., preheating (cf. Chapter 2). It can be most easily

[2]It could be seen most easily from $\lim_{x\gg 1}\tanh^{2n}(x) = (1-e^{-2x})^{2n}$.

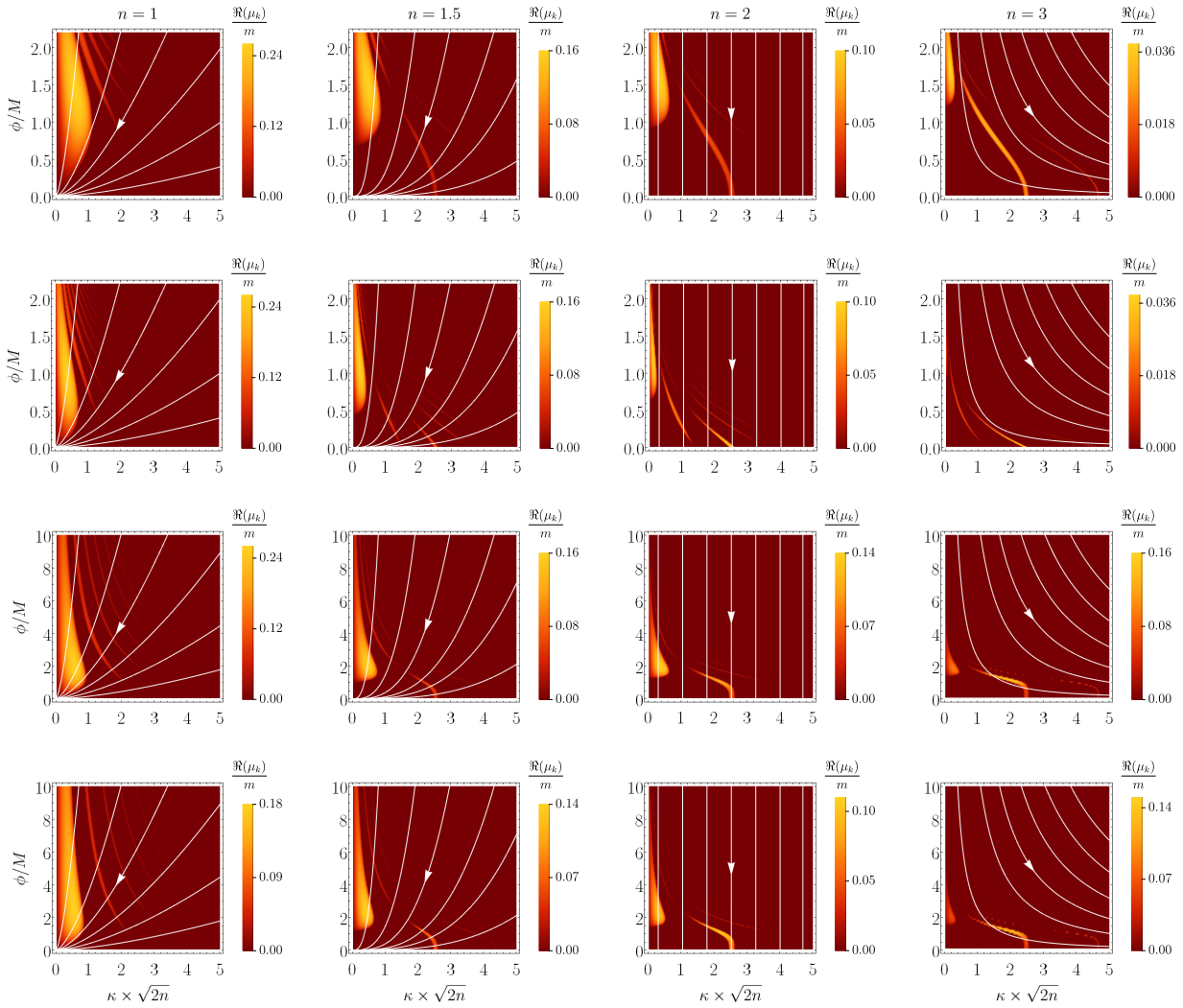

Figure 6.2: The instability regions and Floquet exponents for the T (first row), E (second row), Monodromy $q = 0.5$ (third row) and $q = 1$ (fourth row) models. On the horizontal axis is the dimensionless physical wavenumber $\kappa = k/(am)$ and on the vertical axis the amplitude of inflaton oscillations. The effective mass, m, is defined in eq. (6.7), and determines the characteristic frequency of oscillations. As the universe expands, a given co-moving mode k flows across the chart as the white lines indicate. The factor of $\sqrt{2n}$ on the horizontal axis is chosen to make the narrow instability bands appear at roughly the same place for different n, see also Fig. 6.3. Although, the broad low momentum instability bands seem to vanish for large n, they never go away. It can be shown by a different rescaling of the horizontal axis. In the T and E models slow-roll inflation ends at $\phi_{\rm end} \sim M$ and the amplitude of inflaton oscillations lies in the range $\phi < M$. In the Monodromy models $\phi_{\rm end} \lesssim m_{\rm Pl}$ and the initial amplitude of inflaton oscillations can exceed M.

understood in terms of the linearized field equations

$$\partial_t^2 \delta\phi_{\mathbf{k}} + \left[k^2 + \partial_{\bar\phi}^2 V(\bar\phi)\right] \delta\phi_{\mathbf{k}} = 0\,, \tag{6.5}$$

where we have ignored expansion for simplicity, but shall include it shortly. Since $\partial_t^2\bar\phi + \partial_{\bar\phi} V = 0$, $\partial_{\bar\phi}^2 V$ is a periodic function of time and Floquet theory [66] tells us (see Section 2.2.1) that the general solution to

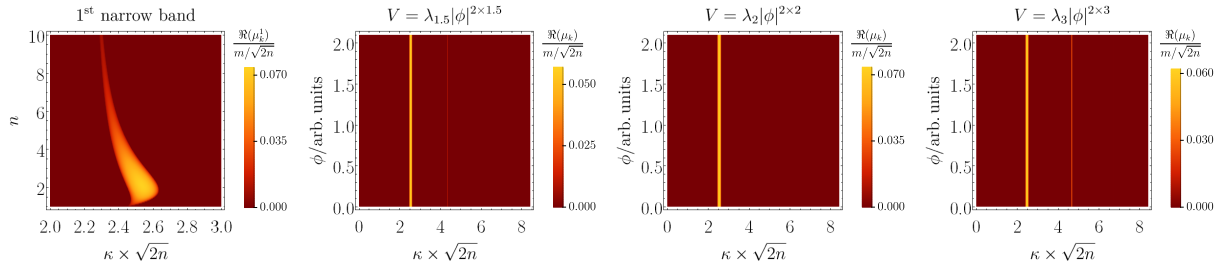

Figure 6.3: The first panel depicts the first narrow instability band for a monomial potential of the form $V = \lambda_n|\phi|^{2n}$. The next three panels give the Floquet charts for $n = 1.5$, 2, 3. Thanks to our choice of κ the instability bands are exactly vertical, independent of the amplitude of inflaton oscillations (the values on the vertical axis). The additional rescaling by $\sqrt{2n}$ makes the first narrow instability band appear at roughly the same place and have roughly the same height, both of which are maximal for $n = 2$, see also Fig. 6.4. For $n = 1.5$ and 3 we have a series of decreasing in height and width instability bands for larger κ. In fact there are four (three) bands in the second (fourth) panel. Interestingly, the second, third, etc. instability bands vanish for $n = 2$.

eq. (6.5) is of the form

$$\delta\phi_k = \mathcal{P}_{k+}(t)\exp(\mu_k t) + \mathcal{P}_{k-}(t)\exp(-\mu_k t)\,. \tag{6.6}$$

$\mathcal{P}_{k\pm}(t)$ are also periodic functions and are determined by the initial conditions. μ_k are the Floquet exponents. If $\Re(\mu_k) \neq 0$, then there is an 'unstable' solution, exponentially growing with time which is a manifestation of non-adiabatic (or resonant) particle production. In Fig. 6.2 we show the instability regions for the inflaton potentials from eqs. (6.1, 6.2, 6.3), for $n = 1$, 1.5, 2, 3 for the T, E and Monodromy models (for $q = 0.5$, 1). The $n = 1$ case features a broad low-k instability region going all the way down to $\bar{\phi} = 0$ and a series of high-k narrow bands, vanishing towards the bottom of the plot. This is common for all slightly flatter than quadratic potentials near $\phi = 0$ [36]. For $n > 1$ the broad low-k band is absent for $\bar{\phi} \lesssim M$. The narrow bands near the bottom of the charts are reminiscent of those for $V \propto |\phi|^{2n}$, see Fig. 6.3. We have defined a mass scale

$$m^2 \equiv \begin{cases} 2n\Lambda^2\left(\frac{\Lambda}{M}\right)^2\left(\frac{\bar{\phi}}{M}\right)^{2(n-1)} & \text{T}\,, \\ 2^{2n+1}n\Lambda^2\left(\frac{\Lambda}{M}\right)^2\left(\frac{\bar{\phi}}{M}\right)^{2(n-1)} & \text{E}\,, \\ q\Lambda^2\left(\frac{\Lambda}{M}\right)^2\left(\frac{\bar{\phi}}{M}\right)^{2(n-1)} & \text{Mon}\,, \end{cases} \tag{6.7}$$

which is what $\partial_{\bar{\phi}}V/\bar{\phi}$ tends to when $\bar{\phi} \ll M$ and is what sets the period of $\bar{\phi}$. We have also defined a dimensionless physical wavenumber $\kappa = k/(am)$. This helps us incorporate the expansion of the universe qualitatively. We recall the general result for the amplitude decay of the inflaton field oscillating in $V \propto |\phi|^{2n}$, $\bar{\phi} \propto a^{-3/(n+1)}$. Hence a given Fourier mode, k, flows through a number of Floquet bands as shown in Fig. 6.2. The mode will grow if the expansion rate, H, is much less than $|\Re(\mu_k)|$. Empirically, strong resonance occurs for $|\Re(\mu_k)|/H \gtrsim 10$. For the broad, low-$k$ band, we find $[|\Re(\mu_k)|/H]_{\rm max} = f(n)m_{\rm Pl}/M$, where $f(n)$ is of order unity. Hence, the expansion of the universe allows for broad self-resonance only for $M \ll m_{\rm Pl}$ for all n.

For $M \gtrsim m_{\rm Pl}$, the amplitude of inflaton oscillations is rapidly redshifted by the expansion of the universe

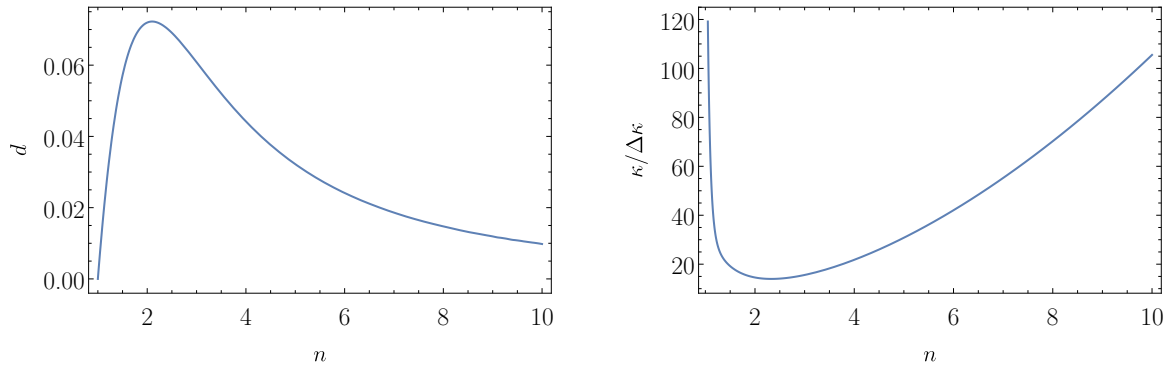

Figure 6.4: The height and width of the first narrow instability band (cf. eq. (6.12) and Fig. 6.3) for $V = \lambda_n|\phi|^{2n}$ and applying also to the T, E and Monodromy models when $\phi \ll M$. Curiously, $d \times \kappa/\Delta\kappa \to 1$.

to the $\bar{\phi} \ll M$ region, i.e., to the bottom of the Floquet charts[3]. Since there are no instability bands in this region for $n = 1$, we do not expect significant particle production. This is anticipated since the condensate is oscillating about a quadratic minimum, and behaves as a free scalar. However, for $n > 1$, we have a series of narrow resonance bands as a consequence of the intrinsic non-linearity. They decrease in height and width for higher κ, cf. Figs. 6.2, 6.3. Hence, the first narrow band plays the dominant role. The particle production can be understood in terms of the white flow lines in Fig. 6.2. The flow lines cross the first narrow band from right to left ($n < 2$), left to right ($n > 2$) or never leave it ($n = 2$). While it is obvious that the narrow resonance will persist until non-linear effects become important in the $n = 2$ case, after a closer look one can argue that the same holds for $n < 2$ and $n > 2$. In these two cases

$$|\dot{\kappa}| \approx \frac{|4-2n|}{n+1} H\kappa\,, \tag{6.8}$$

and since H is decreasing, at some point a given k-mode will spend enough time within the first narrow band for self-resonance to become efficient. This eventually leads to back-reaction on the condensate. We can estimate the moment when this happens. Roughly speaking two conditions have to be met: (i) $|\Re(\mu_k^1)|_{\rm max}\Delta t_{\rm res} \gg 1$ for sufficient particle production and (ii) $|\dot{\kappa}|\Delta t_{\rm res} \ll \Delta\kappa$ for the given k-mode to have spent enough time, $\Delta t_{\rm res}$, within the first narrow resonance band of width $\Delta\kappa$ and height $|\Re(\mu_k^1)|_{\rm max}$. Hence at the time of back-reaction

$$|\Re(\mu_k^1)|_{\rm max} = \frac{H_{\rm br}}{\delta}\frac{\kappa}{\Delta\kappa}\,, \tag{6.9}$$

where the small dimensionless number $\delta \ll 1$ will be determined numerically from our non-linear analysis in the next section. Recalling that $H \sim m\bar{\phi}/\sqrt{2n}m_{\rm Pl}$ and that the initial amplitude of oscillations is $\sim M$, at the end of inflation for $M \sim m_{\rm Pl}$, i.e.,

$$\bar{\phi} \approx \left(\frac{a_{\rm end}}{a}\right)^{3/(n+1)} M\,, \tag{6.10}$$

[3]Recall that the decay rate of the amplitude of $\bar{\phi}$ is set by H, whereas the typical frequency of oscillations is m. Since $H/m \sim \bar{\phi}/m_{\rm Pl} \sim M/m_{\rm Pl}$ at the end of inflation, then $M \sim m_{\rm Pl}$ leads to a rapid decay of the amplitude, within a few oscillations.

then the predicted number of *e*-folds of expansion is[4]

$$\begin{aligned}\Delta N_{\rm br}^{\rm pred} &\equiv \ln\left(\frac{a_{\rm br}}{a_{\rm end}}\right) \\ &\approx \frac{n+1}{3}\ln\left[\frac{1}{d\delta}\frac{\kappa}{\Delta\kappa}\frac{M}{m_{\rm Pl}}\frac{|4-2n|}{n+1}\right] .\end{aligned} \tag{6.11}$$

The ratios $\kappa/\Delta\kappa$ and

$$d \equiv \frac{|\Re(\mu_k^1)|_{\max}}{m/\sqrt{2n}} , \tag{6.12}$$

for the first narrow instability band are given in Fig. 6.4 (also see Fig. 6.3). Curiously, their product is approximately equal to 1.

For power-laws in the region of $n = 2$ condition (ii) is changed to $H\Delta t_{\rm res} \ll 1$, leading to

$$|\Re(\mu_k^1)|_{\max} = \frac{H_{\rm br}}{\delta} , \tag{6.13}$$

whence

$$\Delta N_{\rm br}^{\rm pred} \equiv \ln\left(\frac{a_{\rm br}}{a_{\rm end}}\right) \approx \ln\left[\frac{1}{d\delta}\frac{M}{m_{\rm Pl}}\right] . \tag{6.14}$$

This semi-analytic linear analysis suggests that self-resonance, i.e., inflaton particle production out of the coherent oscillations of the inflaton condensate, can occur after inflation for all values of M. In the following section we investigate numerically the linear and non-linear stages of the post-inflationary evolution. We find that when strong resonance takes place ($M \ll m_{\rm Pl}$), i.e., the inflaton spends enough time in the low-k band, the condensate fragments completely into long-lived (oscillons, $n = 1$) or short-lived (transients, $n > 1$) objects. We also find that even if expansion is significant, i.e., when $M \sim m_{\rm Pl}$, narrow resonance leads to back-reaction and fragmentation.

6.3.2 Non-linear dynamics

In this section we present our results from numerical simulations of the post-inflationary universe. As usual, we map the problem of the inflaton decay onto a classical one [145] which we solve numerically through classical lattice simulations. We use *LatticeEasy* [74] and adopt the standard picture at the time of the beginning of preheating, i.e., a homogeneous inflaton condensate $\bar{\phi}(t)$ with vacuum fluctuation, $\delta\phi_{\mathbf{k}}$, on top of it. The spatial 3d lattice is fixed in co-moving space. The subsequent inflaton evolution and the expansion of the universe are calculated self-consistently, according to the Klein-Gordan, $\Box\phi + \partial_\phi V = 0$, and Friedmann equations. We consider subhorizon scales only, since non-adiabatic resonant particle production happens predominantly on these scales. Ignoring metric fluctuations is also justified. We initialize the simulations around the end of inflation, defined as the first instance when $\ddot{a}(t) = 0$ (the results are insensitive to the exact time of initialization as long as it is near the end of inflation). We set $N_\star = 60$, to find the parameters from eq. (6.4).

As discussed in Section 6.3.1, the interplay between parametric resonance and the Hubble expansion can be divided into two regimes, depending on whether the rate of oscillations is slower ($M \sim m_{\rm Pl}$) or faster ($M \ll m_{\rm Pl}$) than the expansion rate of the universe at the end of inflation. Below, we consider each one in turn.

[4]We use $M/2$ in the place of M for the E-models here and in eq. (6.14).

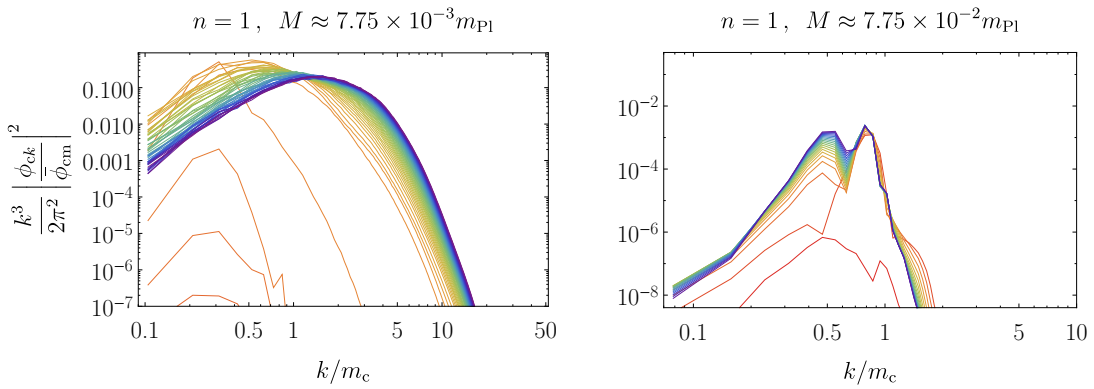

Figure 6.5: The power-spectra of the inflaton field when the rate of oscillations is fast enough for back-reaction to take place (left) and slow enough for the expansion of the universe to shut off the particle production before the condensate can fragment (right). The data is for the T-model. On the vertical axes we have the inflaton power-spectrum which is a measure of the two-point correlation function on co-moving scales $\sim k^{-1}$ or a measure of the autocorrelation per logarithmic k interval. It has been deliberately rescaled by the amplitude of inflaton oscillations – this way if the peak of the power-spectrum reaches unity, the variance becomes comparable to the mean and back-reaction occurs. The subscript 'c' stands for conformal – the Fourier modes are rescaled by $a^{3/(n+1)}$ whereas $\bar{\phi}_{\rm cm}$ is the conformal amplitude, cf. Fig. 6.11, and $m_{\rm c} \equiv m(\bar{\phi}_{\rm cm})$. In both panels time runs from red to purple. Initially, we see particle production due to the broad low-momentum instability band. In the left the growth is eventually shut off by back-reaction and fragmentation, whereas in the right the particle production is quenched by the rapid expansion of the universe, which leads to the quick redshifting of the amplitude of inflaton oscillations below the instability band, cf. Fig. 6.2. In the latter case the condensate remains intact and keeps oscillating, while the energy in the excited modes becomes increasingly subdominant and never leads to back-reaction. The broad peak in the power-spectrum, formed in the case with back-reaction, is slowly shifted towards higher co-moving wavenumbers as the universe expands at late times. This is an indication for the formation of stable objects of fixed physical size – oscillons, cf. left column in Fig. 6.6.

Oscillons & matter domination

For $n = 1$ when the universe expands slowly with respect to the rate of oscillations of $\bar{\phi}(t)$ strong resonance takes place. One can see that from Fig. 6.2 which implies that for $M \lesssim 10^{-2} m_{\rm Pl}$ the broad low-k instability band is important, since $\bar{\phi}(t)$ undergoes a great number of oscillations while in it. Our simulations indeed confirm the expectation from the linear analysis. Initially, we observe the development of a broad low-k peak in the spectrum of the inflaton, cf. left panel in Fig. 6.5. When the energy of the peak becomes comparable to that of the condensate, back-reaction takes place. The back-reaction process is very efficient in the sense that the condensate fragments completely. However, the fragmentation is followed by the formation of interesting non-linear structures of fixed physical size, cf. first column in Fig. 6.6. They remain intact for the entire duration of the simulations. That is why the peak in the power-spectrum never goes away and is only slowly shifted towards higher co-moving wavenumbers.

These non-linear objects are called oscillons [36]. They normally form if V is quadratic near the origin and flatter away from it. Oscillons are long-lived pseudo-solitonic objects. Their field profile is such that the non-linear terms from $\partial_\phi V$ essentially cancel the dispersion term in the equation of motion, i.e., $\partial_t^2 \phi_{\rm osc} + m^2 \phi_{\rm osc} \approx 0$ (for a more detailed explanation cf., e.g., [36, 146, 147]). $\phi_{\rm osc}(r,t)$ is spherically symmetric, peaking at the centre of the oscillon and approaching monotonically zero away from it. The profile is oscillating with time, hence the name. All points oscillate in phase at the same frequency, so one can approximately write $\phi_{\rm osc}(r,t) = R(r)T(t)$. The energy contained in oscillons, however, is constant with

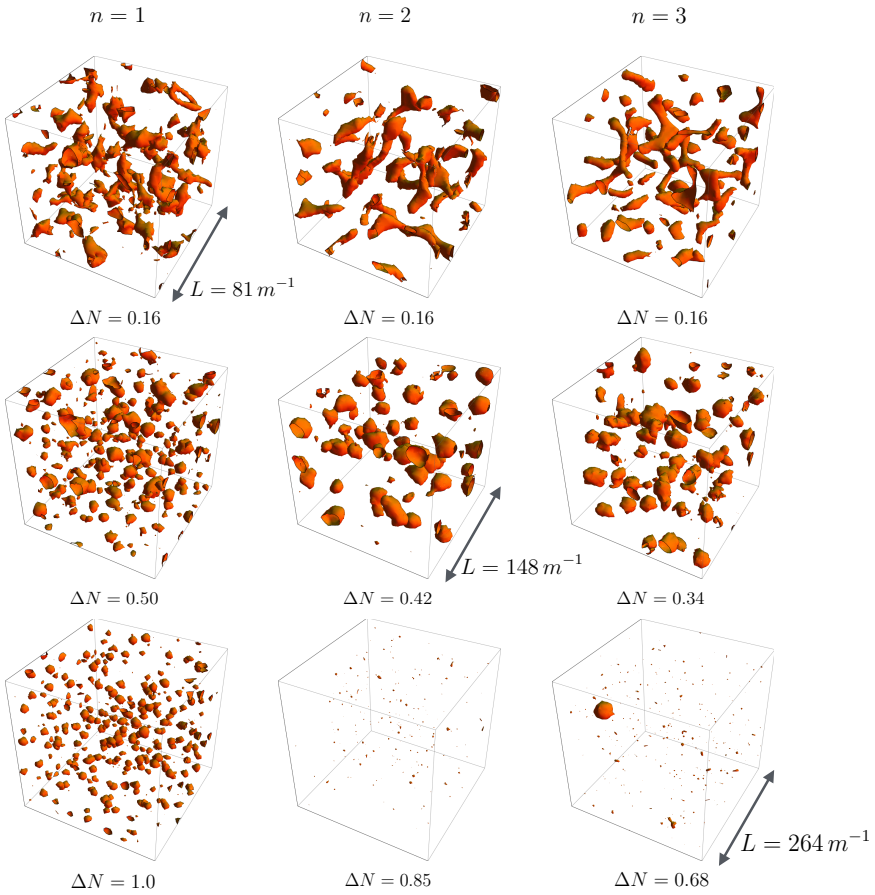

Figure 6.6: The three columns show snapshots of density contours at $5\times$ the mean for $M \approx 0.775 \times 10^{-2} m_{\rm Pl}$ for three different n for the T-model. After the inflaton fragments it can form very stable objects (oscillons, $n = 1$) lasting millions of oscillations or transient objects ($n > 1$) lasting tens of oscillations. They are highly overdense regions, containing a substantial fraction of the energy of the universe for many e-folds of expansion ($n = 1$) or for $\mathcal{O}(1)$ e-folds ($n > 1$). The inflaton becomes virialized after transients decay. The physical size of the co-moving boxes is given in terms of $m(\phi = M)$. The boxes are always subhozrion.

time. They can lock a substantial fraction of the energy of the universe. Oscillons behave as pressureless dust, thereby giving rise to a matter-dominated stage of expansion, cf. Fig. 6.7, where we plot the equation of state parameter defined as

$$w \equiv \frac{\langle p \rangle_{\rm s}}{\langle \rho \rangle_{\rm s}} = \frac{\langle \dot{\phi}^2/2 - (\nabla\phi)^2/6a^2 - V \rangle_{\rm s}}{\langle \dot{\phi}^2/2 + (\nabla\phi)^2/2a^2 + V \rangle_{\rm s}}\,, \tag{6.15}$$

where, ρ and p are the energy density and pressure of the inflaton field, respectively. The symbol $\langle \ldots \rangle_{\rm s}$ stands for spatial average over the lattice. The equation of state often rapidly oscillates compared to the characteristic expansion time-scale – a time average over many oscillations should be assumed when we refer to w unless otherwise stated. The number of e-folds of expansion after inflation is defined as $\Delta N = \int_{a_{\rm end}}^{a(t)} d\ln a$. Note that w is not exactly 0, but rather decays towards it. This is because there is some energy

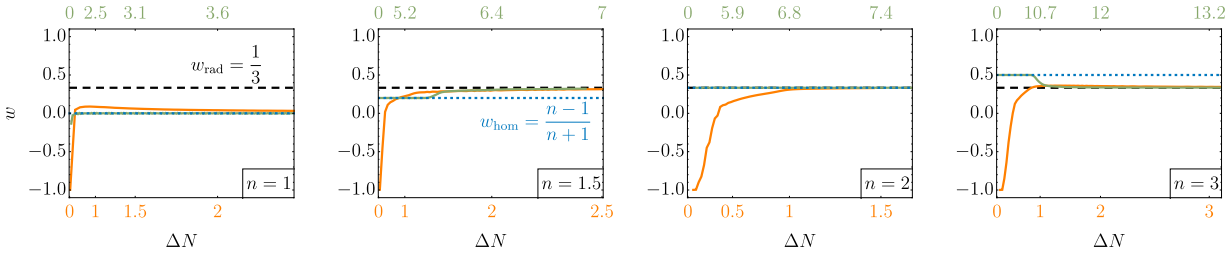

Figure 6.7: The evolution of the equation of state for different M and n in the T-models. On the vertical axes we have the equation of state and on the horizontal axes the number of e-folds of expansion after the end of inflation. In blue we have the expected homogeneous equation of state and in black the equation of state for a radiation dominated universe. In orange and green we give data from representative lattice simulations. In the orange cases ($M \approx 7.75 \times 10^{-3} m_{\rm Pl}$), the resonance is efficient since it leads to the complete fragmentation of the condensate within less than an e-fold of expansion. Afterwards w settles to 0 for a quadratic minimum (since oscillons behave as pressureless dust) or $1/3$ for steeper power-laws (after the transient objects decay away). For $n > 1$ there is a brief intermediate period with a matter-like equation of state, due to the transients (which, like oscillons, behave as pressureless dust). On the other hand, in the green cases ($M \approx 2.45 m_{\rm Pl}$) the resonance is inefficient since the condensate can oscillate for very long times. In fact, if $n = 1$ the condensate never fragments due to self-resonance, cf. Fig. 6.5, whereas if $n > 1$ back-reaction eventually occurs and the equation of state quickly settles to $1/3$ in a step-like manner.

stored in relativistic modes outside the oscillons. However, since the energy in oscillons redshifts as matter, $\rho \propto a^{-3}$, whereas in relativistic modes as $\propto a^{-4}$ it does not take long for $w \to 0$. Note how efficient the entire process is – it takes less than an e-fold of expansion for the field to fragment and form oscillons and reach a matter-like equation of state in the T and E models. In these models the inflaton starts to oscillate in the broad band immediately after inflation, cf. Fig. 6.2 (in the Monodromy models it can take up to 2 e-folds for the amplitude of inflaton oscillations to be redshifted to the broad instability band peak near $\phi \sim M$). For the universe to reach a radiation dominated state necessary for successful BBN, we need extra ingredients in the way of daughter fields coupled to the inflaton which eventually lead to the decay of the oscillons into relativistic matter. We must point out that $\phi_{\rm osc}(r,t)$ is not actually an exact solution to the equations of motion, but only approximate. Oscillons are expected to decay through classical [174] (or quantum [175]) radiation eventually. Nevertheless, oscillons are very long-lived and stable objects that can last for millions of oscillations (corresponding to many Hubble times).

The development of non-linear structures could potentially seed PBHs. We proceed with a qualitative study of the gravitational field induced on the surfaces of the oscillons to roughly estimate how likely it is for them to collapse under their own gravity and form PBHs. We use our lattice simulations which account for gravity only at the background level. For our purposes it is sufficient to solve the Poisson equation within the simulation box, subject to periodic boundary conditions:

$$\Delta \psi_{\rm N} = \frac{\rho}{2 m_{\rm Pl}^2}\,, \tag{6.16}$$

where $\psi_{\rm N}$ is the Newtonian gravitational potential and ρ is the local energy density. If the gravitational potential on the surface of a spherical lump is $\psi_{\rm N}^{\rm s} \gtrsim 1$, then the formation of a PBH should be expected and a more detailed investigation carried out. We can actually estimate the typical $\psi_{\rm N}^{\rm s}$ from very simple considerations. The oscillons are spherically symmetric. A good guess for the gravitational potential on the surface of an individual object would be $\psi_{\rm N}^{\rm s} \sim M_{\rm s}/(m_{\rm Pl}^2 R_{\rm s}) \sim \rho_{\rm c} R_{\rm s}^2/m_{\rm Pl}^2$, where $M_{\rm s}$ and $R_{\rm s}$ are its mass and

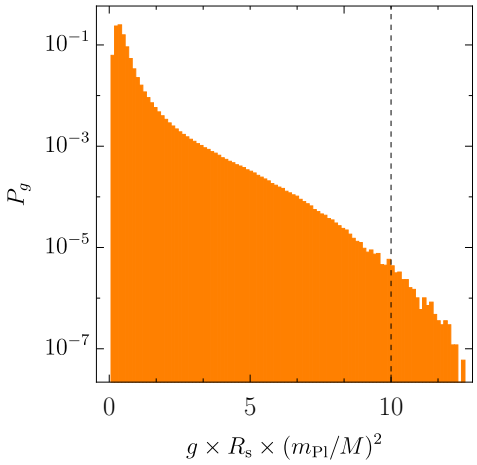

Figure 6.8: A histogram of the gravitational field, g, at $\Delta N = 1$, after oscillons have formed and settled, for the T-model with $n = 1$, $M \approx 0.775 \times 10^{-2} m_{\rm Pl}$. If the Newton potential on the surface of the oscillons $\psi_{\rm N}^{\rm s} \gtrsim 1$, they could become the seeds of primordial black holes. g has its maximum near the surface of the oscillons, $r \sim R_{\rm s}$, hence $g_{\rm max,box} R_{\rm s} \sim g_{\rm s} R_{\rm s} \sim \psi_{\rm N}^{\rm s}$. Our simulations are in agreement with our expectations – vertical dashed line at $g_{\rm s} R_{\rm s} \sim 10^{-1} \times (M/m_{\rm Pl})^2$, cf. eq. (6.17). Since oscillons cannot form from self-resonance for $M > 10^{-2} m_{\rm Pl}$, they cannot lead to the formation of black holes.

radius, respectively, and $\rho_{\rm c}$ is the core energy density. Oscillons formed as a consequence of self-resonance have $\phi_{\rm c} \lesssim \bar{\phi}_{\rm br}$, where $\bar{\phi}_{\rm br}$ is the amplitude of the oscillating inflaton at the time of back-reaction (or fragmentation). Hence, $\rho_{\rm c} \lesssim \bar{\rho}_{\rm br}$ and $\psi_{\rm N}^{\rm s} \lesssim H_{\rm br}^2 R_{\rm s}^2$. According to this criterion only superhorizon objects at the time of back-reaction can collapse and form PBHs. The broad low-k resonance band has a typical lengthscale $R_{\rm res} \sim m^{-1} \sim R_{\rm s}/10$, cf. Fig. 6.2. It is subhorizon at the time of back-reaction since normally $\bar{\phi}_{\rm br} \sim M < 10^{-2} m_{\rm Pl}$, while the Friedmann equation tells us $H_{\rm br}^2 \sim m^2 \bar{\phi}_{\rm br}^2/(6 m_{\rm Pl}^2)$. Therefore, it is unlikely for the pseudo-solitonic lumps to have $\psi_{\rm N}^{\rm s} \gtrsim 1$ and collapse due to their own gravitational field and form PBHs. The actual numerical solution to eq. (6.16) using data from our lattice simulations confirms that, cf. Fig. 6.8. There we show a histogram of the magnitude of the gravitational field, $g = |\boldsymbol{\nabla} \psi_{\rm N}|$, for $M \approx 0.775 \times 10^{-2} m_{\rm Pl}$ at $\Delta N = 1$ for the T-model. We can clearly see that our naive upper bound for $\psi_{\rm N}^{\rm s}$ describes quite well the data. We estimate that $g_{\rm s} \sim \psi_{\rm N}^{\rm s}/R_{\rm s} \sim (M/m_{\rm Pl})^2 m \sim 10 \times (M/m_{\rm Pl})^2/R_{\rm s}$, which indeed corresponds to the maximal value of g up to a factor of order unity.[5] Hence

$$\psi_{\rm N}^{\rm max} \lesssim 10 \times \left(\frac{M}{m_{\rm Pl}}\right)^2 \lesssim 10^{-3} \,. \tag{6.17}$$

Transients & radiation domination

Even if V is steeper than quadratic near the minimum ($n > 1$) we also observe the formation of non-linear objects, when the universe expands slowly with respect to the rate of oscillations of $\bar{\phi}(t)$. We refer to them

[5] We found that the profiles of individual oscillons can be approximated as Gaussian. The maximum of the gravitational field is always near their surface.

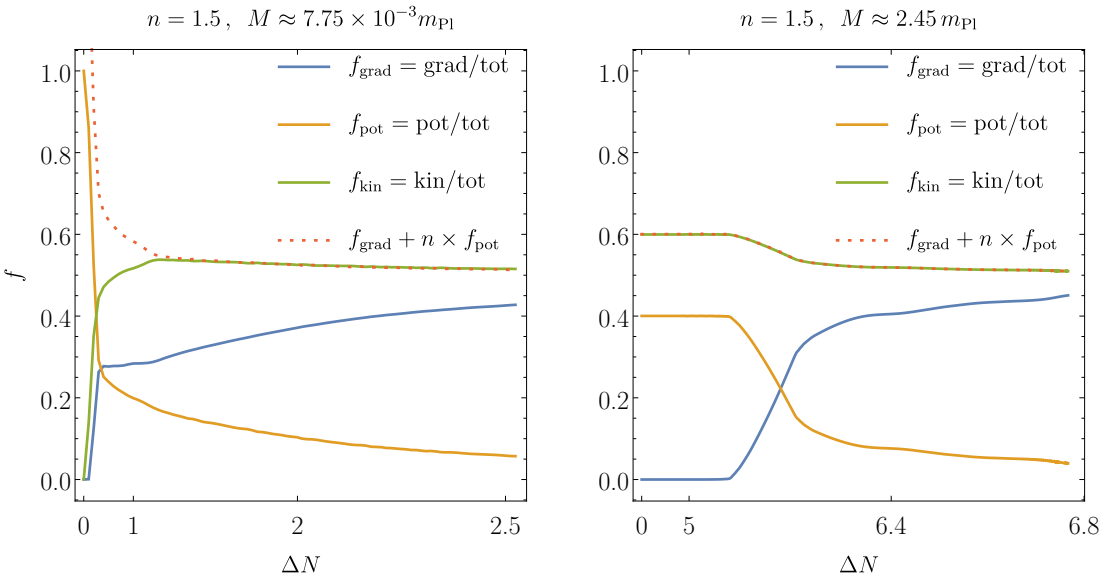

Figure 6.9: The evolution of the fraction of energy, f, stored in gradient (blue), potential (orange) and kinetic (green) terms. The red (dotted) line is the right hand side of the virial expression, cf. eq. (6.18), divided by the total energy. All curves represent time averages over many oscillations and volume averages over the simulation box. The data is for the T-models. In the case on the left, the universe expands slowly enough for the broad instability band to play an important role. The condensate fragments rapidly into transient objects, surviving for about an e-fold of expansion, as one can tell by the initial plateau in $f_{\rm grad}$. After that the transients decay away and the inflaton field becomes virialised. In the right panel, the amplitude of inflaton oscillations is redshifted quickly towards the power-law minimum. Only the first narrow instability band is relevant. It leads to slow but steady particle production. The condensate oscillates for over 5 e-folds, as indicated by the initial plateaus in the three fs. Eventually, the excited modes backreact and the condensate fragments. Interestingly, the field remains completely virialised throughout its evolution. In both cases the self-interaction energy becomes increasingly subdominant with time.

as transients since they are much shorter-lived than oscillons – they survive for tens of oscillations only, cf. second and third columns in Fig. 6.6 and first column in Fig. 6.10. Still, they can dominate the energy budget of the universe for up to an e-fold of expansion, cf. Fig. 6.7, and hence can be of cosmological relevance. Their effect on the equation of state of the universe is quite interesting. Before they decay w is matter-like (since transients, like oscillons, behave as matter), whereas after that it is that of radiation, $w = 1/3$, for *all* $n > 1$. This could be understood if one looks at the evolution of the fraction of energy stored in the form of kinetic, gradient and potential energies, cf. Fig. 6.9. Numerically, we find that after the transients decay, they leave a completely virialized [176] inflaton

$$\frac{1}{2}\langle\dot{\phi}^2\rangle_{\rm s,t} = \frac{1}{2}\langle(\nabla\phi/a)^2\rangle_{\rm s,t} + n\langle V\rangle_{\rm s,t}\,. \tag{6.18}$$

This implies[6]

$$w = \frac{1}{3} + \frac{2}{3}\frac{(n-2)}{(n+1) + \frac{\langle(\nabla\phi/a)^2\rangle_{\rm s,t}}{\langle V\rangle_{\rm s,t}}}\,. \tag{6.19}$$

[6]If we assume that $\left\langle \frac{\langle\ldots\rangle_{\rm s}}{\langle\ldots\rangle_{\rm s}} \right\rangle_{\rm t} = \frac{\langle\ldots\rangle_{\rm s,t}}{\langle\ldots\rangle_{\rm s,t}}$, which turns out to be an excellent approximation at late times.

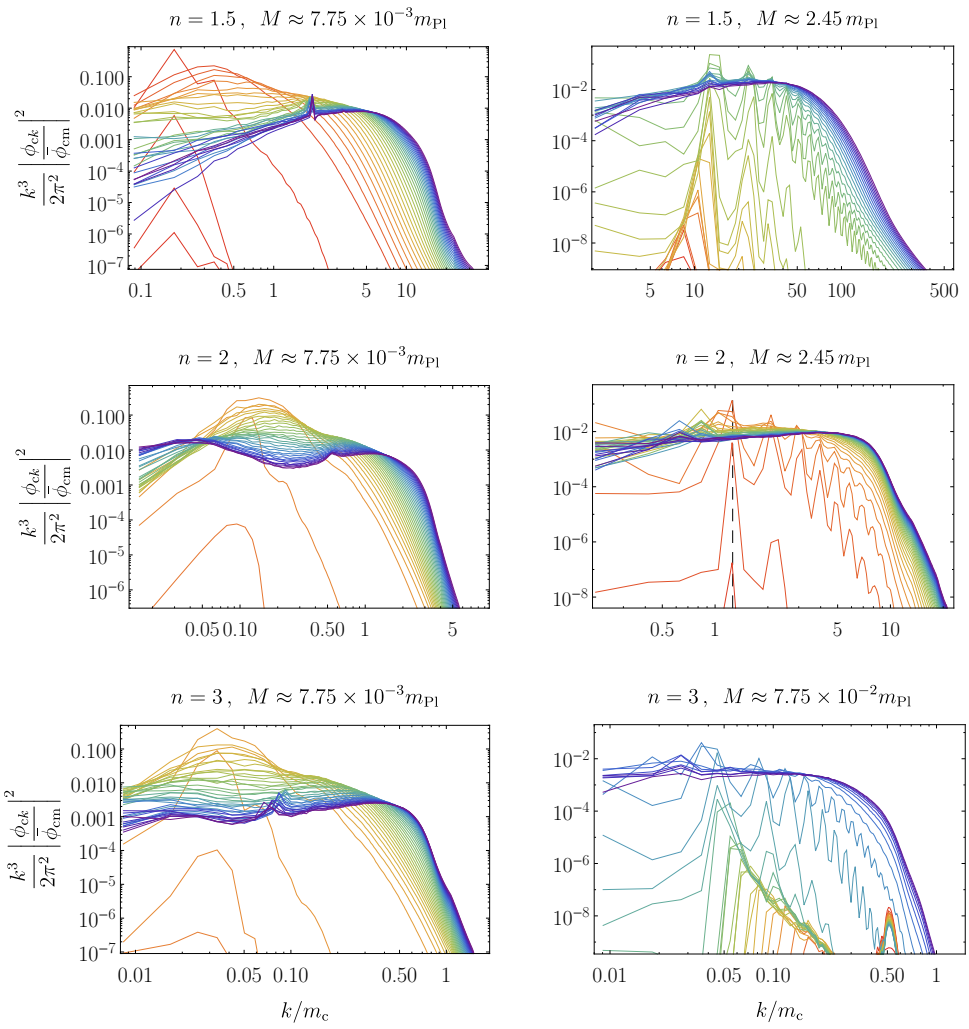

Figure 6.10: Representative power-spectra for $n > 1$. The data is for the T-models (cf. Fig. 6.5 for notation). The left column is for sufficiently small M, allowing for the broad instability band to generate enough particles to fragment the condensate and form transients. As the objects decay, the broad peaks in the power-spectra go away and UV and IR modes become excited. The right column is for larger M, for which the first narrow instability band leads to slow, but steady particle production in a narrow co-moving band whose peak shifts with time towards higher ($n < 2$), lower ($n > 2$) co-moving modes or stays fixed ($n = 2$) at $k \approx 1.27 m_{\rm c}$, cf. Figs 6.2, 6.3. The growth is eventually shut off by back-reaction and fragmentation (without the formation of any transient non-linear objects). For $n = 3$, the chosen M is not too large and allows for some initial particle production due to the lower regions of the broad instability band (the bump around $k \sim 0.5 m_{\rm c}$). In all six panels, power cascades slowly towards the UV at late times. Since there is a subdominant remnant oscillating condensate, cf. Fig 6.11 there is also some particle production due to the first narrow instability band at late times, clearly visible in the first column and not so much in the second column.

Since $\langle V \rangle_{\rm s,t} \ll \langle \dot{\phi}^2 \rangle_{\rm s,t}, \langle (\nabla \phi / a)^2 \rangle_{\rm s,t}$, cf. Fig. 6.9, $w \to 1/3$ – a somewhat unexpected result for $n < 2$. The reason why it is surprising is the following. Recall that the density of a condensate oscillating in $V \propto |\phi|^{2n}$

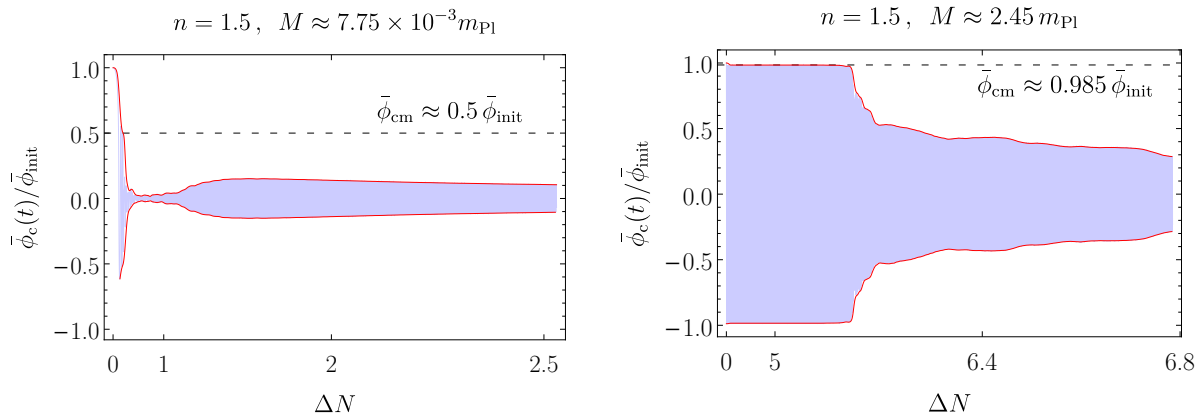

Figure 6.11: The evolution of the volume average of the inflaton field for the T-models. $\bar{\phi}_{\rm init}$ is its initial value, at the beginning of the simulations (around the end of inflation, when $\ddot{a} = 0$ for the first time). We plot the rescaled 'conformal' value $\bar{\phi}_{\rm c}(t) \equiv (a/a_{\rm init})^{3/(n+1)}\bar{\phi}(t)$ – the prefactor compensates for the decay of the amplitude of inflaton oscillations due to the expansion of the universe. The left panel is for a case when the mass M is small enough for the broad instability band to play a major role and lead to the formation of transients. Shortly after initialization, the condensate undergoes several oscillations with a nearly constant conformal amplitude, $\bar{\phi}_{\rm c,m} \approx 0.5\bar{\phi}_{\rm init}$ (for Monodromy models, it can undergo 10s of oscillations). During this period, the broad instability band excites multiple modes, eventually causing back-reaction. The oscillating condensate disappears for about an e-fold of expansion, reflecting its complete fragmentation and the formation of localized transients. As the objects decay away, a part of the condensate reappears, because a non-trivial dynamical equilibrium is established [18, 19, 145]. The new condensate, however, is increasingly subdominant in energy. The right panel is for a case when M is so large, that only the first narrow instability band plays an important role. The condensate undergoes many oscillations with conformal amplitude very close to $\bar{\phi}_{\rm init}$ (this is typical for $M \gtrsim m_{\rm Pl}$). As the slow, but steady particle production due to the first narrow band causes back-reaction, the condensate fragments partially. Non-linear transient objects do not form in this case, but just like after their decay in the other case, the remnant condensate becomes energetically less important with time.

redshifts as $\rho \propto a^{-6n/(n+1)}$,[7] i.e., slower than radiation for $n < 2$. Hence, for such n, whatever condensate (coherent low-k modes) is left after the decay of the transients, its energy should redshift slower than the energy stored in the relativistic modes and eventually become the dominant component, yielding[7]

$$w_{\rm hom} = \frac{n-1}{n+1}\,. \tag{6.20}$$

Instead, numerically we find that power cascades slowly towards the UV akin to the turbulent evolution described in [18, 19] and that the energy stored in the relativistic modes always dominates over the remnant condensate, leading to $w \to 1/3$, for all $n > 1$. This is a purely non-linear effect.

The formation of transients is somewhat unexpected, too. We could try to make a connection with oscillons and assume that the dispersion term is cancelled by all but the lowest order term from $\partial_\phi V$ in the equation of motion, i.e., $\partial_t^2\phi_{\rm tr} + m^2\phi_{\rm tr} \approx 0$. However, this equation does not permit separable solutions. It is impossible to get an approximate solution of the form $\phi_{\rm tr}(r,t) = R(r)T(t)$, since $m^2 \propto \phi_{\rm tr}^{2n-2}$ and therefore the frequency of oscillations will be amplitude dependent, implying that different points of the

[7] For a rapidly oscillating scalar condensate in an expanding universe $0 = \langle\phi(\ddot{\phi} + \partial_\phi V)\rangle_{\rm t} = -\langle\dot{\phi}^2\rangle_{\rm t} + \langle\phi\partial_\phi V\rangle_{\rm t}$, from which follows $\langle\dot{\phi}^2\rangle_{\rm t} = 2n\langle V\rangle_{\rm t}$. After substitution in eq. (6.15) we obtain eq. (6.20), whereas using energy conservation $\dot{\rho}+3H(\rho+p) = 0$, we arrive at $\rho \propto a^{-6n/(n+1)}$.

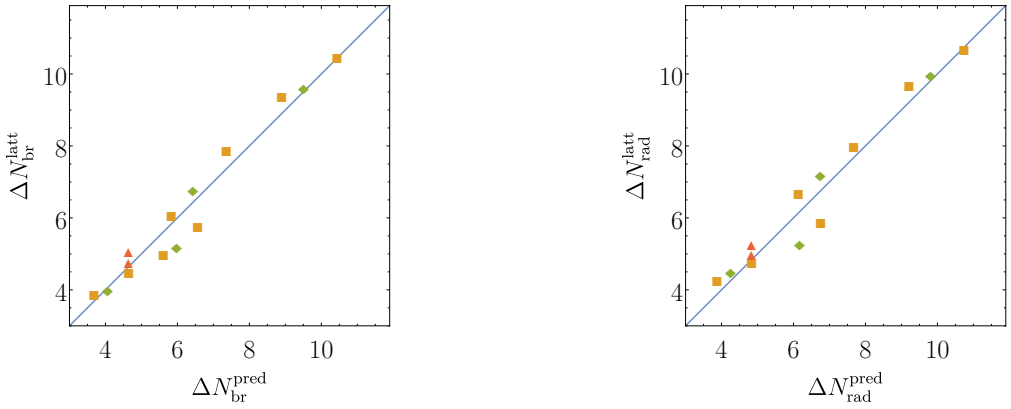

Figure 6.12: On the left we show the number of e-folds of expansion after the end of inflation when back-reaction takes place due to particle production from the first narrow instability band. On the horizontal axis we plot the predicted values (eq. (6.11) for $1 < n \neq 2$ and eq. (6.14) for $n = 2$) and on the vertical axis the measured values from lattice simulations, for different M and n. The orange squares are for the T-models, the green rhombi are for the E-models and the red triangles are for the Monodromy models for $q = 0.5, 1$. We find that for all models and parameters, the data fits the $45^{\rm o}$ degree line for $\delta \approx 0.126$. We also found that changing δ to 0.100 describes well the time the equation of state approaches $w_{\rm rad} = 1/3$, as shown on the right.

profile will oscillate at different rates. In our simulations we indeed observe the formation of ripples on top of the oscillating $\phi_{\rm tr}(r,t)$, which radiate away the energy of the objects, explaining their transient nature. We can in fact go a step further and generalize this statement and claim that any $V \propto |\phi|^{2n}$ $(n > 1)$ near the origin and flattening out away from it can support such transients. To the best of our knowledge this is the first time they have been reported in the literature. It is interesting to think about the longevity of this objects if there is a mechanism which forces their profile to resemble a top-hat (akin to the flat-top oscillons [177]). The constancy of the amplitude within an extended region should suppress the formation of ripples and prolong the lifetime of the transients. We leave this investigation for a future work.

We have also analysed the gravitational field created by the transients. We arrive at qualitatively similar results to $n = 1$, cf. eq. (6.17) and Fig. 6.8, i.e., they are very unlikely to seed PBHs. On the other hand, transients decay away quickly, in a non-spherical manner. Hence, unlike the cases when we have oscillons in which gravitational waves (GWs) are not generated after oscillons are formed [82], the decay of the transients can act as an additional source of GWs and we hope to address this issue in the near future.

1$^{\rm st}$ band & radiation domination

Let us proceed with the case when the expansion of the universe immediately after inflation is more important than the particle production from the broad resonance band, $M \gtrsim 10^{-2} m_{\rm Pl}$. For all n the amplitude of $\bar{\phi}$ decays rapidly, and it does not undergo a significant number of oscillations while the low-k modes lie in the broad instability band, cf. Fig. 6.2. Our simulations indeed reveal that all $\delta\phi_{\mathbf{k}}$ do not grow much initially. They experience brief excitations due to the crossing of multiple instability bands, but not large enough to back-react on the condensate. $\bar{\phi}(t)$ continues to oscillate around the bottom of $V \propto |\phi|^{2n}$.

However, as Fig. 6.2 suggests, despite the fast expansion of the universe, narrow resonance effects play an important role at late times for $n > 1$. Co-moving modes within the narrow bands remain unstable

as Hubble expansion drives $\bar{\phi} \to 0$. However, the unstable k-modes cannot grow indefinitely. Roughly speaking, when their energy becomes comparable to that of the condensate, non-linear effects become important and lattice simulations become essential. We show in the right column in Fig. 6.10 the inflaton spectra at different times. After a short period of excitation of low-k modes, $\bar{\phi}$ has decayed significantly (due to expansion) for the narrow bands to become important. The modes within the first narrow resonance band grow ever faster when compared to the expansion time-scale, since $|\Re(\mu_k)| \propto m$ and $H \sim m\bar{\phi}/m_{\rm Pl}$, i.e., $|\Re(\mu_k)|/H \propto m_{\rm Pl}/\bar{\phi}$, developing a prominent narrow *primary* peak that is shifted towards higher co-moving wavenumbers ($n < 2$), towards lower co-moving wavenumbers ($n > 2$) or is fixed in co-moving space at $k_1 = \kappa_1 a(t)m(t) = \text{const}$, $\kappa_1 \approx 1.27$ ($n = 2$). Interestingly, before the deposited energy in the primary peak becomes comparable to that of the condensate, a series of *secondary* peaks develops. Initially at k near 0 and then at ever higher k. We call them secondary because they do not follow from the linear analysis (the linear analysis yields a much slower growth near the secondary peaks). They result from re-scattering processes (we confirmed their re-scattering origin by removing the initial fluctuations above a certain cut-off, e.g., $k > 1.2k_1$ for $n = 2$). The k close to 0 appears first as a consequence of the strongest re-scattering – between particles from the primary peak and the condensate. The higher k peaks then follow from 'primary-primary' and 'primary-secondary' re-scattering processes. The parametric resonance is eventually shut off by the back-reaction on the condensate. All peaks smear out and again (just like in the transients case) the field is virialized, cf. Fig. 6.9, the power cascades slowly towards the UV and the energy stored in the relativistic modes always dominates over the remnant condensate, leading to $w \to 1/3$. This is a purely non-linear process that has been observed in pure $\lambda\phi^4$ theory [18, 19, 145]. Note that $\bar{\phi}$ never disappears completely, cf. Fig 6.11 – it is in a non-trivial dynamical equilibrium with the highly occupied modes and if it is removed artificially it reappears due to Bose condensation (for more details see the references). Importantly, the inflaton field is again virialized, having kinetic and gradient energies much greater than the potential energy, which implies a $w \approx 1/3$. We find that the fragmented inflaton almost immediately reaches a radiation dominated state of expansion, i.e., $\Delta N_{\rm rad} \gtrsim \Delta N_{\rm br}$. The expected time from the linear analysis in Section 6.3.1, cf. eqs. (6.11,6.14), agrees well with the lattice simulations, cf. Fig. 6.12, when the first narrow instability band plays an important role. The moment of back-reaction obtained from our lattice simulations fits the predictions for $\delta \approx 0.126$, for all four models (T, E and Monodromy $q = 0.5, 1$). We also find that decreasing the small parameter to 0.100 describes well the data for the time when w settles to $1/3$. When the broad instability band causes the fragmentation of the condensate into transient objects we find that $\Delta N_{\rm rad} \gtrsim \Delta N_{\rm br} \sim 1\,(2.5)$ for the T and E (Monodromy) models. These simple results have significant implications for the constraints on $n_{\rm s}$ and r, cf. Section 6.4.

For $n = 1$ when $M \gtrsim 10^{-2} m_{\rm Pl}$, we do not observe sufficient particle production to fragment the condensate. This could be understood again from the stability chart in Fig. 6.2 – since the narrow bands vanish as $\phi \to 0$, there should not be any particle production at late times. Our lattice simulations verify this, cf. right panel in Fig. 6.5. The condensate remains intact and keeps oscillating about a quadratic minimum, implying a matter dominated stage of expansion, $w = 0$, cf. Fig. 6.7.

Numerics

We have carried out various numerical checks. We have tested the robustness of our results against changes in the IR and UV resolutions of our simulations. While often a 256^3 lattice turned out to be large enough to cover the relevant dynamical range, we typically ran 512^3, sometimes going up to 1024^3 to make sure that finite resolution effects do not lead to spurious results.

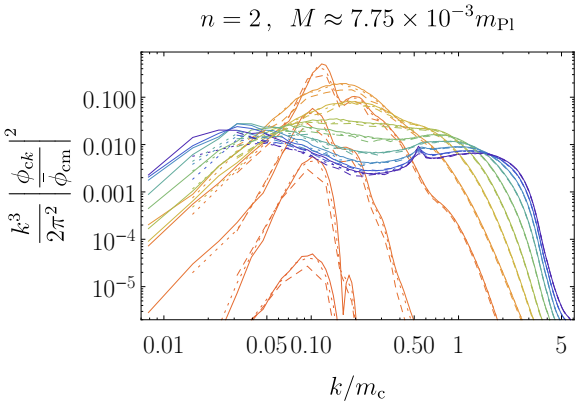

Figure 6.13: The evolution of the power-spectrum for a case when transients form and then decay away. The data is from three simulations, differing in their IR resolution. The solid lines are for a 1024^3 run, the dotted for a 512^3 run and the dashed for a 256^3 run. After the initial particle production in a broad co-moving band, the condensate fragments and forms transient objects, as indicated by the broad peak at intermediate times. As the transients decay, the broad peak goes away, power cascades towards the UV, with low-energy long wavelength modes also being excited. Importantly, the IR cut-off does not affect the evolution of the intermediate and short wavelength modes which dominate the energy budget.

For $n = 1$ the simulations were relatively straightforward. For $M \sim m_{\rm Pl}$, very little energy is transfered from the homogeneous inflaton to relativistic modes, back-reaction never takes place due to self-resonance, the condensate remains intact and keeps oscillating (however, if gravity is included at first order, the condensate must eventually fragment [83]; this is beyond the scope of our work). When $M < 10^{-2} m_{\rm Pl}$ and oscillons form, the only challenges are to make sure that the full width of the broad low-momentum instability band is captured (setting the IR cut-off) while the UV cut-off allows for the resolution of the small (with respect to the horizon) objects. Since the lattice is fixed in co-moving space, i.e., expands along with the universe, and oscillons have fixed physical size, we inevitably run out of resolution on small sales. A 512^3 run with the product of the physical length of the edge of the lattice and the Hubble parameter at the time of back-reaction $(LH)_{\rm br} \sim 0.1$, allows to keep track of the oscillons for about an e-fold of expansion after their formation, while resolving the broad resonance band at earlier times.

When $n > 1$ and transients form we are faced with the same challenges as in the oscillons case. However, as the transient objects decay and the broad peak in the inflaton field power-spectrum goes away and most of the power is transfered to high-k modes, some energy goes to the IR modes, too. We have verified that the IR cut-off does not affect the dynamics on small scales and the features on intermediate scales, cf. Fig. 6.13. The former can be understood from the fact that the IR modes are much less energetic than the UV modes (typically suppressed by a factor of k^2) and the latter from the non-trivial dynamical equilibrium [18, 19, 145] between the energetic (i.e., UV) and subdominant (i.e., intermediate and IR) modes. Hence, the IR cut-off does not affect the evolution of the equation of state, which is determined by the high energy modes. The only quantity that we find to be affected is the spatial average of the inflaton, $\bar{\phi}(t)$, after transients decay, cf. Fig. 6.11. Basically, the amplitude of the oscillations of the condensate that forms after transients go away turns out to vary weakly (normally decreases) as we improve the IR resolution. This is reasonable, since we capture more long wave modes (the non-trivial dynamical equilibrium also implies in general some variation in the occupation number of the IR modes). But again, since the IR modes and the condensate in particular are subdominant in energy, their sensitivity on the IR

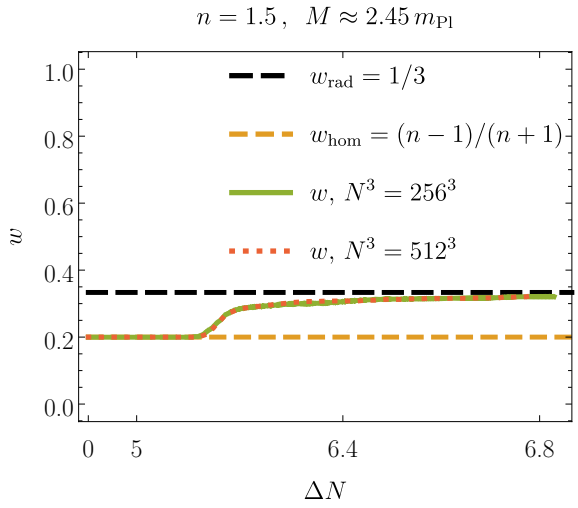

Figure 6.14: The evolution of the equation of state for a case when M is large enough for particle production from the first narrow instability band to cause back-reaction and fragmentation. The green solid and the red dotted lines are for two runs with the same IR cut-off, but different UV resolution. The inflaton dynamics and w are not affected by the UV cut-off for the duration of the simulations.

resolution has a negligible effect on the inflaton dynamics. On the other hand, since in the cases of radiation domination, energy always cascades slowly towards high-k modes it was also important to verify that the UV cut-off does not affect the inflaton dynamics and the evolution of the equation of state, cf. Fig. (6.14). We found that with 256^3 and 512^3 boxes with the same IR cut-off, effects due to the finite UV resolution become important after 2 e-folds after back-reaction for $n \lesssim 2$ and much later for $n > 2$, i.e., always long after radiation domination is established.

6.4 Observational implications

6.4.1 CMB observables

The numerical studies presented in the previous section give us a new look on the expansion history of our universe. We have shown that for all potentials that are steeper than quadratic near the origin, $n > 1$, and any value of M, the oscillating inflaton condensate fragments due to self-resonance. The equation of state approaches that of a radiation dominated universe at sufficiently late times. In fact, the time it takes for the universe to make the transition from an inflationary to a radiation dominated state, in the case of negligible couplings between the inflaton and light species of matter, can be used as an upper bound on the duration of this intermediate period. It is justified because if interactions are stronger (but still perturbative), than the production of relativistic daughter particles is even more effective than due to self-resonance, and the transition is faster. Even with non-perturbative decay to massless fields (say via bi-quadratic interactions), our statement about the upper bound is not expected to change [33].[8] All of

[8]However, care is needed in interpreting our claim. The decay to sufficiently massive fields or non-perturbative dynamics of massless fields coupled to the inflaton when (for example) defects form can change this conclusion.

these insights can help us improve the uncertainties in the predictions of individual models of inflation in a rather general way, without the need for a specific reheating model. In the remainder of the section we derive the improved predictions for two cosmological observables – the scalar spectral index, $n_{\rm s}$, and the tensor-to-scalar ratio, r, and compare them to the most recent constraints from measurements of the CMB.

Slow-roll inflation yields a nearly scale-invariant power-spectrum of the curvature perturbation, $\mathcal{R}$, see eq. (1.59). The amplitude of the curvature perturbations, $A_{\rm s} \approx 2.2 \times 10^{-9}$, is measured at the pivot scale $k_\star = 0.05\,{\rm Mpc}^{-1}$, whereas the observed running of the scalar spectral index, $dn_{\rm s}/d\ln k$, is consistent with 0 [2].

On the other hand, the best constraints on the tensor-to-scalar ratio, r, are evaluated at a pivot scale of $k_\star = 0.002\,{\rm Mpc}^{-1}$ and are shown in Fig. 6.17, together with those for $n_{\rm s}$. Note that the quoted values of $n_{\rm s}$ are for measurements carried out at a different pivot scale – $0.05\,{\rm Mpc}^{-1}$. However, since there is no running in the scalar spectral index, it is safe to assume that the same constraints on it hold for $k_\star = 0.002\,{\rm Mpc}^{-1}$ [2]. Henceforth, we will use $0.002\,{\rm Mpc}^{-1}$ as the value of the pivot scale when calculating predictions for $n_{\rm s}$ and r.[9]

In the slow-roll approximation, see eq. (1.61),

$$\begin{aligned} n_{\rm s} &= 1 - 3m_{\rm Pl}^2\left(\frac{V_\star'}{V_\star}\right)^2 + 2m_{\rm Pl}^2\frac{V_\star''}{V_\star}\,, \\ r &= 8m_{\rm Pl}^2\left(\frac{V_\star'}{V_\star}\right)^2\,, \end{aligned} \tag{6.21}$$

where $V_\star \equiv V(\phi_\star)$, etc. and $\phi_\star$ is the value of the inflaton field at the time when the co-moving pivot scale crossed out the Hubble radius $k = k_\star = a_\star H_\star$. The number of *e*-folds of expansion before the end of inflation, $N_\star$, when this happened, is, cf. eq. (5.2),

$$N_\star = \left|\int_{\phi_\star}^{\phi_{\rm end}} \frac{V}{V'}\frac{d\phi}{m_{\rm Pl}^2}\right|\,. \tag{6.22}$$

Here $\phi_{\rm end}$ is the value of the inflaton field at the end of inflation, $\ddot{a} = 0$.[10] In conventional studies of reheating $N_\star$ is effectively treated as a free parameter in the range $50 < N_\star < 60$ due to uncertainties related to the post-inflationary expansion history. Comparisons with observations can lead to constraints on the duration of the transition from an inflationary to a radiation dominated state, $\Delta N_{\rm rad}$, and the reheating temperature, $T_{\rm th}$, for a given expansion history, $w(\Delta N)$, and inflaton potential parameters [45–47, 51, 134, 135, 137–142]. In this chapter, we tackle the problem from the opposite direction. Thanks to our numerical studies, we have a better understanding of $w(\Delta N)$ and an upper bound on $\Delta N_{\rm rad}$. Thus, we can treat $N_\star$ as a known quantity (with a known variation) and use it to actually constrain inflaton potential parameters. To this end we need to derive an expression for $N_\star$ from mapping modes between horizon crossing, $k_\star = a_\star H_\star$,

[9] For the calculation of the inflaton potential parameters in Section 6.3.2, we have used the value of $A_{\rm s}$ measured at $k_\star = 0.05\,{\rm Mpc}^{-1}$. We have checked that our results do not change with the variation of the model parameters for pivot scales in the range $0.002\,{\rm Mpc}^{-1} \leq k_\star \leq 0.05\,{\rm Mpc}^{-1}$, assuming eq. (1.59).

[10] In principle, one can calculate $\phi_{\rm end}$ from the inflaton dynamics during inflation. Nevertheless, a good estimate, sufficient for our purposes, can be obtained from setting the potential slow-roll parameter, $\epsilon_{\rm V} = m_{\rm Pl}^2\left(V'/V\right)^2/2$, to 1.

during inflation and re-entry, $k_\star = a_0 H_0$, at late times. We start from

$$\begin{aligned}\frac{k_\star}{a_0 H_0} &= \frac{a_\star H_\star}{a_0 H_0} \\ &= \frac{a_\star}{a_{\rm end}}\frac{a_{\rm end}}{a_{\rm rad}}\frac{a_{\rm rad}}{a_0}\frac{\rho_{\rm rad}^{1/4}}{H_0}\frac{\rho_{\rm end}^{1/4}}{\rho_{\rm rad}^{1/4}}\frac{H_\star}{\rho_{\rm end}^{1/4}}\,,\end{aligned} \tag{6.23}$$

where $N_\star \equiv \ln(a_{\rm end}/a_\star)$ and $\Delta N_{\rm rad} \equiv \ln(a_{\rm rad}/a_{\rm end})$. Note that $\rho_{\rm rad}$ is the mean energy density at the beginning of radiation domination, $w \to w_{\rm rad} = 1/3$, which is captured by our lattice simulations. The universe need not be in thermal equilibrium at that time. In fact, thermal equilibrium could be reached much later and we can determine the exact moment from

$$\rho_{\rm rad}^{1/4} a_{\rm rad} = \rho_{\rm th}^{1/4} a_{\rm th}\,, \tag{6.24}$$

where we assume that the universe is dominated by relativistic degrees of freedom while $a_{\rm rad} < a < a_{\rm th}$. Taking the log of eq. (6.23) after plugging-in eq. (6.24) and $H_\star^2 \approx V_\star/(3m_{\rm Pl}^2)$ yields

$$\begin{aligned}N_\star = &\ln\left(\frac{\rho_{\rm th}^{1/4}}{\sqrt{3}H_0}\frac{a_{\rm th}}{a_0}\right) + \frac{1}{4}\ln\left(\frac{V_\star^2}{m_{\rm Pl}^4\rho_{\rm end}}\right) \\ &- \ln\left(\frac{k_\star}{a_0 H_0}\right) - \Delta N_{\rm rad} + \frac{1}{4}\ln\left(\frac{\rho_{\rm rad}}{\rho_{\rm end}}\right)\,.\end{aligned} \tag{6.25}$$

The value of the first term is generally known, since it is determined by the physics of the late universe, while the second term depends only on the inflaton potential parameters and $A_{\rm s}$ through the constraint in eq. (6.30). The third term is a function of the pivot scale which we have already fixed, whereas the fourth and fifth terms can be extracted from the results of our lattice simulations for a given model. Therefore, $N_\star$ is solely a function of the inflaton potential parameters!

Note that the ratios $a_{\rm th}/a_{\rm rad}$ and $\rho_{\rm th}/\rho_{\rm rad}$ do not appear in eq. (6.25). Their absence is a manifestation of the importance of the expansion history over the thermal history of the universe in the context of mapping cosmological perturbation modes to early times. It is sufficient to know the evolution of the scale factor and the moment when $w \to 1/3$. The value of the redshift at which the universe reached local thermal equilibrium has no effect on the mapping of the modes (as long as $w = 1/3$, while $a_{\rm rad} < a < a_{\rm th}$ which is a reasonable assumption). Thus, one can, in principle, employ classical lattice simulations to calculate the expansion history up to $a = a_{\rm rad}$ and, thereby, connect inflationary predictions with observations without having to worry about thermalization, $T_{\rm th}$ and the end of reheating as a whole. To show that this is indeed the case, let us calculate the first term in eq. (6.25). The entropy, $s \sim gT^3$, (g being the number of effective bosonic degrees of freedom in thermal equilibrium) is conserved between the end of reheating and today

$$s_{\rm th} a_{\rm th}^3 = s_0 a_0^3\,, \tag{6.26}$$

whence,

$$\begin{aligned}\frac{\rho_{\rm th}^{1/4}}{\sqrt{3}H_0}\frac{a_{\rm th}}{a_0} &= \frac{\left(\pi^2 g_{\rm th} T_{\rm th}^4/30\right)^{1/4}}{\sqrt{3}H_0}\left(\frac{g_0 T_0^3}{g_{\rm th}T_{\rm th}^3}\right)^{1/3} \\ &= \left(\frac{\pi^2}{30}\right)^{1/4}\frac{g_0^{1/3} g_{\rm th}^{-1/12}}{\sqrt{3}}\frac{T_0}{H_0} \\ &\approx e^{66.89} g_{\rm th}^{-1/12}\,,\end{aligned} \tag{6.27}$$

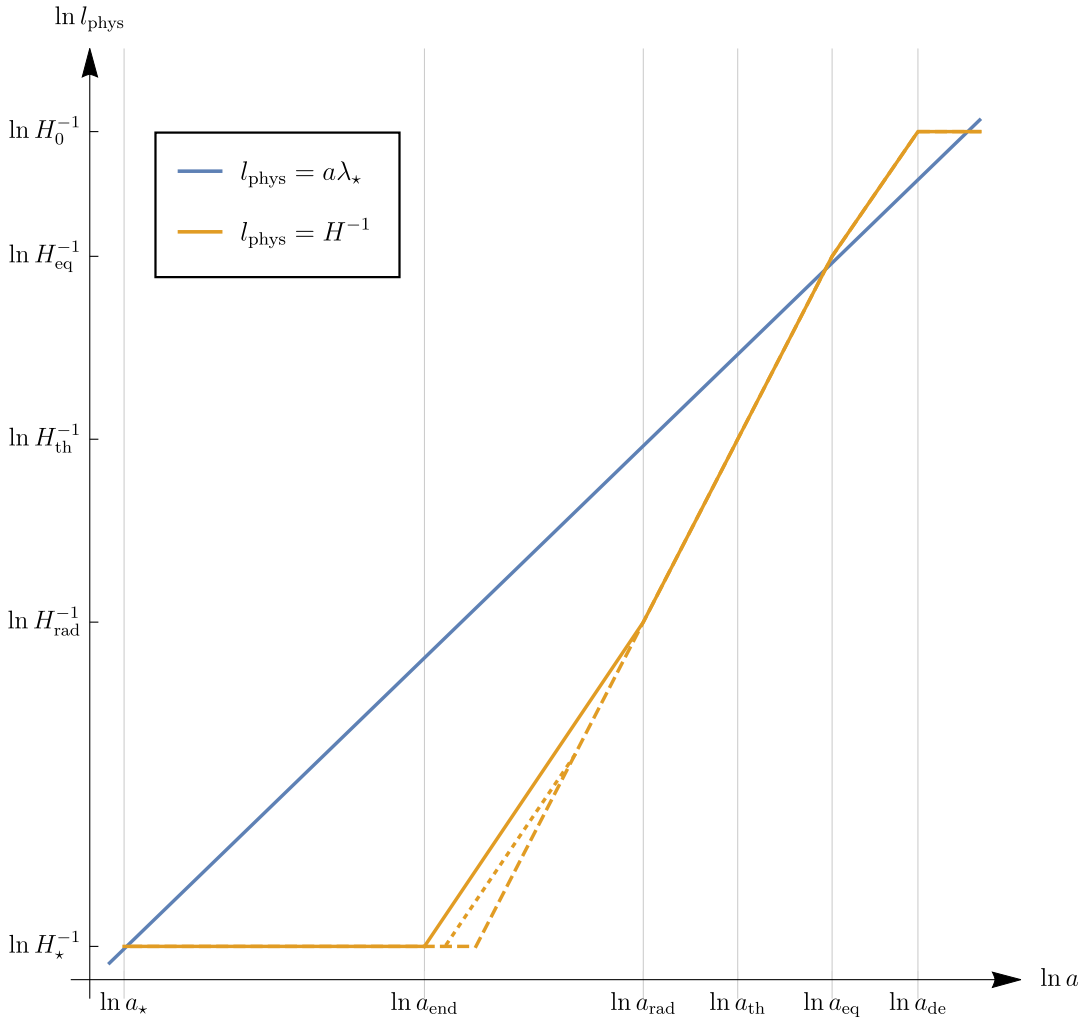

Figure 6.15: The figure illustrates our assumptions about the expansion history of reheating (see also Fig. 5.1 for notation). We assume that after $w = w_{\rm rad} = 1/3$, the equation of state remains constant until thermalization, i.e., for $a_{\rm rad} < a < a_{\rm th}$. We also assume that $w = w_{\rm hom} = (n-1)/(n+1)$ between the end of inflation and radiation domination, i.e., $a_{\rm end} < a < a_{\rm rad}$. The solid orange line shows the maximal value of $\Delta N_{\rm rad} \equiv \ln(a_{\rm rad}/a_{\rm end})$, determined by our lattice studies (for some value of the power in the range $1 < n < 2$; for $n > 2$ see Fig. 6.16) of self-resonance. Perturbative decays to relativistic daughter fields decrease $\Delta N_{\rm rad}$. The dashed line depicts the case of instantaneous transition to radiation domination, $\Delta N_{\rm rad} = 0$, whereas the dotted line stands for some intermediate value of $\Delta N_{\rm rad}$. Note that the dotted and solid orange lines are parallel to each other. Recall that $d(\ln H^{-1})/d(\ln a) = 3(1+w)/2$.

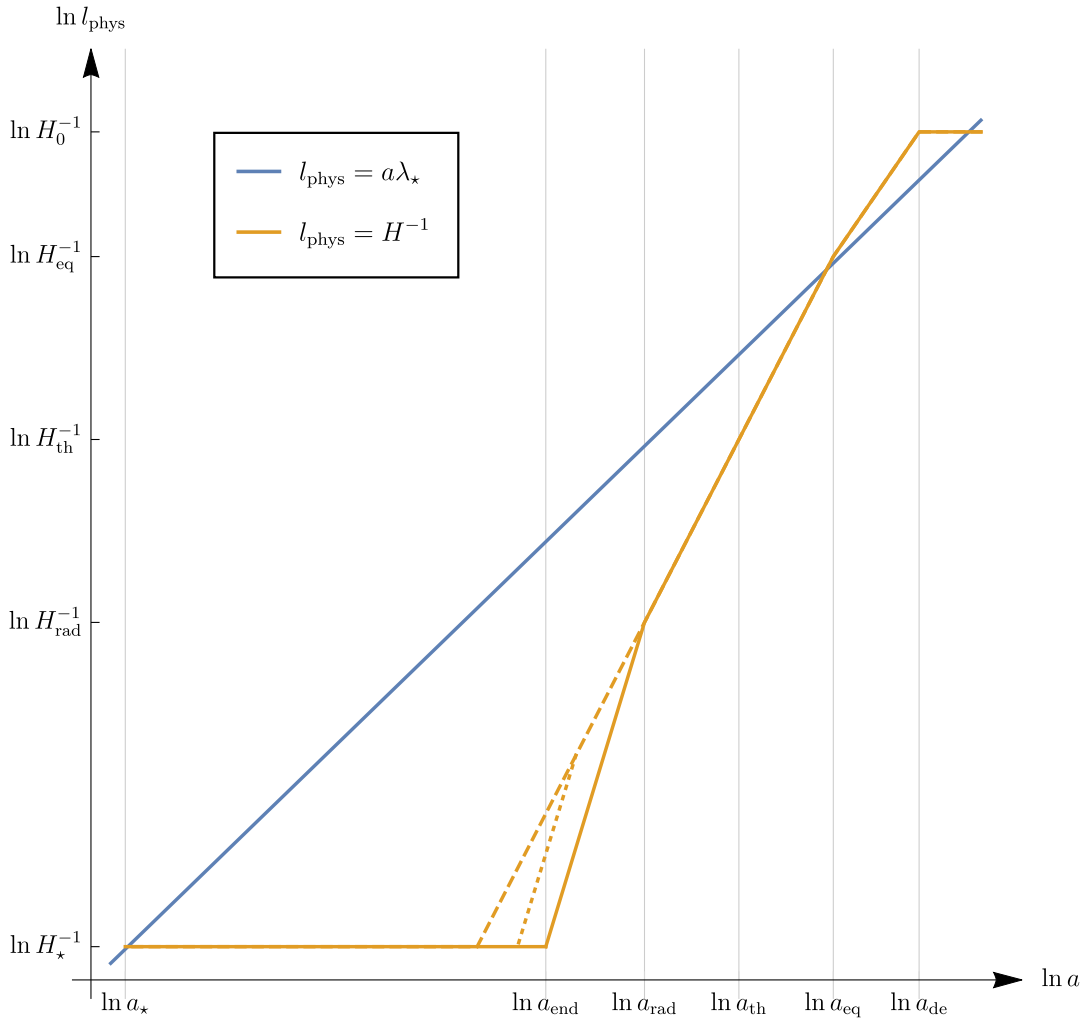

Figure 6.16: Same as Fig. 6.15, but for $n > 2$. Note that the dotted and solid orange lines are parallel to each other.

where $T_0 = 0.235\,\mathrm{meV}$ is the CMB temperature today, $g_0 = 43/11$, $H_0 = 67.6\,\mathrm{km\,s^{-1}\,Mpc^{-1}}$, $1\,\mathrm{Mpc} = 3.086 \times 10^{19}\,\mathrm{km}$. $g_{\rm th}$ is largely unknown. At the time of big-bang nucleosynthesis, $g_{\rm BBN} = 106.75$. In the analysis below, we let $g_{\rm th} = 1 - 10^5$. Luckily, due to the small power it is raised by in eq. (6.27), $g_{\rm th}$ affects the predictions for $n_{\rm s}$ and r negligibly.

In general, the time of $a = a_{\rm rad}$ depends on the specific model of reheating, e.g., the form and strength of the interactions of the inflaton with the other species of matter. Each model has to be dealt with on an individual basis, by carrying out expensive lattice simulations. Furthermore, the broad range of possible interactions leads to various expansion histories, increasing the range of $N_\star$ values for fixed inflaton potential parameters significantly. However, this is not the case for all observationally consistent models with $n > 1$. As we showed in Sections 6.3.2 and 6.3.2, in these models the approach to $w = w_{\rm rad}$ can be realised even with an isolated inflaton, completely decoupled from all other species of matter, evolving under the influence of its self-interactions and gravity only. Since any additional (perturbative) decay channel to

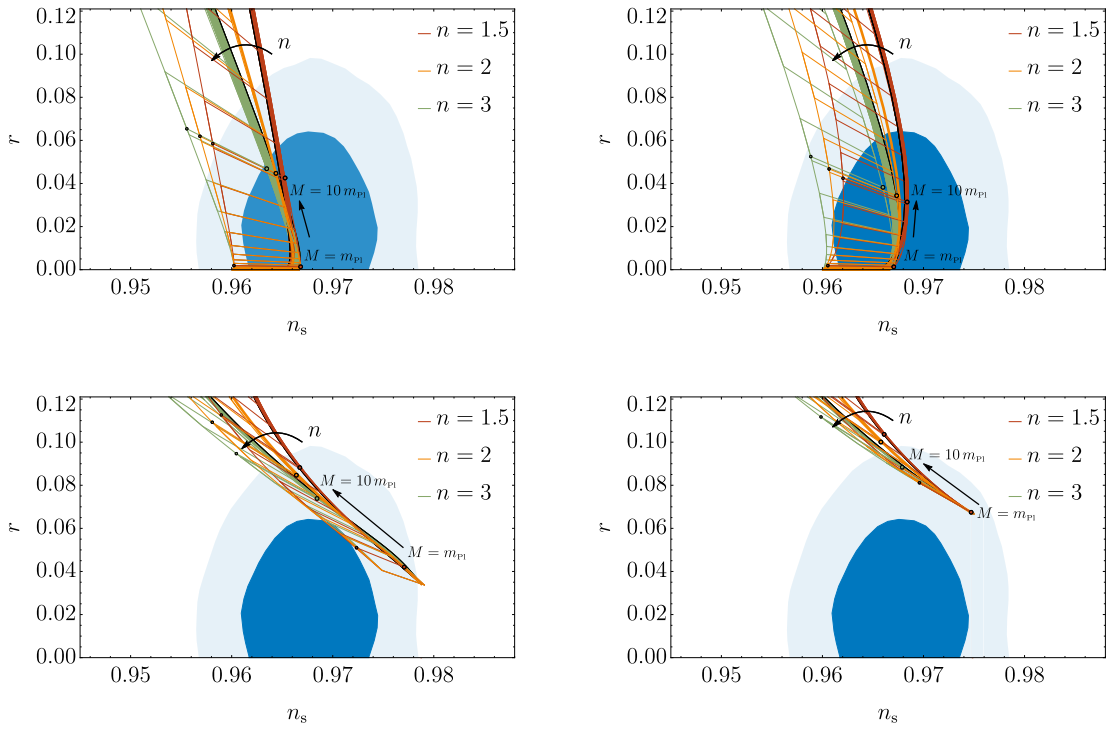

Figure 6.17: Top row from left to right: α-attractor T and E models. Bottom row from left to right: Monodromy models, $q = 0.5,\ 1$. The recently reported constraints on r and n_s by the Planck Collaboration [2] are shown with the blue shaded regions. Our predictions for $n = 1.5,\ 2,\ 3$ are given by the thick green, orange and red lines for different values of M. As the straight arrows indicate, as we increase M we move up the lines. The width of each thick line reflects the uncertainty from our analysis – $\Delta N_{\rm rad} \leq \Delta N_{\rm rad}^{\rm latt}$, i.e., the uncertainty from coupling the inflaton to other light fields. The black edges are for the upper bound. On the other hand the broad green, orange and red striped bands give the standard predictions for the same M and n. The width of each band accounts for the standard reheating-related uncertainties – $50 < N_\star < 60$. Our bounds on the expansion history after inflation, reduce the uncertainties in $N_\star$ significantly and hence in the predictions for the two CMB observables, as can be seen in the figures.

daughter particles (which are typically relativistic) speeds up the approach to $w = w_{\rm rad}$, the $\Delta N_{\rm rad}$ obtained for an isolated inflaton can serve as an upper bound on the duration to radiation domination. Moreover, the expansion history takes a very simple form: $w = w_{\rm hom}$ if $0 < \Delta N < \Delta N_{\rm rad}$ and $w = w_{\rm rad}$ if $\Delta N > \Delta N_{\rm rad}$, where ΔN is the number of e-folds of expansion after inflation. The form of the evolution of w does not change if we turn on the (perturbative) interactions with daughter particles; only $\Delta N_{\rm rad}$ can decrease (down to 0 at most), see Figs. 6.15 and 6.16. This expansion history implies

$$\rho_{\rm end} a_{\rm end}^{6n/(n+1)} = \rho_{\rm rad} a_{\rm rad}^{6n/(n+1)}\,, \tag{6.28}$$

finally leading to

$$\begin{aligned} N_\star = 66.89 &- \frac{1}{12}\ln\left(g_{\rm th}\right) + \frac{1}{4}\ln\left(\frac{V_\star^2}{m_{\rm Pl}^4 \rho_{\rm end}}\right) \\ &- \ln\left(\frac{k_\star}{a_0 H_0}\right) + \frac{n-2}{2(n+1)}\Delta N_{\rm rad}\,. \end{aligned} \tag{6.29}$$

Recalling

$$A_{\rm s} = \frac{1}{12\pi^2}\frac{V_\star^3}{m_{\rm Pl}^6 V_\star'^2}\,, \tag{6.30}$$

we can now solve eqs. (6.22,6.29,6.30) simultaneously for $N_\star$, Λ and $\phi_\star$, for given values of M, n (and q) and substitute the results in eq. (6.21). The obtained values for $n_{\rm s}(M,n)$ and $r(M,n)$ are shown in Fig. 6.17 as thick green, orange and red lines for $n = 1.5$, 2, 3, respectively.[11] The width of each line reflects the uncertainty from coupling to other light fields, i.e., $\Delta N_{\rm rad} \leq \Delta N_{\rm rad}^{\rm latt}(M,n)$. For comparison we also give the predictions for the same M, n (and q), assuming the standard reheating related uncertainties $50 < N_\star < 60$, with the shaded broad bands. The width of each band reflects the uncertainty in $N_\star$. The figures clearly indicate that our analysis significantly reduces the theoretical uncertainties in the predictions for the CMB observables – from the standard broad lines to the thick lines that we have.

6.4.2 Reheating temperature

The analysis in the previous section emphasizes the importance of the expansion history in the determination of the inflationary observables such as the scalar spectral index $n_{\rm s}$ and the tensor-to-scalar ratio r. While it does not tell us much about the thermal history of the universe, it still allows us to calculate an upper bound on $T_{\rm th}$ for an 'isolated' inflaton (i.e., an inflaton whose couplings to additional light fields can be neglected during $a_{\rm end} < a < a_{\rm rad}$) when $n > 1$ and $n \neq 2$. If we assume that soon after the approach to a radiation-dominated state of expansion the universe reaches thermal equilibrium, i.e., $a_{\rm br} \lesssim a_{\rm rad} \lesssim a_{\rm th}$, then

$$\rho_{\rm th} = \frac{\pi^2}{30} g_{\rm th} T_{\rm th}^4 \lesssim 3 m_{\rm Pl}^2 H_{\rm br}^2 \approx \frac{m_{\rm br}^2 \phi_{\rm br}^2}{2n}\,, \tag{6.31}$$

whence, for the case when the first narrow instability band plays a major role,[12]

$$T_{\rm th} \lesssim \frac{\sqrt{b m_{\rm Pl} M}}{(\pi^2 g_{\rm th}/30)^{1/4}} \left[\frac{m_{\rm Pl}}{M}\frac{\Delta\kappa}{\kappa} d\delta \frac{n+1}{|4-2n|}\right]^{n/2}. \tag{6.32}$$

The new parameter appearing under the square root is defined as

$$b \equiv \frac{m/\sqrt{2n}}{m_{\rm Pl}(\bar\phi/M)^{n-1}}\,. \tag{6.33}$$

From eqs. (6.4,6.7) it follows that

$$b \equiv \begin{cases} \sqrt{3\pi^2 A_{\rm s}/N_\star^2} & {\rm T}\,, \\ 2\sqrt{3\pi^2 A_{\rm s}/N_\star^2} & {\rm E}\,, \\ \sqrt{\frac{6q\pi^2 A_{\rm s}/n}{\left(2qN_\star m_{\rm Pl}^2/M^2\right)^{q/4}}}\,(q m_{\rm Pl}/M)^2 & {\rm Mon}\,. \end{cases} \tag{6.34}$$

This upper bound on the reheating temperature holds when the thermal equilibrium is reached after the end of self-resonance when $w = 1/3$. If the inflaton is coupled strongly enough to additional light fields and $w = 1/3$ is reached earlier, due to the inflaton decays into other relativistic degrees of freedom, then the reheating temperature can be even higher, with the upper bound set by the energy scale of inflation.

[11] We have used $g_{\rm th} = 10^3$, however, letting it vary in the range $1 - 10^5$, does not change the location and the thickness of the lines in any visible way.

[12] In eqs. (6.32,6.33) we use $M/2$ in place of M, for the E-models.

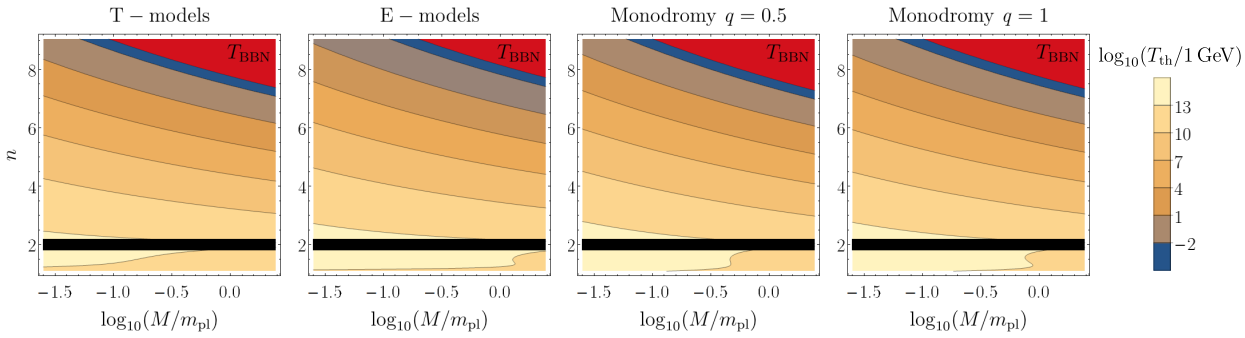

Figure 6.18: The upper bound on the reheating temperature, $T_{\rm th}$, as a function of M and n in the limit when the self-couplings of the inflaton dominate over its couplings to other species of matter. The red areas in the upper right corners in each panel represent regions in parameter space for which the upper bound on $T_{\rm th}$ for an isolated inflaton is less than the lower bound (1 MeV) imposed by the big-bang nucleosynthesis scenario. The horizontal black bands near $n = 2$ remind us that we cannot arrive at an upper bound on the reheating temperature on the basis of the expansion history alone for a quartic potential. The monotonic decrease of $T_{\rm th}$ with n and $M/m_{\rm Pl}$ for $n > 2$ can be understood from the duration of the self-resonance due to the narrow instability band. As upon increasing any of the two parameters it takes longer for fragmentation to take place, the energy density would be redshifted to lower values at the time of back-reaction, too, hence the observed dependence.

On the other hand, BBN provides a lower bound: $T_{\rm th} > T_{\rm BBN} \sim 1\,{\rm MeV}$. If it saturates the upper one in eq. (6.32), then we know that significant couplings to additional light fields have to be introduced explicitly, to make sure that energy is transfered early enough from the condensate to relativistic species of matter and the reheating temperature can be raised to the observationally allowed region. In Fig. 6.18 we plot the numerical values of $T_{\rm th}$ from eq. (6.32) along with the constraints from BBN. They become important only for large n and $M/m_{\rm Pl}$. Qualitatively, this can be understood from the nature of the self-resonance. Since $\Delta N_{\rm br}$ increases monotonically with n and/or $M/m_{\rm Pl}$ for $n > 2$, cf. eq. (6.11), then the energy scale at back-reaction (and the upper bound on $T_{\rm th}$) will decrease because of the prolonged oscillatory period during which the energy of the condensate is redshifted. These dependences can be seen directly in the square brackets in eq. (6.32). Note that the additional M term appearing under the square root in front of the square brackets comes from the energy scale of inflation and has opposite effect, i.e., the higher M is the greater the energy scale at the end of inflation is and hence the greater $T_{\rm th}$ is. However, this effect is not sufficiently strong and the overall dependence on M is determined by the duration of the self-resonance.

Another use of the expression in eq. (6.32) is that it gives us an estimate for the characteristic energy scale at the time of back-reaction and fragmentation. This then tells us the typical frequency of gravitational waves emitted due to the non-linear dynamics. For instance, since the planned mHz gravitational wave detector LISA [120] is expected to probe early universe phase transitions at characteristic temperatures $10^2 - 10^3\,{\rm TeV}$, then from Fig. 6.18 follows that for $n \gtrsim 5$ and $M \gtrsim m_{\rm Pl}$ the peak in the power-spectrum of the stochastic gravitational wave background from phase transitions occurring shortly after self-resonance should be in the $1\,{\rm mHz}$ range today. We present a more detailed discussion in the following section.

6.4.3 Gravitational waves

The fragmentation of the inflaton condensate due to resonant particle production during preheating can lead to the generation of a stochastic gravitational wave background (GWB) [118, 178–180]. For narrow

self-resonance, the power-spectrum of the GWB (at the time of its generation) is peaked near the typical physical momentum of produced particles. In this section we will estimate the frequency of the peak today, as well as its height, for different models and parameters.

Let us start with a derivation of the frequency observed today of a signal with co-moving wavenumber k, generated during the time of back-reaction. The frequency (in Hz) can be written as

$$\begin{aligned} f &= \frac{1}{2\pi}\frac{k}{a_0} \\ &= \frac{1}{2\pi}\frac{k}{a_{\rm br}\rho_{\rm br}^{1/4}}\left(\frac{\rho_{\rm br}}{\rho_{\rm rad}}\right)^{1/4}\frac{a_{\rm br}}{a_{\rm rad}}\frac{a_{\rm rad}}{a_0}\rho_{\rm rad}^{1/4}\,. \end{aligned} \tag{6.35}$$

We now make the mild assumption that $\rho a^4 = \text{const}$ for $a_{\rm rad} < a < a_{\rm th}$, define a mean equation of state $\rho a^{3(1+w)} = \text{const}$ for $a_{\rm br} < a < a_{\rm rad}$ and recall that entropy conservation for $a > a_{\rm th}$ implies

$$\frac{\rho_{\rm th}^{1/4} a_{\rm th}}{\rho_{\rm rel,0}^{1/4} a_0} = \left(\frac{g_{\rm th}}{g_0}\right)^{-1/12}\,, \tag{6.36}$$

where $\rho_{\rm rel,0}$ is the energy stored in relativistic degrees of freedom today. All of this yields

$$f = \frac{1}{2\pi}\frac{k}{a_{\rm br}\rho_{\rm br}^{1/4}}\left(\frac{a_{\rm br}}{a_{\rm rad}}\right)^{(1-3w)/4}\left(\frac{g_{\rm th}}{g_0}\right)^{-1/12}(3\Omega_{\rm rel,0})^{1/4}\sqrt{m_{\rm Pl}H_0}\,. \tag{6.37}$$

It can be further simplified, by substituting for the known parameters $\Omega_{\rm rel,0} = 4.3\times10^{-5}h_{100}^{-2}$, $h_{100} = 0.67$ and again assuming $g_{\rm th} = 10^3$ and $a_{\rm br} \approx a_{\rm rad}$, to

$$f = \frac{k}{a_{\rm br}}\frac{1}{\rho_{\rm br}^{1/4}} \times 4\times10^{10}\,{\rm Hz}\,. \tag{6.38}$$

The planned GW detectors LISA, BBO and Ligo O5 [120, 181] will have their best sensitivities in the mHz, Hz and 10^2 Hz ranges, respectively. We would like to see for what model parameters f will fall into these ranges. By looking at eq. (6.38) one can see two competing effects. The first factor giving the physical wavenumber at the time of the generation of the GWB is proportional to the Hubble parameter at that moment. The earlier the GWB is generated, the smaller the horizon at that time is and hence the higher the frequency is. The energy density in the second term has the opposite effect. The more efficient the resonance is (i.e., the earlier the time of back-reaction is) the greater the mean energy density of the universe is and hence the lower the frequency is. This second effect is a manifestation of the redshifting of the gravitational waves – the earlier in time they are generated the longer they are redshifted to lower frequencies. Overall, the first effect wins, since the Hubble parameter is proportional to the square root of the mean energy density. Hence, if we wish to drive f from eq. (6.38) to small enough values to be of observational interest, we need to consider 'inefficient' self-resonance (i.e., sufficiently slow particle production). This can be seen explicitly from the following expressions

$$\frac{k}{a_{\rm br}} \sim \frac{m_{\rm br}}{\sqrt{2n}} \equiv \beta^{-1}H_{\rm br}\,, \tag{6.39}$$

$$f \sim \beta^{-1} \sqrt{\frac{H_{\rm br}}{\sqrt{3} m_{\rm Pl}}} \times 4 \times 10^{10}\,{\rm Hz}\,. \tag{6.40}$$

Finally, after applying what we have learned for the fragmentation of the condensate from the previous sections we find that

$$\beta = d\delta \times \begin{cases} (\Delta\kappa/\kappa)(n+1)/|4-2n|\,, & n \neq 2\,, \\ 1\,, & n = 2\,, \end{cases} \tag{6.41}$$

and that the frequency reduces to[13]

$$f \sim \left(\frac{m_{\rm Pl}}{M}\right)^{(n-1)/2} \beta^{(n-2)/2} \sqrt{b} \times 10^{10}\,{\rm Hz}\,, \tag{6.42}$$

where we have ignored factors of order unity. We will use the last expression to calculate predictions for the gravitational wave signal in the remainder of this section. However, the frequency as written in eq. (6.40) can shed some light on what values of the parameters n and M fall in the mHz–10^2 Hz range. The typical value of β for self-resonance is 10^{-3}, hence an energy scale of back-reaction $\sim 10^2 - 10^3\,{\rm TeV}$ leads to $f \sim 1\,{\rm Hz}$. According to Section 6.4.2, such energy scales are expected for $n \gtrsim 5$ and $M \gtrsim m_{\rm Pl}$.[14]

To check whether GWBs, whose peak falls in the observationally interesting frequency range, can be indeed probed with upcoming experiments, we need to consider the actual strength of the signal itself. Normally, it is characterized by the ratio of the GW energy density by logarithmic co-moving momentum interval and the critical energy density of the universe today, i.e.,

$$\Omega_{\rm GW,0} h_{100}^2 = \frac{h_{100}^2}{\rho_{\rm c,0}} \frac{d\rho_{\rm GW,0}}{d\ln k}\,. \tag{6.43}$$

We are again interested in the value of this quantity for the peak of the GWB. Since $\rho_{\rm GW} a^4 = {\rm const}$ one can easily show that

$$\Omega_{\rm GW,0} h_{100}^2 = \Omega_{\rm GW,br} \left(\frac{a_{\rm br}}{a_{\rm rad}}\right)^{1-3w} \left(\frac{g_{\rm th}}{g_0}\right)^{-1/3} \Omega_{\rm rel,0} h_{100}^2\,. \tag{6.44}$$

Since

$$\rho_{\rm GW,br} \sim \dot{h}_{ij}^2 m_{\rm Pl}^2 \sim \left(\frac{\nabla h_{ij}}{a_{\rm br}}\right)^2 m_{\rm Pl}^2\,, \tag{6.45}$$

and

$$\ddot{h}_{ij} \sim \frac{\Delta h_{ij}}{a_{\rm br}^2} \sim \frac{[\partial_i\phi\partial_j\phi]^{TT}}{m_{\rm Pl}^2} \tag{6.46}$$

and if we assume that a fraction $\delta_{\rm grad}$ of the mean energy density at the time of back-reaction is stored in the form of gradients then

$$\begin{aligned} \rho_{\rm GW,br} &\sim H_{\rm br}^2 m_{\rm Pl}^2 \left(\frac{H_{\rm br}}{k/a_{\rm br}}\right)^2 \delta_{\rm grad}^2 \\ &\sim \rho_{\rm c,br} \left(\frac{H_{\rm br}\delta_{\rm grad}}{m_{\rm br}/\sqrt{2n}}\right)^2 = \rho_{\rm c,br}\beta^2\delta_{\rm grad}^2\,, \end{aligned} \tag{6.47}$$

[13] We again use $M/2$ in the place of M for the E-models.

[14] Note that for phase transitions $\beta \sim 1$ and such energy scales lead to $f \sim 1\,{\rm mHz}$.

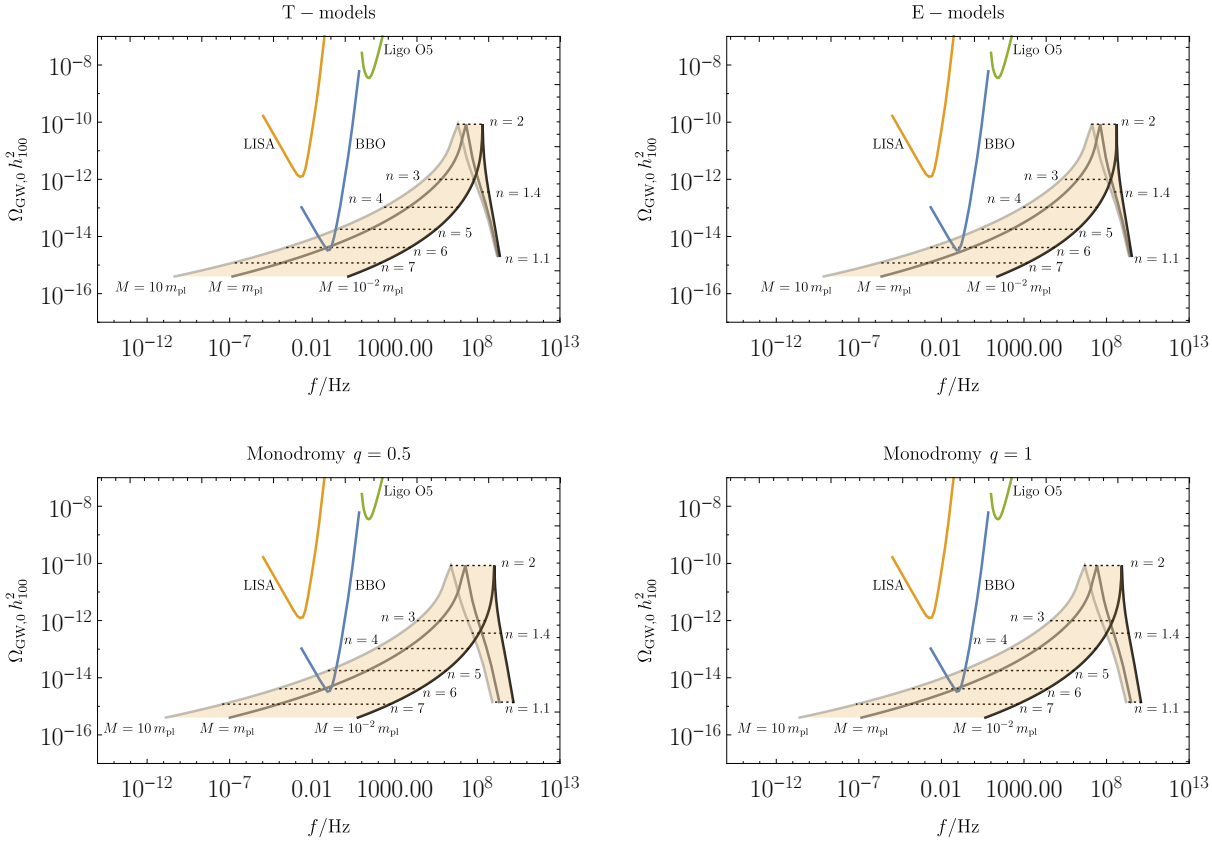

Figure 6.19: The contemporary typical gravitational wave energy density from fragmentation due to particle production from the first narrow instability band (vertical axes) as a function of its frequency today (horizontal axes). The light gray, gray, dark gray lines are for $M = 10m_{\rm Pl}$, $m_{\rm Pl}$, $10^{-2}m_{\rm Pl}$, respectively, for different values of n. The green, blue and orange 'buckets' give the target regions for planned gravitational wave detectors [120, 181].

implying $\Omega_{\rm GW,br} \sim \beta^2\delta^2_{\rm grad}$. After substituting for it in eq. (6.44) we arrive at

$$\Omega_{\rm GW,0}h^2_{100} \sim \beta^2\delta^2_{\rm grad}\left(\frac{a_{\rm br}}{a_{\rm rad}}\right)^{1-3w}\left(\frac{g_{\rm th}}{g_0}\right)^{-1/3}\Omega_{\rm rel,0}h^2_{100}\,. \tag{6.48}$$

Plugging in the values of the known parameters and setting $a_{\rm br} \approx a_{\rm rad}$, finally yields

$$\Omega_{\rm GW,0}h^2_{100} \sim 10^{-5}\beta^2\delta^2_{\rm grad}\,. \tag{6.49}$$

In the calculations below we will use $\delta_{\rm grad} = 1/3$ for a virialised scalar field. The typical values of $\Omega_{\rm GW,0}h^2_{100} < 10^{-10}$ are quite small. Qualitatively, this could be understood from the following reasoning. The factor of 10^{-5} in eq. (6.49) comes from $\Omega_{\rm rel,0}$. Since gravitational waves redshift as radiation (or relativistic matter) we expect $\Omega_{\rm GW}$ to scale linearly with $\Omega_{\rm rel}$, which has been decreasing since the epoch of equality. The additional β suppression is a consequence of the suppression of GW production on subhorizon scales sourced by the anisotropic part of the energy momentum tensor of the scalar field, cf. eq. (6.47).

Our estimates for the peak of the stochastic GWB, due to the fragmentation of the condensate after particle production from the first narrow instability band, are summarized in Fig. 6.19. The shape for a set of n and fixed M does not change significantly as we vary M. The prominent maximum at $n = 2$ and the decrease as we move away from it can be understood in terms of $\beta(n)$. Unfortunately, most of the parameter space is unlikely to be probed by planned GW detectors. Only $5 < n < 6$ and $M > m_{\rm Pl}$ lies within the target space of BBO. However, a natural justification for this values of the parameters is not clear, whereas observations of the CMB introduce additional constraints: $M < 10 m_{\rm Pl}$. Furthermore, in this scenarios slow-roll inflation occurs at high energies $\sim 10^{15}\,\mathrm{GeV}$. Then the inflaton oscillates for ~ 25 *e*-folds before particle production from the first narrow instability band can cause back-reaction and fragmentation, again posing some serious questions about the naturalness of this scenario.

6.5 Conclusions

We investigated the post-inflationary dynamics of the inflaton field governed by observationally consistent potentials that are sufficiently flat away from the origin and going as simple power-laws, $\propto |\phi|^{2n}$, near it. Through a combination of semi-analytic and numerical methods we showed that self-resonance can be important even when the inflaton is not coupled to other fields. We observed that for different parts of parameter space, the inflaton can fragment through a narrow self-resonance or broad self-resonance. In the latter case, the complete fragmentation of the inflaton in combination with the profile of its potential lead to the formation of pseudo-solitonic objects, that are long-lived (short-lived) for $n = 1$ ($n > 1$). The long-lived objects, also known as oscillons [36, 146, 147] dominate the energy budget of the universe, and since they behave as dust, $w \approx 0$, and can survive for many *e*-folds of expansion, the inflaton needs to have an additional channel to decay into relativistic matter and set the stage for BBN. The short-lived objects also behave as dust and can survive for up to $\mathcal{O}(1)$ *e*-folds of expansion. We have shown that the objects cannot collapse under their own gravity and form black holes. Nevertheless, it might be worthwhile to include gravitational interactions in simulations that run for much longer times to see if sufficient local densities can be build up by accretion and collisions to produce a population of blackholes, or at least additional structure on small scales [148–150].

As the transients decay away, the universe becomes radiation dominated. A similar trend is observed for back-reaction after narrow self-resonance for $n > 1$, although we do not observe the formation of any transient objects. In both cases, we find that at late times the field evolves in a turbulent manner [18, 19, 145] and that the relativistic modes dominate the energy budget of the universe, leading to a radiation-dominated period of expansion[15], $w \to w_{\rm rad} = 1/3$. We show that this simple result can be relevant for the bounds on CMB observables such as $n_{\rm s}$ and r. The fact that a completely decoupled inflaton from the rest of the matter sector attains a radiation-like equation of state allows us to put limits on the duration of the transition between the inflationary and radiation-dominated states of expansion. The length of the period, $\Delta N_{\rm rad}$, is maximal if we ignore couplings of the inflaton to other light fields and is set by self-resonance, whereas it can decrease (down to 0 *e*-folds of expansion) if we introduce (perturbative) interactions with other light fields. We provide analytical expressions for the upper bound on $\Delta N_{\rm rad}$. This is then transferred on the number of *e*-folds, $N_\star$, before the end of inflation when the pivot scale left the Hubble horizon and leads to substantial reduction in the uncertainties in the predictions for $n_{\rm s}$ and r.

[15]This is a purely empirical result which calls for a further analytical study.

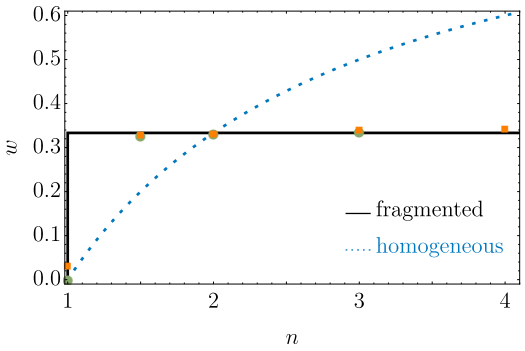

Figure 6.20: A summary for the *asymptotic* equation of state without coupling to additional fields. The numerical results from lattice simulations are shown as green circles for $M \approx 2.45\, m_{\rm Pl}$, and orange squares for $M \approx 7.75 \times 10^{-3} m_{\rm Pl}$. The dotted blue line is the expectation from a homogeneous, oscillating condensate.

We have shown that our results hold for quite general potential profiles. In this work we considered symmetric (asymmetric) models – α-attractor T (E) models [159, 160], which are extremely flat away from (only on one side of) the origin, as well as power-law potentials inspired by Monodromy inflation [161, 162]. The only requirement for broad self-resonance to be efficient and for formation of localized objects is the potential profile to be flatter than $\propto |\phi|^{2n}$ in some region away from the origin. The field scale where the potential makes the transition from flat to power-law, M, has to be also $\ll m_{\rm Pl}$ in order for the expansion rate of the universe to be much lower than the resonant excitation rate. Otherwise, when $M \sim m_{\rm Pl}$ the amplitude of inflaton oscillations decays away faster than the particle production rate due to the broad instability band. But still, at late times the condensate oscillates in the $V \propto |\phi|^{2n}$ region, and the non-linearities give rise to narrow instability bands and to a slow and steady particle production. However, the potential with $n = 1$ does not feature any narrow instability bands and the condensate remains. Hence, for a quadratic minimum, no matter what the value of M in terms of $m_{\rm Pl}$ is, the inflaton always ends up with a matter-like equation of state, $w = 0$. To ensure the transition to a radiation-dominated state of expansion, required as an initial condition for primordial nucleosynthesis, we need to introduce couplings to other light fields [35]. We plan to return to this issue in a future work.

In the $n = 1$ case, when coupling to other massless fields is included, the dynamics can be quite complex, especially for $M \ll m_{\rm Pl}$ due to the existence of oscillons [31, 36, 182]. For general n, the inclusion of additional decay channels to massive fields and non-minimal couplings [23, 25, 97], gravitational effects [83, 183], as well as certain quantum aspects [184] not captured by our classical simulations can influence predictions from this epoch. Finally, note that for $n > 1$, our results hold even if the inflaton has an additional small mass as long as this mass is much smaller than the effective mass due to the curvature of the potential during the approach to radiation domination. Eventually, this small mass as well as the masses of the daughter fields the inflaton is coupled to, might play a role in the decays and the equation of state.

We have also estimated the peaks in the power-spectrum of stochastic gravitational wave backgrounds generated by the gradual fragmentation for $M \sim m_{\rm Pl}$, $n > 1$ and found small ranges in parameter space that could be probed with future gravitational wave detectors. We leave the investigation of gravitational waves emitted by the decay of the transients when $M \ll m_{\rm Pl}$, $n > 1$ for a future work.

In summary, for the class of observationally consistent models considered in this chapter, we have determined the post-inflationary equation of state of the universe by taking the fragmentation of the inflaton

field into account. We found a rather general result at sufficiently late times:

$$w \to \begin{cases} 0 & \text{if } n = 1\,, \\ 1/3 & \text{if } n > 1\,, \end{cases} \tag{6.50}$$

i.e., for potentials with non-quadratic minima, the equation of state parameter reaches $1/3$ even without couplings to other massless fields; for quadratic minima, the equation of state is zero with or without fragmentation, see Fig. 6.20. Under the stated assumptions, we provided an upper bound on the duration to radiation domination as a function of general features of the potential using a linear stability analysis, and verified this time-scale using numerical simulations. Finally, we showed that such bounds can reduce the uncertainty in inflationary observables.

Part III

Reheating with a charged inflaton

In this part of the thesis we consider different natural models of reheating in which the inflaton is charged under a symmetry. We consider non-perturbative particle production in the linear stage of preheating and also the ensuing non-linear evolution. We begin in Chapter 7 with a study of a reheating baryogenesis model in which the inflaton is a complex scalar, showing that post-inflationary non-linear dynamics should not be ignored when calculating global quantities such as the baryon-to-photon ratio, η. We then proceed in Chapter 8 with an investigation of the resonant particle production of gauge fields in models with an inflaton charged under a local symmetry. We pay particular attention to technical issues such as choice of gauge and initial conditions from inflation for parametric resonance in order to rigorously study non-perturbative production of gauge fields during the linear stage of preheating. In Chapter 9 we present a numerical scheme for studying the subsequent non-linear evolution of the combined inflaton gauge fields system.

Chapter 7

Generating the observed matter-antimatter asymmetry

Abstract

The dynamics at the end of inflation can generate an asymmetry between particles and anti-particles of the inflaton field. This asymmetry can be transferred to baryons via decays, generating a baryon asymmetry in our Universe. We explore this idea in detail for a complex inflaton governed by an observationally consistent – "flatter than quadratic"– potential with a weakly broken global $U(1)$ symmetry. We find that most of the inflaton asymmetry is locked in non-topological soliton like configurations (oscillons) produced copiously at the end of inflation. These solitons eventually decay into baryons and generate the observed matter-antimatter asymmetry for a range of model parameters. Through a combination of three dimensional lattice simulations and a detailed linearized analysis, we show how the inflaton asymmetry depends on the fragmentation, the magnitude of the symmetry breaking term and initial conditions at the end of inflation. We discuss the final decay into baryons, but leave a detailed analysis of the inhomogeneous annihilation, reheating and thermalization to future work. As part of our work, we pay particular attention to generating multifield initial conditions for the field fluctuations (including metric perturbations) at the end of inflation for lattice simulations.

7.1 Introduction

Can the observed matter-antimatter asymmetry in our Universe be connected to the dynamics at the end of inflation? An affirmative answer would allow us to connect the earliest stages of the Universe's history to this intriguing asymmetry in our Universe.

Inflation provides the necessary initial conditions for the formation of structure in our Universe [3, 4]. However, once inflation ends the energy of the inflaton must eventually be converted into standard model particles as well as dark matter (reheating). Reheating connects inflationary physics with better understood physics of the Standard Model, possibly via intermediaries. The end of inflation and reheating can be complex, with non-linear dynamics giving rise to a number of distinctly non-perturbative phenomena such

as inflaton fragmentation, explosive particle production, defect formation etc. [11, 14, 36]. It also has a number of challenging but important observational consequences (see for example [16]).

Experiences from our immediate surroundings, as well as from cosmological observations tell us that there are more baryons than anti-baryons in our Universe [185]. Moreover, the number of baryons compared to photons is extremely small [2]

$$\eta \approx 6 \times 10^{-10}. \tag{7.1}$$

These observations beg the question of how such an asymmetry was generated. Sakharov [110] (see Sec. 5.2.1) provided the conditions necessary to generate such an asymmetry (i) departure from thermal equilibrium (ii) CP and C violation (iii) non-conservation of baryon number. Within the Standard Model, baryogenesis is difficult [186]. A number of ideas for the generation of baryon asymmetry, with ingredients from beyond the Standard model have been put forth (see for example [187, 188]). Amongst the many proposals, the Affleck-Dine mechanism [103] is often invoked to generate the requisite asymmetry using extra scalar fields. Such fields are easily available in supersymmetric extensions of the Standard Model.

Recently, a variation of the Affleck-Dine mechanism using the inflaton as the Affleck-Dine scalar field was proposed in [38, 189] (for an earlier, related work, see [190]). The authors provide an elegant analysis of asymmetry generation from the *homogeneous* dynamics of the inflaton at the end of inflation and provide possible particle physics embeddings to generate the observed baryon asymmetry. While the homogeneous analysis is sufficient for the quadratic inflation scenario (analyzed in detail in these papers), such an analysis is insufficient when nonlinearities in the potential are present and lead to fragmentation of the inflaton.

The main goal of this chapter is understanding the effects of inflaton fragmentation on the generated asymmetry. We will show that when nonlinearities in the potential are present, the asymmetry can be qualitatively and quantitatively different from the homogeneous scenario. Moreover, the fragmentation leads to copious formation of pseudo-solitonic configurations (oscillons [177, 191–194]) after inflation which lock up most of the energy density as well as the asymmetry. Some of these oscillons have an inflaton excess, others have an anti-inflaton excess. They eventually decay to generate the observed baryon asymmetry in the Universe.

We model the inflaton as a complex scalar field with a potential motivated by monodromy inflation [161, 162, 195–197]. As in [189], we add a small $U(1)$ breaking term to generate the inflaton/anti-inflaton asymmetry. While we focus on this particular model for concreteness, we expect our qualitative results to hold for a much broader class of "flatter than quadratic" potentials because of the results in [36].

In this chapter, we focus on the non-linear aspects of the inflaton asymmetry generated at the end of inflation. We provide an estimate of the generated baryon-to-photon ratio under some simplifying assumptions. However, we leave the problem of detailed quark/baryon dynamics, annihilation and thermalization for future work. The highly inhomogeneous nature of the field configurations of the inflaton, the particle physics details of decay to quarks/baryons and their diffusion along with subsequent annihilations make a more detailed calculation necessary.

We briefly review some of the previous work related to this chapter. This review is not exhaustive; our aim is to try and put our work in the context of previous literature. Inhomogeneous fragmentation of the inflaton and soliton formation, but without baryogenesis, has been analyzed before (for example see [36, 198, 199]). Q-ball [200, 201] formation has also been analysed in the context of Affleck-Dine baryogenesis with supersymmetric flat directions (for example see [104, 105]). In our case, the inflaton acting as the Affleck-Dine field fragments into oscillons (rather than Q-balls) which carry most of the asymmetry. The connection between Q-balls and baryogensis has been discussed extensively in the literature

[104]. Oscillons have been found in a number of reheating studies as well (for example [36, 147, 199, 202]). In this chapter, our focus has been inflaton fragmentation, soliton formation and asymmetry generation within the context of the scenario in [189]: inflationary asymmetry generation due to a small breaking of global $U(1)$ symmetry. We also believe that our work provides the first explicit connection between oscillons and baryogenesis. For a different inhomogeneous baryogenesis scenario, see for example [203]. For further reviews on baryogenesis see [187, 204]

The rest of the chapter is organized as follows. In Sec. 7.2 we explicitly write down the complex inflaton model along with the $U(1)$ symmetry breaking term and define the inflaton asymmetry. In Sec. 7.3 we discuss initial conditions for our lattice simulations, linear instability in the oscillating inflaton condensate and the non-linear dynamics of the complex inflaton field. In this section we also discuss the formation of oscillons. In Sec. 7.4 we show how the inflaton asymmetry is generated in the homogeneous and fully fragmented case. We discuss the dependence of the asymmetry on the parameters of the model. We also discuss the decay into baryons, as well as the relation of the baryon asymmetry to the inflaton asymmetry. We conclude in Sec. 8.8, with a summary of our work, comments on additional observational implications and future directions. In Appendix A, we provide a formal, linearized calculation of the asymmetry.

We will assume an approximately Friedmann-Robertson-Walker (FRW) universe with a metric of the form[1]

$$ds^2 = [1 + 2\Psi(t, \mathbf{x})]\, dt^2 - a^2(t)\, [1 - 2\Psi(t, \mathbf{x})]\, d\mathbf{x}^2, \tag{7.2}$$

where $a(t)$ is the scalefactor. We include the metric perturbations for the calculation of *initial conditions* for our lattice simulations. However, for subsequent non-linear evolution after the end of inflation (on subhorizon scales), we assume an FRW metric.

7.2 Inflaton model and asymmetry

In this section we model the inflaton, the breaking of global $U(1)$ symmetry and define some relevant measures of the inflaton/anti-inflaton asymmetry.

7.2.1 The inflaton model

We model the inflaton as a complex scalar field ϕ, whose action is given by

$$S = \int d^4x \sqrt{-g} \left[-\frac{m_{\rm Pl}^2}{2} R + g^{\mu\nu} \partial_\mu \phi \partial_\nu \phi^* - V(\phi, \phi^*) \right], \tag{7.3}$$

where $g_{\mu\nu}$ is the metric, g is the determinant of $g_{\mu\nu}$ and R is the Ricci scalar. The equation of motion of the inflaton ϕ is

$$g^{\mu\nu} \nabla_\mu \nabla_\nu \phi + \partial_{\phi^*} V(\phi, \phi^*) = 0. \tag{7.4}$$

The conjugate of eq. (7.4) yields the equation of motion for ϕ^*.

The potential $V(\phi, \phi^*)$ consists of two parts:

$$V(\phi, \phi^*) = V_{\rm s}(|\phi|) + V_{\rm br}(\phi, \phi^*), \tag{7.5}$$

[1]We set the two metric potentials equal to each other. This is valid for a linear calculation in both the metric and the field fluctuations for canonical scalar fields.

where $V_{\rm s}(|\phi|)$ respects the global $U(1)$ symmetry: $\phi \to e^{i\theta}\phi$. This part of the potential controls the dynamics of the field during and after inflation (though there are some corrections from $V_{\rm br}$). $V_{\rm br}(\phi, \phi^*)$ on the other hand, breaks the global $U(1)$ symmetry, and is chosen to be subdominant, at least energetically, at all times. For concreteness, we assume the following form for $V_{\rm s}(|\phi|)$:

$$\begin{aligned} V_{\rm s}(|\phi|) &= m^2 M^2 \left[\sqrt{1+2\frac{|\phi|^2}{M^2}} - 1\right], \\ &= \begin{cases} m^2|\phi|^2 - \frac{m^2}{2M^2}|\phi|^4 + \ldots & |\phi| \ll M \\ \\ \sqrt{2}m^2 M|\phi| - m^2M^2 + \ldots & |\phi| \gg M. \end{cases} \end{aligned} \tag{7.6}$$

During inflation $|\phi| \gtrsim m_{\rm Pl} \gg M \gg m$. The form of the potential is motivated by the monodromy inflation scenarios [161, 195–197]. Such "flattened" potentials are not only well motivated theoretically, but are consistent with observations [2].

For the symmetry breaking term, $V_{\rm br}(\phi, \phi^*)$, we can choose

$$V_{\rm br}(\phi, \phi^*) = \frac{c_3}{3}\frac{m^2}{M}\left(\phi^3 + \phi^{*3}\right). \tag{7.7}$$

This is the lowest dimension symmetry breaking term considered in [189] (note that in terms of notation, our c_3 is different from the one defined there). The cubic power ensures that the symmetry breaking term is subdominant at late times after the end of inflation when the inflaton potential is $V_{\rm s}(|\phi|) \approx m^2|\phi|^2$. The coefficient m^2/M is chosen to make c_3 dimensionless. For the large field values (i.e. during inflation), this symmetry breaking term might dominate unless c_3 is small enough. To avoid this, we must have

$$c_3 \ll \frac{1}{N}\left(\frac{M}{m_{\rm Pl}}\right)^2, \tag{7.8}$$

where N is the number of e-folds of inflation. For $N = 55$ and $M = 10^{-2}m_{\rm Pl}$ we get $c_3 \ll 10^{-6}$.

However, if we do not want c_3 to be very small, $V_{\rm br}$ can be modified as

$$\begin{aligned} V_{\rm br}(\phi, \phi^*) &= \frac{c_3}{3}\frac{m^2}{M}\frac{\left(\phi^3 + \phi^{*3}\right)}{f(|\phi|)}, \\ f(|\phi|) &= \left(1 + 2\frac{|\phi|^2}{M^2}\right)^2. \end{aligned} \tag{7.9}$$

Since $f(|\phi|) \gg 1$ during inflation, it naturally suppresses the symmetry breaking term during inflation.[2] We prefer to work with this form of the symmetry breaking term since we wish to explore the c_3 dependence, even when c_3 is close to 1. While appearing innocuous here, this also leads to an extra suppression of this term in inhomogeneous regions with large field values (even after the end of inflation).

For future reference, note that at the end of inflation $|\phi|_{\rm end} \sim m_{\rm Pl} \gg M$. Hence $V_{\rm s}(|\phi|_{\rm end}) \gg V_{\rm br}(\phi_{\rm end}, \phi^*_{\rm end})$.

[2]One could imagine such a factor arising due to a conformal transformation from the Jordan to Einstein frame.

7.2.2 Inflationary constraints

In our potential, we have two mass scales: m and M. If one of them is chosen, the other is determined based on the amplitude of the curvature fluctuations observed in the cosmic microwave background [2] (see eq. (1.61)):

$$\begin{aligned} A_{\rm s} &= \frac{1}{12\pi^2}\left(\frac{m}{m_{\rm Pl}}\right)^2\left(\frac{M}{m_{\rm Pl}}\right)(2N_\star)^{3/2}, \\ &\approx 2.2\times 10^{-9}, \end{aligned} \tag{7.10}$$

where we have ignored the symmetry breaking term during inflation. More explicitly for $N_\star = 55$ we have

$$m = 1.5\times 10^{-5}\left(\frac{m_{\rm Pl}}{M}\right)^{3/2} M. \tag{7.11}$$

For example with $M = 10^{-2}m_{\rm Pl}$, we get $m = 1.5\times 10^{-4}m_{\rm Pl}$. For the rest of the chapter, we will only consider M as a free parameter.

For our model (with $N_\star = 55$), we get a scalar spectral index $n_s = 0.97$ and the tensor-to-scalar ratio $r_{0.002} = 0.07$; consistent with Planck [2] (see Fig. 6.17).

7.2.3 Inflaton asymmetry

The difference between the number of inflaton and anti-inflaton particles can be written in terms of the fields as follows[3]

$$\Delta N_\phi = N_\phi - N_{\phi^*} = i\int d^3x a^3(\phi^*\dot\phi - \dot\phi^*\phi). \tag{7.12}$$

In absence of a symmetry breaking term, this number is conserved. Using the equations of motion we get

$$\frac{d}{dt}\Delta N_\phi = i\int d^3x a^3\left[\phi\partial_\phi - \phi^*\partial_{\phi^*}\right]V_{\rm br}. \tag{7.13}$$

For the particular symmetry breaking term defined in eq. (7.9), we get

$$\begin{aligned} \frac{d}{dt}\Delta N_\phi &= ic_3\frac{m^2}{M}\int d^3x a^3\frac{\left(\phi^3 - \phi^{*3}\right)}{f(|\phi|)}, \\ &= -2c_3\frac{m^2}{M}\int d^3x a^3\frac{|\phi|^3\sin 3\theta}{f(|\phi|)}, \end{aligned} \tag{7.14}$$

where we used $\phi = |\phi|e^{i\theta}$. We define a spatially averaged asymmetry density and a spatially averaged energy density:

$$\begin{aligned} \Delta n_\phi(t) &\equiv \frac{\Delta N_\phi}{a^3 V_{\rm com}}, \\ \bar\rho_\phi(t) &\equiv \frac{\int d^3x a^3\left[|\dot\phi|^2 + a^{-2}|\nabla\phi|^2 + V(\phi,\phi^*)\right]}{(a^3 V_{\rm com})}, \end{aligned} \tag{7.15}$$

[3]We define this quantity assuming an FRW metric. As we discuss later, this is justified since the asymmetry generation from fragmentation happens on subhorizon scales where the metric perturbations can be ignored.

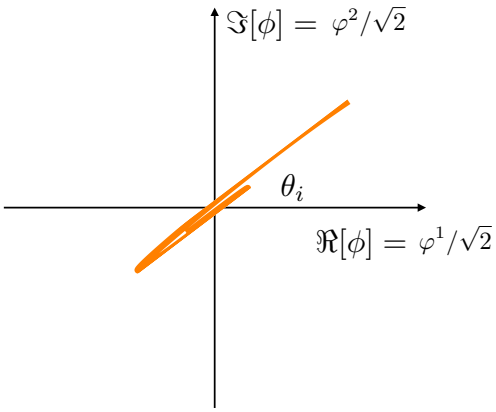

Figure 7.1: A qualitative picture of the homogenous evolution of the complex inflaton field. During inflation, the symmetry breaking term is suppressed. As a result $\theta_i = \theta_{\rm inf} =$ constant. Note that the field typically starts spiraling around $|\phi| \lesssim m_{\rm Pl}$.

where $V_{\rm com}$ is the comoving volume of interest. A dimensionless ratio characterizing the inflaton asymmetry [189] is given by

$$A_\phi(t) = \frac{\Delta n_\phi}{(\bar{\rho}_\phi/m)}. \tag{7.16}$$

From now on, we will refer to this ratio as the inflaton asymmetry. For future convenience, we define another useful spatially dependent quantity, an "asymmetry density" as follows:

$$\mathcal{A}_\phi(t,\mathbf{x}) = \frac{\phi^*(t,\mathbf{x})\dot{\phi}(t,\mathbf{x}) - \dot{\phi}^*(t,\mathbf{x})\phi(t,\mathbf{x})}{(\bar{\rho}_\phi/m)}. \tag{7.17}$$

7.3 Inflaton dynamics

The equation of motion for the scalar field is given by eq. (7.4). Both for numerical and analytic calculations, we find it is convenient to decompose the field into its "cartesian components":

$$\phi = \frac{\varphi^1 + i\varphi^2}{\sqrt{2}}. \tag{7.18}$$

The equation of motion can then be written as

$$g^{\mu\nu}\nabla_\mu\nabla_\nu\varphi^J + \partial^J\mathcal{V} = 0, \tag{7.19}$$

where $J = 1, 2$. Note that the covariant derivatives include the homogeneous and the inhomogeneous parts of the metric. The potential in terms of the two fields is as follows:

$$\begin{aligned}\mathcal{V} &= \mathcal{V}_{\rm s} + \mathcal{V}_{\rm br},\\ \mathcal{V}_{\rm s} &= m^2 M^2 \left[\sqrt{1 + \frac{\delta_{IJ}\varphi^I\varphi^J}{M^2}} - 1\right],\\ \mathcal{V}_{\rm br} &= \frac{c_3}{3\sqrt{2}}\frac{m^2}{M}\frac{(\varphi^1)^3 - 3\varphi^1(\varphi^2)^2}{f(\varphi^1,\varphi^2)}.\end{aligned} \tag{7.20}$$

As usual, repeated indices are summed over.

We can solve eq. (7.19) along with appropriate Einstein equations on a lattice, without further approximations. However, it would be a waste of computational resources to use the lattice simulations when the perturbations are small. For evolution during inflation and up to the end of inflation (or until the fluctuations in the field remain small compared to the background), we will solve the above system after linearizing in the field fluctuations. We include the metric fluctuations here since they are important for perturbations on horizon and superhorizon scales. At the end of inflation, we switch to a lattice code, which solves the full non-linear field equation, but ignores the fluctuations of the metric. This is reasonable because although the field becomes highly nonlinear, the metric fluctuation still remains small. Moreover, we chose a simulation volume which is comparable to the comoving size of the horizon at the end of inflation since fragmentation happens on subhorizon scales (for the model considered). After the end of inflation modes never leave the horizon since the horizon grows faster than the scale factor. As a result, horizon related metric effects only matter right at the end of inflation for our simulation volume, and can be ignored thereafter. With these considerations, we include metric fluctuations in calculating the initial conditions for the fluctuations at the end of inflation, but ignore them in the lattice simulation.

7.3.1 Homogeneous inflaton dynamics

The homogeneous dynamics of the field and the metric are controlled by

$$\begin{aligned}&\ddot{\varphi}^I + 3H\dot{\varphi}^I + \partial^I\mathcal{V} = 0,\\ &H^2 = \frac{1}{3m_{\rm Pl}^2}\left[\frac{1}{2}\delta_{IJ}\dot{\varphi}^I\dot{\varphi}^J + \mathcal{V}\right].\end{aligned} \tag{7.21}$$

Recall that $\varphi^1 = \sqrt{2}|\phi|\cos\theta$ and $\varphi^2 = \sqrt{2}|\phi|\sin\theta$. Solving the above system numerically, we find that in the $\varphi^1 - \varphi^2$ plane, the field maintains a constant angle during inflation when the symmetry breaking terms are subdominant:

$$\theta_{\rm inf} = \tan^{-1}(\varphi^2/\varphi^1) = \text{const.} \tag{7.22}$$

After the end of inflation θ can vary, but its variation is suppressed by the size of the symmetry breaking term. In Fig. 7.1 we show a typical homogeneous trajectory. Note that this is a qualitative picture, the spiral is invisible for typical values of our chosen parameters.

In the usual Affleck-Dine baryogenesis, the Affleck-Dine condensate is rotating in the complex plane. In contrast, the homogeneous mode here maintains a collinear motion in the complex plane.

7.3.2 Linearized perturbations

For this section, our results are valid for N real fields. For the case at hand, $N = 2$.

When the field fluctuations are small, we can linearize the equations of motion for the field perturbations around the homogeneous values: $\varphi^I + \delta\varphi^I$. In Fourier space, the linearized equations of motion become

$$\delta\ddot{\varphi}^I_{\mathbf{k}} + 3H\delta\dot{\varphi}^I_{\mathbf{k}} + \left[\delta^I_J \frac{k^2}{a^2} + \partial^I\partial_J\mathcal{V}\right]\delta\varphi^J_{\mathbf{k}} = -2\Psi_{\mathbf{k}}\partial^I\mathcal{V} + 4\dot{\Psi}_{\mathbf{k}}\dot{\varphi}^I. \tag{7.23}$$

The potential $\Psi_{\mathbf{k}}$ and its derivative $\dot{\Psi}_{\mathbf{k}}$ are determined from the linearlized Einstein equations:

$$\begin{aligned} \dot{\Psi}_{\mathbf{k}} + H\Psi_{\mathbf{k}} &= \frac{1}{2m_{\text{Pl}}^2}\delta_{IJ}\dot{\varphi}^I\delta\varphi^J_{\mathbf{k}}, \\ \left(\dot{H} + \frac{k^2}{a^2}\right)\Psi_{\mathbf{k}} &= \frac{1}{2m_{\text{Pl}}^2}\delta_{IJ}\left[-\dot{\varphi}^I\delta\dot{\varphi}^J_{\mathbf{k}} + \delta\varphi^J_{\mathbf{k}}\ddot{\varphi}^I\right]. \end{aligned} \tag{7.24}$$

One can substitute the gravitational potential $\Psi_{\mathbf{k}}$ and its derivative $\dot{\Psi}_{\mathbf{k}}$ into the field equations for $\delta\varphi^J_{\mathbf{k}}$ to get a (coupled) linear system for $\delta\varphi^J$. Formally, we can write this linear system as

$$\mathbb{L}_k(t)\cdot\delta\vec{\varphi}_{\mathbf{k}}(t) = 0, \tag{7.25}$$

where

$$\delta\vec{\varphi}_{\mathbf{k}}(t) = \left[\delta\varphi^1_{\mathbf{k}}(t), \ldots, \delta\varphi^N_{\mathbf{k}}(t)\right]^T. \tag{7.26}$$

In the above equation $\mathbb{L}_k(t)$ is a linear, second-order-in-time differential operator that depends on k and t. It is a $N \times N$ matrix. For our case the operator $\mathbb{L}_k$ has the form

$$\begin{aligned} \mathbb{L}_k\cdot\delta\varphi_{\mathbf{k}}(t) = \delta\ddot{\vec{\varphi}}_{\mathbf{k}}(t) + 3H\delta\dot{\vec{\varphi}}_{\mathbf{k}}(t) + \frac{k^2}{a^2}\delta\vec{\varphi}_{\mathbf{q}} + \mathbb{M}(t)\cdot\delta\vec{\varphi}_{\mathbf{k}} \\ + \frac{1}{m_{\text{Pl}}^2}\left[\mathbb{X}(t,k)\cdot\delta\vec{\varphi}_{\mathbf{k}} + \left(\frac{aH}{k}\right)^2\mathbb{Y}(t,k)\cdot\delta\dot{\vec{\varphi}}_{\mathbf{k}}\right] = 0. \end{aligned} \tag{7.27}$$

The above system includes scalar gravitational perturbations (terms $\propto m_{\text{Pl}}^{-2}$). The matrices $\mathbb{X}(t,k)$ and $\mathbb{Y}(t,k)$ have the property $\mathbb{X}(t,k), H\mathbb{Y}(t,k) \ll (m_{\text{Pl}}^2H^2)(k/aH)^2$ as $k/aH \to \infty$.

The solution to this linear system can be written formally as

$$\delta\vec{\varphi}_{\mathbf{k}}(t) = \sum_{n=1}^{N} a_{\mathbf{k}n}\vec{u}_n(t,k) + a^*_{-\mathbf{k}n}\vec{u}^*_n(t,k), \tag{7.28}$$

where for each n,

$$\begin{aligned} \vec{u}_n(t,k) &= \left[u^1_n(t,k), \ldots, u^N_n(t,k)\right]^T, \\ \mathbb{L}_k(t)\cdot\vec{u}_n(t,k) &= 0. \end{aligned} \tag{7.29}$$

Note that the solution has $2N$ constants of integration and $2N$ "vector" solutions. The appearance of $a^*_{-n\mathbf{k}}$ is due to our assumption that $\delta\varphi^J_{\mathbf{k}}$ are Fourier transforms of real fields. In component form

$$\delta\varphi^J_{\mathbf{k}}(t) = \sum_{n=1}^{N} a_{\mathbf{k}n}u^J_n(t,k) + a^*_{-\mathbf{k}n}u^{J*}_n(t,k). \tag{7.30}$$

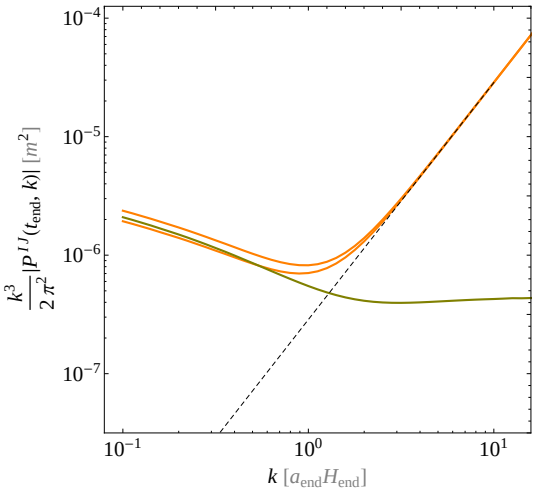

Figure 7.2: Different components of the power-spectra of the fields at the end of inflation (with $\theta_i = 0.7 \times \pi/3$). Inside the horizon, the diagonal components match the Minkowski space power-spectrum, whereas the cross spectra are small. Outside the horizon, the perturbation spectra (diagonal spectra (orange) and cross spectra(green)) are much larger that the Minkowski space approximations (dashed line). Starting from Bunch-Davies initial conditions deep inside the horizon during inflation, we evolved the perturbations including metric perturbations self consistently. Ignoring metric perturbations underestimates the spectra on superhorizon scales.

Quantization and power-spectra

We now follow the usual canonical quantization procedure and elevate $a_{n\mathbf{k}}$ and $a^*_{n\mathbf{k}}$ to operators

$$\begin{aligned} a_{\mathbf{k}n} &\to \hat{a}_{\mathbf{k}n}, \\ a^*_{\mathbf{k}n} &\to \hat{a}^\dagger_{\mathbf{k}n}, \end{aligned} \tag{7.31}$$

that satisfy the following commutation relations

$$\begin{aligned} [\hat{a}_{\mathbf{q}n}, \hat{a}_{\mathbf{k}m}] &= 0, \\ \left[\hat{a}_{\mathbf{q}n}, \hat{a}^\dagger_{\mathbf{k}m}\right] &= \delta(\mathbf{q}-\mathbf{k})\delta_{nm}. \end{aligned} \tag{7.32}$$

Notationally, this means putting "hats" on $\delta\varphi^J_{\mathbf{k}}$ and $\{a_{n\mathbf{k}}, a^*_{-n\mathbf{k}}\}$ in the mode expansion in eq. (7.30). This expansion in terms of creation and annihilation operators is consistent with the one provided in the last chapter of [55].[4] Following [55], we chose the Bunch-Davies vacuum as initial conditions. When the modes are sufficiently deep inside the horizon during inflation

$$u^J_n(t,k) \to \delta^J_n \frac{\exp\left[-ik\int_{t_{\rm in}}^t \frac{d\tau}{a(\tau)}\right]}{(2\pi)^{3/2}a(t)\sqrt{2k}}. \tag{7.33}$$

Here, $t_{\rm in}$ stands for a time when modes of interest are deep inside the horizon.

[4]We thank D. Kaiser, M. Hertzberg and J. Karouby for discussion on two field initial conditions. A further discussion of multifield initial conditions is presented in the review article [17].

We can now evolve $u_n^J(t,k)$ from deep inside the horizon during inflation, through horizon crossing and up to the end of inflation. It is convenient to decompose the complex u_n^J in terms of two real functions as follows

$$u_n^J(t,k) = \frac{1}{(2\pi)^{3/2}a(t_{\rm in})\sqrt{2k}}\left[f_n^J(t,k) - H(t_{\rm in})g_n^J(t,k) - i\frac{k}{a(t_{\rm in})}g_n^J(t,k)\right]. \tag{7.34}$$

The benefit of using f_n^J and g_n^J is numerical ease. They are real functions satisfying

$$\begin{aligned} f_n^J(t_{\rm in},k) &= \dot{g}_n^J(t_{\rm in},k) = \delta_n^J, \\ \dot{f}_n^J(t_{\rm in},k) &= g_n^J(t_{\rm in},k) = 0. \end{aligned} \tag{7.35}$$

The Bunch-Davies initial conditions are taken care of using the k dependent coefficients. Evolving f_n^J and g_n^J we can obtain the mode functions as well as the power-spectra at any time where the linearized analysis is valid. Once we have the mode evolution, we can calculate correlation functions for the fields on any scale.

Using the commutation relations, the correlation functions for the fields are then given by

$$\langle 0|\delta\hat{\varphi}_{\mathbf{q}}^I(t)\delta\hat{\varphi}_{\mathbf{k}}^{J\dagger}(t)|0\rangle = \delta(\mathbf{q}-\mathbf{k})P^{IJ}(t,k), \tag{7.36}$$

where

$$P^{IJ}(t,k) = \sum_{n=1}^{N} u_n^I(t,k)u_n^{J*}(t,k). \tag{7.37}$$

Note that the cross correlations are not necessarily zero and can be important, especially on superhorizon scales. This aspect has been ignored in the literature for setting up initial conditions for lattice simulations (to the best of our knowledge).[5]

For our two field model at hand, we plot the different components of the power-spectra at the end of inflation in Fig. 7.2. Note that the diagonal spectra converge to the Minkowski one deep inside the horizon, whereas the cross-spectra have an interesting plateau like behavior resulting from higher order corrections in aH/k (which can be derived by a careful WKB analysis):

$$\begin{aligned} P^{II}(k,t) &\to \frac{1}{(2\pi)^3 a^2(t)2k} \qquad k \gg aH, \\ P^{IJ}(k,t) &\to \mathcal{O}[(aH/k)^3] \qquad I \neq J, k \gg aH. \end{aligned} \tag{7.38}$$

Above we assume that k/a is larger than the effective mass from the potential and from gravitational effects. On superhorizon scales, the departure from Minkowski space power-spectrum as well as the effect of metric perturbations is significant. Moreover the cross spectra are also non-negligible on superhorizon scales.

Once we obtain $P^{IJ}(t,k)$ at the end of inflation, we can populate the modes on the lattice assuming a Gaussian distribution of amplitude with uncorrelated phases. To do so, it is convenient to chose a basis where $P^{IJ}(t_{\rm end},k)$ is diagonal. After populating the lattice using the above spectra, we rotate back to the original basis in the complex plane. This rotation back to the original basis is necessary. The final asymmetry generated depends on the breaking of $U(1)$ symmetry, and is sensitive to the angle of the homogeneous trajectory in the complex plane.

[5]Multifield mode evolution for calculating for example, cosmic microwave background observables, has been done before. See for example [205–208].

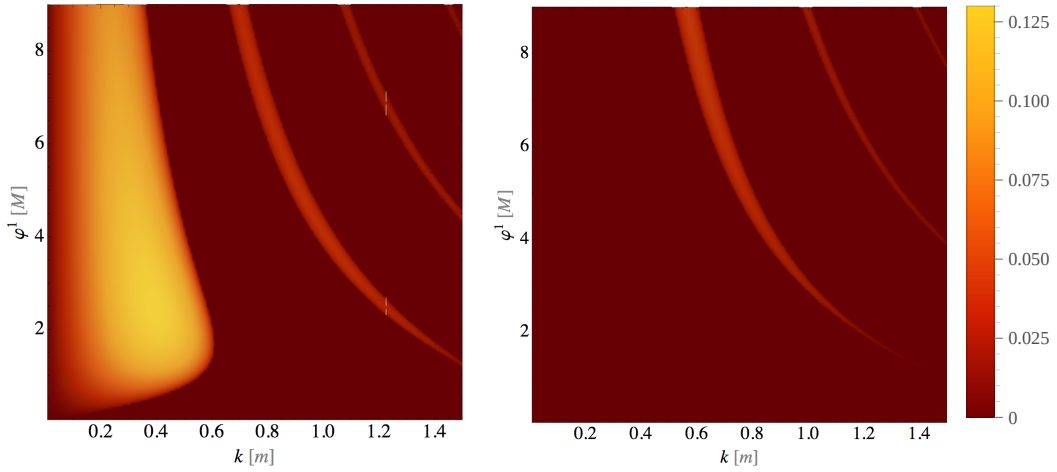

Figure 7.3: Floquet charts for field fluctuations: parallel to the motion of the homogeneous field (left) and perpendicular to the motion of the homogeneous field (right). The vertical axis is the amplitude of oscillation of the homogeneous mode (assumed to be in the φ^1 directions). Lighter colors correspond to unstable regions. The legend shows the magnitude of the real part of the Floquet exponent: $\Re(\mu_k)/m$. Note that the parallel perturbations have a broad, strong instability band near $k \lesssim 0.5m$ which is not present for the perpendicular perturbations.

Note that we have decided to self-consistently evolve mode functions with Bunch-Davies initial conditions from the time that modes are deep inside the horizon during inflation, up to the end of inflation. We could have chosen an instantaneous lowest energy state for each mode at the end of inflation. However, such a lowest energy state becomes ill-defined for modes outside the horizon [70]. While other prescriptions might be possible, we believe that our prescription is unambiguous and physically well-grounded because we start with initial conditions deep inside the horizon where all gravitational effects as well as interactions can be ignored.

Once the initial conditions are set, we use *LatticeEasy* [74] to evolve the fields. Before presenting the results of our simulations, we provide a linear analysis of the instabilities in the oscillating inflaton condensate. For the interested reader, we also provide the formalism to calculate the inflaton asymmetry based on the linearized fluctuations in Appendix A.

Floquet analysis

Soon after inflation ends, the almost homogeneous inflaton field starts oscillating around the minimum. The nonlinearities in the potential lead to an instability in the field fluctuations. The instability can be understood in terms of Floquet theory (see Section 2.2.1) that applies to linear equations of motion with periodic coefficients. Our linearized equations of motion for the fluctuations do not have strictly periodic coefficients because of expansion as well as due to the symmetry breaking terms. For sufficiently subhorizon scales and rapid growth, we can ignore the Hubble expansion (i.e. we set $H = 0$ and $a = 1$ for this section). For this section we also assume that $\mathcal{V}_{\rm br} \ll \mathcal{V}_{\rm s}$. With these assumptions, as a first approximation, we arrive at

$$\delta\ddot{\varphi}^I_{\mathbf{k}} + \left[\delta^I_J k^2 + \partial^I\partial_J\mathcal{V}_{\rm s}\right]\delta\varphi^J_{\mathbf{k}} \approx 0. \tag{7.39}$$

In absence of the symmetry breaking term, one can always rotate our field axes so that the homogeneous field is entirely along the φ^1 direction. In this case the equations of motion become:

$$\begin{aligned}\delta\ddot{\varphi}^1_{\mathbf{k}} + \left[k^2 + \frac{m^2}{(1+(\varphi^1)^2/M^2)^{3/2}}\right]\delta\varphi^1_{\mathbf{k}} \approx 0,\\ \delta\ddot{\varphi}^2_{\mathbf{k}} + \left[k^2 + \frac{m^2}{\sqrt{1+(\varphi^1)^2/M^2}}\right]\delta\varphi^2_{\mathbf{k}} \approx 0.\end{aligned} \tag{7.40}$$

As the field oscillates, the coefficients of both equations are periodic in time. According to Floquet theory, for each equation, the growing solution can be written as

$$\delta\varphi^J_{\mathbf{k}}(t,k) = \mathcal{P}^J_{\mathbf{k}+}(t)e^{\mu^J_k t} + \mathcal{P}^J_{\mathbf{k}-}(t)e^{-\mu^J_k t}, \tag{7.41}$$

where $\mathcal{P}^J_{\mathbf{k}\pm}(t)$ are periodic functions of time whereas μ^J_k are Floquet exponents. For a simple algorithm to calculate the exponents, in similar notation, see Appendix A of [209]. If the Floquet exponents have a real part, then we have exponentially growing solutions. We plot the real part of the Floquet exponents as a function of the amplitude of oscillations of the background field and the wavenumber k in Fig. 7.3. The lighter regions are regions of instability. It is evident, that fluctuations along φ^1 (i.e. parallel to the direction of the field) have broad regions of instability in contrast with the direction perpendicular to φ^1.[6] For the remainder of this section we concentrate on $\delta\varphi^1_{\mathbf{k}}$. In an expanding FRW universe, expansion of space counteracts the exponential growth discussed above. For the instability to be efficient in an expanding universe, we have to compare the Floquet exponents (the growth rate of perturbations) to the rate of expansion. If this ratio is large compared to 1 then we get a rapid growth of perturbations even in an expanding universe.

For the case at hand, the nonlinearities in the potential become important when $|\phi| \sim M$. For $|\phi| = \varphi^1/\sqrt{2} \sim M$, $H \sim m(M/m_{\rm Pl})$. From the results of Floquet analysis we get $\Re[\mu_k] \lesssim m$ for $\varphi^1 \sim M$. Putting in the appropriate numerical factors, the condition for efficient growth of perturbations is given by

$$\left[\frac{\Re(\mu^1_k)}{H}\right]_{\rm max} \approx \frac{1}{4}\frac{m_{\rm Pl}}{M} \gg 1. \tag{7.42}$$

For the factor of $1/4$ above, see [36]. Thus for fragmentation we need $M \ll m_{\rm Pl}$. From the full lattice simulations we find that fragmentation is efficient when $m_{\rm Pl}/M \gtrsim 40$.

7.3.3 Non-linear dynamics

Inflaton fragmentation

Soon after the beginning of parametric resonance, the perturbations become non-linear and back-react on the homogeneous field marking a breakdown of our linearized analysis. About 20 oscillations after the end of inflation, the inflaton field fragments. This fragmentation leads to the formation of long-lived, localized pseudo-solitonic "lumps". The fragmentation of the inflaton and formation of these pseudo-solitonic lumps is shown in Fig. 7.4. The "lumps" are highly over-dense regions, the contours in the above plots are drawn at

[6] Very recently, an analysis for linearized, uncoupled perturbations in the parallel and perpendicular directions was also provided by [40, 41].

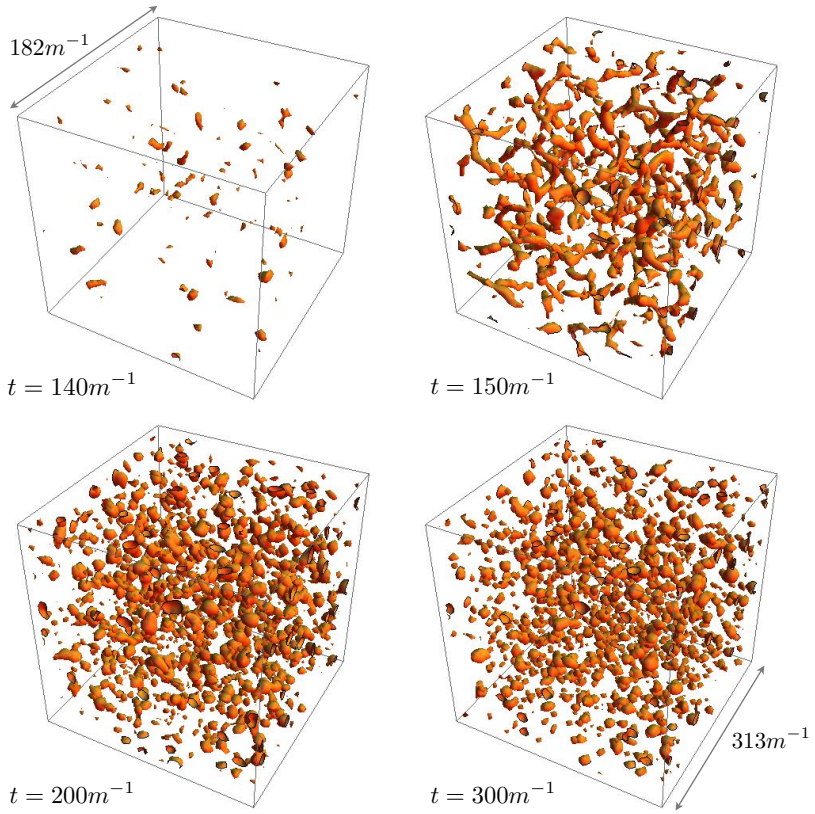

Figure 7.4: The homogeneous inflaton condensate starts fragmenting within ~ 20 oscillations after the end of inflation. The fragmentation is driven by parametric resonance in the fluctuations along the direction of motion of the field. After the perturbations become nonlinear, localized, long-lived field configurations called oscillons form and dominate the energy density of the inflaton field. The oscillons once formed maintain a fixed size and density, and can be very long lived with lifetimes $\gg m^{-1}, H^{-1}$. They are highly over dense regions, the contours in the above plots are drawn at $5\times$ the average density. Most of the inflaton asymmetry is locked in these oscillons although they occupy a small fraction of the volume. The co-moving size of the box is comparable to the Hubble horizon at the end of inflation.

$5\times$ the average density. Their central densities are often more than an order of magnitude above the average density. The lumps maintain a fixed central density and physical size as the universe expands.

A closer analysis of the lumps, reveals that they are "oscillon-like" configurations [191–193]. Oscillons are field configurations that are localized in space and oscillatory in time. Their field configuration rather than specific parameters in the Lagrangian controls their longevity [174, 175].

Oscillons are similar to Q-balls [200] in that they are localized, non-topological solitons [201]. However unlike Q-balls, the fields do not rotate in the complex plane and do not have a conserved charge. Below, we provide justification for why we call our "lumps" oscillons rather than Q-balls.

Oscillons vs. Q-balls

Ignoring the influence of the symmetry breaking terms, the general form of oscillons and Q-balls is given by

$$\begin{aligned}\phi_{\rm osc}(r,t) &= \epsilon\left[f_1(r) + i f_2(r)\right]\sin\omega t + \mathcal{O}[\epsilon^3],\\ \phi_{\rm Q}(r,t) &= f(r)e^{i\omega t},\end{aligned} \tag{7.43}$$

where $\omega < m$ and ϵ characterizes the amplitude of the oscillon. Heuristically, both objects arise when the scalar potential is effectively "shallower-than-quadratic" for some field values [194, 201, 210]. For oscillons, the field oscillates along a particular direction in the complex plane (in essentially 1 dimensional motion), whereas for Q-balls, the field rotates in the complex plane. Note that in the literature oscillons are usually defined for real fields. We have generalized this definition to a complex field. For oscillons, the higher order terms neglected here can be important when their central amplitude is large.

To determine whether our localized overdensities in our simulation are Q-balls or oscillons, we carried out the following two tests for a sample of 10 objects selected at random from our simulations. For the first test, we focus on the behavior of the field profiles. Note that

$$\begin{aligned}|\phi_{\rm osc}(r,t)|^2 &= \left[f_1^2(r) + f_2^2(r)\right]\sin^2(\omega t) + \ldots,\\ |\phi_{\rm Q}(r,t)|^2 &= f^2(r).\end{aligned} \tag{7.44}$$

We found that for our sample of solitons, the magnitude-squared of the field profile matched better with a sinusoidal time-dependence. [7]

Furthermore, the ratio of the real and imaginary parts of the field inside the two types of pseudo-solitons is given by

$$\frac{\Re(\phi)}{\Im(\phi)} \approx \begin{cases}\text{const}, & \text{oscillons},\\ \tan(\omega t), & \text{Q-balls}.\end{cases} \tag{7.45}$$

Again, for our sampled objects we found that this ratio was constant, consistent with oscillons.

For the length of the simulation, we found that our sample objects were oscillons. However, [198] have argued that similar fragmentation, albeit in a different potential and without a symmetry breaking term, generates Q-balls. We cannot rule out the possibility that if one waits for a longer time ($t \gg 300m^{-1}$) some of the oscillons will become Q-balls.

We note that the motion of the field inside the scalar field lumps cannot be purely radial, since in this case the asymmetry is obviously zero. Some deviation from collinear motion in the complex plane, sourced by the symmetry breaking term and/or by non-linear couplings between the radial and tangential directions, is necessary for there to be non-zero asymmetry. The exact nature of "oscillon like" solutions and their corresponding asymmetry is left for future work. We will continue to call our overdensities oscillons in what follows.

Although we are dealing with a two field model (or one complex field), the dynamics is very similar to a single real field scenario discussed in [36]. We find that the oscillons are $\sim 10m^{-1}$ in width with varying amplitudes $\gtrsim M$. The fields inside oscillons oscillate in phase with a frequency $\lesssim m$. The detailed profiles of oscillons and their lifetimes [175, 177, 210, 211], interactions [212, 213], their size distribution [146, 147] etc. will be studied elsewhere.

[7] We also note that the oscillons we find here have a breathing mode (as seen in [36]) making the higher order terms ignored above also relevant.

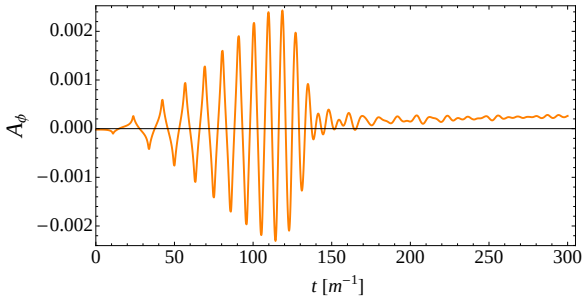

Figure 7.5: Evolution of the inflaton/anti-inflaton asymmetry as a function of time. The asymmetry is zero at the end of inflation ($t = 0$). Asymmetry is generated during the explosive dynamics after the end of inflation. After the inflaton fragments into localized solitons ($t \sim 150m^{-1}$), the asymmetry settles down to a constant value. We have not checked the asymmetry for significantly longer time-scales due to numerical considerations. Although not shown above, a similar plot for the asymmetry for the homogeneous case continues to show large oscillations and settles down at a much later time $t \geq 10^3 m^{-1}$.

Simulation details

We carry out a 3+1 dimensional lattice simulation of the fields in an expanding universe using a modified version of *LatticeEasy* [74]. As noted earlier, we ignore metric perturbations in the lattice code (although we include them in the initial conditions). Explicitly we solve the following equations in their discretized form

$$\begin{aligned} &\ddot{\varphi}^I + 3H\dot{\varphi}^I - \frac{\nabla^2}{a^2}\varphi^I + \partial^I \mathcal{V} = 0, \\ &H^2 = \frac{1}{3m_{\rm Pl}^2}\left[\frac{1}{2}\delta_{IJ}\left(\dot{\varphi}^I\dot{\varphi}^J + \frac{\nabla\varphi^I}{a}\cdot\frac{\nabla\varphi^J}{a}\right) + \mathcal{V}\right]_{\rm avg}, \end{aligned} \tag{7.46}$$

where $I, J = 1, 2$ and the potential is defined in eq. (7.20). The right-hand side of the H^2 equation is spatially averaged.

Our initial simulation volume was chosen to be $L = 25m^{-1}$, whereas the Hubble horizon at this initial time is $H^{-1} \approx 23m^{-1}$. We also varied the initial size of the box between $L = 25m^{-1}$ and $L = 50m^{-1}$ and found no significant difference between the results. This is due to the fact that resonance in our model is restricted to subhorizon scales. For $L = 50m^{-1}$, the initial power-spectrum on superhorizon scales is needed so as to not underestimate the power on those scales. While for this particular model, this superhorizon power does not affect the answers significantly, this need not be the case in general.

We ran our simulations for a period of $300m^{-1}$ after the end of inflation during which the universe expands by a factor of ≈ 12 (and the simulation volume continues to remain sub-Hubble). Beyond this point, we run into resolution issues, mainly because oscillons maintain a fixed physical size as the 'grid' expands. It is certainly feasible to run longer, higher resolution simulations. But for our purposes, we found a lattice with 128^3 points to be sufficient. We have checked that up to $t - t_{\rm end} \sim 300m^{-1}$ there were no qualitative difference between a 256^3 and 128^3 run.

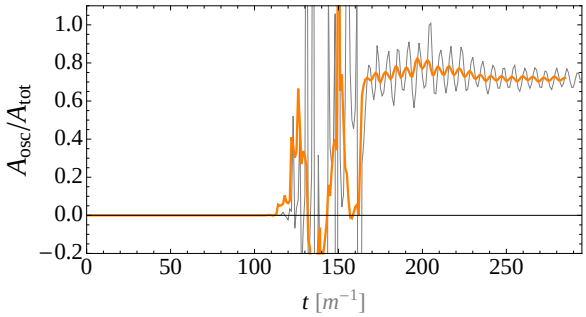

Figure 7.6: The ratio of the inflaton asymmetry in regions with twice the average density to the total asymmetry (orange curve is smoothed over a few oscillations). After $t \approx 150$, the over dense regions are composed of localized pseudo-solitons (oscillons). Once oscillons are formed, most of the asymmetry is locked inside them with a final value of $A_{\rm osc}/A_{\rm tot} \approx 0.7$. A qualitatively similar behavior is found if we consider regions with ten times the average density instead. For that case we get $A_{\rm osc}/A_{\rm tot} \approx 0.6$.

7.4 Inflaton asymmetry

In the previous section we could have ignored the symmetry breaking term $\mathcal{V}_{\rm br}$ in setting up the initial conditions (though we did not). The term was included in the lattice simulations, but the results discussed so far have not depended significantly on $\mathcal{V}_{\rm br}$. In both cases the dominant contribution to the quantities of interest: the power-spectrum for initial conditions and overdensities from lattice simulations, were primarily determined by the $U(1)$ symmetric piece $\mathcal{V}_{\rm s}$ of the Lagrangian. We now turn to the inflaton asymmetry, whose value is explicitly zero when evaluated using $\mathcal{V}_{\rm s}$ alone.

As a reminder, recall that we defined a dimensionless measure of the difference between inflaton and anti-inflaton particle numbers as follows (see Sec. 7.2.3):

$$A(t) = \frac{m}{\bar{\rho}_\phi(t) V_{\rm com}} \int d^3\mathbf{x} \left[\dot{\varphi}^1 \varphi^2 - \dot{\varphi}^2 \varphi^1\right] . \tag{7.47}$$

Note that we have written the asymmetry in terms of two real fields: the real and imaginary parts of a complex inflaton.

7.4.1 Asymmetry generation

The dimensionless asymmetry (defined in eq. (7.47)) generated at the end of inflation is shown in Fig. 7.5. The asymmetry is zero during inflation, and is generated after the end of inflation. After fragmentation is completed, the asymmetry settles to a fixed value. This behavior is evident in Fig. 7.5. We have checked that similar qualitative behavior is seen for a wide range of parameters.

Apart from the total asymmetry, we explored the spatial distribution of the asymmetry using the asymmetry density: $\mathcal{A}(t, \mathbf{x})$ defined in equation (7.17). After fragmentation more than 50% of the asymmetry is locked in regions which are at least two times overdense compared to the average density. More precisely, for overdensities more than twice the average density, the ratio of asymmetry in the overdensity compared to the total is 70%, whereas for $10\times$ the average density, the ratio is 60%. Thus, the energy overdensity and asymmetry density are spatially localized within the oscillons. A ratio of the

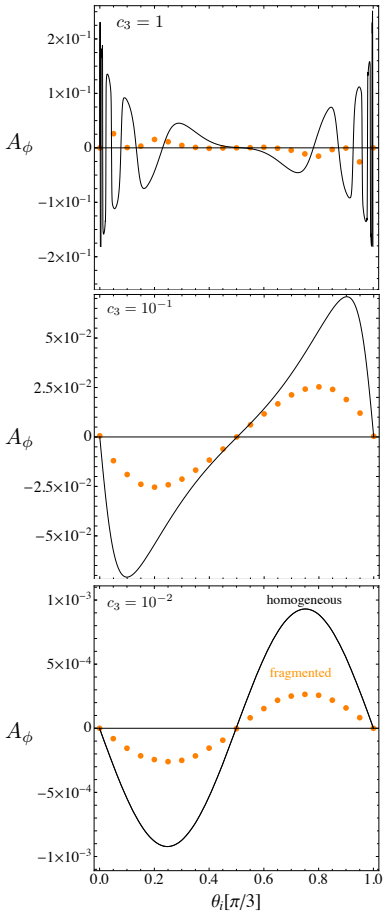

Figure 7.7: Inflaton asymmetry as a function of the initial angle made by the homogeneous inflaton field in the complex plane for different values of c_3. The black curve corresponds to the homogeneous case, whereas the orange points are results of lattice simulations. This sinusoidal behavior seen for $c_3 = 10^{-2}$ is seen for all $c_3 \ll 1$. The $\pi/3$ period is related to the form of the symmetry breaking term. When $c_3 \lesssim 1$, both the homogeneous and fragmented curves become much more complicated, no longer remaining sinusoidal. However, the $\pi/3$ period is still respected.

asymmetry inside significant overdensities (oscillons) to the total spatially averaged asymmetry is shown in Fig. 7.6. Note the 'jump' in overdensity and subsequent stabilization of the ratio around $t \approx 150m^{-1}$.

7.4.2 Parameter dependence

In this section we describe how the asymmetry depends on the parameters in the Lagrangian based on (i) the full lattice simulations (ii) an analysis assuming a homogeneous inflaton. For the full lattice simulations, we find that for $c_3 \ll 1$ and $M \ll m_{\rm Pl}$ we get

$$A_\phi \sim \mathcal{O}[10^2] \frac{M}{m_{\rm Pl}} c_3^2 \sin 3\theta_i, \tag{7.48}$$

where M is the scale where the potential changes shape, c_3 is the coefficient of the symmetry breaking term, and θ_i is the initial angle of the trajectory in the $\varphi^1 - \varphi^2$ plane. We discuss each of these dependencies in

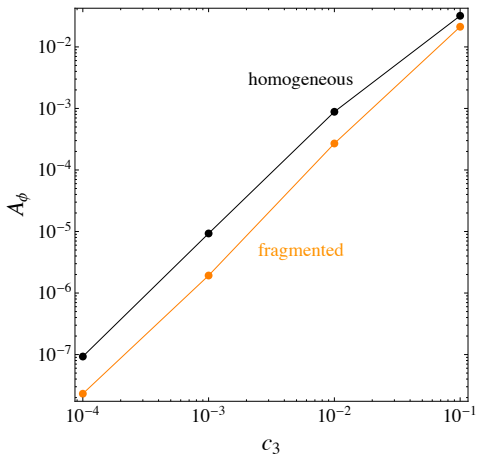

Figure 7.8: Inflaton asymmetry as a function of symmetry breaking parameter, with all other parameters fixed ($\theta_i = 0.7 \times \pi/3, M = 10^{-2} m_{\rm Pl}$). The black points correspond to the homogeneous case, whereas the orange points correspond to the results from a full lattice simulation. For $c_3 \ll 1$, in both cases $A_\phi \propto c_3^2$, with the inhomogeneous value always being below the homogeneous one.

turn below. The parameter m does not make an appearance because in our simulations, once M is chosen, m is determined based on the constraints on the amplitude of curvature fluctuations observed in the cosmic microwave background (see eq. (7.11)).

For comparison with the asymmetry from lattice simulations, the homogeneous asymmetry is (for $c_3 \ll 1$)

$$A_\phi^{\rm hom} \sim \mathcal{O}[10^{-1}] \frac{m_{\rm Pl}}{M} c_3^2 \sin 3\theta_i. \tag{7.49}$$

Note that the dependence of $m_{\rm Pl}/M$ is reversed between the homogeneous and the fragmented cases.

Dependence on initial conditions

The asymmetry is a strong, but simple function of the initial angle of the trajectory in $\varphi^1 - \varphi^2$ for the homogeneous and fragmented case when $c_3 \ll 1$. For small enough c_3, the dependence is sinusoidal $A_\phi \propto \sin(3\theta_i)$ where the number 3 is related directly to the power of the fields in the asymmetry term $V_{\rm br} \propto (\phi^3 + \phi^{*3})$. This dependence is shown in Fig. 7.7. As c_3 approaches 1 the behavior of the asymmetry in the homogeneous as well as the fully fragmented cases becomes much more complicated.

Dependence on magnitude of the symmetry breaking term

When $c_3 \ll 1$ we find that $A_\phi \propto c_3^2$ for both the homogeneous and fragmented cases, with a smaller value for the fragmented case. However, as c_3 approaches 1, we start seeing deviations from this behavior. In Fig. 7.8 we show the dependence of A_ϕ on c_3 with a fixed initial angle and fixed M. Similar behavior is seen for different choices of θ_i.

The quadratic dependence on c_3 helps in reducing the value of the asymmetry when $c_3 \ll 1$. This is different from the linear dependence on c_3 found for $m^2|\phi|^2$ inflation [189]. The quadratic dependence on the small parameter is also different from the linear dependence discussed in [40] where they considered a

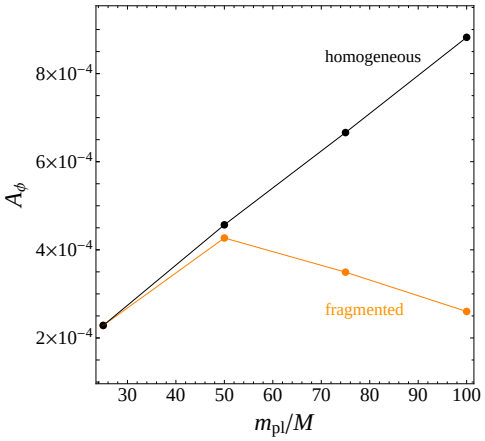

Figure 7.9: Asymmetry as a function of $m_{\rm Pl}/M$ (with all other parameters fixed). The black points and curve correspond to the homogeneous case, whereas the orange points correspond to the results from lattice simulations. Note that the difference between the homogeneous and lattice case becomes larger and larger as $m_{\rm Pl}/M$ increases. The ratio $m_{\rm Pl}/M$ can be interpreted as the fragmentation efficiency parameter (see eq. (7.42)). However, the symmetry breaking term also gets suppressed in the high density regions resulting from fragmentation. Hence both the fragmentation into high density regions *and* the suppression of asymmetry in high density regions due to the form of the symmetry breaking term determine the decrease in asymmetry as a function of $m_{\rm Pl}/M$ seen in the above figure.

symmetry breaking term of the form $\phi^4 + \phi^{*4}$. For small c_3, we expect symmetry should go as $\sim c_3 X_1 + c_3^2 X_2 + \ldots$. For the case at hand, and for the range of c_3 chosen, the linear term is $c_3 X_1 \ll c_3^2 X_2$.

Dependence on fragmentation

The parameter M controls the field value where the potential changes from a quadratic, to a non-linear potential (see Sec. 7.2). In terms of the dynamics of the inflaton the ratio $\sim m_{\rm Pl}/M$ controls the efficiency with which the inflaton fragments due to parametric resonance in an expanding universe (see Sec. 8.4.1). We plot the dependence of the asymmetry on $m_{\rm Pl}/M$ in Fig. 7.9. The asymmetry for the fragmented scenario starts deviating from the homogeneous case when $m_{\rm Pl}/M \gtrsim 50$. After that point, as the fragmentation efficiency increases the asymmetry decreases. This shows the importance of considering a full lattice simulation for calculating the asymmetry compared to the homogeneous case.

While it is clear that fragmentation plays a role, the actual reason behind the asymmetry suppression when $M \ll m_{\rm Pl}$ is nontrivial. The symmetry breaking term, $V_{\rm br} \propto |\phi|^3/(1+|\phi|^2/M^2)^2$. For $|\phi| \gg M$, we get $V_{\rm br} \propto M/|\phi|$. As a result in large field amplitude regions generated by fragmentation, the effect of the symmetry breaking terms (and hence the asymmetry) is suppressed.

7.4.3 Inflaton asymmetry to observed baryon-to-photon ratio

So far we have discussed the inflaton asymmetry in great detail. However, the observable we are ultimately interested in is the baryon asymmetry, more specifically the baryon-to-photon ratio η. The discussion below is based on [189], however a fragmented inflaton introduces additional subtleties. Along with the field fragmentation, note that a matter dominated phase that results in our scenario before reheating would lead to additional non-linear structure formation (for a low enough reheating temperature). Our main aim here

is to connect the inflaton asymmetry to η observed today. We will comment on the differences between the homogeneous case (studied in [189]) and our highly fragmented scenario as we present a *sketch* of how the decay might proceed below.

First, at some time t_ϕ the asymmetry A_ϕ freezes out as seen in Fig. 7.5. Thereafter, the inflaton/anti-inflatons decay into baryons and anti-baryons[8], by some time

$$t_\Gamma \sim \Gamma_\phi^{-1}, \tag{7.50}$$

where Γ_ϕ is the decay rate of the inflaton to baryons. Within any particular particle physics embedding (see for example [189]) we can calculate Γ_ϕ for "incoherent" decay. However, the high density, coherent oscillon/Q-balls configurations might affect the decay rate [175, 214, 215] significantly. We treat Γ_ϕ as a free parameter in what follows. [9]After t_Γ we assume that there are no baryon number violating processes. At t_Γ we have

$$N_b - N_{\bar{b}} = b_\phi (N_\phi - N_{\phi^*})_{t_\Gamma}, \tag{7.51}$$

where $b_\phi = 1$ or $1/3$ is the baryon number associated with the inflaton particles. For the right-hand side, we assume that $(N_\phi - N_{\phi^*})$ is approximately constant between t_ϕ and t_Γ. We can write it in terms of our asymmetry parameter as follows:

$$(N_\phi - N_{\phi^*})_{t_\Gamma} = \left(A_\phi \frac{E_\phi}{m} \right)_{t_\Gamma} = \left(A_\phi \frac{E_\phi}{m} \right)_{t_\phi}, \tag{7.52}$$

where we used the definition of the inflaton asymmetry and E_ϕ is the energy of the inflaton field(s) in the volume of interest. The expression evaluated at t_ϕ is what we have calculated in the previous sections.

On the left-hand-side of eq. (7.51), the number of baryons minus the number of anti-baryons is fixed, after t_Γ. Hence this quantity is constant and can be evaluated at late times (after thermalization, and after photon number changing processes have become inefficient):

$$N_b - N_{\bar{b}} = (\eta N_\gamma)_{\rm late}, \tag{7.53}$$

where N_γ is the number of photons for the volume of interest. Using eqs. (7.51, 7.52 and 7.53) and using spatially averaged densities, we have

$$\eta_{\rm late} = b_\phi m^{-1} \frac{\left(A_\phi a^3 \bar{\rho}_\phi \right)_{t_\phi \text{ or } t_\Gamma}}{(a^3 \bar{n}_\gamma)_{\rm late}}. \tag{7.54}$$

Note that this relates the A_ϕ we have calculated carefully to the observable $\eta_{\rm late}$. However evaluating the denominator is a bit subtle.

After t_Γ the baryons and anti-baryons produced by the decay will annihilate to produce photons. The annihilation within the solitons might be rapid, but the excess baryons/anti-baryons left over would have to diffuse through the "plasma" to find their anti-particles to annihilate. It is unclear how long this process takes.

[8]More precisely, quarks rather than baryons since the energy scale at this time $\gg 200\mathrm{MeV}$. For simplicity we will continue to refer to baryons

[9]It is possible to imagine $t_\phi \ll t_\Gamma$ or they might be comparable depending on the details of the decay.

Furthermore, the inflaton also decays into other particles and radiation, with the entire mix eventually reaching thermal equilibrium with a radiation like equation of state at some time $t_{\rm reh}$ (equivalently a reheating temperature, $T_{\rm reh}$). It is not easy to estimate the time-scale of this process and to what value $(a^3\bar{n}_\gamma)_{\rm late}$ eventually settles. As a result, without a careful analysis, we cannot provide a good estimate of the denominator.

To make further progress, we have to make some strong assumptions. We will assume that

$$t_{\rm late} \sim t_{\rm reh} \sim t_\Gamma. \tag{7.55}$$

This essentially means that annihilations and thermalization happen rapidly after t_Γ, and photon number changing processes also become inefficient soon after. In this case, we can evaluate the denominator and numerator at the same time $t \sim t_\Gamma$ and get an expression for the late time baryon-to-photon ratio, $\eta_{\rm late}$, in terms of the inflaton asymmetry, A_ϕ, the reheating temperature, $T_{\rm reh}$, and the inflaton mass, m.

Under the assumption in eq. (7.55), we get

$$\begin{aligned}(\rho_\phi)_{t_\Gamma} \sim (\rho_\phi)_{t_{\rm reh}} \sim& \frac{\pi^2}{30} g_* T_{\rm reh}^4, \\ (\bar{n}_\gamma)_{\rm late} \sim (\bar{n}_\gamma)_{t_{\rm reh}} \sim& \frac{2\zeta(3)}{\pi^2} T_{\rm reh}^3,\end{aligned} \tag{7.56}$$

where g_* is the number of relativistic degrees of freedom at that time. Using eq. (7.56) in eq. (7.54) we have

$$\eta_{\rm late} = \beta \times \frac{b_\phi \pi^4 g_*}{60\zeta(3)} A_\phi \left(\frac{T_{\rm reh}}{m}\right). \tag{7.57}$$

The factor β is meant to account for a number of simplifications we have made such as rapid annihilation, reheating and thermalization. Assuming g_* the numerical pre-factor is ≈ 160. The inflaton asymmetry A_ϕ is the value of the asymmetry at t_ϕ (i.e. after it settles down). The details of annihilation, decay rates etc. are hidden in $T_{\rm reh}$ and β.

We are finally ready to compute a numerical value of $\eta_{\rm late}$ and how it relates to the parameters that determine the inflaton asymmetry. Note that the observed value of $\eta_{\rm late} \approx 6 \times 10^{-10}$. Hence $A_\phi \ll 1$ and/or $T_{\rm reh} \ll m$. Both are rather natural and possible. Below we provide a combination of parameters that allows us to get the desired $\eta_{\rm late}$:

$$\eta_{\rm late} \sim 10^{-9}\beta \left(10^2 \frac{M}{m_{\rm Pl}}\right) \left(\frac{c_3}{10^{-2}}\right)^2 \left(10^{-4}\frac{m_{\rm Pl}}{m}\right) \left(\frac{T_{\rm reh}}{10^4 {\rm TeV}}\right) \sin 3\theta_i. \tag{7.58}$$

In general, if we want a high reheating temperature, c_3 has to be small and vice-versa. Although we have not used that relationship above, m and M are related via the constraint on the amplitude of curvature fluctuations.

7.5 Summary and future directions

We have investigated the generation of matter/antimatter asymmetry from the complex and rich dynamics at the end of inflation. We have shown that in a class of models with a complex inflaton and a small breaking of $U(1)$ symmetry, the inflaton fragments into localized soliton-like configurations called oscillons. These

configurations not only contain most of the energy density of the inflaton, they also carry most of the inflaton/anti-inflaton asymmetry. The oscillons decay into baryons/anti-baryons eventually giving rise to the observed baryon-to-photon ratio in our Universe for a broad range of parameters.

We took care in specifying multifield initial conditions on the lattice on super/subhorizon scales. Instead of using the instantaneous lowest energy state at the end of inflation, we self-consistently evolved all independent mode functions with Bunch-Davies initial conditions from deep inside the horizon during inflation up to the end of inflation. We carried out a linearized analysis of the field fluctuations with and without gravitational perturbations where applicable (see Sec. 7.3.2 and Appendix A). Because of the structure of resonance in our model, the details of the initial power-spectra on superhorizon scales were not relevant for us. However, we note that multifield initial conditions on horizon and superhorizon scales could be important for setting initial conditions for lattice simulations in other models.

We carried out detailed numerical simulations using a modified version of *LatticeEasy* to explore the non-linear dynamics of the inflaton field and the asymmetry generation. We explored how the asymmetry depends on the parameters of the Lagrangian, as well as the fragmentation dynamics. We found that the fragmentation does affect the inflaton asymmetry significantly. The value of the asymmetry as well as its spatial distribution are qualitatively and quantitatively different from the homogeneous case. In general, the asymmetry in the fragmented case is smaller than the one derived by ignoring the fragmentation. Inspite of the complex dynamics, we were able to provide a simple (empirical) formula for the inflaton asymmetry, expressing it in terms of the parameters of the Lagrangian and initial conditions in a physically transparent manner (see eq. (7.48)).

While we provided a detailed analysis of the asymmetry generation in the inflaton, we provided a comparatively simple analysis of the decay to quarks/baryons. How this decay takes place in a highly inhomogeneous inflaton field configuration, and the details of subsequent annihilation of the quarks/anti-quarks (baryons/anti-baryons) is left for future work. We provided an estimate for the baryon-to-photon ratio (see eqs. (7.57) and (7.58)) under simplified assumption of rapid thermalization (amongst others). This estimate should be checked by a detailed analysis of the inflaton decay, inhomogeneous annihilation and subsequent thermalization.

On the theoretical side a few additional problems need to be addressed. While we argued heuristically for the form of the inflaton asymmetry, a more detailed understanding is needed. We have not explored the properties of oscillons generated here in detail. Their lifetimes, distribution of amplitudes, sizes and interactions would be useful. Importantly, longer time-scale simulations (with an initial higher resolution) are needed to quantify the long term behavior of the asymmetry. It would be a useful check to carry out these simulations using other existing codes (besides *LatticeEasy*), each with their own benefits [75, 76, 78–80].

The results for the inflaton asymmetry and the baryon-to-photon ratio should be sensitive to the form of $V_{\rm br}$. It will be interesting to test if successful baryogenesis can be realised with different $V_{\rm br}$ in the presence of oscillons.

7.5.1 Additional observational consequences

Beyond the baryon-to-photon ratio, the scenario for baryogenesis is rich in terms of other potential observational implications. We briefly discuss a few of them below.

Isocurvature modes are generated during inflation due to the presence of the light "angular" component of the complex field [189]. For our model, this leads to an isocurvature fraction, $\alpha_{II} \sim 2.6 \times 10^{-4}$, which is two orders of magnitude below the current constraints [2]. Note that these isocurvature modes are not due

to fragmentation.[10] Another connection between baryogenesis *during* inflation and isocurvature modes is discussed in [217, 218].

The initial fragmentation, and soliton formation can lead to the generation of gravitational waves (see for example [81, 82, 219]). In addition, a long phase of soliton domination leads to a matter dominated expansion history before reheating takes place. This change in the expansion history affects the mapping of modes between horizon exit during inflation and re-entry at late times, thus affecting our interpretation of inflationary observables [133, 139, 220] (see Chapter 6). The long matter dominated phase also leads to additional gravitational structure formation in the early Universe before the inflaton decays away.

The solitons found in the simulation might be extremely long lived, serving as dark matter candidates [221][11] or they might decay into dark matter [222].

The inhomogeneous annihilation, if it is inefficient might lead to signatures during big bang nucleosynthesis or in the late Universe [223]. We hope that our work will motivate a more detailed analysis of inhomogeneous decay, annihilation and subsequent thermalization in similar models.

[10]Note that in a number of Affleck-Dine Baryogeneis scenarios the isocurvature modes are unacceptabely large for high energy scale inflation (see for example [216]). However, the large vacuum expectation value of the inflaton field (which doubles as the Affleck-Dine field) suppresses the isocurvature modes [39].

[11]These authors considered Q-balls rather than oscillons. Q-balls are likely to live longer than oscillons because of their (approximately) conserved $U(1)$ charge.

Chapter 8

Gauge fields production

Abstract

We calculate particle production during inflation and in the early stages of reheating after inflation in models with a charged scalar field coupled to Abelian and non-Abelian gauge fields. A detailed analysis of the power-spectra of primordial electric fields, magnetic fields and charge fluctuations at the end of inflation and preheating is provided. We carefully account for the Gauss constraints during inflation and preheating, and clarify the role of the longitudinal components of the electric field. We calculate the time-scale for the back-reaction of the produced gauge fields on the inflaton condensate, marking the onset of non-linear evolution of the fields. We provide a prescription for initial conditions for lattice simulations necessary to capture the subsequent non-linear dynamics. On the observational side, we find that the primordial magnetic fields generated are too small to explain the origin of magnetic fields on galactic scales and the charge fluctuations are well within observational bounds for the models considered in this chapter.

8.1 Introduction

Particle production during inflation [3–6] and reheating [10–12, 14–17, 224] sets up the initial conditions for the formation of observed structure and the beginning of the hot big bang. Particle production in models with gauge fields is particularly interesting because of the ubiquity of gauge fields in the Standard Model (SM) and their natural appearance in extensions beyond the SM. Gauge fields coupled to scalar fields can have important consequences for the generation of curvature [225–251] and charge perturbations [38, 39, 52, 247, 252–254], gravitational waves [27, 91, 242, 244, 255–261] as well as seeding primordial magnetic fields [53, 253, 262–275] during inflation. Such gauge fields can significantly affect the transition to a radiation dominated universe after inflation [37, 276] and can lead to novel non-perturbative phenomena [26, 29, 277–282].

An analysis of particle production with gauge fields in the early universe has been undertaken in many previous studies. For example, gauge field production during inflation and its consequences was reviewed in [283]. Non-perturbative gauge field production during and after inflation was explored in [24, 28, 92, 94–96, 247, 284–287] (see also Section 4.3), whereas non-linear dynamics of gauge fields after inflation was considered in [21, 22, 26, 37, 276, 288, 289] for Abelian fields and [29, 277–281] for non-Abelian ones.

In this chapter we re-visit particle production in locally gauge invariant models with Abelian and non-Abelian fields coupled to charged scalar fields. In these models we assume that a component of the charged scalar field plays the role of the inflaton condensate. Care has to be taken with gauge fields because they have to satisfy certain constraint equations (along with the usual evolution equations). The natural gauge redundancy can lead to complications in quantization or to spurious gauge modes during numerical evolution. The non-zero vacuum expectation value (vev) of the inflaton condesate during inflation and reheating changes some of the common results for gauge fields coupled to scalar fields with zero vevs. Moreover, certain common gauge choices become ill-defined when the inflaton condensate starts oscillating at the end of inflation. Finally, if significant particle production occurs, back-reaction becomes important and classical lattice simulations are needed to fully explore the non-linear dynamics of the fields. Initial conditions for such lattice simulations can be nontrivial because of the constraints on the different variables that must be satisfied. We pay special attention to all of these issues in this work. While we restrict ourselves to "minimal" models consistent with local gauge invariance, our techniques and results should carry over to more complicated scenarios such as [24, 286].

We calculate particle production during inflation using gauge invariant variables and with proper accounting for the constraints (Section 8.3). The use of gauge invariant variables naturally avoids issues with spurious gauge degrees of freedom and makes the quantization and subsequent evolution of perturbations particularly transparent. We provide power-spectra for the electric and magnetic fields at the end of inflation, along with simple analytic estimate for their shape. In Appendix B we explain their shape via approximate analytic calculations.

While useful during inflation, gauge invariant variables become ill-defined when the inflaton starts oscillating. We argue for the use of well defined Coulomb gauge variables for analysing non-perturbative particle production during preheating at the end of inflation. In Section 8.4, we carry out a Floquet like analysis for the resonant production of the gauge fields. Here, we point out some minor discrepancies in the literature regarding the productions of the gauge invariant longitudinal component of the electric field. We then estimate the end of preheating by calculating the time when back-reaction of the resonantly produced gauge fields becomes important (Section 8.4.2). In Appendix C we provide technical details for quantizing and calculating the back-reaction in the Coulomb gauge.

Once non-linear effects become important, simulations become essential. Non-linear simulations with gauge fields (especially non-Abelian fields) can be challenging because of the large number of components and the necessity of satisfying constraint equations. In Section 8.5 of this work we provide a simple prescription for setting up initial conditions for such lattice simulations which can be applied in any gauge. In our prescription, the lattice initial conditions naturally satisfy the necessary gauge constraints. We note that our initial conditions accurately account for metric perturbations, field interactions and gauge constraints to linear order. We provide an example of lattice initial conditions in temporal gauge which is a common choice for simulations. We arrive at these initial conditions via gauge invariant variables; this serves as a model to set up initial conditions in any gauge. We will carry out detailed lattice simulations in future work (a novel algorithm for simulating Abelain gauge fields is presented in Chapter 9).

We have tried to make the present chapter self-contained, so that it can be used for future reference easily. To this end, we provide the necessary equations for the perturbations of metric and matter fields (scalar and gauge fields) in position and Fourier space for gauge invariant variables. While we work with gauge invariant variables as far as possible, we also provide a dictionary to translate our results to other popular gauges.

For pedagogical purposes, we carry out the analysis for Abelian fields first (Section 8.2). We show in

the later half of the chapter (Section 8.6) how the non-Abelian analysis can be reduced to an analysis of multiple copies of the Abelian case in the linear regime. Hence, the analysis for the Abelian case, including the setting up of the lattice initial conditions, can be easily carried over to the non-Abelian case. We show how to apply the developed techniques to a $SU(2)$ model and its extension: a $SU(2) \times U(1)$ model.

We discuss the observational consequences of a charged inflaton and its gauge fields in Section 8.7. We summarize our results in the Conclusions section and discuss future directions.

8.2 The Abelian model

We consider an action with matter minimally coupled to gravity

$$S = -\frac{m_{\rm Pl}^2}{2}\int d^4x\sqrt{-g}R + S_{\rm m}\,, \tag{8.1}$$

where R is the Ricci scalar, g is the determinant of the metric. The matter action contains a complex scalar field φ and the gauge field A_μ:

$$S_{\rm m} = \int {\rm d}^4x\sqrt{-g}\mathcal{L}_{\rm m} = \int {\rm d}^4x\sqrt{-g}\left[(D_\mu\varphi)^*(D^\mu\varphi) - \mathcal{V}(|\varphi|) - \frac{1}{4}F_{\mu\nu}F^{\mu\nu}\right]\,, \tag{8.2}$$

where the field tensor $F_{\mu\nu}$ for the gauge fields and the gauge-covariant derivative $D_\mu\varphi$ are given by

$$F_{\mu\nu}(A) = \nabla_\mu A_\nu - \nabla_\nu A_\mu\,, \qquad D_\mu\varphi = \left(\nabla_\mu + i\frac{g_A}{2}A_\mu\right)\varphi\,. \tag{8.3}$$

In the above equations, ∇_μ is the usual Levi-Civita connection. The action $S_{\rm m}$ is invariant under local $U(1)$ gauge transformations

$$\varphi \to e^{-i\frac{g_A}{2}\alpha(x^\nu)}\varphi\,, \qquad A_\mu \to A_\mu + \nabla_\mu\alpha(x^\nu)\,, \tag{8.4}$$

where $\alpha(x^\nu)$ is an arbitrary real function of space and time. The total action is also invariant under space-time differomorphisms. The gauge symmetry implies that not all of the components of the 4-vector A_μ and the real and imaginary parts of the scalar field are physical degrees of freedom (dof). We remedy this redundancy by working in the appropriate set of gauge invariant variables or by fixing the gauge. The redundancy due to space-time diffeomorphisms is handled in a similar fashion.

We will present our answers as power-spectra of the electric and magnetic fields, which are defined in the usual way [290]:[1]

$$E_i \equiv F_{0i} = \nabla_0 A_i - \nabla_i A_0\,, \qquad B_i \equiv \frac{1}{2}\epsilon^{ilm}F_{lm} = \frac{1}{2}\epsilon^{ilm}\left(\nabla_l A_m - \nabla_m A_l\right)\,. \tag{8.5}$$

8.2.1 $U(1)$ gauge invariants

When the field $\varphi \neq 0$, it can be written in polar co-ordinates as

$$\varphi(x^\mu) = \frac{1}{\sqrt{2}}\rho(x^\mu)e^{i\frac{g_A}{2}\Omega(x^\mu)}\,. \tag{8.6}$$

[1] ϵ^{ijk} is the antisymmetric Levi-Civita tensor. It does not raise or lower (spatial) indices.

Under the local $U(1)$ gauge transformation (see eq. (8.4)) $\rho \to \rho$ and $\Omega \to \Omega - \alpha$. It is convenient to work in local $U(1)$ gauge invariant variables given by the following five fields:

$$\rho(x^\nu) \qquad \text{and} \qquad G_\mu(x^\nu) \equiv A_\mu(x^\nu) + \nabla_\mu \Omega(x^\nu)\,. \tag{8.7}$$

In these variables the matter action becomes

$$S_{\rm m} = \int \mathrm{d}^4x\sqrt{-g}\Big[\frac{1}{2}\nabla_\mu\rho\nabla^\mu\rho + \frac{1}{2}\left(\frac{g_A\rho}{2}\right)^2 G_\mu G^\mu - V(\rho) - \frac{1}{4}F_{\mu\nu}\left(G\right)F^{\mu\nu}\left(G\right)\Big]\,, \tag{8.8}$$

where $V(\rho) = \mathcal{V}(|\varphi|)$. It is worth noting that the variable Ω appearing in eq. (8.6) does not make an appearance in the above action. There is no need to worry about the $U(1)$ gauge redundancy when working with gauge invariant variables.

Note that the E and B fields are invariant with respect to $U(1)$ transformations and their expressions in terms of G_μ are identical to those in terms of A_μ:

$$E_i = \nabla_0 G_i - \nabla_i G_0\,, \qquad B_i = \frac{1}{2}\epsilon^{ilm}\left(\nabla_l G_m - \nabla_m G_l\right)\,. \tag{8.9}$$

8.2.2 Diffeomorphism invariants

We will work in a perturbed Friedmann-Roberston-Walker space-time with the metric:

$$\begin{aligned} ds^2 &= (\bar{g}_{\mu\nu} + \delta g_{\mu\nu})dx^\mu dx^\nu \\ &= (1+2\phi)\,a^2(\tau)d\tau^2 + 2\left(\partial_i\mathcal{B} + \mathcal{S}_i\right)a^2(\tau)dx^i d\tau \\ &\quad - \left[\,(1-2\psi)\,\delta_{ij} - 2\partial_i\partial_j\mathcal{E} - \partial_j\mathcal{K}_i - \partial_i\mathcal{K}_j - \tilde{h}_{ij}\right]a^2(\tau)dx^i dx^j\,, \end{aligned} \tag{8.10}$$

where $\phi(x^\sigma)$, $\mathcal{B}(x^\sigma)$, $\psi(x^\sigma)$, $\mathcal{E}(x^\sigma)$ are scalar perturbations, $\mathcal{S}_i(x^\sigma)$, $\mathcal{K}_i(x^\sigma)$ are divergence-free 3-vector perturbations, and $\tilde{h}_{ij}(x^\sigma)$ is a traceless transverse 3-tensor perturbation.

In this perturbed space-time, we define the perturbations of the following $U(1)$ invariant variables:

$$\begin{aligned} \rho(x^\mu) &= \bar{\rho}(\tau) + \delta\rho(x^\mu)\,, \\ G_\mu(x^\mu) &= \left[G_0(x^\mu), \partial_i G^{\parallel}(x^\mu) + G_i^{\perp}(x^\mu)\right]\,, \end{aligned} \tag{8.11}$$

where $G_0(x^\sigma)$ and $G^{\parallel}(x^\sigma)$ are scalars and $G_i^{\perp}(x^\sigma)$ is a divergence-free 3-vector. Note that the gauge fields vanish at the background level: the spatial components are zero from isotropy of the Friedmann-Robertson-Walker (FRW) background and the equations of motion will set the background temporal component to zero. Hence we will work at the linear level in G_μ.

For our scenario, there are two physical scalar metric perturbations, with scalar field perturbation and scalar parts of the gauge field adding three more. We choose to work with the following five diffeomorphism invariant combinations:

$$\begin{aligned} \Phi &= \phi - \frac{1}{a}\partial_\tau\left[a\left(\mathcal{B} - \partial_\tau\mathcal{E}\right)\right]\,, \\ \Psi &= \psi + \mathcal{H}\left(\mathcal{B} - \partial_\tau\mathcal{E}\right)\,, \\ \delta\tilde{\rho} &= \delta\rho - \left(\partial_\tau\bar{\rho}\right)\left(\mathcal{B} - \partial_\tau\mathcal{E}\right)\,, \\ &G_0\,, \\ &G^{\parallel}\,, \end{aligned} \tag{8.12}$$

where $\mathcal{H} = \partial_\tau \ln a$. The first two are the standard Bardeen variables. G_0 and $G^{\parallel}$ are diffeomorphism invariant since the gauge field vanishes at the background level.

Similarly, for the vectors we chose to work with the following diffeomorphism invariant combinations

$$\begin{aligned} &\tilde{V}_i \equiv \mathcal{S}_i - \partial_\tau \mathcal{K}_i \,, \\ &G_i^{\perp} \,, \end{aligned} \tag{8.13}$$

where $\tilde{V}$ and $G^{\perp}$ are divergence free.

The traceless, transverse 3-tensor perturbation $\tilde{h}_{ij}$ is already diffeomorphism invariant. Similarly, the electric and magnetic fields defined in eq. (8.9) are already diffeomorphism invariant. It is convenient to split the electric and magnetic fields into divergence-free and curl-free parts

$$E_i(x^\mu) = \partial_i E^{\parallel}(x^\mu) + E_{\perp i}(x^\mu) \,, \qquad B_i(x^\mu) = B_i^{\perp}(x^\mu) \,. \tag{8.14}$$

Note that $B^{\parallel} = 0$ from the definition of B_i in eq. (8.9).

8.2.3 Equations of motion

The general equations of motion for the matter and metric fields in curved space-time take the following form:

$$\begin{aligned} &D_\mu D^\mu \varphi + \frac{\partial \mathcal{V}}{\partial \varphi^*} = 0 \,, \\ &\nabla_\mu F^{\mu\sigma} + i\frac{g_{\scriptscriptstyle A}}{2}\left(\varphi\left(D^\sigma\varphi\right)^* - \varphi^* D^\sigma \varphi\right) = 0 \,, \\ &\mathcal{G}_{\mu\nu} = \frac{1}{m_{\rm Pl}^2} T_{\mu\nu} \,, \end{aligned} \tag{8.15}$$

where $\mathcal{G}_{\mu\nu}$ is the Einstein tensor and the energy momentum tensor is given by

$$T_{\mu\nu} = 2\left(D_{(\mu}\varphi\right)^* D_{\nu)}\varphi - F_{\mu\alpha}F_\nu{}^\alpha - g_{\mu\nu}\left[\left(D^\alpha\varphi\right)^* D_\alpha\varphi - \mathcal{V} - \frac{1}{4}F_{\alpha\beta}F^{\alpha\beta}\right] . \tag{8.16}$$

In terms of the $U(1)$ gauge invariant variables defined in Section 8.2.1, the above equations become

$$\nabla_\mu\nabla^\mu\rho + \frac{\partial V}{\partial\rho} - \rho\left(\frac{g_{\scriptscriptstyle A}}{2}\right)^2 G_\mu G^\mu = 0 \,, \tag{8.17}$$

$$\nabla_\mu F^{\mu\sigma}(G) + \left(\frac{\rho g_{\scriptscriptstyle A}}{2}\right)^2 G^\sigma = 0 \,, \tag{8.18}$$

$$\begin{aligned} T_{\mu\nu} = {} & \nabla_\mu\rho\nabla_\nu\rho - \left(\frac{g_{\scriptscriptstyle A}\rho}{2}\right)^2 G_\mu G_\nu - F_{\mu\alpha}(G)F_\nu{}^\alpha(G) \\ & - g_{\mu\nu}\left[\frac{1}{2}\nabla_\alpha\rho\nabla^\alpha\rho - \frac{1}{2}\left(\frac{g_{\scriptscriptstyle A}\rho}{2}\right)^2 G_\alpha G^\alpha - V(\rho) - \frac{1}{4}F_{\alpha\beta}(G)F^{\alpha\beta}(G)\right] . \end{aligned} \tag{8.19}$$

Equation (8.18) implies the following definition of the conserved 4-current:

$$j^\mu = \left(\frac{\rho g_{\scriptscriptstyle A}}{2}\right)^2 G^\mu \,, \qquad \nabla_\mu j^\mu = 0 \,. \tag{8.20}$$

The equivalent of Maxwell's equations for the electric and magnetic fields are

$$\nabla^i E_i = \left(\frac{\rho g_A}{2}\right)^2 G_0 = j_0\,, \qquad \epsilon^{ilm}\nabla^l B_m - \nabla^0 E_i = \left(\frac{\rho g_A}{2}\right)^2 G_i = j_i\,. \tag{8.21}$$

Next, we write down the equations of motion for the background (space independent) fields and linearized perturbations around these background fields in terms of gauge invariant variables.

Background

Assuming the scalar field plays the role of the inflaton and treating the gauge fields as perturbations, the evolution of $\bar{\rho}(\tau)$ can be determined from eq. (8.17):

$$\partial_\tau^2\bar{\rho} + 2\mathcal{H}\partial_\tau\bar{\rho} + a^2\frac{\partial V}{\partial\bar{\rho}} = 0\,, \tag{8.22}$$

where $\mathcal{H}$ is given by the 00 background Einstein equation

$$\mathcal{H}^2 = \frac{a^2}{3m_{\rm pl}^2}\left(\frac{(\partial_\tau\bar{\rho})^2}{2a^2} + V\right)\,. \tag{8.23}$$

The electric and magnetic fields vanish at the background level.

Linearized perturbations in position space

From eq. (8.17) and eq. (8.18) we get the equations of motion for diffeomorphism and $U(1)$ gauge invariant *scalar* perturbations:

$$\partial_\tau^2\delta\tilde{\rho} + 2\mathcal{H}\partial_\tau\delta\tilde{\rho} - \Delta\delta\tilde{\rho} + a^2\frac{\partial^2 V}{\partial\bar{\rho}^2}\delta\tilde{\rho} - \partial_\tau\bar{\rho}\,(3\partial_\tau\Psi + \partial_\tau\Phi) + 2a^2\frac{\partial V}{\partial\bar{\rho}}\Phi = 0\,, \tag{8.24}$$

$$\partial_\tau^2 G^{\parallel} + a^2\left(\frac{\bar{\rho}g_A}{2}\right)^2 G^{\parallel} - \partial_\tau G_0 = 0\,, \tag{8.25}$$

$$\partial_\tau\Delta G^{\parallel} - \Delta G_0 + a^2\left(\frac{\bar{\rho}g_A}{2}\right)^2 G_0 = 0\,, \tag{8.26}$$

where eq. (8.26) is the linearized version of the Gauss constraint. Note that the scalar components of the gauge fields G_0 and $G^{\parallel}$ do not couple to the metric perturbations.

The evolution of the $U(1)$ gauge and diffeomorphism invariant *vector* perturbations involving matter fields can be obtained from

$$\partial_\tau^2 G_i^{\perp} - \Delta G_i^{\perp} + a^2\left(\frac{\bar{\rho}g_A}{2}\right)^2 G_i^{\perp} = 0\,. \tag{8.27}$$

The perturbations $G_i^{\perp}$ also do not couple to metric perturbations. As mentioned earlier, the *tensor* perturbations are also decoupled from the matter fields at the linear level. We shall not consider tensor perturbations any further in this chapter.

We now turn to the Einstein equations. The energy-momentum tensor in eq. (8.19) is quadratic in the G_μ (with $G_\mu = 0$ at the background level). Hence, to linear order in the perturbations, the energy-momentum

tensor depends only on the perturbations in ρ and the metric. Also $T^i_j = 0$ for $i \neq j$; there is no anisotropic stress. The linearised Einstein equations (for scalar perturbations) yield

$$\begin{aligned}
&\Phi = \Psi\,, \\
&\left(\partial_\tau \mathcal{H} - \mathcal{H}^2 - \Delta\right)\Psi = \frac{1}{2m_{\rm pl}^2}\left[-\partial_\tau\bar{\rho}\left(\partial_\tau\delta\tilde{\rho} + \mathcal{H}\delta\tilde{\rho}\right) + \delta\tilde{\rho}\partial_\tau^2\bar{\rho}\right]\,, \\
&\partial_\tau\Psi + \mathcal{H}\Psi = \frac{1}{2m_{\rm pl}^2}\delta\tilde{\rho}\partial_\tau\bar{\rho}\,.
\end{aligned} \tag{8.28}$$

Note that the gauge fields are completely decoupled from the scalar metric perturbations.

The picture for vector perturbations is even simpler - the linearized Einstein equations for the vector perturbations involve only metric perturbations:

$$\Delta\tilde{V}_i = 0 \qquad \text{and} \qquad \partial_\tau\left(\partial_j\tilde{V}_i + \partial_i\tilde{V}_j\right) + 2\mathcal{H}\left(\partial_j\tilde{V}_i + \partial_i\tilde{V}_j\right) = 0\,, \tag{8.29}$$

which do not affect the matter vector perturbations.

At the linearized level, the equations of motion for the electric and magnetic fields defined in eq. (8.9) are simple[2]

$$\begin{aligned}
&-\Delta E^{\parallel} = a^2\left(\frac{\bar{\rho}g_{_A}}{2}\right)^2 G_0 = a^2 j_0\,, \\
&-\partial_\tau E^{\parallel} = a^2\left(\frac{\bar{\rho}g_{_A}}{2}\right)^2 G^{\parallel} \equiv a^2 j^{\parallel}\,, \\
&\epsilon^{ilm}\partial^l B^{\perp}_m - \partial_\tau E^{\perp}_i = a^2\left(\frac{\bar{\rho}g_{_A}}{2}\right)^2 G^{\perp}_i \equiv a^2 j^{\perp}_i\,.
\end{aligned} \tag{8.30}$$

On the right-hand sides of the last two equations, we have defined the scalar perturbations and divergence-free vector perturbations in the 3-current density, respectively.

Linearized perturbations in Fourier space

For calculational purposes, we move to Fourier space. Fourier space is also particularly convenient for solving the various constraint equations, which essentially become algebraic in the relevant variables.

We begin with the equations of motion for the scalar perturbations. From the (Fourier space version of the) constraints, eqns. (8.28), we can substitute the gravitational potential $\Psi_{\mathbf{k}}$ and its derivative into the evolution equation for $\delta\tilde{\rho}_{\mathbf{k}}$ (cf. eq. (8.24)) to obtain an equation of motion which only involves $\delta\tilde{\rho}_{\mathbf{k}}$:

$$\begin{aligned}
&\partial_\tau^2\delta\tilde{\rho}_{\mathbf{k}} + 2\mathcal{H}\partial_\tau\delta\tilde{\rho}_{\mathbf{k}} + k^2\delta\tilde{\rho}_{\mathbf{k}} + a^2\frac{\partial^2 V}{\partial\bar{\rho}^2}\delta\tilde{\rho}_{\mathbf{k}} \\
&\qquad + \frac{2}{m_{\rm Pl}^2}\left[\left(\mathcal{H}\partial_\tau\bar{\rho} + \frac{a^2}{2}\frac{\partial V}{\partial\bar{\rho}}\right)\frac{\delta\tilde{\rho}_{\mathbf{k}}\partial_\tau^2\bar{\rho} - \partial_\tau\bar{\rho}\left(\partial_\tau\delta\tilde{\rho}_{\mathbf{k}} + \mathcal{H}\delta\tilde{\rho}_{\mathbf{k}}\right)}{\partial_\tau\mathcal{H} - \mathcal{H}^2 + k^2} - \left(\partial_\tau\bar{\rho}\right)^2\delta\tilde{\rho}_{\mathbf{k}}\right] = 0\,.
\end{aligned} \tag{8.31}$$

The remaining scalar perturbations, G_0 and $G^{\parallel}$, are governed again by an evolution equation, eq. (8.25), and a constraint, eq. (8.26). Before moving to the Fourier transformed versions of these equations we define the longitudinal (i.e., curl-free) component of the space-like part of G_μ:

$$\left(\boldsymbol{G}^L\right)_i = \partial_i G^{\parallel}\,. \tag{8.32}$$

[2]Note that in FRW background with conformal time $\nabla_\mu F^{\mu\nu} = g^{\nu\alpha}\nabla^\mu F_{\mu\alpha} = g^{\nu\alpha}\partial^\mu F_{\mu\alpha}$.

The Fourier transform of $\boldsymbol{G}^L$ can be expressed in terms of a longitudinal polarisation vector, $\boldsymbol{\epsilon}^L_{\mathbf{k}}$, as follows:

$$\boldsymbol{G}^L_{\mathbf{k}} = \boldsymbol{\epsilon}^L_{\mathbf{k}} G^L_{\mathbf{k}}\,, \tag{8.33}$$

where we shall call the scalar $G^L_{\mathbf{k}}$, the *longitudinal mode*. The polarisation vector has the following properties:

$$\boldsymbol{\epsilon}^L_{\mathbf{k}} = \boldsymbol{\epsilon}^{L*}_{-\mathbf{k}}\,, \qquad \boldsymbol{\epsilon}^{L*}_{\mathbf{k}} \cdot \boldsymbol{\epsilon}^L_{\mathbf{k}} = 1\,, \qquad i\mathbf{k}\cdot\boldsymbol{\epsilon}^L_{\mathbf{k}} = k\,, \qquad i\mathbf{k}\times\boldsymbol{\epsilon}^L_{\mathbf{k}} = 0\,. \tag{8.34}$$

The Fourier transformed equations, eqns. (8.25) and (8.26), then take the form

$$\left(\frac{g_A\bar{\rho}a}{2}\right)^2 G_{0\mathbf{k}} = -k^2 G_{0\mathbf{k}} - k\partial_\tau G^L_{\mathbf{k}}\,, \tag{8.35}$$

$$\partial^2_\tau G^L_{\mathbf{k}} + k\partial_\tau G_{0\mathbf{k}} + \left(\frac{g_A\bar{\rho}a}{2}\right)^2 G^L_{\mathbf{k}} = 0\,. \tag{8.36}$$

There is a similarity between the pairs $\left(G^L_{\mathbf{k}}, G_{0\mathbf{k}}\right)$ and $(\delta\tilde{\rho}_{\mathbf{k}}, \Psi_{\mathbf{k}})$. $G^L_{\mathbf{k}}$ and $\delta\tilde{\rho}_{\mathbf{k}}$ are both dynamical fields, evolved according to second order in time equations of motion, eq. (8.36) and eq. (8.24), respectively. Each of these perturbations has its own auxiliary field, $G_{0\mathbf{k}}$ and $\Psi_{\mathbf{k}}$ respectively, determined by a constraint equation. Substituting the auxiliary field (i.e., $G_{0\mathbf{k}}$) into the equation of motion we obtain the following expression in terms of $G^L_{\mathbf{k}}$ only:

$$\partial^2_\tau G^L_{\mathbf{k}} + 2\left(\mathcal{H} + \frac{\partial_\tau\bar{\rho}}{\bar{\rho}}\right)\frac{\partial_\tau G^L_{\mathbf{k}}}{1+\left(\frac{g_A\bar{\rho}a}{2k}\right)^2} + \left[k^2 + \left(\frac{g_A\bar{\rho}a}{2}\right)^2\right] G^L_{\mathbf{k}} = 0\,. \tag{8.37}$$

We now turn to vector perturbations. The matter vector perturbations are decoupled from the metric vector perturbations. Similarly to the longitudinal case, we introduce a pair of transverse polarisation vectors $\boldsymbol{\epsilon}^{T\pm}_{\mathbf{k}}$ which satisfy

$$\boldsymbol{\epsilon}^{T\pm}_{\mathbf{k}} = \boldsymbol{\epsilon}^{T\pm *}_{-\mathbf{k}}, \qquad \boldsymbol{\epsilon}^{T\lambda'*}_{\mathbf{k}} \cdot \boldsymbol{\epsilon}^{T\lambda}_{\mathbf{k}} = \delta^{\lambda'\lambda}\,, \qquad i\mathbf{k}\cdot\boldsymbol{\epsilon}^{T\pm}_{\mathbf{k}} = 0, \qquad i\mathbf{k}\times\boldsymbol{\epsilon}^{T\pm}_{\mathbf{k}} = \pm k\boldsymbol{\epsilon}^{T\pm}_{\mathbf{k}}\,. \tag{8.38}$$

The divergence-free perturbations in terms of these polarization vectors are

$$\boldsymbol{G}^\perp_{\mathbf{k}}(\tau) = \sum_{\lambda=\pm} \boldsymbol{\epsilon}^{T\lambda}_{\mathbf{k}} G^{T\lambda}_{\mathbf{k}}(\tau)\,, \tag{8.39}$$

with the equations of motion

$$\partial^2_\tau G^{T\pm}_{\mathbf{k}} + \left[k^2 + \left(\frac{g_A\bar{\rho}a}{2}\right)^2\right] G^{T\pm}_{\mathbf{k}} = 0\,. \tag{8.40}$$

The fact that Hubble friction does not appear in the evolution equations for the transverse modes is because of conformal invariance of massless gauge fields. However, the longitudinal components (which exist when the gauge field is effectively massive) do feel Hubble friction.

One can also rewrite the electric and magnetic fields, and the 3-current, in terms of longitudinal and transverse modes, e.g.,

$$E_i = \partial_i E^\parallel + E^\perp_i = (\boldsymbol{E}^L)_i + E^\perp_i\,, \tag{8.41}$$

which in terms of the polarization vectors in Fourier space becomes

$$\boldsymbol{E}_{\mathbf{k}} = \boldsymbol{\epsilon}^{L}_{\mathbf{k}} E^{L}_{\mathbf{k}} + \sum_{\lambda=\pm} \boldsymbol{\epsilon}^{T\lambda}_{\mathbf{k}} E^{T\lambda}_{\mathbf{k}} \,. \tag{8.42}$$

Similar expansions hold for j_i and B_i with the exception $B^{L}_{\mathbf{k}} = 0$. Below we give the expressions used in the subsequent sections to calculate the primordial power-spectra of the longitudinal and transverse modes of E and B

$$\begin{aligned} E^{L}_{\mathbf{k}} &= k G_{0\mathbf{k}} + \partial_\tau G^{L}_{\mathbf{k}} = \frac{\left(\frac{\bar{\rho} g_A}{2}\right)^2}{\frac{k^2}{a^2} + \left(\frac{\bar{\rho} g_A}{2}\right)^2} \partial_\tau G^{L}_{\mathbf{k}} \,, \\ E^{T\pm}_{\mathbf{k}} &= \partial_\tau G^{T\pm}_{\mathbf{k}} \,, \qquad B^{T\pm}_{\mathbf{k}} = \pm k G^{T\pm}_{\mathbf{k}} \,. \end{aligned} \tag{8.43}$$

The charge and current densities can also be expressed in terms of the G field's longitudinal and transverse modes

$$j_{0\mathbf{k}} = \left(\frac{\bar{\rho} g_A}{2}\right)^2 G_{0\mathbf{k}} = \frac{-\left(\frac{\bar{\rho} g_A}{2}\right)^2}{\frac{k^2}{a^2} + \left(\frac{\bar{\rho} g_A}{2}\right)^2} \frac{k}{a^2} \partial_\tau G^{L}_{\mathbf{k}} \,, \qquad j^{L}_{\mathbf{k}} = \left(\frac{\bar{\rho} g_A}{2}\right)^2 G^{L}_{\mathbf{k}} \,, \qquad j^{T\pm}_{\mathbf{k}} = \left(\frac{\bar{\rho} g_A}{2}\right)^2 G^{T\pm}_{\mathbf{k}} \,. \tag{8.44}$$

The first identity is simply $-k E^{L}_{\mathbf{k}} = a^2 j_{0\mathbf{k}}$, i.e., the Gauss constraint. In a consistent quantum analysis of the perturbations during and after inflation, one cannot set $j_{0\mathbf{k}}$ and $j^{L}_{\mathbf{k}}$ to zero by hand (this differs from the treatment in [269], [291]). This is because the vacuum fluctuations in $G^{L}_{\mathbf{k}}$ can be enhanced due to horizon crossing during inflation or non-adiabatic particle production during preheating. We shall see this aspect in detail in the subsequent sections.

8.2.4 Gauge transformations

In the upcoming sections we will use either the gauge invariant variables discussed above or work in some particular gauge depending on which approach is best for the problem at hand. In this short section we provide the relationships between variables in some of the popular gauges used in the literature and the gauge invariant ones. These relationships can also be used to move from one gauge to another. When the variables are well defined, we can use the equations of motion and the solutions in the gauge invariant case to recover the corresponding expressions in our gauge of choice. Occasionally, some of the variables become ill-defined or the relationships between variables require a patching up of co-ordinate maps (for example during reheating). Such cases can be dealt with on an individual basis, or one simply derives the equations of motion and solutions directly from the equations of motion themselves.

In different gauges (but not the gauge invariant case) the complex scalar field is represented as $\varphi = (\varphi^0 + i\varphi^1)/\sqrt{2}$, and the gauge fields by A^μ. For perturbations, we will always work around an FRW background. Using the global $U(1)$ invariance, we set the homogeneous, imaginary part of φ, $\bar{\varphi}^1 = 0$. That is $\varphi = (\bar{\varphi}^0 + \delta\varphi^0 + i\delta\varphi^1)/\sqrt{2}$. For the homogeneous part $\bar{\varphi}^0 = \pm\rho$ with the $\pm$ sign accounting for the change in sign during an oscillation through zero. In Fourier space, the transverse modes and the scalar perturbations along the direction of motion of the homogeneous field (in all the gauges discussed below) are related to the gauge invariant variables as follows:

$$\delta\varphi^0_{\mathbf{k}} = \delta\rho_{\mathbf{k}} \,, \qquad A^{T\pm}_{\mathbf{k}} = G^{T\pm}_{\mathbf{k}} \,, \tag{8.45}$$

with the equations of motion for $\delta\varphi^0_{\mathbf{k}}$ and $A^{T\pm}_{\mathbf{k}}$ being identical to the gauge invariant case with $\rho \to \bar{\varphi}^0$.

Coulomb gauge:
In this gauge $\partial_i A^i = 0$. In Fourier space we get

$$\delta\varphi^1_{\mathbf{k}} = -\frac{\bar{\rho} g_{_A}}{2k} G^L_{\mathbf{k}}\,, \qquad A_{0\mathbf{k}} = G_{0\mathbf{k}} + \frac{1}{k}\partial_\tau G^L_{\mathbf{k}}\,, \qquad A^L_{\mathbf{k}} = 0\,. \tag{8.46}$$

Unitary gauge:
In this gauge $\varphi^1 = 0$, which yields

$$\delta\varphi^1_{\mathbf{k}} = 0\,, \qquad A_{0\mathbf{k}} = G_{0\mathbf{k}}\,, \qquad A^L_{\mathbf{k}} = G^L_{\mathbf{k}}\,. \tag{8.47}$$

The equations in the Unitary gauge are identical to those in the gauge invariant one.

Temporal gauge:
In this gauge $A_0 = 0$. However, the theory is still invariant under the time-independent transformation $A_i \to A_i + \partial_i\alpha(\mathbf{x})$ and $\delta\varphi^1 \to \delta\varphi^1 - \bar{\varphi}^0 g_{_A}\alpha(\mathbf{x})/2$, which in Fourier space translates to $A^L_{\mathbf{k}} \to A^L_{\mathbf{k}} - k\alpha_{\mathbf{k}}$ and $\delta\varphi^1_{\mathbf{k}} \to \delta\varphi^1_{\mathbf{k}} - \bar{\varphi}^0 g_{_A}\alpha_{\mathbf{k}}/2$. Hence, we completely fix the gauge by choosing an α such that at some moment of time, $\tau = \tau_{\rm in}$, $\delta\varphi^1_{\mathbf{k}}(\tau_{\rm in}) = 0$. With this condition, we have

$$\delta\varphi^1_{\mathbf{k}} = \frac{\bar{\rho} g_{_A}}{2}\int_{\tau_{\rm in}}^{\tau} G_{0\mathbf{k}}(\eta)d\eta\,, \qquad A_{0\mathbf{k}} = 0\,, \qquad A^L_{\mathbf{k}} = G^L_{\mathbf{k}} + k\int_{\tau_{\rm in}}^{\tau} G_{0\mathbf{k}}(\eta)d\eta\,. \tag{8.48}$$

Lorenz gauge:
In this gauge $\nabla_\mu A^\mu = 0$. In this case

$$\begin{aligned} &\delta\varphi^1_{\mathbf{k}} = \bar{\rho} g_{_A}(A^L_{\mathbf{k}} - G^L_{\mathbf{k}})/(2k)\,, \qquad A_{0\mathbf{k}} = G_{0\mathbf{k}} + \partial_\tau(G^L_{\mathbf{k}} - A^L_{\mathbf{k}})/k\,, \\ &A^L_{\mathbf{k}} = \int \mathcal{G}(\tau,\eta)\left(\partial_\eta + 2\mathcal{H}(\eta)\right)\left(kG_{0\mathbf{k}}(\eta) + \partial_\eta G^L_{\mathbf{k}}(\eta)\right)d\eta\,, \end{aligned} \tag{8.49}$$

where $\mathcal{G}(\tau,\eta)$ is the Greens function of the linear operator $\mathcal{L}_\tau \equiv \partial^2_\tau + 2\mathcal{H}(\tau)\partial_\tau + k^2$. Arriving at the above form of the relationship between variables requires a bit of explanation. In Fourier space the Lorenz gauge condition translates to $\partial_\tau A_{0\mathbf{k}} + 2\mathcal{H}A_{0\mathbf{k}} - kA^L_{\mathbf{k}} = 0$, and the equation governing $A^L_{\mathbf{k}}$ yields $\mathcal{L}_\tau A^L_{\mathbf{k}} = (\partial_\tau + 2\mathcal{H})(kG_{0\mathbf{k}} + \partial_\tau G^L_{\mathbf{k}})$. This equation yields the particular solution above only if we can set the complementary solution to zero. This can always be done since there is a residual degree of freedom χ such that under the transformations $A_\mu \to A_\mu + \nabla_\mu\chi$ and $\delta\varphi^1 \to \delta\varphi^1 - \bar{\varphi}^0 g_{_A}\chi/2$, the theory remains invariant; provided χ obeys $\nabla_\mu\nabla^\mu\chi = 0$. In Fourier space we get $\mathcal{L}_\tau\chi_{\mathbf{k}} = 0$. Since the operator evolving $\chi_{\mathbf{k}}$ is identical to the one evolving $A^L_{\mathbf{k}}$, we can always choose $\chi_{\mathbf{k}}$ such that the complementary part of $A^L_{\mathbf{k}}$ vanishes, thus arriving at the particular solution provided above.

8.3 Inflationary dynamics

The background dynamics are relatively straightforward during inflation. At the phenomenological level, with an appropriate choice of the potential V and initial conditions we can easily arrange for $-\partial_t H/H^2 =$

$-a\partial_\tau(\mathcal{H}/a)/\mathcal{H}^2 \ll 1$ for sufficient number of e-folds. For simple models, this corresponds to $H = (\mathcal{H}/a) \approx$ const and $\bar{\rho} \approx$ const during inflation. Inflation ends when $\partial_\tau \mathcal{H} = 0$, when accelerated expansion stops and the field starts rolling quickly. Assuming such a background solution has been found, we focus on the quantum fluctuations around this classical background. Quantization of constrained systems, like the problem at hand, can be tricky. We find that by working in Fourier space with gauge invariant variables and substituting the constraints before quantizing, the process becomes straightforward. Once the appropriate quantized solutions for the scalar and gauge fields are available, we construct the power-spectra of the electric and magnetic fields at the end of inflation.

8.3.1 Quantized scalar and vector perturbations

For the purposes of quantization, it is convenient to write down the action for the Fourier components of the dynamical perturbation variables left after imposing the constraints. The equations of motion for these variables $\delta\tilde{\rho}_{\mathbf{k}}, G^L_{\mathbf{k}}$ and $G^{T\pm}_{\mathbf{k}}$ were provided in the previous section (see eqns. (8.31), (8.37) and (8.40)). The total quadratic action of these variables naturally splits into four parts:

$$S^{(2)}_{\rm m} = S^\rho + S^L + S^{T+} + S^{T-} = \sum_I S^I \,, \tag{8.50}$$

where S^I are the quadratic actions for the perturbations in the I-th variable f^I with

$$S^I = \int \mathrm{d}\tau L^I(\tau) = \int d\tau \int d^3k \; b_I(k,\tau) \left[\frac{1}{2}|\partial_\tau f^I_{\mathbf{k}}|^2 - \frac{1}{2}\omega_I^2(k,\tau)|f^I_{\mathbf{k}}|^2\right]. \tag{8.51}$$

The explicit forms of $b_I(k,\tau)$ and $\omega_I(k,\tau)$ will be provided below for the different components. We first outline the general quantization procedure common to all of the components. The conjugate momentum density of the I-th variable

$$\pi^I_{\mathbf{k}}(\tau) = \frac{\delta\left(L^I(\tau)\right)}{\delta\left(\partial_\tau f^I_{-\mathbf{k}}\right)} = b_I \partial_\tau f^I_{\mathbf{k}} \,, \tag{8.52}$$

where we have made use of $f^{I*}_{\mathbf{k}} = f^I_{-\mathbf{k}}$. The field operators $\hat{f}^I_{\mathbf{k}}$ along with their conjugate momenta operators $\pi^I_{\mathbf{k}}$ must obey the standard equal time commutators:

$$\left[\hat{f}^I_{\mathbf{k}}(\tau), \hat{f}^J_{\mathbf{q}}(\tau)\right] = 0 \,, \quad \left[\hat{\pi}^I_{\mathbf{k}}(\tau), \hat{\pi}^J_{\mathbf{q}}(\tau)\right] = 0 \,, \quad \left[\hat{f}^I_{\mathbf{k}}(\tau), \hat{\pi}^J_{\mathbf{q}}(\tau)\right] = i\,(2\pi)^{-3}\,\delta^{IJ}\delta(\mathbf{k}+\mathbf{q}) \,. \tag{8.53}$$

Note that our fields are not canonically normalized. The non-vanishing commutator and eq. (8.52) imply

$$\left[\hat{f}^I_{\mathbf{k}}(\tau), \partial_\tau \hat{f}^J_{\mathbf{q}}(\tau)\right] = i\,(2\pi)^{-3}\,(b_I(k,\tau))^{-1}\,\delta^{IJ}\delta(\mathbf{k}+\mathbf{q}) \,. \tag{8.54}$$

The field operators $\hat{f}^I_{\mathbf{k}}$ can be expanded in terms of operators $\hat{a}^I_{\mathbf{k}}$ and mode functions $u^I_k(\tau)$ as

$$\hat{f}^I_{\mathbf{k}}(\tau) = \hat{a}^I_{\mathbf{k}} u^I_k(\tau) + \hat{a}^{I\dagger}_{-\mathbf{k}} u^{I*}_k(\tau) \,, \tag{8.55}$$

where each of the mode functions $u^I_k(\tau)$ satisfies the corresponding field equations of motion obtained by varying the action S^I (same equations as those satisfied by $f^I_{\mathbf{k}}$)

$$\partial^2_\tau u^I_k + (\partial_\tau \ln b_I)\,\partial_\tau u^I_k + \omega_I^2 u^I_k = 0 \,. \tag{8.56}$$

The final ingredient needed for evolving the mode function $u_k^I(\tau)$ (and hence the field operators), are the initial conditions for the mode functions. Their normalization will in turn also determine the commutation relation for the operators $\hat{a}_{\mathbf{k}}^I$. We will determine the initial conditions by constructing WKB solutions for the mode functions satisfying eq. (8.56) at very early times.

To proceed to the WKB solutions for the initial conditions we need the explicit forms of $b_I(k,\tau)$ and $\omega_I(k,\tau)$, which are provided below. For $I=\rho$, i.e., when $f_{\mathbf{k}}^\rho = \delta\tilde{\rho}_{\mathbf{k}}$ we have

$$\begin{aligned} b_\rho(k,\tau) &= a^2 \exp\left[\frac{1}{2m_{\rm Pl}^2}\int_{\tau_i}^{\tau} d\tau \left(\frac{\partial_\tau(\partial_\tau\bar{\rho})^2}{\partial_\tau\mathcal{H}-\mathcal{H}^2+k^2}\right)\right], \\ \omega_\rho^2(k,\tau) &= k^2 + a^2\partial_{\bar{\rho}}^2 V - \frac{1}{m_{\rm Pl}^2}\left[\partial_\tau^2\bar{\rho}\left(\frac{\partial_\tau^2\bar{\rho}-\mathcal{H}\partial_\tau\bar{\rho}}{\partial_\tau\mathcal{H}-\mathcal{H}^2+k^2}\right)+2(\partial_\tau\bar{\rho})^2\right]. \end{aligned} \tag{8.57}$$

Similarly, for $I=L,T\pm$, i.e., when $f_{\mathbf{k}}^I = G_{\mathbf{k}}^L, G_{\mathbf{k}}^{T\pm}$ we have

$$\begin{aligned} b_L(k,\tau) &= \left[1+\left(\frac{2k}{\bar{\rho}g_{_A}a}\right)^2\right]^{-1}, \qquad \omega_L^2(k,\tau) = k^2+\left(\frac{\bar{\rho}g_{_A}a}{2}\right)^2, \\ b_{T\pm}(k,\tau) &= 1, \qquad \omega_{T\pm}^2(k,\tau) = k^2+\left(\frac{\bar{\rho}g_{_A}a}{2}\right)^2. \end{aligned} \tag{8.58}$$

One can check that extremising the action in eq. (8.50) with respect to each of the field perturbations gives the corresponding equations of motion from the previous section, namely eqns. (8.31), (8.37) and (8.40).

At early enough times during inflation as $a\to 0$, a given k mode of interest will be deep inside the horizon $k\gg\mathcal{H}$ and will dominate all other physical scales (for example, $k\gg(\bar{\rho}g_{_A}a)$) as $a\to 0$. At such early enough times during inflation $\partial_\tau^2\ln b_I$, $(\partial_\tau\ln b_I)^2 \ll \omega_I^2$. This hierarchy can be verified by noting that for each component $\omega_I^2\to k^2$ and $(\partial_\tau\ln b_{\rho,L})^2, \partial_\tau^2\ln b_{\rho,L}\to\mathcal{O}[\mathcal{H}^2]$, $\partial_\tau\ln(b_{T\pm})=0$. With this information at hand, the WKB solution of eq. (8.56) at early enough times during inflation is[3]

$$u_k^I(\tau)\to\frac{1}{(2\pi)^{3/2}\sqrt{2}}\frac{1}{\sqrt{b_I(k,\tau)\omega_I(k,\tau)}}\exp\left(-i\int_{\tau_{\rm in}}^{\tau}{\rm d}\tau'\omega_I(k,\tau')\right), \tag{8.59}$$

where for the WKB solution to be valid

$$\left|\partial_\tau\left[\omega_I^2-\frac{1}{2}\partial_\tau^2\ln b_I-\frac{1}{4}(\partial_\tau\ln b_I)^2\right]^{-1/2}\right| \ll 1. \tag{8.60}$$

The time independent normalization of the mode functions ($\left[(2\pi)^{3/2}\sqrt{2}\right]^{-1}$) was chosen so that the usual commutation relation for the creation and annihilation operators is satisfied. That is, using the above mode functions in eqns. (8.54) and (8.55) implies that at early times

$$\left[\hat{a}_{\mathbf{k}}^I,\hat{a}_{-\mathbf{k}}^J\right]=0, \qquad \left[\hat{a}_{\mathbf{k}}^I,\hat{a}_{-\mathbf{q}}^{J\dagger}\right]=\delta^{IJ}\delta(\mathbf{k}+\mathbf{q}). \tag{8.61}$$

Since these operators are time-independent, these relationships remain true at all times. Thus by starting with the initial conditions for the mode functions u_k^I in eq. (8.59), we can evolve them using eq. (8.56) to any later

[3]This can be obtained by making the usual transformation to eliminate the "friction term" from eq. (8.56) and then using the general form of the 1st order WKB solution. The final form also assumes that ω_I^2 dominates over other terms in the WKB solution.

time and obtain the necessary power-spectra. The forward time evolution will take the initially sub-horizon and/or ultra-relativistic ($k \gg \mathcal{H}$ and/or $k \gg \bar{\rho} g_{_A} a$) solutions to superhorizon and non-relativistic ones.

Before ending this section we make some general comments about the early time solutions for the mode functions u_k^I during inflation written explicitly below:

$$\begin{aligned} u_k^{\rho}(\tau) &\to \frac{\mathrm{e}^{-ik\tau}}{(2\pi)^{3/2}\, a(\tau)\sqrt{2k}}\,, \\ u_k^{L}(\tau) &\to \frac{\left(\frac{2k}{\bar{\rho} g_{_A}}\right) \mathrm{e}^{-ik\tau}}{(2\pi)^{3/2}\, a(\tau)\sqrt{2k}}\,, \\ u_k^{T\pm}(\tau) &\to \frac{\mathrm{e}^{-ik\tau}}{(2\pi)^{3/2}\, \sqrt{2k}}\,. \end{aligned} \tag{8.62}$$

The early time solution for the mode function u_k^{ρ} of $\delta\hat{\bar{\rho}}_{\mathbf{k}}$ reflects the fact that at early enough times, we are simply dealing with an effectively massless ($k^2 \gg a^2 \partial_{\rho}^2 V$) field on subhorizon $k \gg \mathcal{H}$ scales where metric perturbations are negligible. The early time solution is identical to the mode functions for the Minkowski vacuum apart from the trivial $a(\tau)$ scaling. The mode function u_k^L of the longitudinal component of the gauge fields $\hat{G}_{\mathbf{k}}^L$ is related to u_k^{ρ} in a simple way: $u_k^L = \left(\frac{2k}{\bar{\rho} g_{_A}}\right) u_k^{\rho}$. The rescaled field $(\bar{\rho} g_{_A}/2k)\hat{G}_{\mathbf{k}}^L$ behaves as a massless scalar field, which is a manifestation of the Goldstone Boson Equivalence Theorem. The scalefactor does not appear in the early time mode functions $u_k^{T\pm}$ of the transverse gauge field modes $\hat{G}_{\mathbf{k}}^{T\pm}$. This reflects the fact that massless transverse modes of gauge fields are conformally invariant.

Finally, we note that the above early solutions were constructed assuming slow roll inflation. However, for large enough k these solutions remain valid even at the end of inflation as is to be expected, albeit with slightly different conditions on k. The conditions for these solutions to be valid are $k^2 \gg \mathcal{H}^2, a^2\partial_{\rho}^2 V$ for u_k^{ρ}; $k \gg \partial_{\tau}(a\bar{\rho})/(a\bar{\rho}), a\bar{\rho} g_{_A}/2$ and $k^2 \gg |\partial_{\tau}^2(a\bar{\rho})/(a\bar{\rho})|$ for u_k^L; and $k \gg a\bar{\rho} g_{_A}/2$ for $u_k^{T\pm}$. These are useful for checking the ultra-relativistic solutions at the end of inflation.

8.3.2 Inflationary power-spectra

Let us now use the developed formalism to compute the power-spectra of the matter fields at the end of inflation – the first moment when $\partial_{\tau}\mathcal{H} = 0$.[4] We will calculate the power-spectra of the gauge invariant electric and magnetic fields.

The correlation functions of the electric and magnetic fields can be written in terms of the longitudinal and transverse mode functions as follows:

$$\begin{aligned} \langle 0|\, \hat{E}_{j\mathbf{q}} \hat{E}_{j\mathbf{k}}^{\dagger}\, |0\rangle &= \delta\left(\mathbf{q}-\mathbf{k}\right)\left(\left|u_k^{E^L}\right|^2 + \sum_{\lambda=\pm}\left|u_k^{E^{T\lambda}}\right|^2\right)\,, \\ \langle 0|\, \hat{B}_{j\mathbf{q}} \hat{B}_{j\mathbf{k}}^{\dagger}\, |0\rangle &= \delta\left(\mathbf{q}-\mathbf{k}\right)\sum_{\lambda=\pm}\left|u_k^{B^{T\lambda}}\right|^2\,, \end{aligned} \tag{8.63}$$

[4] Which is equivalent to the standard expression $\ddot{a}(t) = 0$, where t is cosmic time.

where from eq. (8.43)

$$u_k^{E^L} = \left[1 + \left(\frac{2k}{\bar{\rho} g_{_A} a}\right)^2\right]^{-1} \partial_\tau u_k^L \,, \qquad u_k^{E^{T\lambda}} = \partial_\tau u_k^{T\lambda} \,, \qquad u_k^{B^{T\pm}} = \pm k u_k^{T\pm} \,. \tag{8.64}$$

The power-spectra of the electric and magnetic fields are defined as[5]

$$\Delta^2_{E^{T\pm}} = 4\pi k^3 \frac{|u_k^{E^{T\pm}}|^2}{a^4} \,, \qquad \Delta^2_{B^{T\pm}} = 4\pi k^3 \frac{|u_k^{B^{T\pm}}|^2}{a^4} \,, \qquad \Delta^2_{E^{L}} = 4\pi k^3 \frac{|u_k^{E^{L}}|^2}{a^4} \,. \tag{8.65}$$

For concreteness, we compute these power-spectra at the end of inflation for the chaotic inflation scenario with $V(\rho) = (1/2)m^2\rho^2$. However, our results hold more generally. For an analytic understanding of the features in the power-spectra we solve the equations of motion in de Sitter space to zeroth order in slow-roll (i.e., we ignore time derivatives of the inflaton) in Appendix B. We assume that inflation lasts 60 e-folds and take the inflaton mass to be $m = 10^{-6}\, m_{\rm pl}$. The longitudinal and transverse fields, $\hat{G}^L_{\mathbf{k}}$ and $\hat{G}^{T\pm}_{\mathbf{k}}$ are evolved numerically from very early times when they are deep inside the horizon with $k \gg \mathcal{H}$, $k \gg a\bar{\rho} g_{_A}/2$ and $k^2 \gg \left|\partial^2_\tau (a\bar{\rho})/a\bar{\rho})\right|$, and have corresponding electric and magnetic WKB power-spectra (cf. eqns. (8.62), (8.64), (8.65))

$$\Delta^2_{E^{T\pm}} = \frac{H^4}{4\pi^2}\left(\frac{k}{\mathcal{H}}\right)^4 , \qquad \Delta^2_{B^{T\pm}} = \frac{H^4}{4\pi^2}\left(\frac{k}{\mathcal{H}}\right)^4 , \qquad \Delta^2_{E^{L}} = \frac{H^4}{4\pi^2}\left(\frac{k}{\mathcal{H}}\right)^2 \left(\frac{k_{_C}}{\mathcal{H}}\right)^2 . \tag{8.66}$$

The power-spectra of the electric and magnetic fields at the end of inflation are shown in Fig. 8.1. To understand these plots, a 'Compton wavenumber' $k_{_C}$ corresponding to the effective mass is particularly important:

$$k_{_C} \equiv a\bar{\rho} g_{_A}/2 \,, \tag{8.67}$$

where the time-dependent quantities on the right-hand side are all evaluated at the time of interest (usually at the end of inflation). The spectra behave differently based on the relative size of $k_{_C}$ and the Hubble scale $\mathcal{H}$. When the Compton wavenumber of $\hat{G}^L_{\mathbf{k}}$ and $\hat{G}^{T\pm}_{\mathbf{k}}$ is subhorizon, i.e., $k_{_C} \gtrsim \mathcal{H}$, we have

$$\begin{aligned}
\Delta^2_{B^{T\pm}} &\approx \frac{H^4}{4\pi^2} \times \begin{cases} (k/\mathcal{H})^4 \, (k/k_{_C}) \,, & \text{if } k \ll k_{_C} \,, \\ (k/\mathcal{H})^4 \,, & \text{if } k \gg k_{_C} \,, \end{cases} \\
\Delta^2_{E^{T\pm}} &\approx \frac{H^4}{4\pi^2} \times \begin{cases} (k/\mathcal{H})^3 \, (k_{_C}/\mathcal{H}) \,, & \text{if } k \ll k_{_C} \,, \\ (k/\mathcal{H})^4 \,, & \text{if } k \gg k_{_C} \,, \end{cases} \\
\Delta^2_{E^{L}} &\approx \frac{H^4}{4\pi^2} \times \begin{cases} (k/\mathcal{H})^3 \, (k_{_C}/\mathcal{H}) \,, & \text{if } k \ll k_{_C} \,, \\ (k/\mathcal{H})^2 \, (k_{_C}/\mathcal{H})^2 \,, & \text{if } k \gg k_{_C} \,. \end{cases}
\end{aligned} \tag{8.68}$$

As is evident from the above scalings, the magnetic field and both the transverse and longitudinal electric field power-spectra have double power-law forms, with $k_{_C}$ setting the break in all three of them. This is indeed expected for $\Delta^2_{E^{T\pm}}$, $\Delta^2_{B^{T\pm}}$, since $\hat{G}^{T\pm}_{\mathbf{k}}$ cares only about $k_{_C}$ (cf. eq. (8.40)). However, $\hat{G}^L_{\mathbf{k}}$ is affected

[5]The two transverse modes would have different power-spectra if there was axion coupling which we do not consider here. The way we have split the transverse modes into states $\pm$ with well-defined helicities makes our analysis easily extendible to the case of charged Higgs with an additional axion-like interaction.

by the expansion rate as well. From its equation of motion we would expect to see something in $\Delta^2_{E^L}$ near $k_{_C}$ and the Hubble scale, $\mathcal{H}$. The reason why there are no features in $\Delta^2_{E^L}$ near $\mathcal{H}$ in the strong coupling regime is given in Appendix B.

On the other hand when $k_{_C} \lesssim \mathcal{H}$, we find that

$$\begin{aligned}
\Delta^2_{B^{T\pm}} &\approx \frac{H^4}{4\pi^2}\left(\frac{k}{\mathcal{H}}\right)^4 , \\
\Delta^2_{E^{T\pm}} &\approx \frac{H^4}{4\pi^2} \times \begin{cases} (k/\mathcal{H})^2 \, (k_{_C}/\mathcal{H})^2 \, , & \text{if } k \ll k_{_C}^2/\mathcal{H} \, , \\ (k/\mathcal{H})^4 \, , & \text{if } k \gg k_{_C}^2/\mathcal{H} \, , \end{cases} \\
\Delta^2_{E^L} &\approx \frac{H^4}{4\pi^2} \times \begin{cases} \mathcal{T}_k \, (k/\mathcal{H})^2 \, (k_{_C}/\mathcal{H})^2 \, , & \text{if } k \ll \mathcal{H} \, , \\ (k/\mathcal{H})^2 \, (k_{_C}/\mathcal{H})^2 \, , & \text{if } k \gg \mathcal{H} \, . \end{cases}
\end{aligned} \tag{8.69}$$

In this regime, the transverse modes are still unaffected upon crossing the Hubble horizon. $\Delta^2_{E^{T\pm}}$ is again a double power-law. However, this time the break is at $k = k_{_C}(k_{_C}/\mathcal{H})$. The additional suppression of $k_{_C}/\mathcal{H}$ is unexpected, at least if one looks at the equation of motion of $\hat{G}^{T\pm}_{\mathbf{k}}$, eq. (8.40). For the interested reader, we explain this in Appendix B. Also note that in this regime $\Delta^2_{B^{T\pm}}$ is a single power-law, given by the deep subhorizon Minkowskian power-spectrum. For $0.1 < k_{_C}/\mathcal{H} < 1$ there is a crossover behaviour from a double power-law of the $k_{_C} \gg \mathcal{H}$ regime to the single power-law of $k_{_C} \ll \mathcal{H}$. The power-spectrum for the longitudinal component of the electric field $\Delta^2_{E^L}$ exhibits a power excess on super-Hubble scales, with the correction factor found numerically to be $1 < \mathcal{T}_k < 2$ at the end of inflation. On super-Compton scales, $k < k_{_C}$, $\mathcal{T}_k \approx 2$. We also do not see any features in the range $k_{_C} < k < \mathcal{H}$ in $\Delta^2_{E^L}$ because the k-dependent pre-factor multiplying $\partial_\tau \hat{G}^L_{\mathbf{k}}$ in the definition of $\hat{E}^L_{\mathbf{k}}$, eq. (8.43), cancels the additional k-dependence. Note that $\mathcal{T}_k$ is time-dependent and $\mathcal{T}_k \to 1$ in de Sitter space-time (see Appendix B for the evaluation of the power-spectra in de Sitter space-time). The deviation of $\mathcal{T}_k$ from 1 is observed towards the end of inflation. It is thus important to solve for the mode functions in a background that deviates from de Sitter in order to capture this effect and obtain the correct power-spectra at the end of inflation.

We also give the power-spectra calculated under the assumption that $H = 0$ and $\bar{\rho} = \text{const}$ (hence $k_{_C} = \text{const}$), cf. dashed lines in Fig. 8.1. These are 'quasi-Minkowski' conditions in the sense that the effects of expansion are ignored. We can then calculate the evolution of the mode functions and obtain the following expressions for the power for electric and magnetic fields:

$$\begin{gathered}
\Delta^2_{E^{T\pm}} = \frac{H^4}{4\pi^2}\left(\frac{k}{\mathcal{H}}\right)^4 \left(1 + \frac{k_{_C}^2}{k^2}\right)^{1/2} , \qquad \Delta^2_{B^{T\pm}} = \frac{H^4}{4\pi^2}\left(\frac{k}{\mathcal{H}}\right)^4 \left(1 + \frac{k_{_C}^2}{k^2}\right)^{-1/2} , \\
\Delta^2_{E^L} = \frac{H^4}{4\pi^2}\left(\frac{k}{\mathcal{H}}\right)^2 \left(\frac{k_{_C}}{\mathcal{H}}\right)^2 \left(1 + \frac{k_{_C}^2}{k^2}\right)^{-1/2} .
\end{gathered} \tag{8.70}$$

When $k_{_C} \ll \mathcal{H}$ expansion is important for superhorizon modes $k < \mathcal{H}$. However, if $k_{_C} \geq \mathcal{H}$ the effects due to expansion are negligible and eq. (8.70) is a good approximation to the power-spectrum in the electric and magnetic fields.

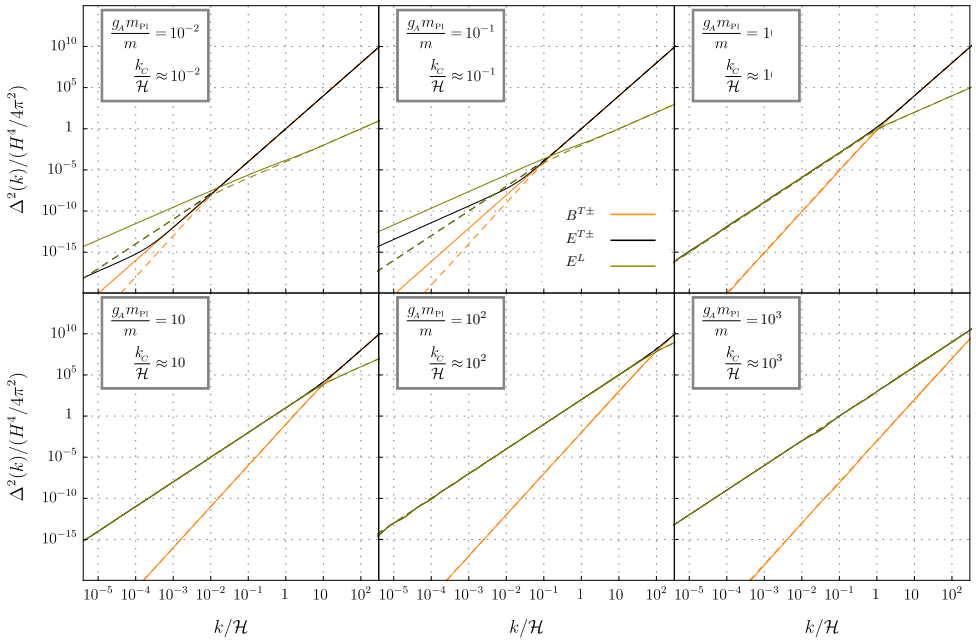

Figure 8.1: The power-spectra of the transverse and longitudinal electric and magnetic fields at the end of inflation for $m^2|\varphi|^2$ inflation (solid lines) for different strengths of the couplings g_A between gauge fields and the inflaton condensate. Power-spectra at the end of inflation ignoring the effects of expansion (dashed lines) are shown for comparison. We show three different spectra: the longitudinal electric field, $\Delta^2_{E^L}$ (green), the transverse electric field, $\Delta^2_{E^{T\pm}}$ (black), and the magnetic field, $\Delta^2_{B^{T\pm}}$ (orange). The mode functions of the fields responsible for these spectra can have two distinct forms depending on the magnitude of the scale $k_C \equiv a\bar{\rho}g_A/2$ where $\bar{\rho}$ is the magnitude of the inflaton field at the end of inflation. For the upper row with $k_C \lesssim \mathcal{H}$, $\Delta^2_{E^L}$ (green) and $\Delta^2_{B^{T\pm}}$ (orange) are nearly single power-laws, whilst $\Delta^2_{E^{T\pm}}$ (black) is a double power-law with a break $k \sim k_C(k_C/\mathcal{H})$. For the lower row with $k_C \gtrsim \mathcal{H}$, all three power-spectra have double power-law forms, with a break at $k \sim k_C$. Note that one can also use these plots to read-off the power-spectrum of the charge density, $\Delta^2_{j_0} = (k/a)^2\Delta^2_{E^L}$. More detailed expressions for the spectra are provided in eqns. (8.68) and (8.69). An analysis of these spectra in de Sitter space (which explains the different power-laws) is provided in Appendix B. Note that the Hubble parameter H (and its conformal counterpart $\mathcal{H}$) *at the end of inflation* was used to make the relevant quantities dimensionless on the horizontal and vertical axes.

8.4 Preheating dynamics

At the end of inflation the inflaton field begins to oscillate around the minimum of its potential. The linearised equations describing the evolution of the fluctuations in the inflaton and gauge fields will then contain oscillating terms. Such oscillating terms can lead to an exponential growth of matter fluctuations. As we discussed in Chapter 2, this *preheating* period begins soon after the end of inflation and its end is marked by the back-reaction of the fluctuations on the inflaton condensate and/or the moment when the linearised analysis of the fluctuations stops being a good approximation.

The power-spectra of electric and magnetic fields at the end of the preheating era are shown in Fig. 8.2. These spectra are calculated numerically (for quadratic inflation) and properly account for the quantum nature of the fields, effects of expansion and metric perturbations. A detailed understanding of these spectra is the main goal of this section. As we will see, calculating these spectra using gauge invariant variables

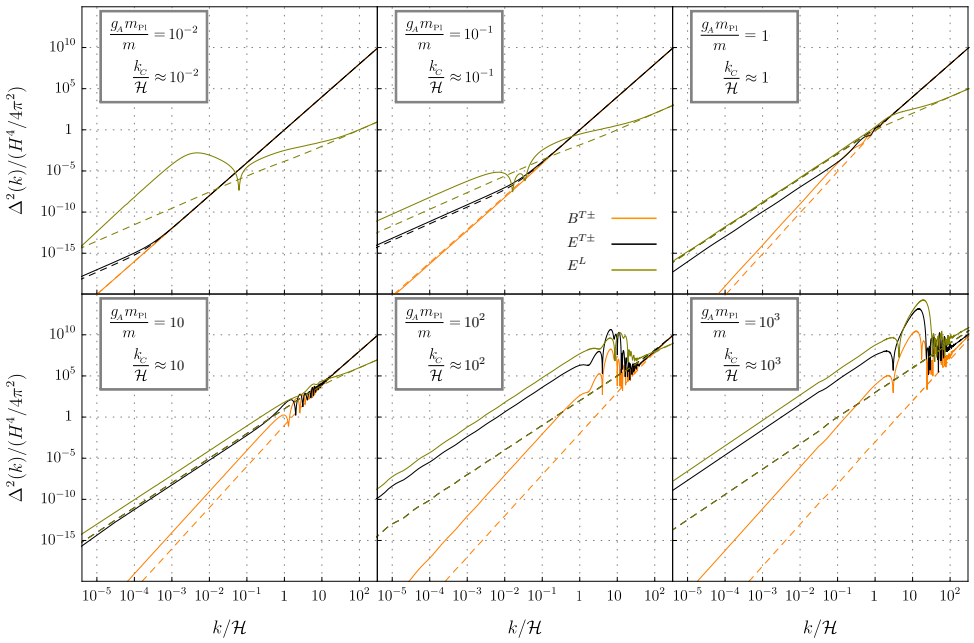

Figure 8.2: The power-spectra of the transverse and longitudinal electric and magnetic fields *after* a few inflaton oscillations at the end of inflation: the longitudinal electric field, $\Delta^2_{E^L}$ (green), the transverse electric field, $\Delta^2_{E^{T\pm}}$ (black), and the magnetic field, $\Delta^2_{B^{T\pm}}$ (orange). Each plot was evaluated for a different coupling g_A, and the result is presented at a fixed time $t_{\rm br} \approx 10^2\, m^{-1}$ after inflation. $t_{\rm br}$ is the time of back-reaction for the specific coupling $g_A m_{\rm Pl}/m = 10^3$ (lower right corner). The effects of non-adiabatic particle production during preheating is clearly visible in the lower row (large coupling) for $k/\mathcal{H} \lesssim \sqrt{m/H}\sqrt{k_C/\mathcal{H}} \sim \sqrt{k_C/\mathcal{H}}$. The boundary between small and large coupling $g_A m_{\rm Pl}/m \approx 1$, can be understood via a Floquet analysis of the instabilities. A requirement of *broad resonance* [14], leads to the upper bound on k. The features in the top row (small couplings) can be also understood in terms of the inflaton oscillations. We have rescaled $\Delta^2_{E^{T\pm}}$ and $\Delta^2_{B^{T\pm}}$ by a^4, and rescaled $\Delta^2_{E^L}$ by a^5 (with $a = 1$ at the end of inflation) to roughly separate the effects of resonant particle production from the expected red-shifting of the fields. We also plot the power-spectra before resonant particle production begins, i.e., right at the end of inflation (dashed lines) for comparison. For ease of comparison with Fig. 8.1, H (and its conformal counterpart $\mathcal{H}$) at the end of inflation was used for constructing the relevant dimensionless ratios on the horizontal and vertical axes. Note that $\mathcal{H}_{\rm br} \approx 0.25\mathcal{H}$, that is $k/\mathcal{H}_{\rm br} \approx 4k/\mathcal{H}$, so the main features in the lower row are all significantly subhorizon at the time of evaluation.

(and *Unitary gauge* variables) becomes somewhat unwieldy (in particular for the longitudinal components of the gauge fields). The *Coulomb gauge* turns out to be well suited for this calculation.

In Section 8.4.1, we will use Floquet theory to explore the instabilities in matter perturbations using gauge invariant variables and gauge dependent variables. In Section 8.4.2, a Hartree approximation is used to understand the effects of back-reaction on the homogeneous condensate and quantify a time when preheating ends.

8.4.1 Floquet analysis

We ignore metric perturbations for the Floquet analysis of the instabilities in the matter perturbations. This is a plausible approximation since the vector and tensor metric perturbations are decoupled from matter anyway, while the scalar metric perturbations are suppressed on subhorizon scales. We also ignore expansion

at the background level since the universe does not expand much during the short period of preheating. For notational simplicity we drop quantum operators from our expressions while carrying out Floquet analysis.[6] The linearized equations of motion for the Fourier modes of the matter fields have the general form (cf. Section 8.3.1, but now ignoring expansion, quantum operators and metric perturbations)

$$\partial_\tau^2 f_{\mathbf{k}}^I + (\partial_\tau \ln b_I)\, \partial_\tau f_{\mathbf{k}}^I + \omega_I^2 f_{\mathbf{k}}^I = 0\,, \tag{8.71}$$

where $\omega_I(k,\tau)$ and $b_I(k,\tau)$ are periodic because of the oscillating inflaton. Floquet theory tells us (see also Section 2.2.1) that eq. (8.71) has solutions of the form

$$f_{\mathbf{k}}^I(\tau) = \mathcal{P}_{\mathbf{k}+}^I(\tau)\exp(\mu_k^I\tau) + \mathcal{P}_{\mathbf{k}-}^I(\tau)\exp(-\mu_k^I\tau)\,, \tag{8.72}$$

where $\mathcal{P}_{\mathbf{k}\pm}^I(\tau)$ are periodic functions having the same period T as the inflaton, and μ_k^I is the Floquet exponent. The Floquet exponents and the periodic functions can be calculated by solving the equation of motion for $f_{\mathbf{k}}^I$ twice in the interval $\tau_0 \le \tau \le \tau_0 + T$ with $\left(f_{\mathbf{k}}^{I(1)}, \partial_\tau f_{\mathbf{k}}^{I(1)}\right) = (1,0)$ and $\left(f_{\mathbf{k}}^{I(2)}, \partial_\tau f_{\mathbf{k}}^{I(2)}\right) = (0,1)$ as initial conditions. The real part of the Floquet exponents is given by

$$\Re[\mu_k] = \frac{1}{T}\ln\left|\frac{1}{2}\left(f_{\mathbf{k}}^{I(1)} + \partial_\tau f_{\mathbf{k}}^{I(2)} + \sqrt{\left\{f_{\mathbf{k}}^{I(1)} - \partial_\tau f_{\mathbf{k}}^{I(2)}\right\}^2 + 4 f_{\mathbf{k}}^{I(2)}\partial_\tau f_{\mathbf{k}}^{I(1)}}\right)\right| \tag{8.73}$$

where $f_{\mathbf{k}}^{I(i)}$ and $\partial_\tau f_{\mathbf{k}}^{I(i)}$ are evaluated at $\tau = \tau_0 + T$. The effects of the more general initial conditions (for example, those from the end of inflation) can then be incorporated by appropriately scaling the periodic solutions.

Gauge invariant analysis

For the gauge invariant variables, the specific forms of the coefficients b_I and ω_I in eq. (8.72) are quite simple in flat spacetime. For the inflaton perturbations $f_{\mathbf{k}}^\rho = \delta\rho_{\mathbf{k}}$, (cf. eq. (8.57), with $a = 1$, $m_{\rm Pl}^2 \to \infty$)

$$b_\rho = 1\,, \qquad \omega_\rho^2 = k^2 + \partial_{\bar\rho}^2 V(\bar\rho)\,. \tag{8.74}$$

Similarly, for the transverse components of the gauge fields $f_{\mathbf{k}}^{T\pm} = G_{\mathbf{k}}^{T\pm}$,

$$b_T = 1\,, \qquad \omega_T^2 = k^2 + \left(\frac{g_A\bar\rho}{2}\right)^2\,. \tag{8.75}$$

In both of these cases, one can calculate the respective Floquet exponents μ_k^ρ and $\mu_k^{T\pm}$ once $\bar\rho(\tau)$ is obtained from the background dynamics using the usual techniques.[7] For a chaotic inflation potential $V(\rho) = (1/2)m^2\rho^2$, $\Re[\mu_k^\rho] = 0$ whereas $\Re[\mu_k^T]$ is shown in Fig. 8.3.

[6] More explicitly, we could have done the calculation with the mode functions with operators coming along for the ride rather than notationally using classical Fourier modes of the fields. However, this gets rather cumbersome.

[7] From the background equation of motion for $\bar\rho$ near the minimum of $V(\bar\rho)$, eq. (8.22), one might infer that $\bar\rho$ is oscillatory with positive and negative values. This seems apparently at odds with the positive definiteness of $\bar\rho$ as implied by its definition as a "radial" variable. This is of course a minor inconvenience due to our choice of "radial" gauge invariant variables and can be understood in terms of a discontinuous jump of the angular variable at the origin which we have ignored. There is the other issue of the definition G_μ when $\bar\rho = 0$, cf. eq. (8.7), though it remains well defined away from this point.

Longitudinal mode: The analysis of the longitudinal mode of the gauge field $f^L_{\mathbf{k}} = G^L_{\mathbf{k}}$ is a bit more subtle. For this case

$$b_L(k,\tau) = \left[1+\left(\frac{2k}{\bar{\rho}g_A}\right)^2\right]^{-1}, \qquad \omega_L^2(k,\tau) = k^2 + \left(\frac{g_A\bar{\rho}}{2}\right)^2. \tag{8.76}$$

To deal with the singularity, $\bar{\rho}=0$, in the coefficient $\partial_\tau \ln b_L$ of $\partial_\tau G^L_{\mathbf{k}}$ (the "damping" term) appearing in eq. (8.71), we make the following change of variables

$$G^L_{\mathbf{k}}(\tau) = \check{h}(\bar{\rho}(\tau))\check{G}^L_{\mathbf{k}}(\tau) \qquad \text{where} \qquad \check{h}(\bar{\rho}(\tau)) = \sqrt{1+\left(\frac{2k}{g_A\bar{\rho}(\tau)}\right)^2}. \tag{8.77}$$

Thereby, we lose the singular damping term in eq. (8.71) for $f^L_{\mathbf{k}} = \check{G}^L_{\mathbf{k}}$, at the expense of the singularity in $\check{h}(\bar{\rho}(\tau))$. The explict form of the coefficients after the transformation are

$$\check{b}_L(k,\tau) = 1\,, \qquad \check{\omega}_L^2(k,\tau) = \frac{3\left(\frac{g_A\partial_\tau\bar{\rho}}{2k}\right)^2}{\left[1+\left(\frac{g_A\bar{\rho}}{2k}\right)^2\right]^2} - \frac{\frac{\partial_\tau^2\bar{\rho}}{\bar{\rho}}}{1+\left(\frac{g_A\bar{\rho}}{2k}\right)^2} + k^2 + \left(\frac{g_A\bar{\rho}}{2}\right)^2. \tag{8.78}$$

We note that the second term in $\check{\omega}_L^2$, proportional to $\partial_\tau^2\bar{\rho}(\tau)/\bar{\rho}(\tau)$, is never singular provided $\bar{\rho}^{-1}\partial_{\bar{\rho}}V(\bar{\rho})$ is well-defined at the origin $\bar{\rho}=0$[8,9], which is usually the case. Hence the solutions

$$\check{G}^L_{\mathbf{k}}(\tau) = \check{\mathcal{P}}^L_{\mathbf{k}+}(\tau)\exp\left(\mu^L_k\tau\right) + \check{\mathcal{P}}^L_{\mathbf{k}-}(\tau)\exp\left(-\mu^L_k\tau\right), \tag{8.79}$$

are well behaved with no singularities present in the Floquet exponents or in the periodic functions. Reverting back to the original variables, cf. eq. (8.77), we have

$$\begin{aligned} G^L_{\mathbf{k}}(\tau) &= \mathcal{P}^L_{\mathbf{k}+}(\tau)\exp\left(\mu^L_k\tau\right) + \mathcal{P}^L_{\mathbf{k}-}(\tau)\exp\left(-\mu^L_k\tau\right), \\ \mathcal{P}^L_{\mathbf{k}\pm}(\tau) &= \check{h}(\bar{\rho}(\tau))\check{\mathcal{P}}^L_{\mathbf{k}\pm}(\tau)\,. \end{aligned} \tag{8.80}$$

The Floquet exponents, μ^L_k, remain unaffected and singularity-free and are shown in Fig. 8.3. Only the periodic functions, $\mathcal{P}^L_{\mathbf{k}\pm}(\tau)$, are singular (or have 'spikes') at the zeroes of $\bar{\rho}$, because of the $\check{h}(\bar{\rho}(\tau))$ factor. Importantly, the physical observables: the longitudinal electric field $E^L_{\mathbf{k}}$ and the charge and current densities, $j_{0\mathbf{k}}$ and $j^L_{\mathbf{k}}$, are immune to the singularities because of the $\bar{\rho}$-dependent pre-factors in their definitions cancel appropriately (cf. eqns. (8.43) and (8.44)).

We note that an identical analysis holds for the *Unitary gauge* ($\Im[\varphi]=0$) as well. In that gauge, the equation of motion for the $A^L_{\mathbf{k}}$ has b_L and ω_L given in eq. (8.76) with $\bar{\rho}\to\Re[\bar{\varphi}]$ (cf. Section 8.2.4). Hence $A^L_{\mathbf{k}}$ grows exponentially as well with periodic spikes occurring whenever $\Re[\bar{\varphi}]=0$. This still leads

[8] Recall that $\partial_\tau^2\bar{\rho}/\bar{\rho} = -\bar{\rho}^{-1}\partial_{\bar{\rho}}V(\bar{\rho})$.

[9] If we are in a broken-symmetry, static state with $\partial_{\bar{\rho}}V(\bar{\rho})|_{\bar{\rho}\neq 0} = 0$ and $\partial_\tau\bar{\rho}=0$, the effective equations of motion $G^L_{\mathbf{k}}$ (seen more easily with $\check{G}^L_{\mathbf{k}}$) and $G^{T\pm}_{\mathbf{k}}$ are equal. Equal effective masses and similar behaviors for $G^L_{\mathbf{k}}$ and $G^{T\pm}_{\mathbf{k}}$ were assumed for example in [24, 286]. However, since during preheating $\partial_{\bar{\rho}}V(\bar{\rho})|_{\bar{\rho}\neq 0}\neq 0$ and $\partial_\tau\bar{\rho}\neq 0$ and hence $G^L_{\mathbf{k}}$ and $G^{T\pm}_{\mathbf{k}}$ have different effective masses (although the masses still remain comparable).

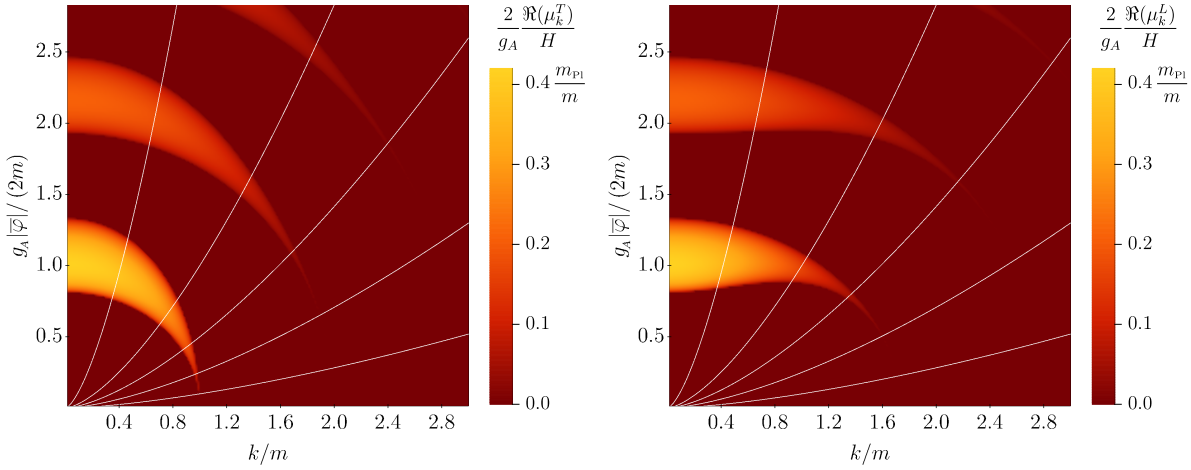

Figure 8.3: The above figures show Floquet exponents μ_k of the transverse (left) and longitudinal (right) modes of the gauge fields during preheating as a function of the physical wavenumber k and the scaled amplitude of the inflaton field oscillations. The gauge fields are coupled to an inflaton with a coupling strength g_A, and the inflaton potential is $m^2|\varphi|^2$. Note that there is no qualitative difference between the longitudinal and transverse modes. As the universe expands, a rough estimate of the amount of particle production in a given Fourier mode can be made by flowing across this plot towards the origin along the white lines (momentum k on the horizontal axis redshifts as a^{-1} and the inflaton field amplitude decays on the vertical axis as $\sim a^{-3/2}$). Note that in the light colored bands the ratio of the "local" Floquet exponent μ_k and the instantaneous expansion rate H is: $\Re[\mu_k]/H \sim g_A\, m_{\rm Pl}/m$, with $m_{\rm Pl}/m \sim 10^6$ from CMB observations. However, whether a given Fourier mode passes through these bands depends on g_A. To see this note that at the beginning of preheating $|\bar{\varphi}| \approx 0.1 m_{\rm Pl}$, hence $g_A|\bar{\varphi}|/m \lesssim 10^5 g_A$. Hence, for $g_A \lesssim 10^{-5}$, most of the low momentum modes start "below" the lowest resonance bands and never experience significant growth. For $g_A \gg 10^{-5}$ the unstable momentum modes pass through many Floquet bands as the universe expands and this can lead to significant particle production.

to *spike-free* exponential growth of the longitudinal electric field and charge and current densities. We also confirm this result below by carrying out the calculation in the Coulumb gauge where no singularities are present in the equations of motion. Our conclusion is different from that of [28], where the authors argued that the coefficient, $\partial_\tau \ln b_L$, of the $\partial_\tau A^L_{\mathbf{k}}$ would drive $A^L_{\mathbf{k}}(\tau) \to 0$ due to its large amplitude near $\Re[\bar{\varphi}(\tau)] = 0$. We also note that the authors in [93] argued that there should be strong resonance in the longitudinal modes (stronger than the transverse modes), though they did not pursue this issue in detail. We find that the resonance in both longitudinal and transverse modes is comparable.

Coulomb gauge analysis

One might be troubled by the presence of singularities in the intermediate steps of the gauge invariant analysis, especially if one wishes to carry out numerical calculations. In the Coulumb gauge the calculation of the physical observables $E^L_{\mathbf{k}}$, $j^0_{\mathbf{k}}$ and $j^L_{\mathbf{k}}$, is 'clean' throughout, i.e., no singularities arise whatsoever in the intermediate steps.

For more details on the well defined field content and the equations of motion in the Coulomb gauge see Section 8.2.4 and Appendix C.

The equations of motion for perturbations $\delta\varphi^0_{\mathbf{k}}$ and $A^{T\pm}_{\mathbf{k}}$ in the Coulumb gauge are identical to the ones for $\delta\rho_{\mathbf{k}}$ and $G^T_{\mathbf{k}}$, respectively, in the gauge invariant scenario (with $\bar{\rho} \to \bar{\varphi}^0$). For a chaotic inflation potential

$V(\bar{\varphi}^0) = (1/2)m^2(\bar{\varphi}^0)^2$, $\Re[\mu_k^0] = 0$ whereas $\Re[\mu_k^{T\pm}]$ is shown in Fig. 8.3 and are identical to the related Floquet exponents in the gauge invariant case.

In the Coulumb gauge we need to analyse $\delta\varphi_{\mathbf{k}}^1$ instead of the longitudinal mode $A_{\mathbf{k}}^L$. For $f_{\mathbf{k}}^1 = \delta\varphi_{\mathbf{k}}^1$ in eq. (8.72), the coefficients are

$$b_1(k,\tau) = \left[1 + \left(\frac{g_A\bar{\varphi}^0}{2k}\right)^2\right]^{-1}, \qquad \omega_1^2(k,\tau) = -\frac{\partial_\tau^2\bar{\varphi}^0}{\bar{\varphi}^0} + \frac{2\left(\frac{g_A\partial_\tau\bar{\varphi}^0}{2k}\right)^2}{1+\left(\frac{g_A\bar{\varphi}^0}{2k}\right)^2} + k^2 + \left(\frac{g_A\bar{\varphi}^0}{2}\right)^2. \tag{8.81}$$

Both coefficients are non-singular (assuming $\left(\bar{\varphi}^0\right)^{-1}\partial_{\bar{\varphi}^0}V(\bar{\varphi}^0)$ is well-defined at the origin $\bar{\varphi}^0 = 0$ as is usually the case). We can calculate the Floquet exponents based on this equation, however, we shall change variables and remove the damping term for reasons that will become clear below. We make the non-singular transformation

$$\delta\varphi_{\mathbf{k}}^1(\tau) = \check{l}(\bar{\varphi}^0(\tau))\delta\check{\varphi}_{\mathbf{k}}^1(\tau) \qquad \text{where} \qquad \check{l}(\bar{\varphi}^0(\tau)) \equiv \sqrt{1+\left(\frac{g_A\bar{\varphi}^0(\tau)}{2k}\right)^2}, \tag{8.82}$$

which yields $\check{b}_1 = \check{b}_L$ and $\check{\omega}_1 = \check{\omega}_L$ with $\bar{\rho} \to \bar{\varphi}^0$ (cf. eq. (8.78)). This identification immediately yields $\delta\check{\varphi}_{\mathbf{k}}^1 = \check{G}_{\mathbf{k}}^L$ where $\check{G}_{\mathbf{k}}^L$ was provided explicitly in eq. (8.79). Finally undoing our transformation of variables in eq. (8.82), we have the solution

$$\delta\varphi_{\mathbf{k}}^1(\tau) = \mathcal{P}_{\mathbf{k}+}^1(\tau)\exp\left(\mu_k^L\tau\right) + \mathcal{P}_{\mathbf{k}-}^1(\tau)\exp\left(-\mu_k^L\tau\right), \tag{8.83}$$

with $\mathcal{P}_{\mathbf{k}\pm}^1(\tau) = \check{l}(\bar{\varphi}_0(\tau))\check{\mathcal{P}}_{\mathbf{k}\pm}^L(\tau)$. The Floquet exponent $\mu_{\mathbf{k}}^L$ is identical to the one in eq. (8.79). A numerical computation of this exponent assuming a chaotic inflationary potential is shown in Fig. 8.3. Also note that now the periodic functions, $\mathcal{P}_{\mathbf{k}\pm}^1(\tau)$, have no troublesome spikes since $\check{l}$ is non-singular everywhere. This is an improvement over the gauge invariant analysis. In that case, $G_{\mathbf{k}}^L = \check{h}\check{G}_{\mathbf{k}}^L$, had singular spikes because $\check{h}$ was singular.

Hence, the Coulomb gauge allows us to calculate $\delta\varphi_{\mathbf{k}}^1(\tau)$, in a safe, singularity-free way. It is well suited for numerical computations. There is no problem with calculating physical variables such as $E_{\mathbf{k}}^L$, $B_{\mathbf{k}}^{T\pm}$ and $E_{\mathbf{k}}^{T\pm}$. For example the longitudinal electric field (cf. Appendix C)

$$E_{\mathbf{k}}^L = \frac{g_A k}{2}\frac{\left[\delta\varphi_{\mathbf{k}}^1\partial_\tau\bar{\varphi}^0 - \bar{\varphi}^0\partial_\tau\delta\varphi_{\mathbf{k}}^1\right]}{k^2+\left(\frac{g_A\bar{\varphi}^0}{2}\right)^2}, \tag{8.84}$$

has no singularities in it.

Before moving on to back-reaction, let us revisit the features seen in Fig. 8.2 in light of what we now understand from our Floquet analysis. The resonance structure of the transverse mode, eq. (8.75), is identical to that of χ in the popular $\tilde{g}^2\varphi^2\chi^2$ toy model [92]. Making use of well-known results about this model (see for example Fig. 2.3 and [292]), the parametric excitation of transverse modes is expected to be most efficient in the broad resonance regime $g_A|\bar{\varphi}|/m \sim g_A m_{\rm Pl}/m \gg 1$ for modes in the range $k \lesssim m\sqrt{g_A|\bar{\varphi}|/m} \sim m\sqrt{g_A m_{\rm Pl}/m}$. This should be true for the longitudinal mode as well based on the Floquet plots shown in Fig. 8.3. The lower three plots in Fig. 8.2 show how for $g_A m_{\rm Pl}/m \gg 1$, the transverse and longitudinal modes in the range $k/\mathcal{H} \lesssim \sqrt{m/H}\sqrt{k_C/\mathcal{H}} \sim \sqrt{k_C/\mathcal{H}}$ are significantly enhanced, in agreement with the analysis of this section (once expansion is appropriately included).

8.4.2 Back-reaction and end of preheating

So far we have extensively relied on a linear analysis of perturbations. As we have seen, during preheating, the covariant derivative coupling between the gauge fields and the inflaton causes resonant Fourier modes of electric and magnetic fields to grow exponentially fast. This growth cannot proceed forever. The resonance is eventually shut-off by the gauge field's back-reaction on the oscillating inflaton condensate, which ultimately leads to the condensate's fragmentation and our linear analysis stops holding any more.

To estimate the time of back-reaction, we shall investigate the effective equation of motion of the inflaton condensate in the Hartree approximation. We shall work in the non-singular Coulomb gauge, and include the background expansion as well (but ignore metric perturbations). Assuming that the slow-roll inflation happens along the real $\bar{\varphi}^0$ axis, the effective condensate equation in the Hartree approximation becomes

$$\begin{aligned}\partial_\tau^2\bar{\varphi}^0 + 2\mathcal{H}\partial_\tau\bar{\varphi}^0 + a^2\left[m^2 - \left(\frac{g_A}{2}\right)^2\langle 0|\,\hat{A}_\mu\hat{A}^\mu\,|0\rangle\right]\bar{\varphi}^0 = \\ a^2\frac{g_A}{2}\Re\Big[2\langle 0|\,\partial_\mu\delta\hat{\varphi}^1\hat{A}^\mu\,|0\rangle + \langle 0|\,\delta\hat{\varphi}^1\partial^\mu\hat{A}_\mu\,|0\rangle + 2\mathcal{H}\langle 0|\,\delta\hat{\varphi}^1\hat{A}^0\,|0\rangle\Big]\,.\end{aligned} \tag{8.85}$$

During preheating the occupation numbers become much greater than one, and the fields are expected to approach the classical limit. In this limit, the commutators of non-commuting variables are unimportant and the ambiguity regarding operator ordering is not significant. Moreover, note that the expectation values of non-commuting operators above can be complex. However, taking the real part is a reasonable approximation since in the classical limit the imaginary part becomes negligible compared to the real one (we have verified this numerically as well).

Our next step is to derive expressions for the expectation values in eq. (8.85) in terms of mode functions for the different fields. In the Coulomb gauge, and in Fourier space, the temporal component of the gauge field can be written in terms of $\delta\varphi^1_{\mathbf{k}}$ (see Appendix C):

$$\hat{A}_{0\mathbf{k}} = \frac{g_A}{2}\frac{\left[\delta\hat{\varphi}^1_{\mathbf{k}}\partial_\tau\bar{\varphi}^0 - \bar{\varphi}^0\partial_\tau\delta\hat{\varphi}^1_{\mathbf{k}}\right]}{\left(\frac{k}{a}\right)^2 + \left(\frac{g_A\bar{\varphi}^0}{2}\right)^2}\,, \tag{8.86}$$

and its first derivative, after taking into account the equations of motion, conveniently reduces to

$$\partial_\tau\hat{A}_{0\mathbf{k}} = a^2\frac{g_A}{2}\bar{\varphi}^0\delta\hat{\varphi}^1_{\mathbf{k}}\,. \tag{8.87}$$

These then translate to the mode functions, $u^1_k(\tau)$ and $u^{A_0}_k(\tau)$, of the quantised fluctuations

$$\delta\hat{\varphi}^1(\boldsymbol{x},\tau) = \int \mathbf{d}^3\mathbf{k}e^{i\boldsymbol{k}.\boldsymbol{x}}\delta\hat{\varphi}^1_{\mathbf{k}}(\tau) = \int \mathbf{d}^3\mathbf{k}e^{i\boldsymbol{k}.\boldsymbol{x}}\left[\hat{a}^L_{\mathbf{k}}u^1_k(\tau) + \hat{a}^{L\dagger}_{-\mathbf{k}}u^{1*}_k(\tau)\right]\,, \tag{8.88}$$

$$\hat{A}_0(\boldsymbol{x},\tau) = \int \mathbf{d}^3\mathbf{k}e^{i\boldsymbol{k}.\boldsymbol{x}}\hat{A}_{0\mathbf{k}}(\tau) = \int \mathbf{d}^3\mathbf{k}e^{i\boldsymbol{k}.\boldsymbol{x}}\left[\hat{a}^L_{\mathbf{k}}u^{A_0}_k(\tau) + \hat{a}^{L\dagger}_{-\mathbf{k}}u^{A_0*}_k(\tau)\right]\,. \tag{8.89}$$

This immediately yields the following expectation values:

$$\begin{aligned}
\langle 0|\,\hat{A}_0\hat{A}^0\,|0\rangle &= \int \frac{dkk^2}{2\pi^2}\left(\frac{g_A}{2a}\right)^2\left|\frac{\partial_\tau\bar{\varphi}^0 u_k^1-\bar{\varphi}^0\partial_\tau u_k^1}{\left(\frac{k}{a}\right)^2+\left(\frac{g_A\bar{\varphi}^0}{2}\right)^2}\right|^2\,,\\
\langle 0|\,\partial_\mu\delta\hat{\varphi}^1\hat{A}^\mu\,|0\rangle &= \langle 0|\,\partial_\tau\delta\hat{\varphi}^1\hat{A}^0\,|0\rangle = \int \frac{dkk^2}{2\pi^2}\frac{g_A}{2a^2}\frac{\partial_\tau u_k^1\left[\partial_\tau\bar{\varphi}^0 u_k^{1*}-\bar{\varphi}^0\partial_\tau u_k^{1*}\right]}{\left(\frac{k}{a}\right)^2+\left(\frac{g_A\bar{\varphi}^0}{2}\right)^2}\,,\\
\langle 0|\,\delta\hat{\varphi}^1\partial^\mu\hat{A}_\mu\,|0\rangle &= \langle 0|\,\delta\hat{\varphi}^1\partial^\tau\hat{A}_0\,|0\rangle = \int \frac{dkk^2}{2\pi^2}\frac{g_A}{2}\bar{\varphi}^0\left|u_k^1(\tau)\right|^2\,,\\
\langle 0|\,\delta\hat{\varphi}^1\hat{A}^0\,|0\rangle &= \int \frac{dkk^2}{2\pi^2}\frac{g_A}{2a^2}u_k^1\frac{\left[\partial_\tau\bar{\varphi}^0 u_k^{1*}-\bar{\varphi}^0\partial_\tau u_k^{1*}\right]}{\left(\frac{k}{a}\right)^2+\left(\frac{g_A\bar{\varphi}^0}{2}\right)^2}\,.
\end{aligned} \tag{8.90}$$

The only term which involves transverse modes is

$$\langle 0|\,\hat{A}_j\hat{A}^j\,|0\rangle = -\int \frac{dkk^2}{2\pi^2}a^{-2}\left[|u_k^{T+}|^2+|u_k^{T-}|^2\right]\,, \tag{8.91}$$

defined in the Coulomb gauge as

$$\hat{A}_j(\boldsymbol{x},\tau) = \int \mathbf{d}^3\mathbf{k}\sum_{\lambda=\pm} e^{i\boldsymbol{k}.\boldsymbol{x}}(\boldsymbol{\epsilon}_{\mathbf{k}}^{T\lambda})_j\hat{A}_{\mathbf{k}}^{T\lambda}(\tau) = \int \mathbf{d}^3\mathbf{k}\sum_{\lambda=\pm} e^{i\boldsymbol{k}.\boldsymbol{x}}(\boldsymbol{\epsilon}_{\mathbf{k}}^{T\lambda})_j\left[\hat{a}_{\mathbf{k}}^{T\lambda}u_k^{T\lambda}+\hat{a}_{-\mathbf{k}}^{T\lambda\dagger}u_k^{T\lambda *}\right]. \tag{8.92}$$

With these expressions, we can now calculate back-reaction effects iteratively. We first evolve the mode functions from vacuum initial conditions in eq. (8.62), using the background solution $\bar{\varphi}^0$ of eq. (8.85) with the correction terms (quadratic in the perturbations) ignored. These then allow us to get the necessary expectation values explicitly. Next, we re-evaluate the background solution, now including the correction terms (quadratic in the perturbations) in eq. (8.85). The moment when the new background solution deviates from the uncorrected one (see the left panel in Fig. 8.4) back-reaction has become important. For large couplings, $g_A > 10^{-4}$ in the Chaotic inflation model ($V = m^2\rho^2/2$, $m = 10^{-6}m_{\rm Pl}$), we get the following expression for the number of e-folds of expansion after the end of inlation when gauge fields back-react on the condensate $\Delta N_{\rm br} \approx 1.72 g_A^{-0.1}$. We caution that this scaling is to be taken as a very rough guide in the range of $3\times10^{-4} < g_A < 2.5\times10^{-3}$ (see the right panel in Fig. 8.4), the true dependence is likely non monotonic. Below the lowest value of g_A we have considered, the Hubble expansion quickly redshifts all modes below the lowest resonance band and we see negligible gauge field production.

8.5 Initial conditions for lattice simulations

In this section we give a concise description of initial conditions for numerical lattice studies of reheating. Our linearlized calculations including expansion, metric perturbations and the quantum nature of the fields were sufficient during inflation and preheating. However, *after* preheating the dynamics of matter fields on subhorizon scales can become highly non-linear. Since (i) the matter field occupation numbers grow rapidly during preheating, (ii) predominantly on subhorizon scales, while (iii) the metric perturbations remain

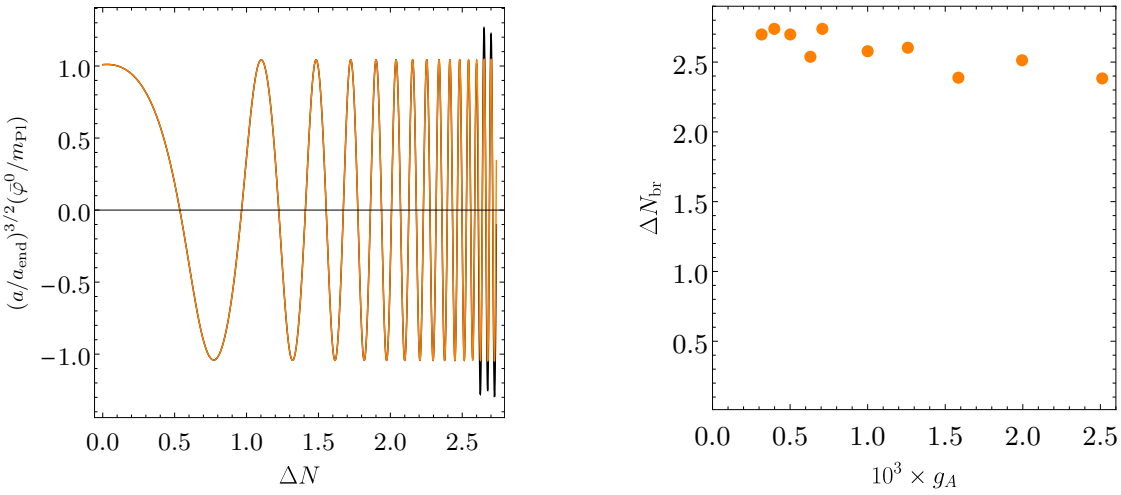

Figure 8.4: Left: The evolution of the homogeneous inflaton field as a function of number of e-folds after the end of inflation with no back-reaction (orange) and with back-reaction taken into account (black) for $g_A \approx 1.26 \times 10^{-3}$. Right: The number of e-folds after the end of inflation for the back-reaction to become important as a function of g_A.

small, one can evolve the classical equations of motion of the matter fields numerically after preheating using subhorizon 3+1d lattice simulations including gravity only at the background level. This standard approximation captures all of the relevant physical phenomena during the non-linear stage of reheating.

There are two distinct parts to setting up initial conditions on the lattice. First, for making the transition from quantized fluctuations to classical ones in the continuum limit, a prescription is needed. The classical field fluctuations must also satisfy the necessary constraints. The second is discretizing these initialized continuous fields on the lattice. We first focus on getting from quantized fluctuations to classical ones, with an accounting for the constraints. We will move from gauge invariant variables to variables in the temporal gauge (a popular choice of lattice simulations), but the prescription is applicable in any gauge.

Working in the local $U(1)$ gauge invariant variables, the matter fields with the quantized fluctuations at the end of preheating, written in terms of the mode functions in Fourier space (in the continuum limit) are as follows. In the expressions below, the time τ is the time of specification of the initial conditions on the lattice (this could be the end of inflation or some time before back-reaction).

$$\delta\hat{\rho}(\boldsymbol{x},\tau) = \int \mathbf{d}^3\mathbf{k} e^{i\boldsymbol{k}\cdot\boldsymbol{x}} \delta\hat{\rho}_{\mathbf{k}}(\tau) = \int \mathbf{d}^3\mathbf{k} e^{i\boldsymbol{k}\cdot\boldsymbol{x}} \left[\hat{a}^{\rho}_{\mathbf{k}} u^{\rho}_k(\tau) + \hat{a}^{\rho\dagger}_{-\mathbf{k}} u^{\rho *}_{\rho k}(\tau)\right],$$

$$\hat{G}^L_j(\boldsymbol{x},\tau) = \int \mathbf{d}^3\mathbf{k} e^{i\boldsymbol{k}\cdot\boldsymbol{x}} \left(\boldsymbol{\epsilon}^L_{\mathbf{k}}\right)_j \hat{G}^L_{\mathbf{k}}(\tau) = \int \mathbf{d}^3\mathbf{k} e^{i\boldsymbol{k}\cdot\boldsymbol{x}} \left(\boldsymbol{\epsilon}^L_{\mathbf{k}}\right)_j \left[\hat{a}^L_{\mathbf{k}} u^L_k(\tau) + \hat{a}^{L\dagger}_{-\mathbf{k}} u^{L*}_k(\tau)\right], \tag{8.93}$$

$$\hat{G}^T_j(\boldsymbol{x},\tau) = \int \mathbf{d}^3\mathbf{k} \sum_{\lambda=\pm} e^{i\boldsymbol{k}\cdot\boldsymbol{x}} \left(\boldsymbol{\epsilon}^{T\lambda}_{\mathbf{k}}\right)_j \hat{G}^{T\lambda}_{\mathbf{k}}(\tau) \tag{8.94}$$

$$= \int \mathbf{d}^3\mathbf{k} \sum_{\lambda=\pm} e^{i\boldsymbol{k}\cdot\boldsymbol{x}} \left(\boldsymbol{\epsilon}^{T\lambda}_{\mathbf{k}}\right)_j \left[\hat{a}^{T\lambda}_{\mathbf{k}} u^{T\lambda}_k(\tau) + \hat{a}^{T\lambda\dagger}_{-\mathbf{k}} u^{T\lambda *}_k(\tau)\right], \tag{8.95}$$

$$\hat{G}_0(\boldsymbol{x},\tau) = -\int \mathbf{d}^3\mathbf{k} e^{i\boldsymbol{k}\cdot\boldsymbol{x}} \frac{\partial_\tau \hat{G}^L_{\mathbf{k}}(\tau)}{k^2 + \left(\frac{\bar{\rho}(\tau) g_A\, a(\tau)}{2}\right)^2} = -\int \mathbf{d}^3\mathbf{k} e^{i\boldsymbol{k}\cdot\boldsymbol{x}} \frac{\left[\hat{a}^L_{\mathbf{k}} \partial_\tau u^L_k(\tau) + \hat{a}^{L\dagger}_{-\mathbf{k}} \partial_\tau u^{L*}_k(\tau)\right]}{k^2 + \left(\frac{\bar{\rho}(\tau) g_A\, a(\tau)}{2}\right)^2} \,. \tag{8.96}$$

We also need time derivatives of the above expressions. In that case, the mode functions u^I_k get differentiated; the creation and annihilation operators $(\hat{a}^I_{\mathbf{k}}, \hat{a}^{I\dagger}_{\mathbf{k}})$ are time independent. By switching from the quantum two point function in real space $\langle 0|\hat{f}^I(\mathbf{x})\hat{f}^J(\mathbf{x}+\mathbf{r})|0\rangle$ to the classical 2-point correlation functions in real space $\langle f^I(\mathbf{x}) f^J(\mathbf{x}+\mathbf{r})\rangle = V^{-1}\int d^3\mathbf{x} f^I(\mathbf{x}) f^J(\mathbf{x}+\mathbf{r})$ with $V \to \infty$, we switch from a quantum to a classical description.[10] We now treat the creation and annihilation operators as complex numbers

$$\hat{a}^I_{\mathbf{k}} \to a^I_{\mathbf{k}} \qquad \text{and} \qquad \hat{a}^{I\dagger}_{\mathbf{k}} \to a^{I*}_{\mathbf{k}} \,, \tag{8.97}$$

with phases distributed uniformly on $[0, 2\pi)$, and with a Rayleigh distributed amplitudes set in the following manner [293]:

$$\left|a^I_{\mathbf{k}}\right| = \sqrt{-\ln\left(X^I_{\mathbf{k}}\right)/2} \qquad \text{and} \qquad \arg\left(a^I_{\mathbf{k}}\right) = 2\pi Y^I_{\mathbf{k}} \,. \tag{8.98}$$

Here $X^I_{\mathbf{k}}$ is a uniform deviate on $(0,1)$ and $Y^I_{\mathbf{k}}$ is a uniform deviate on $[0,1)$. The amplitude is governed by the requirement of consistency with the quantum 2-point function. The index I denotes the field under consideration, i.e., $I = \{\rho, L, T^+, T^-\}$. Note that the complex numbers $a^L_{\mathbf{k}}$ in eq. (8.93) and eq. (8.96) are the same.

So far the analysis have been carried out in a gauge invariant framework. It is not difficult to find the initial conditions for lattice simulations in a particular gauge. For example, in the $A_0 = 0$ (temporal) gauge – the common gauge choice for numerical simulations, the conversion between gauge invariant variables and gauge dependent fields is given in eqns. (8.45) and (8.48). For convenience one can choose $\tau_{\text{in}} = \tau$ in eq. (8.48), so that $\delta\varphi^1_{\mathbf{k}}(\tau) = 0$ and $A^L_{\mathbf{k}}(\tau) = G^L_{\mathbf{k}}$, but $\partial_\tau \delta\varphi^1_{\mathbf{k}}(\tau) = \bar{\rho} g_A G_{0\mathbf{k}}/2$ and

$$\partial_\tau A^L_{\mathbf{k}}(\tau) = \partial_\tau G^L_{\mathbf{k}} + k G_{0\mathbf{k}} \,. \tag{8.99}$$

We note that despite the random nature of the complex numbers in eq. (8.98), the Gaussian constraint on the lattice is automatically satisfied to linear order in the perturbations, since the expression for $G_0(\mathbf{x},\tau)$ in eq. (8.96), in terms of the complex $a^L_{\mathbf{k}}$, takes care of the first order terms in eq. (8.18).

If one wishes the Gauss constraint to be met to machine precision on the lattice, a simple correction has to be made. After initialising $\delta\rho(\mathbf{x},\tau)$, $\partial_\tau\delta\rho(\mathbf{x},\tau)$, $G_i(\mathbf{x},\tau)$, $\partial_\tau G_i(\mathbf{x},\tau)$, $G_0(\mathbf{x},\tau)$ we define the corrected time derivative

$$\partial_\tau G^{L,\text{corr}}_j(\mathbf{x},\tau) = \int \mathbf{d}^3\mathbf{k} e^{i\boldsymbol{k}\cdot\boldsymbol{x}} \left(\boldsymbol{\epsilon}^L_{\mathbf{k}}\right)_j \partial_\tau G^{L,\text{corr}}_{\mathbf{k}}(\tau) \,, \tag{8.100}$$

where

$$\partial_\tau G^{L,\text{corr}}_{\mathbf{k}} = -k G_{0\mathbf{k}} - \frac{\tilde{j}_{0\mathbf{k}}}{k} \,, \qquad \tilde{j}_{0\mathbf{k}} = \int \frac{\mathbf{d}^3\mathbf{x}}{(2\pi)^3} e^{-i\boldsymbol{k}\cdot\boldsymbol{x}} (\bar{\rho} + \delta\rho)\bar{\rho} \left(\frac{g_A a}{2}\right)^2 G_0 \,. \tag{8.101}$$

[10] That is, we replace the creation and annihilation operators with stochastic complex numbers (with Gaussian probability distribution) whose covariance matrix is determined by the mode functions. This holds for fields whose mode functions have increased (are occupied) significantly [293]. This is not necessarily true for the gauge fields at the end of inflation. However, if gauge field modes are resonantly excited during preheating, the stochastic approach becomes consistent.

Note the $\delta\rho$ appearing on the right-hand side of the last equation. We then use $\partial_\tau G_j^{L,\text{corr}}(\mathbf{x},\tau)$ in place of $\partial_\tau G_j^L(\mathbf{x},\tau)$ to generate the necessary gauge dependent variable in eq. (8.99).

We remind the reader that all expressions so far in this section are for fields on a continuous space-time manifold. The reason is transparency of the transition from quantum to classical fields accounting for the constraints. For completeness we outline the discrete lattice counterparts to the continuous variables. Let Δ be the separation between neighbouring lattice points and L the length of the lattice. Then the following substitutions should be used to define the fields on the lattice[11]

$$\begin{aligned}\mathbf{x} &\to \mathbf{x}_n = \boldsymbol{n}\Delta\,,\\ \mathbf{k} &\to \mathbf{k}_n = \frac{2\pi}{L}\boldsymbol{n}\,,\end{aligned} \tag{8.102}$$

where $\boldsymbol{n} = [n_x, n_y, n_z]$ with $-L/(2\Delta) \leq n_{x,y,z} \leq L/(2\Delta)$. For example

$$\delta\rho(\mathbf{x}_n,\tau) = \left(\frac{2\pi}{L}\right)^{3/2}\sum_{\mathbf{k}_n} e^{i\mathbf{k}_n\cdot\mathbf{x}_n}\delta\rho_{\mathbf{k}_n}(\tau) = \left(\frac{2\pi}{L}\right)^{3/2}\sum_{\mathbf{k}_n} e^{i\mathbf{k}_n\cdot\mathbf{x}_n}\left[a^{\rho}_{\mathbf{k}_n}u^{\rho}_{k_n}(\tau) + a^{\rho*}_{-\mathbf{k}_n}u^{\rho*}_{k_n}(\tau)\right]. \tag{8.103}$$

There is a minor subtlety in the definition of the polarisation vectors. Consider a finite difference lattice code in which the discrete divergence of a vector is given by[12]

$$\left(\boldsymbol{\nabla}\cdot\mathbf{G}\right)(\mathbf{x},\tau) \to \frac{1}{\Delta}\sum_{i=x,y,z}\left[G_i(\mathbf{x}+\hat{i}\frac{\Delta}{2},\tau) - G_i(\mathbf{x}-\hat{i}\frac{\Delta}{2},\tau)\right]. \tag{8.104}$$

Then the continuous directional definitions of the longitudinal and transverse polarisation vectors from eq. (8.34) and eq. (8.38) should be modified to

$$\begin{aligned} i\mathbf{k}\cdot\boldsymbol{\epsilon}^{T\pm}_{\mathbf{k}} = 0 \to 2i\frac{\sin\left(\mathbf{k}\frac{\Delta}{2}\right)}{\Delta}\cdot\boldsymbol{\epsilon}^{T\pm}_{\mathbf{k}} = 0\,,\\ i\mathbf{k}\times\boldsymbol{\epsilon}^{L}_{\mathbf{k}} = 0 \to 2i\frac{\sin\left(\mathbf{k}\frac{\Delta}{2}\right)}{\Delta}\times\boldsymbol{\epsilon}^{L}_{\mathbf{k}} = 0\,.\end{aligned} \tag{8.105}$$

These modifications hold for the spatial discretization stencil in eq. (8.104). For other stencils one can derive similar expressions for the orientation of polarisation vectors (eq. (9.52)). We stress that if the spatial discretization is not accounted for by polarization vectors, there will be a violation of the Gauss constraint.

8.6 The non-Abelian models

We now show that the developed techniques in the previous sections can be used for more complicated non-Abelian models. The main purpose here is to reduce calculations of these complicated models (as far as possible) to the ones we have carried out in the Abelian case. We shall first consider the case of $SU(2)$ non-Abelian gauge fields and then extend to $SU(2)\times U(1)$, describing the Electroweak sector of the Standard Model.

[11]The normalization factor of $(2\pi/L)^{3/2}$ is needed to make sure that the two-point correlation function on the lattice is equal to the continuous one [74].

[12]E.g., in the standard Wilsonian approach to lattice gauge theories, gauge fields live on *space-time* links, $G_\mu(x_\mu + \hat{\mu}\frac{\Delta}{2})$ and scalar fields live on the nodes of the space-time lattice, $\rho(x^\mu)$. Here $\hat{\mu}$ is the space-time unit vector and Δ is the separation between two neighbouring points on the space-time lattice.

8.6.1 $SU(2)$ gauge fields

We consider the following action for a charged scalar doublet

$$S_{\rm m} = \int {\rm d}^4x\sqrt{-g}\mathcal{L}_{\rm m} = \int {\rm d}^4x\sqrt{-g}\Big[\left(\mathbf{D}_\mu\boldsymbol{\varphi}\right)^\dagger \left(\mathbf{D}^\mu\boldsymbol{\varphi}\right) - \mathcal{V}(|\boldsymbol{\varphi}|) - \frac{1}{2}{\rm tr}\,\mathbf{F}^2(\mathbf{A})\Big] , \tag{8.106}$$

where

$$\begin{aligned} \mathbf{D}_\mu\boldsymbol{\varphi} &= \nabla_\mu\boldsymbol{\varphi} + ig_{_A}\mathbf{A}_\mu\boldsymbol{\varphi} , \\ \mathbf{F}_{\mu\nu} &= \nabla_\mu\mathbf{A}_\nu - \nabla_\nu\mathbf{A}_\mu + ig_{_A}\left(\mathbf{A}_\mu\mathbf{A}_\nu - \mathbf{A}_\nu\mathbf{A}_\mu\right) . \end{aligned} \tag{8.107}$$

The action is invariant under the local $SU(2)$ transformation

$$\begin{aligned} \boldsymbol{\varphi} &\to \mathbf{U}\boldsymbol{\varphi} = e^{-ig_{_A}\boldsymbol{\beta}(x^\nu)}\boldsymbol{\varphi} , \\ \mathbf{A}_\mu &\to \mathbf{U}\mathbf{A}_\mu\mathbf{U}^{-1} + \frac{i}{g_{_A}}\left(\nabla_\mu\mathbf{U}\right)\mathbf{U}^{-1} , \end{aligned} \tag{8.108}$$

where the non-Abelian gauge fields are $\mathbf{A}_\mu = A^a_\mu\boldsymbol{\sigma}^a/2$, and $\boldsymbol{\beta}(x^\nu) = \beta^a(x^\nu)\boldsymbol{\sigma}^a/2$, with $\left\{\boldsymbol{\sigma}^1, \boldsymbol{\sigma}^2, \boldsymbol{\sigma}^3\right\}$ being the three Pauli matrices. The repeated indices are summed over (both for field and spacetime indices).

It is possible to write the above action in terms of local $SU(2)$ invariant fields (analogous to the Abelian case). We will show below that these gauge invariant fields decouple from each other at the linear level and the problem reduces to three identical copies of the Abelian model. The quantisation scheme, preheating analysis as well as setting up of lattice initial conditions discussed in the previous sections then carries over without any difficulty.

We begin by writing the scalar doublet as [292]

$$\boldsymbol{\varphi} = \frac{\rho}{\sqrt{2}}\mathbf{M}\begin{pmatrix} 0 \\ 1 \end{pmatrix} , \tag{8.109}$$

where ρ will be our real scalar field which forms a condensate during inflation (e.g., the inflaton), and $\mathbf{M}$ is a *unitary* matrix of *unit* determinant

$$\mathbf{M} = \exp\left(i\frac{g_{_A}}{2}\Omega^a\boldsymbol{\sigma}^a\right) . \tag{8.110}$$

This $\{\rho, \Omega^a\}$ decomposition is similar to the polar one give in eq. (8.6) for the Abelian model. In a now familiar way, cf. eq. (8.7), we proceed to define $SU(2)$ invariant non-Abelian fields

$$\mathbf{G}_\mu \equiv \mathbf{M}^{-1}\mathbf{A}_\mu\mathbf{M} - \frac{i}{g_{_A}}\mathbf{M}^{-1}\nabla_\mu\mathbf{M} . \tag{8.111}$$

More explicitly, $\mathbf{G}_\mu = G^a_\mu\boldsymbol{\sigma}^a/2$, which in component form is

$$\mathbf{G}_\mu = \frac{1}{2}\begin{pmatrix} G^3_\mu & G^1_\mu - iG^2_\mu \\ G^1_\mu + iG^2_\mu & -G^3_\mu \end{pmatrix} . \tag{8.112}$$

The action in eq. (8.106) then simplifies to

$$S_{\rm m} = \int {\rm d}^4x\sqrt{-g}\left[\frac{\nabla_\mu\rho\nabla^\mu\rho}{2} - V(\rho) + \frac{g_{_A}^2\rho^2}{8}G^a_\mu G^{a\mu} - \frac{1}{4}F^a_{\mu\nu}(G)F^{a\mu\nu}(G)\right] , \tag{8.113}$$

where the interactions between the gauge bosons are hidden in the definition of the field tensor

$$F^a_{\mu\nu}(G) \equiv \nabla_\mu G^a_\nu - \nabla_\nu G^a_\mu - g_A \epsilon^{abc} G^b_\mu G^c_\nu \,. \tag{8.114}$$

We will again work at the linear level in G^a_μ, since the arguments for the vanishing backgrounds of the gauge fields used in the Abelian model apply to this case as well. The inflaton fluctuations ($\delta\rho$) are decoupled from the gauge fields, G^a_μ. Furthermore $\delta\rho$ is the only field coupled to the metric perturbations. At linear order we can ignore the interactions between the gauge bosons, i.e., the last term in (8.114). Thereby, the three gauge fields, G^a_μ, are decoupled from each other and each of them is treated as the gauge field from the Abelian model. The quadratic action for the matter perturbations splits into (cf. eq. (8.50))

$$S^{(2)}_{\rm m} = S^\rho + \sum_{a=1}^{3} \left(S^{aL} + S^{aT+} + S^{aT-} \right) = \sum_I S^I \,. \tag{8.115}$$

Each S^I is of the general form given in eq. (8.51). The coefficients $b_\rho(k,\tau)$, $\omega_\rho(k,\tau)$ are those in eq. (8.57), and $b_{aL}(k,\tau)$, $\omega_{aL}(k,\tau)$ and $b_{aT\pm}(k,\tau)$, $\omega_{aT\pm}(k,\tau)$ are equal to the longitudinal and transverse ones in eq. (8.58), respectively. Therefore, the inflationary power-spectra will be those of three identical copies of longitudinal modes and six identical copies of transverse modes (i.e., one longitudinal and two transverse modes per gauge field). The quantization procedure is identical to the Abelian case with no additional subtleties.

The inflaton oscillations during preheating again present a problem for the gauge invariant fields. The gauge invariant fields, G^a_μ, are ill-defined when Ω^a are ill-defined which happens every time $\boldsymbol{\varphi} = \mathbf{0}$. In analogy with the Abelian case, we will work in the Coulomb gauge. In terms of its "cartesian" components,

$$\boldsymbol{\varphi}(x^\mu) = \frac{1}{\sqrt{2}} \begin{pmatrix} \delta\varphi^2 + i\delta\varphi^1 \\ \bar\varphi^0 + \delta\varphi^0 - i\delta\varphi^3 \end{pmatrix} , \tag{8.116}$$

where we have used the global $SU(2)$ invariance of the action to rotate the internal $\boldsymbol{\varphi}$ axes to align with the direction of motion of the homogeneous field. We have taken this direction to be along $\bar\varphi^0$, with all the other homogeneous components set to zero.[13] In the Coulomb gauge for each $a = 1, 2, 3$, the longitudinal modes $A^{aL}_{\mathbf{k}} = 0$ from the gauge condition $\partial_i A^{ai} = 0$. The relevant perturbative degrees of freedom in this gauge are $\{\delta\varphi^0_{\mathbf{k}}, \delta\varphi^a_{\mathbf{k}}\}$ and the transverse components of the gauge field $A^{aT\pm}_{\mathbf{k}}$. The equation of motion for

[13]Note that $\Omega^a \ll 1$, and to linear order in perturbations, the scalar doublet in eq. (8.109) can be written as

$$\boldsymbol{\varphi}(x^\mu) = \frac{\bar\rho + \delta\rho}{\sqrt{2}} \begin{pmatrix} \frac{g_A}{2}\Omega^2 + i\frac{g_A}{2}\Omega^1 \\ 1 - i\frac{g_A}{2}\Omega^3 \end{pmatrix} \approx \frac{1}{\sqrt{2}} \begin{pmatrix} \frac{g_A}{2}\bar\rho\Omega^2 + i\frac{g_A}{2}\bar\rho\Omega^1 \\ \bar\rho + \delta\rho - i\frac{g_A}{2}\bar\rho\Omega^3 \end{pmatrix} . \tag{8.117}$$

This explains the choice of signs and labeling of components in $\boldsymbol{\varphi}$. The terms on the right-hand side in eq. (8.111) reduce to

$$\begin{aligned} \mathbf{M}^{-1}\mathbf{A}_\mu\mathbf{M} &= \frac{1}{2} \begin{pmatrix} A^3_\mu & A^1_\mu - iA^2_\mu \\ A^1_\mu + iA^2_\mu & -A^3_\mu \end{pmatrix} , \\ -\frac{i}{g_A}\mathbf{M}^{-1}\nabla_\mu\mathbf{M} &= \frac{\nabla_\mu}{2} \begin{pmatrix} \Omega^3 & \Omega^1 - i\Omega^2 \\ \Omega^1 + i\Omega^2 & -\Omega^3 \end{pmatrix} . \end{aligned} \tag{8.118}$$

Recalling eq. (8.112), one arrives at the familiar expression for the gauge invariant fields at linear order in perturbations (cf. eq. (8.7)): $G^a_\mu = A^a_\mu + \nabla_\mu\Omega^a$. This relation, along with $\delta\varphi^a = g_A\bar\rho\Omega^a/2$ and $\bar\rho = \bar\varphi^0$, then allows us to easily derive the equations of motion for A^a_μ and $\delta\varphi^a$ from the equations for G^a_μ, since $G^a_\mu = A^a_\mu + \nabla_\mu(2\delta\varphi^a/g_A\bar\rho)$.

$\bar{\varphi}^0$ and its perturbation in Fourier space ($\delta\tilde{\varphi}^0_{\mathbf{k}}$) is identical to eq. (C.1) and the first equation in eq. (C.2), respectively. This field plays the role of the inflaton. The equations of motion for $\delta\varphi^a_{\mathbf{k}}$ are copies of the second equation in eq. (C.2).

8.6.2 The "Electroweak" sector: $SU(2) \times U(1)$

Let us consider a more realistic scenario in which the scalar has $SU(2) \times U(1)$ charges

$$S_{\rm m} = \int {\rm d}^4x\sqrt{-g}\mathcal{L}_{\rm m} = \int {\rm d}^4x\sqrt{-g}\Big[\left(\mathbf{D}_\mu\boldsymbol{\varphi}\right)^\dagger \left(\mathbf{D}^\mu\boldsymbol{\varphi}\right) - \mathcal{V}(|\boldsymbol{\varphi}|) - \frac{1}{4}\mathcal{F}^2(B) - \frac{1}{2}{\rm tr}\mathbf{F}^2(\mathbf{A})\Big] , \tag{8.119}$$

where

$$\mathbf{D}_\mu\boldsymbol{\varphi} = \nabla_\mu\boldsymbol{\varphi} + ig_{_A}\mathbf{A}_\mu\boldsymbol{\varphi} - \frac{i}{2}g_{_B}B_\mu\boldsymbol{\varphi} , \tag{8.120}$$

and $\mathcal{F}_{\mu\nu}(B)$ and $\mathbf{F}_{\mu\nu}(\mathbf{A})$ are the field tensors defined in eqns. (8.3) and (8.107), respectively. The coefficients in the covariant derivative are defined in this particular way, so that one can refer the scalar doublet to the Standard Model Higgs field, whose hypercharge is $-1/2$. The action is invariant under the local $U(1)$ and $SU(2)$ transformations

$$\boldsymbol{\varphi} \to \exp[ig_{_B}\alpha(x^\nu)/2]\mathbf{U}\boldsymbol{\varphi} , \qquad B_\mu \to B_\mu + \nabla_\mu\alpha(x^\nu) , \qquad \mathbf{A}_\mu \to \mathbf{U}\mathbf{A}_\mu\mathbf{U}^{-1} + \frac{i}{g_{_A}}\left(\nabla_\mu\mathbf{U}\right)\mathbf{U}^{-1} , \tag{8.121}$$

where $\mathbf{U}$ was defined in eq. (8.108).

We can write the $SU(2)$ sector (but not the $U(1)$ sector) in terms of gauge invariant variables, ρ and G^a_μ, by repeating the initial steps (eqns. (8.109)-(8.112)) from Section 8.6.1. We could have defined $SU(2)$ *and* $U(1)$ invariant fields. However, following the standard treatment of the Electroweak sector of the Standard Model of Particle Physics, we will fix the gauge for the $U(1)$ sector. With an eye towards the preheating analysis, we will choose Coulomb gauge for the $U(1)$ fields, where $\partial_i B^i = 0$ (in Fourier space, $B^L_{\mathbf{k}} = 0$). In addition, instead of proceeding to quantization and then to a preheating analysis, we will work with certain linear combinations of G and B fields to make contact with the Standard Model. To this end, we define the charged *W* bosons as (cf. eq. (8.112)) $W^\pm_\mu = (G^1_\mu \mp iG^2_\mu)/\sqrt{2}$. The *Z* boson and the massless photon, $\mathcal{A}$, emerge after rotating in the G^3B space

$$\begin{pmatrix}\mathcal{A}_\mu \\ Z_\mu\end{pmatrix} \equiv \begin{pmatrix}\cos\theta_{_W} & \sin\theta_{_W} \\ -\sin\theta_{_W} & \cos\theta_{_W}\end{pmatrix}\begin{pmatrix}B_\mu \\ G^3_\mu\end{pmatrix} , \tag{8.122}$$

through the Weinberg angle

$$\cos\theta_{_W} \equiv -\frac{g_{_A}}{\sqrt{g^2_{_A} + g^2_{_B}}} . \tag{8.123}$$

The action from eq. (8.119) becomes

$$\begin{aligned} S_{\rm m} = \int {\rm d}^4x\sqrt{-g}\Bigg[&\frac{\nabla_\mu\rho\nabla^\mu\rho}{2} - V(\rho) + \frac{\left(g^2_{_A} + g^2_{_B}\right)\rho^2}{8}Z_\mu Z^\mu - \frac{1}{4}F^2(\mathcal{A}) - \frac{1}{4}F^2(Z) \\ &+ \frac{g^2_{_A}\rho^2}{4}W^+_\mu W^{-\mu} - \frac{1}{2}F_{\mu\nu}(W^+)F^{\mu\nu}(W^-)\Bigg] , \end{aligned} \tag{8.124}$$

where the interactions between the gauge bosons are included into the definitions of the field tensors

$$\begin{aligned} F_{\mu\nu}(Z) &\equiv \nabla_\mu Z_\nu - \nabla_\nu Z_\mu - ig_{_A}\cos\theta_{_W}\left(W_\mu^- W_\nu^+ - W_\nu^- W_\mu^+\right), \\ F_{\mu\nu}(\mathcal{A}) &\equiv \nabla_\mu \mathcal{A}_\nu - \nabla_\nu \mathcal{A}_\mu - ig_{_A}\sin\theta_{_W}\left(W_\mu^- W_\nu^+ - W_\nu^- W_\mu^+\right), \\ F_{\mu\nu}(W^\pm) &\equiv \mathcal{D}_\mu^\pm W_\nu^\pm - \mathcal{D}_\nu^\pm W_\mu^\pm, \end{aligned} \tag{8.125}$$

where

$$\mathcal{D}_\mu^\pm W_\nu^\pm \equiv \nabla_\mu W_\nu^\pm \pm ig_{_A}\sin\theta_{_W}\mathcal{A}_\mu W_\nu^\pm \pm ig_{_A}\cos\theta_{_W} Z_\mu W_\nu^\pm . \tag{8.126}$$

Note that ρ, $\mathcal{A}_\mu$, Z_μ and $W_\mu^\pm$ are invariant under $SU(2)$ transformations, eq. (8.108). However, $\mathcal{A}_\mu$ and $W_\mu^\pm$ change under a $U(1)$ transformation, eq. (8.121), as follows:

$$\mathcal{A}_\mu \to \mathcal{A}_\mu + \frac{1}{\cos\theta_{_W}}\nabla_\mu\alpha(x^\nu), \quad W_\mu^\pm \to e^{\pm ig_{_B}\alpha(x^\nu)}W_\mu^\pm . \tag{8.127}$$

That is why, to remove this redundancy, we choose $B_{\mathbf{k}}^L = 0$, which implies $\mathcal{A}_{\mathbf{k}}^L = Z_{\mathbf{k}}^L\tan\theta_{_W}$, cf. eq. (8.122). This is also a good place to point out that $W_\mu^\pm$ are a conjugate pair of *complex* fields. The '$\pm$' should not be confused with the two transverse polarisation states.

We work at the linear level in $\delta\rho$, $W_\mu^\pm$, Z_μ, $\mathcal{A}_\mu$ (the arguments for the vanishing backgrounds of the gauge fields used in the previous cases apply here as well). Once again the inflaton fluctuations $\delta\rho$ are decoupled from the rest of the matter fields, and the only ones coupled to the metric perturbations. Neglecting the interactions between the gauge bosons, i.e., the second order terms in eq. (8.125) and expressing $W_\mu^\pm$ in terms of G_μ^1, G_μ^2, the second order in perturbations matter action splits into, cf. eqns. (8.50) and (8.115),[14]

$$\begin{aligned} S_{\rm m}^{(2)} &= S^\rho + S^{ZL} + S^{ZT+} + S^{ZT-} + S^{\mathcal{A}T+} + S^{\mathcal{A}T-} + \sum_{a=1}^{2}\left(S^{aL} + S^{aT+} + S^{aT-}\right) \\ &= \sum_I S^I . \end{aligned} \tag{8.128}$$

The S^I have the form shown in eq. (8.51). For $I = \rho$, $b_\rho(k,\tau)$ and $\omega_\rho(k,\tau)$ are given in eq. (8.57). For $I = aL, aT\pm$ (with $a = \{1,2\}$), the coefficient pairs $\{b_{aL}(k,\tau), \omega_{aL}(k,\tau)\}$ and $\{b_{aT\pm}(k,\tau), \omega_{aT\pm}(k,\tau)\}$ are the longitudinal and transverse coefficients in eq. (8.58), respectively. The other coefficients are

$$\begin{aligned} &b_{ZL}(k,\tau) = \left[1 + \left(\frac{2k\cos\theta_{_W}}{\bar\rho g_{_A} a}\right)^2\right]^{-1}, \qquad \omega_{ZL}^2(k,\tau) = k^2 + \left(\frac{\bar\rho g_{_A} a}{2\cos\theta_{_W}}\right)^2, \\ &b_{ZT\pm}(k,\tau) = 1, \qquad \omega_{ZT\pm}^2(k,\tau) = k^2 + \left(\frac{\bar\rho g_{_A} a}{2\cos\theta_{_W}}\right)^2, \\ &b_{\mathcal{A}T\pm}(k,\tau) = 1, \qquad \omega_{\mathcal{A}T\pm}^2(k,\tau) = k^2 . \end{aligned} \tag{8.129}$$

Notice that only the transverse modes of the photon, $\mathcal{A}$, contribute to the action. The longitudinal modes of $\mathcal{A}$ do not contribute since the photon is *massless* - a manifestation of the Ward identity. We can now quantise the transverse modes of $\mathcal{A}$ and the longitudinal and transverse modes of Z, G^1, G^2 as done in Section 8.3.1.

[14] While defined $W_\mu^\pm$ because of our desire to connect to the Standard Model, we write the action for the perturbations in terms of G_μ^1 and G_μ^2, because it brings part of the action in a form which looks like multiple copies of the Abelian case.

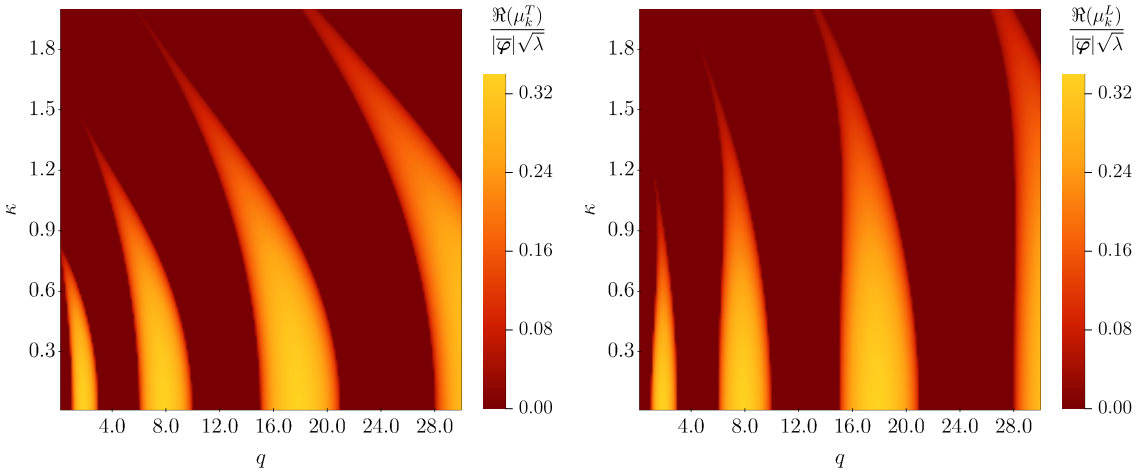

Figure 8.5: Floquet exponents of transverse and longitudinal modes of *W* and *Z* bosons during preheating with non-Abelian fields. The Floquet plot for the transverse modes on the left is the same as Figure 1 in [28]. Our analysis shows a similar qualitative behavior for the longitudinal modes as well (right). For this plot the scalar field potential is taken to be $V(\rho) = \lambda(\boldsymbol{\varphi}^\dagger\boldsymbol{\varphi})^2 = \lambda\rho^4/4$. We use the same notation as in [28]: $\kappa = k/\sqrt{2\lambda|\overline{\boldsymbol{\varphi}}|^2} = k/\sqrt{\lambda\bar{\rho}^2}$, $q_W = g_A^2/4\lambda$ and $q_Z = (g_A^2 + g_B^2)/4\lambda$. The amplitude of the oscillating scalar field and the momentum redshift as a^{-1}, rendering κ redshift-independent. That is why the flow lines from Fig. 8.3 do not appear here. As the universe expands, Fourier modes do not cross through multiple bands. This is a manifestation of the conformal nature of the quartic potential after the end of inflation.

We remind the reader that the procedure outlined above is well-defined during inflation, when $\rho^2/2 = \boldsymbol{\varphi}^\dagger\boldsymbol{\varphi} \neq 0$. Similarly to the Abelian and the $SU(2)$ cases, $\mathbf{G}_\mu$, are ill-defined when $\rho = 0$ and this can generally happen during preheating. Once again the right prescription is to work in well-defined variables in a non-singular gauge. In the Coulomb gauge, $B^L = 0$ and $A^{aL} = 0$, the longitudinal modes G^{1L}, G^{2L} and Z^L can be expressed in terms of the well-defined perturbations of $\boldsymbol{\varphi}$: $\delta\varphi^1$, $\delta\varphi^2$ and $\delta\varphi^3$ respectively. In this gauge, the transverse modes are even easier to handle: $G^{1T\pm}$ and $G^{2T\pm}$ reduce to $A^{1T\pm}$ and $A^{2T\pm}$, respectively; similarly $Z^{T\pm} \to -\sin\theta_W B^{T\pm} + \cos\theta_W A^{1T\pm}$ and $\mathcal{A}^{T\pm} \to \cos\theta_W B^{T\pm} + \sin\theta_W A^{1T\pm}$. Hence we can keep the expressions for the transverse modes since they have no singularities in them with $\rho \to \bar{\varphi}^0$. As usual, using the $SU(2)$ global invariance, we have rotated our internal axes along the direction of motion of the inflaton.

For purposes of comparison with the literature, we provide the Floquet charts for the longitudinal and transverse modes of the *W* and *Z* fields which are excited by the oscillations of the Higgs condensate for the case when $V(|\boldsymbol{\varphi}|) = \lambda\left(\boldsymbol{\varphi}^\dagger\boldsymbol{\varphi}\right)^2 = \lambda\rho^4/4$, see Fig. 8.5. The longitudinal modes are excited parametrically during reheating. The inflaton decay to transverse modes of the gauge fields mimics the well studied $\varphi^2\chi^2$ scalar field model [84] (see also Fig. 4.1).

Without the longitudinal modes, the back-reaction of the transverse gauge fields would be identical to the one in $\varphi^2\chi^2$. However, recent numerical experiments [26] indicate that there are small differences between the behaviour of the inflaton decaying to scalars and to Abelian gauge fields. This might be due to the longitudinal modes being excited and playing a role in the back-reaction process. In general, calculations during (p)reheating and estimation of the effects of non-Abelian interaction terms are convenient in the Coulomb gauge (or some other well-defined gauge during preheating). The traditional unitary gauge is *not*

a good choice because the inflaton oscillates through the origin. Although as we saw in the Abelian case, the electric and magnetic fields can be well defined even when using gauge invariant variables, the intermediate steps leading up their calculation often involve singular behaviour which at the very least leads to numerical unpleasantness. The same comment holds for the unitary gauge since the equations of motion are identical to those in gauge invariant variables.

8.7 Observational consequences

Particle production during and after inflation in models with a charged inflaton coupled to gauge fields may leave potentially observable signatures such as primordial magnetic fields, charge fluctuations as well as scalar and tensor metric perturbations. We schematically discuss each one in turn.

8.7.1 Magnetic fields

At the end of inflation the magnetic field power-spectrum on superhorizon scales is blue and given by a power-law, see eqns. (8.68) and (8.69). If the gauge fields are 'lighter' than the co-moving Hubble scale during inflation, i.e., for $k_{\scriptscriptstyle C} \lesssim \mathcal{H}$ we have $\Delta_{B^{T\pm}} \propto k^2$. If the gauge fields are "massive" enough, $k_{\scriptscriptstyle C} \gtrsim \mathcal{H}$, the power-spectrum is much steeper: $\Delta_{B^{T\pm}} \propto k^{5/2}$. After inflation, the oscillating inflaton can resonantly amplify the gauge fields. For the $m^2|\varphi|^2$ model considered in Section 8.3.2, the resonance is broad and effective for $k_{\scriptscriptstyle C}/a \sim g_{\scriptscriptstyle A}|\bar{\varphi}| \gtrsim m$, where $\bar{\varphi}$ is the vev of the inflaton during the early stages of preheating at the end of inflation.[15]

The above considerations show that the optimal range for production of magnetic fields on superhorizon scales is $k_{\scriptscriptstyle C} \lesssim \mathcal{H}$ during inflation and $k_{\scriptscriptstyle C}/a \gtrsim m$ during preheating. However, for $m^2|\varphi|^2$ inflation, $k_{\scriptscriptstyle C}/(am) \gtrsim 1$ during preheating implies $k_{\scriptscriptstyle C}/\mathcal{H} \gtrsim 1$ during inflation, thus excluding the possibility of broad resonance *and* a relatively shallow power law for the magnetic field spectrum. We reached the same conclusion via a more detailed calculation whose results were summarized in Fig. 8.2. We have to settle for two separate regimes: $\Delta_{B^{T\pm}} \propto k^2$ which receives no resonant amplification during preheating, or $\Delta_{B^{T\pm}} \propto k^{5/2}$ which can be resonantly amplified until it backreacts.

As discussed in Section 5.2.2, in the contemporary universe, observations indicate a magnetic field strength of $\sim 10^{-6}\,\mathrm{G}$ on $1\,\mathrm{Mpc}$ scales (for example, see [53]). If a *seed* magnetic field $B_{\rm seed} \gtrsim 10^{-25}\,\mathrm{G}$ is present on comoving scales corresponding to $1\,\mathrm{Mpc}$ at the time of matter-radiation equality, the galactic dynamo mechanism can potentially amplify $B_{\rm seed}$ to the observed values today [53]. As we show below, the seed field generated in the models under consideration are far too small compared to what is required observationally.

For the case when $k_{\scriptscriptstyle C} \lesssim \mathcal{H}$ during inflation, the magnetic field has a shallow spectrum $\propto k^2$ on superhorizon scales but is not resonantly amplified during preheating. At the time of decoupling we obtain $B_{\rm seed} \sim \Delta^{\rm dec}_{B^{T\pm}} \sim (2\pi)^{-1}\,(k/a_{\rm dec})^2 \sim 10^{-50}\,\mathrm{G}$ (for example, see [269]) where we used $a_{\rm dec} \sim 10^{-3}$, $k = \text{few}\,\mathrm{Mpc}^{-1} \sim 10^{-38}\,\mathrm{GeV}$ and $1\,\mathrm{GeV}^2 \sim 10^{20}\,\mathrm{G}$. When $k_{\scriptscriptstyle C} \gtrsim \mathcal{H}$, the magnetic field can be resonantly amplified, with an amplification factor that can be as large as $\sim 10^4 - 10^5$. The maximum value is set by back-reaction considerations. However, there is a suppression factor $\sqrt{k/k_{\scriptscriptstyle C}}$ (see eq. (8.68)) which turns out to be more important. The net effect is that $B_{\rm seed}$ is suppressed compared to the no-resonance scenario. For

[15] In the more popular notation, the parameter determining the strength of the resonance, q, is given by $q = k_{\scriptscriptstyle C}/(am)$. The resonance is broad when $q \gg 1$ and narrow or absent when $q \lesssim 1$ (see Section 2.2).

the case when $k_{_C} = 10^3\,\mathcal{H}$ at the end of inflation (shown in Fig. 8.2), $B_{\rm seed} \sim 10^{-58}\,$G. For this estimate we assumed that the back-reaction takes place 2.5 e-folds after inflation, and subsequently the magnetic field redshifts in the usual way: $a^4\Delta^2_{B^{T\pm}} = $ const for another 57.5 e-folds.

We note that while broad resonance does not happen for $k_{_C} \lesssim \mathcal{H}$ for the $m^2|\varphi|^2$ models, it can occur for $k_{_C} < \mathcal{H}$ for steeper potentials (e.g., $\lambda|\varphi|^4$). It might be possible to boost the amplitude of the seed field up to $10^{-45}\,$G in such cases. However, this is still too small to be observationally relevant. Successful magnetogenesis from reheating has been recently discussed in models different from ours (see for example, [95, 96]).

8.7.2 Charge fluctuations

Just like the magnetic field, the charge fluctuations also have a blue power-spectrum at the end of inflation. Recalling Gauss law, $-kE^L_{\boldsymbol{k}} = a^2 j_{0\boldsymbol{k}}$, we arrive at the useful expression $\Delta_{j_0} = (k/a)\Delta_{E^L}$. Indeed eqns. (8.68) and (8.69) imply that on superhorizon scales $\Delta_{j_0} \propto k^2$ and $k^{5/2}$ for $k_{_C} \lesssim \mathcal{H}$ and $k_{_C} \gtrsim \mathcal{H}$ respectively, reminiscent of the magnetic field spectrum. After inflation, parametric resonance can amplify the charge fluctuations in the $m^2|\varphi|^2$ model, provided we are in the broad resonance regime $g_{_A}|\bar{\varphi}| \gtrsim m$ (i.e., $k_{_C} \gtrsim \mathcal{H}$ with a spectrum $\propto k^{5/2}$ on superhorizon scales). Note that unlike the magnetic field case, we see some production of charge fluctuations on superhorizon scales at the end of inflation even when $m \gtrsim g_{_A}|\bar{\varphi}|$. This fluctuation production is related to the oscillation of the inflaton, but cannot be analysed with simple Floquet analysis since it occurs on superhorizon scales where expansion plays a significant role.

If we imagine that the gauge field in question is the electromagnetic field and put $g_{_A} = 2e$ one can compare the charge fluctuations to the observational bounds from vorticity and cosmological magnetic fields on the electrical charge asymmetry of the universe [294], namely that $\Delta_{j_0}/(en_{_B}) \lesssim 10^{-26}$ on co-moving scales corresponding to $10^2\,$kpc today, where $n_{_B} \sim 1.5\times 10^{-10}\,T^3$ is the number of baryons and T is the photon temperature. For $k_{_C} < \mathcal{H}$, we can assume the universe reheats immediately after the end of inflation and the charge fluctuation is transferred to a charge asymmetry in the ordinary matter. The charge asymmetry will then redshift as $a^3\Delta_{j_0} = $ const, akin to number density. Then the fractional charge asymmetry $\Delta_{j_0}/en_{_B} \sim 10^9 \times (k/a_{\rm rh}T_{\rm rh})^2\,(g_{_A}|\varphi_{\rm inf}|/T_{\rm rh}) \sim 10^{-36}$, where we used $|\varphi_{\rm inf}| \sim m_{\rm Pl}$, $k = 10\,{\rm Mpc}^{-1}$, $T_{\rm end} \sim 10^{16}\,$GeV and $a_{\rm end}T_{\rm end} \sim T_0 = 2.5\times 10^{-4}$eV. [16] For the broad resonance regime, $k_{_C} \gtrsim \mathcal{H}$, the amplitude of the charge fluctuations can be parametrically amplified up to $10^3 - 10^4$. However, there is also a suppression factor which dominates on the scales of interest. Explicitly, for $k_{_C} = 10^3\,\mathcal{H}$ discussed in Fig. 8.2, if we assume that the universe reheats immediately after back-reaction has taken place (2.5 e-folds after the end of inflation) and then the universe expands for another 57.5 e-folds, the suppression factor is roughly $\sim \sqrt{\exp(-2.5)k/k_{_C}}$, implying $\Delta_{j_0}/(en_{_B}) \approx 10^{-45}$.

Again, we recall that in the $m^2|\varphi|^2$ model, broad resonance does not happen for $k_{_C} \lesssim \mathcal{H}$. For steeper power-law potentials, parametric resonance is efficient for light gauge fields and the excess of charged particles per baryon can go up to 10^{-32}. We once again caution the reader that the calculations here are meant to be schematic.

8.7.3 Metric perturbations

The production of gauge fields may affect the primordial metric perturbations, giving rise to (for example) non-gaussianities and gravitational waves. Since the gravitational production of gauge fields during

[16] We caution the reader that this is a very rough estimate.

inflation is not significant, they are not expected to give rise to any interesting signals. However, if the post-inflationary dynamics include parametric amplification of fields then interesting signatures are possible. For example, light scalar fields might develop a non-zero vev across the observable universe today along with perturbations around this vev within each Hubble patch at the time of preheating. The details of the following non-linear stage might depend on the vev in each separate universe. For instance, in [43, 125, 126] it was shown that as the inflaton decays to a light χ field in $\phi^2\chi^2$ models, the back-reaction depends on the initial vev $\bar{\chi}_{\rm i}$ within the Hubble patch. This in turn affects the expansion history within the Hubble patch and therefore may lead to non-gaussianities. $\bar{\chi}_{\rm i}$ also affects the gravitational waves produced during the non-linear evolution within the separate patches. This may lead to low-multiple corrections to the stochastic gravitational wave background [121, 122].

For $k_{_C} \lesssim \mathcal{H}$ one can show that the gauge field sector has a light scalar with a scale-invariant power-spectrum – it is $\delta\varphi^1$ in the Coulomb gauge, see eq. (8.46) and Appendix B. This implies that $\delta\varphi^1$ develops a non-zero vev across the sky with deviations from it within each Hubble patch at the time of preheating. Its back-reaction should lead to similar effects to the $\varphi^2\chi^2$ models, since the resonance structure is similar. Note that for the $m^2|\varphi|^2$ model we have been considering, back-reaction cannot happen because resonance is inefficient if $k_{_C} \lesssim \mathcal{H}$ (which was necessary for developing a vev for $\delta\varphi^1$ during inflation). The absence of resonance for $k_{_C} \lesssim \mathcal{H}$ is a feature of $m^2|\varphi|^2$ model. For steeper potentials (e.g $\lambda|\varphi|^4$), broad resonance can occur for $k_{_C} \lesssim \mathcal{H}$.

8.8 Conclusions

In this chapter, we carried out a self-contained analysis of particle production during and after inflation in models with charged scalars coupled to Abelian and non-Abelian fields. We calculated the power-spectra of the produced gauge fields in the regime where the equations of motion could be linearized. We also provided a prescription for setting up initial conditions for lattice simulations to further evolve the fields nonlinearly.

To make our treatment self-contained, we provided the necessary equations for linear perturbations (including metric fluctuations) in terms of gauge invariant variables, and provided a dictionary to relate these variables to those in some common gauges. This should allow results to be translated between gauges quite easily. For pedagogical purposes, we carried out the initial analysis for the Abelian model. In the later half of the chapter we provided the explicit generalization to the non-Abelian cases.

We carried out the quantization and evolution of the perturbations during inflation in terms of gauge invariant variables. After substituting the constraint equations into the original action, the quantization and subsequent evolution was carried out in a straightforward manner. Gauge invariant variables have the advantage of automatically dealing with the correct number of degrees of freedom; we never have to worry about spurious gauge modes. We numerically calculated the electric and magnetic field power-spectra at the end of inflation for a simple $m^2|\varphi|^2$ inflation (see Fig. 8.1). We provided an understanding of the shape of the spectra (blue tilt and broken power law behavior – see eqns. (8.68) and (8.69)) in terms of two scales: the co-moving Compton wavenumber of the gauge fields $k_{_C} \equiv a|\bar{\varphi}|g_{_A}/2$ ($\bar{\varphi}$ is the vev of the inflaton condensate during inflation, $g_{_A}$ is the coupling strength and a is the scalefactor) and the conformal Hubble scale $\mathcal{H}$. We found that the transverse modes are always dominant over the longitudinal ones on sub-Compton scales, $k \gtrsim k_{_C}$. For gauge fields with $k_{_C} \gtrsim \mathcal{H}$ the longitudinal modes are as energetic as the transverse ones on super-Compton scales, $k \lesssim k_{_C}$, whereas when $k_{_C} \lesssim \mathcal{H}$ the longitudinal modes dominate on super-Compton scales. The longitudinal mode of the electric field is directly proportional to

charge fluctuations, and hence charge fluctuations are also generated during inflation. While our numerical calculations assumed a particular model, these results are expected to hold more generally for potentials where the inflaton is rolling slowly. As a further check, we carried out a semi-analytic analysis in a de Sitter universe and confirmed the shapes of the electric and magnetic field spectra.

While gauge invariant variables are suited for calculations during inflation, they become ill-defined when the inflaton starts oscillating after inflation. After inflation, the Coulomb gauge turns out to be a particularly well-suited for preheating studies. We carried out an explicit numerical calculation of resonant gauge field production during preheating and provided power-spectra of the corresponding electric and magnetic fields at the end of preheating (see Fig. 8.2). For an analytic understanding of the main features of the spectra, we carried out a Floquet analysis of the instabilities with the gauge constraints included (see Fig. 8.3). In both calculations, we found that the longitudinal modes are as prone to resonant excitation during preheating as the transverse ones. The characteristic wavenumber range of the instability is $k \lesssim m(g_A m_{\rm Pl}/m)^{1/2}$, whereas the growth rate of fluctuations is determined by $g_A m_{\rm Pl}/m$. We also estimated that the gauge fields back-react on the scalar condensate within about 10 oscillations in the case of a $m^2|\varphi|^2$ potential and for couplings, $g_A \gtrsim 10^{-3}$ (see Fig. 8.4). For $g_A \lesssim 10^{-4}$ gauge fields are not produced significantly enough to back-react.

If back-reaction becomes important, the occupation numbers in the gauge fields are usually very high. Further evolution, which is usually highly nonlinear, can be investigated by numerical lattice simulations within the classical approximation. We provided a scheme for initializing such simulations with the gauge constraints being violated only at second order in the perturbations. We also provide a work-around enabling the gauge constraints to be satisfied more precisely at the expense of insignificant (second order in perturbations) modification to the spectrum of the gauge fields. Our prescription for initial conditions is not restricted to a particular gauge; we provide an explicit example of setting up such conditions in the temporal gauge which is commonly used for simulations (see Section 8.5 and also Section 9.5). The derived power-spectra as well as the initial conditions prescription might be useful for lattice simulations of Abelian and non-Abelian fields at the end of inflation (for example, [21, 22, 26, 27, 29, 37, 276, 277, 279, 281]).

We considered two non-Abelian models. In the $SU(2)$ model we showed that to linear order in perturbations, the problem conveniently reduces to three decoupled identical replicas of the Abelian model. We then extended the local group to $SU(2) \times U(1)$, with the Electroweak sector of the Standard Model of Particle Physics in mind. Again, to linear order in the perturbations, the problem splits into three copies of the Abelian model. There are two identical copies, describing the evolution of the massive W bosons, and a similar one for the massive Z boson, the only difference being the coupling constants. The massless photon $\mathcal{A}$ remains decoupled from the other sectors of the theory. The framework describing the longitudinal and transverse modes in the Abelian model can be straightforwardly applied to the W and Z sectors, including the scheme for initialising lattice simulations. We provided Floquet charts to capture the instability of these fields during preheating, assuming the scalar condensate to be characterised by $\lambda(\boldsymbol{\varphi}^\dagger\boldsymbol{\varphi})^2$ self-interaction (see Fig. 8.5). In this case, we again confirm that the longitudinal and transverse mode can be excited at a comparable level.

Our analysis allowed us to estimate the magnetic field and charge fluctuations from inflation and preheating in a self-consistent manner. We found that the charged inflaton produces a magnetic field that cannot exceed $\sim 10^{-50}\,$G on $1\,$Mpc scales today (consistent with [92]) for an $m^2|\varphi|^2$ potential. Parametric resonance in models with steeper potentials, e.g., $\lambda|\varphi|^4$ may boost the magnetic field by a factor of 10^5, which is still not enough to seed an efficient galactic dynamo mechanism. The charge fluctuations are shown to be also below the observational bounds, if the inflaton is assumed to be electrically charged. The excess charged particles per baryon are found to be at most $\lesssim 10^{-36}$ on $0.1\,$Mpc scales for an $m^2|\varphi|^2$

potential. Preheating in models with steeper potentials, e.g., $\lambda|\varphi|^4$ may amplify this by a factor of 10^4. This is well within the observational bound of $\lesssim 10^{-26}$ [294]. The possibility of an electrically charged inflaton is not ruled out.

Our analysis also reveals that the azimuthal degree of freedom of the charged inflaton develops a scale-invariant power-spectrum if the gauge fields are lighter than the Hubble scale. This gives us the possibility of generating non-Gaussianities and gravitational waves [27, 43, 121, 122, 125, 126] from the non-linear stage of reheating which we leave for future work.

Chapter 9

Non-linear dynamics

Abstract

To understand inflation and the subsequent stage of reheating: the period when the Universe first got populated with particles during the hot big bang, we need highly accurate numerical methods. In this chapter we present a symplectic integrator for non-linear partial differential equations describing the evolution of charged scalar fields coupled to abelian gauge fields in an expanding universe.

9.1 Introduction

The non-perturbative particle production of preheating can lead to non-linear effects [17, 32] (see also Chapter 8). To study the non-linear post-inflationary dynamics in models with a charged scalar field coupled to gauge fields we have developed a novel, precise numerical scheme for the integration of the equations of motion with the space-time curvature included at the back-ground level. The basic idea is that the action, instead of the equations of motion, is discretized. This way the approximate problem is solved 'exactly', rather than the exact problem approximately. To be specific, the action is discretized in space on a 3d cubic lattice, first (keeping the time derivatives continuous). This allows us to use the Hamiltonian formalism. Only after we derive the Hamiltonian for the problem we carry out the temporal symplectic discretization of the equations of motion by operator splitting [295]. This allows us to have different order of accuracy in space and time. The current version of the code is 2-nd order in space and could be much higher in time (so far tested up to 8-th order).

Although, such discretization seems straightforward for scalar field models [75, 296], it is not clear whether it could be applied to more complicated systems involving gauge fields. The issue is that with gauge fields come non-dynamical equations (constraint equations) following from the gauge invariant action, which have to be met exactly by the numerical integrator for consistency. That is why one of the most common approaches is to use 2-nd order discretization of spatial and temporal derivatives, the Method of Link variables [22, 54], which preserves the gauge invariance of the action, but could be quite expensive to implement if one needs good accuracy in time. Another (not very common) alternative is to ignore the constraint equations when discretizing, and integrate the system of equations, while keeping track of the violation of the consistency of the theory [31, 37]. This method could work for short periods of time, but inevitably breaks down and leads to spurious effects.

What we have found is that if one works in a specific gauge (the temporal gauge) in the Abelian-Higgs system in Friedmann-Robertson-Walker (FRW) spacetime, the temporal symplectic discretization of the equations of motion by the operator splitting technique leads to the exact preservation of the constraint (Gauss) equation, even if the universe expands self-consistently. To the best of our knowledge this is the first algorithm that has this feature (none of the above mentioned methods have it). This lets us not only enjoy the advantages of the symplectic integrators (separate control over space and time accuracy; no need for extra storage of intermediate results unlike Runge-Kutta schemes, which can be vital for large three dimensional simulations), but also answer physical questions related to the expansion history of our Universe. We can go beyond the conventional Abelian-Higgs model and consider conformal couplings between the scalar and the gauge fields and/or adding fermions on the lattice. We expect none of these extensions to cause any issues with the Gauss constraint. Non-Abelian theories and/or the presence of Chern-Simons terms are problematic in this respect. However, we could in principle still use our algorithm and keep track of the violation of the Gauss constraint. We can even address non-Abelian problems such as reheating after Higgs-inflation, since it is known that before and even during the non-linear phase the non-Abelain interaction terms are suppressed, i.e., one can safely split the non-Abelian Lagrangian into identical copies of the Abelian-Higgs model [23, 24, 26, 32].

We begin with a brief reminder of conservation laws in dynamical systems described by invariant Lagrangians under continuous symmetry transformations, Section 9.2. The results from this section are useful for the derivation of the Gauss law in the discretized Abelian-Higgs system, outlined in Sectoin 9.3. The actual integrator is presented in Section 9.4. A prescription for physically accurate initial conditions, taking into account the particle production during inflation and preheating, as well as the gauge constraints is given in Section 9.5 (cf. also our earlier work [32] and Section 8.5).

9.2 Conserved currents and symmetries

9.2.1 Infinite d.o.f.

Let us begin with the action of a continuous classical system

$$S = \int d^4x \sqrt{-\eta}\, \mathcal{L}(f_i(x^\mu), \partial_\mu f_i(x^\nu))\,, \tag{9.1}$$

describing *i* fields, $f_i(x^\mu)$, each of which encodes an infinite number of degrees of freedom, in Minkowski spacetime. If there exists a continuous transformation that leaves the Lagrangian density invariant, infinitesimally written as

$$f_i \to f_i + \delta f_i\,, \quad \mathcal{L} \to \mathcal{L}\,, \tag{9.2}$$

then according to the Noether theorem there exists a conserved current

$$\partial_\mu j^\mu = 0\,, \quad j^\mu = \sum_i (\partial_{\partial_\mu f_i}\mathcal{L})\delta f_i\,. \tag{9.3}$$

The second expression can be obtained after assuming that the Euler-Lagrange equations

$$\partial_{f_i}\mathcal{L} = \partial_\mu \partial_{\partial_\mu f_i}\mathcal{L}\,, \tag{9.4}$$

are obeyed. The conservation of the current implies the existence of a constant net charge

$$Q = \int d^3x\, j^0 = \text{const} \tag{9.5}$$

if $\lim_{|\boldsymbol{x}|\to\infty} \boldsymbol{j}(\boldsymbol{x}) = \boldsymbol{0}$.

9.2.2 Finite d.o.f.

The discrete counterpart of the above system has an action of the standard form

$$S = \int d\tau\, L(f_i(\tau), f_i'(\tau))\,, \tag{9.6}$$

describing i generalized coordinates, $f_i(x^\tau)$[1]. If again there is a continuous symmetry, leaving the Lagrangian invariant, written infinitesimally as

$$f_i \to f_i + \delta f_i\,, \quad L \to L\,, \tag{9.7}$$

then the quantity

$$J = \sum_i (\partial_{f_i'} L)\delta f_i\,, \tag{9.8}$$

is conserved

$$J' = 0\,, \tag{9.9}$$

provided the equations of motion hold, $\partial_{f_i} L = (\partial_{f_i'} L)'$. Note that the number of conserved quantities, $J = \text{const}$, corresponds to the number of symmetry transformations leaving the Lagrangian, eq. (9.7), invariant.

9.3 Abelian-Higgs in FRW

The system that we wish to solve is the Abelian-Higgs model (or the Ginzburg-Landau model with a general Higgs potential)

$$S = \int d^4x\sqrt{-g}\mathcal{L} = \int d^4x\sqrt{-g}\left[-\frac{m_{\text{Pl}}^2}{2}R + |\mathcal{D}^q\varphi|^2 - \frac{1}{4e^2}F_{\mu\nu}F^{\mu\nu} - \mathcal{V}(|\varphi|)\right]\,, \tag{9.10}$$

in FRW spacetime, using conformal time[2] ($' \equiv d/d\tau$)

$$g_{\mu\nu} = a^2\eta_{\mu\nu}\,, \quad R = -6\frac{a''}{a^3}\,. \tag{9.11}$$

The covariant derivative and the field tensor are defined as follows[3]

$$\mathcal{D}_\mu^q = \partial_\mu + iqA_\mu\,, \quad F_{\mu\nu} = \mathcal{D}_\mu^{q=1}A_\nu - \mathcal{D}_\nu^{q=1}A_\mu\,. \tag{9.12}$$

[1]The number of generalized coordinates does not correspond to the number of fields from Section 9.2.1.

[2]We assume spatially flat FRW, $k = 0$, for simplicity. The integrator derived in the following sections can be easily generalised and works equally well for $k \neq 0$.

[3]Since the gauge field is Abelian, the field tensor reduces to $F_{\mu\nu} = \partial_\mu A_\nu - \partial_\nu A_\mu$.

Note that the actual coupling between the Higgs and the gauge fields is qe. You can think of e as the actual charge, related to the 'fine structure constant' of the theory, whereas q is the fractional charge given in units of e. This deliberate split makes it more convenient to generalize the algorithm we are going to derive below to multiple scalar and gauge fields with arbitrary couplings.

Sometimes, it is more convenient to work in terms of the real and imaginary parts of the Higgs, redefining its potential as well

$$\varphi = \frac{1}{\sqrt{2}}(\varphi_1 + i\varphi_2)\,, \quad \mathcal{V}(|\varphi|) = V\left(\sqrt{\varphi_1^2 + \varphi_2^2}\right)\,. \tag{9.13}$$

The Lagrangian density, eq. (9.10), is invariant under the local (gauge) symmetry transformation

$$\varphi \to \exp[-iq\alpha(x^\nu)]\varphi\,, \quad A_\mu \to A_\mu + \partial_\mu\alpha(x^\nu)\,, \quad \mathcal{L} \to \mathcal{L}\,. \tag{9.14}$$

In the next subsections we shall fix the gauge by making a specific choice for the gauge fields at the level of the Lagrangian, rather than the equations of motion, and see what implications this approach has for the non-dynamical constraint equations. Afterwards we shall discretize the Lagrangian on a 3d grid and discuss the discrete constraint equations. As it will be shown in Section 9.4, our gauge choice and the discretization scheme make symplectic integrators particularly suitable, preserving the constraint equations exactly.

9.3.1 Continuous case in $A_0 = 0$ gauge

We choose to work in the temporal gauge, setting $A_0 = 0$. The action, eq. (9.10), then reduces to

$$\begin{aligned} S &= \int d^4x \mathcal{L}_\mathrm{c} \\ &= \int d^4x \left[-3m_\mathrm{Pl}^2 a'^2 + \frac{(a\varphi_1')^2}{2} + \frac{(a\varphi_2')^2}{2} - a^2|\boldsymbol{\mathcal{D}}^q\varphi|^2 - a^4 V + \frac{\mathbf{A}'^2}{2e^2} - \frac{(\boldsymbol{\nabla}\times\mathbf{A})^2}{2e^2}\right]\,. \end{aligned} \tag{9.15}$$

This specific gauge choice allows us to apply the Hamiltonian formalism straightforwardly, since all variables are dynamical

$$\varphi_1 = \varphi_1(\tau,\mathbf{x})\,, \quad \varphi_2 = \varphi_2(\tau,\mathbf{x})\,, \quad \mathbf{A} = \mathbf{A}(\tau,\mathbf{x}) = [A_1(\tau,\mathbf{x})\,, A_2(\tau,\mathbf{x})\,, A_3(\tau,\mathbf{x})]^T\,, \quad a = a(\tau)\,. \tag{9.16}$$

Their conjugate momenta densities defined as

$$\pi_1(\tau,\mathbf{x}) = \frac{\partial}{\partial\varphi^{1\prime}}\mathcal{L}_\mathrm{c}\,, \quad \pi_2(\tau,\mathbf{x}) = \frac{\partial}{\partial\varphi^{2\prime}}\mathcal{L}_\mathrm{c}\,, \quad \boldsymbol{\pi}_A(\tau,\mathbf{x}) = \frac{\partial}{\partial\mathbf{A}'}\mathcal{L}_\mathrm{c}\,, \quad \pi_a(\tau) = \frac{\partial}{\partial a'}\mathcal{L}_\mathrm{c}\,, \tag{9.17}$$

reduce to

$$\pi_1 = a^2\varphi_1'\,, \quad \pi_2 = a^2\varphi_2'\,, \quad \boldsymbol{\pi}_A = e^{-2}\mathbf{A}'\,, \quad \pi_a = -6m_\mathrm{Pl}^2 a'\,. \tag{9.18}$$

Before we switch to the Hamiltonian description of the system it is worth thinking about what happens to the constraint equation (Gauss constraint) after we set the non-dynamical variable A_0 to zero at the level of the Lagrangian, cf., e.g., [297]. Normally, the Gauss constraint follows after varying the action with respect to the non-dynamical A_0. However, since the action in eq. (9.15) has no A_0 it is not clear whether the constraint should be imposed additionally or that the evolution of the system governed by eq. (9.15) will

obey it automatically, without any additional modifications to the action. The answer lies in the residual gauge symmetry. Even after setting $A_0 = 0$, we are free to make time-independent gauge transformations

$$\varphi \to \exp[-iq\alpha(\mathbf{x})]\varphi\,, \quad \mathbf{A} \to \mathbf{A} + \boldsymbol{\nabla}\alpha(\mathbf{x})\,, \quad \mathcal{L}_\mathrm{c} \to \mathcal{L}_\mathrm{c}\,, \tag{9.19}$$

written infinitesimally as

$$\delta\varphi_1 = \varphi_2 q\alpha\,, \quad \delta\varphi_2 = -\varphi_1 q\alpha\,, \quad \delta\mathbf{A} = \boldsymbol{\nabla}\alpha\,, \tag{9.20}$$

if $\alpha(\mathbf{x}) \ll 1$. As discussed in Section 9.2, it implies the existence of a conserved current

$$j^\mu = \sum_i (\partial_{\partial_\mu f_i}\mathcal{L}_\mathrm{c})\delta f_i\,. \tag{9.21}$$

The constant net charge is

$$\begin{aligned} Q = \int d^3x\, j^0 &= \int d^3x\, [\boldsymbol{\pi}_A \cdot \boldsymbol{\nabla}\alpha + (\pi_1\varphi_2 - \pi_2\varphi_1)q\alpha] \\ &= \oint \alpha\boldsymbol{\pi}_A \cdot \mathbf{dS} - \int d^3x\, \alpha\, [\boldsymbol{\nabla}\cdot\boldsymbol{\pi}_A - q(\pi_1\varphi_2 - \pi_2\varphi_1)]\ , \end{aligned} \tag{9.22}$$

Since $Q = \text{const}$ for all $\alpha(\mathbf{x})$, then

$$\boldsymbol{\nabla}\cdot\boldsymbol{\pi}_A(\tau,\mathbf{x}) - q\,[\pi_1(\tau,\mathbf{x})\varphi_2(\tau,\mathbf{x}) - \pi_2(\tau,\mathbf{x})\varphi_1(\tau,\mathbf{x})] = \text{const}\,, \tag{9.23}$$

provided $\lim_{|\boldsymbol{x}|\to\infty} \alpha(\mathbf{x})\boldsymbol{\pi}_A(\tau,\mathbf{x}) = \mathbf{0}$, which always holds, because both α and $\boldsymbol{\pi}_A$ vanish separately at spatial infinity – the former by the definition of a gauge transformation and the latter trivially. Hence, if we make sure that the constant on the right hand side in eq. (9.23) is set to zero initially for all $\mathbf{x}$, then the whole equation reduces to the Gauss constraint and it is automatically preserved by the equations of motion.

9.3.2 Discrete case in $A_0 = 0$ gauge

The last step we need to make before proceeding with the numerical integration of the Abelian-Higgs model is to discretize the fields on a 3d spatial grid. We assume a cubic lattice with periodic boundary conditions and N^3 lattice points, the length of the edge of the unit cell being equal to b. The scalar fields, $\{\varphi_{1,\mathbf{x}}, \varphi_{2,\mathbf{x}}\}$, live on the lattice points with spatial coordinates $\mathbf{x}$, whereas the gauge fields, $A_{j,\mathbf{x}}$, live on the lattice links, connecting the points $\mathbf{x}$ and $\mathbf{x} + \mathbf{n}_j$. The unit vectors are defined as

$$\mathbf{n}_1 = [1,0,0]^T\,, \quad \mathbf{n}_2 = [0,1,0]^T\,, \quad \mathbf{n}_3 = [0,0,1]^T\,. \tag{9.24}$$

We now introduce the link variables, $U_{j,\mathbf{x}}$, and the plaquettes, $P_{ij,\mathbf{x}}$, [54]

$$U_{j,\mathbf{x}} = \exp[ibA_{j,\mathbf{x}}]\,, \quad P_{ij,\mathbf{x}} = U_{i,\mathbf{x}}U_{j,\mathbf{x}+\mathbf{n}_i b}U^*_{i,\mathbf{x}+\mathbf{n}_j b}U^*_{j,\mathbf{x}}\,, \quad P_{ij,\mathbf{x}} = P^*_{ji,\mathbf{x}}\,. \tag{9.25}$$

We use them to derive the spatial derivative terms (no summation is implied over repeated indices)

$$(\mathcal{D}^q_j\varphi)_{(\mathbf{x})} \to \frac{U^q_{j,\mathbf{x}}\varphi_{\mathbf{x}+\mathbf{n}_j b} - \varphi_\mathbf{x}}{b}\,, \quad (F_{ij}F^{ij})_{(\mathbf{x})} \to \frac{2 - P_{ij,\mathbf{x}} - P_{ji,\mathbf{x}}}{b^4}\,, \tag{9.26}$$

in the lattice version of the continuous action, eq. (9.15),

$$S = \int d\tau\, L = \int d\tau \Bigg\{ -3m_{\rm Pl}^2 a'^2 N^3 + \sum_{\mathbf{x}}^{N^3} \Bigg(\frac{(a\varphi'_{1,\mathbf{x}})^2}{2} + \frac{(a\varphi'_{2,\mathbf{x}})^2}{2} - a^4 V_{\mathbf{x}} + \frac{1}{2e^2} \sum_{j}^{1,2,3} A'^2_{j,\mathbf{x}} \\ - \frac{1}{2e^2 b^4} \sum_{i,j}^{1,2,3} [1 - P_{ij,\mathbf{x}}] - \frac{a^2}{2b^2} \sum_{j}^{1,2,3} \Big[(\varphi^2_{1,\mathbf{x}+\mathbf{n}_j b} + \varphi^2_{2,\mathbf{x}+\mathbf{n}_j b}) + (\varphi^2_{1,\mathbf{x}} + \varphi^2_{2,\mathbf{x}}) \\ - \Big((\varphi_{1,\mathbf{x}} - i\varphi_{2,\mathbf{x}}) U^q_{j,\mathbf{x}} (\varphi_{1,\mathbf{x}+\mathbf{n}_j b} + i\varphi_{2,\mathbf{x}+\mathbf{n}_j b}) + c.c. \Big) \Big] \Bigg) \Bigg\} . \tag{9.27}$$

Note that we have carried out the summation over the lattice points and we have rescaled the action by a factor of $(dx)^3 = b^3$ – an overall rescaling of the action does not affect Euler-Lagrange and Hamilton equations of motions. The continuous system of five fields describing infinitely many degrees of freedom and the scale factor has been transformed to one having $5 \times N^3 + 1$ generalized coordinates, with conjugate momenta

$$\pi_{1,\mathbf{x}} = a^2 \varphi'_{1,\mathbf{x}} , \quad \pi_{2,\mathbf{x}} = a^2 \varphi'_{2,\mathbf{x}} , \quad \pi_{Aj,\mathbf{x}} = e^{-2} A'_{j,\mathbf{x}} , \quad \pi_a = -6m_{\rm Pl}^2 a' N^3 . \tag{9.28}$$

The use of links and plaquettes also preserves the important invariance of the action on the grid, eq. (9.27), under time-independent symmetry transformations, eq. (9.19). Their lattice version looks as follows

$$\varphi_{\mathbf{x}} \to \Omega^q_{\mathbf{x}} \varphi_{\mathbf{x}} , \quad U_{j,\mathbf{x}} \to \Omega_{\mathbf{x}} U_{j,\mathbf{x}} \Omega^*_{\mathbf{x}+\mathbf{n}_j b} , \quad L \to L , \quad \Omega_{\mathbf{x}} = \exp[-i\alpha_{\mathbf{x}}] , \tag{9.29}$$

and it can be written infinitesimally as

$$\delta\varphi_{1,\mathbf{x}} = \varphi_{2,\mathbf{x}} q \alpha_{\mathbf{x}} , \quad \delta\varphi_{2,\mathbf{x}} = -\varphi_{1,\mathbf{x}} q \alpha_{\mathbf{x}} , \quad \delta A_{j,\mathbf{x}} = \frac{\alpha_{\mathbf{x}+\mathbf{n}_j b} - \alpha_{\mathbf{x}}}{b} , \tag{9.30}$$

if $\alpha_{\mathbf{x}} \ll 1$. According to Noether theorem, cf. Section 9.2, for an arbitrary $\alpha_{\mathbf{x}}$, there is a conserved current

$$J = \sum_i (\partial_{f'_i} L) \delta f_i = \sum_{\mathbf{x}}^{N^3} \left[q\alpha_{\mathbf{x}} (\pi_{1,\mathbf{x}} \varphi_{2,\mathbf{x}} - \pi_{2,\mathbf{x}} \varphi_{1,\mathbf{x}}) + \sum_{j}^{1,2,3} \pi_{Aj,\mathbf{x}} \frac{\alpha_{\mathbf{x}+\mathbf{n}_j b} - \alpha_{\mathbf{x}}}{b} \right] = \text{const} , \tag{9.31}$$

which can be simplified, after relabeling the dummy indices under the second summation, to

$$J = \sum_{\mathbf{x}}^{N^3} \alpha_{\mathbf{x}} \left[q(\pi_{1,\mathbf{x}} \varphi_{2,\mathbf{x}} - \pi_{2,\mathbf{x}} \varphi_{1,\mathbf{x}}) - \sum_{j}^{1,2,3} \frac{\pi_{Aj,\mathbf{x}} - \pi_{Aj,\mathbf{x}-\mathbf{n}_j b}}{b} \right] = \text{const} . \tag{9.32}$$

Since $J = \text{const}$ is valid for all $\alpha_{\mathbf{x}}$, then

$$\sum_{j}^{1,2,3} \left[\frac{\pi_{Aj,\mathbf{x}} - \pi_{Aj,\mathbf{x}-\mathbf{n}_j b}}{b} \right] - q(\pi_{1,\mathbf{x}} \varphi_{2,\mathbf{x}} - \pi_{2,\mathbf{x}} \varphi_{1,\mathbf{x}}) = \text{const} . \tag{9.33}$$

This is the lattice version of the Gauss constraint from eq. (9.23), provided we set initially the right hand side to zero at all lattice points. If we now evolve the generalized coordinates according to the classical continuous in time Euler-Lagrange or Hamilton equations of motion, the Gauss constraint, eq. (9.33), will be preserved automatically. The question that remains is whether there is a temporal discretization that leads to the preservation of eq. (9.33) after carrying out the numerical integration of the discretized equations of motion. As we show in the next section, there is a scheme based on symplectic discretization.

9.4 Time evolution

To numerically integrate the Abelian-Higgs system with lattice action eq. (9.27) and meet the Gauss constraint, eq. (9.33), everywhere on the lattice, we have discovered that we should use symplectic integrators. To this end we need to switch from a Lagrangian to Hamiltonian description. The Legendre transformation gives us the Hamiltonian of the system

$$H = \sum_i \pi_{f_i} f_i' - L \,, \tag{9.34}$$

which splits into three non-commuting parts[4]

$$H = H_1 + H_2 + H_3 \,, \tag{9.35}$$

each of which contains commuting terms only

$$\begin{aligned} H_1 &= -\frac{\pi_a^2}{12 m_{\rm Pl}^2 N^3} \,, \qquad H_2 = \sum_{\mathbf{x}}^{N^3} \left[\frac{\pi_{1,\mathbf{x}}^2}{2a^2} + \frac{\pi_{2,\mathbf{x}}^2}{2a^2} + e^2 \sum_j^{1,2,3} \frac{\pi_{Aj,\mathbf{x}}^2}{2} \right] \,, \\ H_3 &= \sum_{\mathbf{x}}^{N^3} \Bigg\{ a^4 V_{\mathbf{x}} + \frac{1}{2e^2 b^4} \sum_{i,j}^{1,2,3} [1 - P_{ij,\mathbf{x}}] + \frac{a^2}{2b^2} \sum_j^{1,2,3} \Big[(\varphi_{1,\mathbf{x}+\mathbf{n}_j b}^2 + \varphi_{2,\mathbf{x}+\mathbf{n}_j b}^2) \\ &\qquad + (\varphi_{1,\mathbf{x}}^2 + \varphi_{2,\mathbf{x}}^2) - \Big((\varphi_{1,\mathbf{x}} - i\varphi_{2,\mathbf{x}}) U_{j,\mathbf{x}}^q (\varphi_{1,\mathbf{x}+\mathbf{n}_j b} + i\varphi_{2,\mathbf{x}+\mathbf{n}_j b}) + c.c. \Big) \Big] \Bigg\} \,. \end{aligned} \tag{9.36}$$

The full Hamiltonian governs the evolution of the generalized coordinates and their conjugate momenta

$$\begin{pmatrix} f_i' \\ \pi_{f_i}' \end{pmatrix} = \{\cdot, H\}_{\text{Poisson}} \begin{pmatrix} f_i \\ \pi_{f_i} \end{pmatrix} \,. \tag{9.37}$$

The numerical solution to this system can be made arbitrarily close to the true one if we use a symplectic method of integration that is based on operator splitting techniques [295]

$$\begin{pmatrix} f_i \\ \pi_{f_i} \end{pmatrix}_{(\tau+\Delta\tau)} = \exp[K^{(k)} \Delta\tau] \begin{pmatrix} f_i \\ \pi_{f_i} \end{pmatrix}_{(\tau)} \,, \tag{9.38}$$

where the $k = 2$-nd order operator is of the form

$$\begin{aligned} \exp[K^{(2)}\Delta\tau] &\equiv \exp[K_1 \Delta\tau/2] \exp[K_2 \Delta\tau/2] \exp[K_3 \Delta\tau] \exp[K_2 \Delta\tau/2] \exp[K_1 \Delta\tau/2] \\ &= \exp[\{\cdot, H\}_{\text{Poisson}} \Delta\tau] + \mathcal{O}(\Delta\tau^3) \,, \\ K_i &= \{\cdot, H_i\}_{\text{Poisson}} \,. \end{aligned} \tag{9.39}$$

Higher-order operators can be obtained recursively

$$\begin{aligned} \exp[K^{(k+2)}\Delta\tau] &\equiv \exp[K^{(k)}\Delta\tau/\beta] \exp[K^{(k)}\Delta\tau(1 - 2\beta^{-1})] \exp[K^{(k)}\Delta\tau/\beta] \\ &= \exp[\{\cdot, H\}_{\text{Poisson}} \Delta\tau] + \mathcal{O}(\Delta\tau^{k+3}) \,, \\ \beta &= 2 - 2^{1/(k+1)} \,. \end{aligned} \tag{9.40}$$

[4] We use the usual Poisson brackets to calculate commutators.

Thus, an integrator of arbitrary accuracy requires only the results of the operation of $\exp[K_1\Delta\tau]$, $\exp[K_2\Delta\tau]$, $\exp[K_3\Delta\tau]$ in some particular combination and taking the appropriate values for the time interval $\Delta\tau$. To derive the expressions below, we have made an extensive use of the operator identity for the Abelian-Higgs system: $\exp[K_i\Delta\tau] = 1 + K_i\Delta\tau$ when applied to any f_j or π_{f_j}, eq. (9.38). Thus after acting with $\exp[K_1\Delta\tau/2]$ on all f_j and π_{f_j} we get

$$a \to a - \left(\frac{\Delta\tau}{2}\right)\frac{\pi_a}{6m_{\rm Pl}^2 N^3}\,, \tag{9.41}$$

with the rest of the generalized coordinates and momenta unchanged. After acting with $\exp[K_2\Delta\tau/2]$

$$\begin{aligned}
&\varphi_{1,\mathbf{x}} \to \varphi_{1,\mathbf{x}} + \left(\frac{\Delta\tau}{2}\right)\frac{\pi_{1,\mathbf{x}}}{a^2}\,, \quad \varphi_{2,\mathbf{x}} \to \varphi_{2,\mathbf{x}} + \left(\frac{\Delta\tau}{2}\right)\frac{\pi_{2,\mathbf{x}}}{a^2}\,, \\
&A_{j,\mathbf{x}} \to A_{j,\mathbf{x}} + \left(\frac{\Delta\tau}{2}\right)e^2\pi_{Aj,\mathbf{x}}\,, \quad \pi_a \to \pi_a + \left(\frac{\Delta\tau}{2}\right)\sum_{\mathbf{x}}^{N^3}\left[\frac{\pi_{1,\mathbf{x}}^2}{a^3} + \frac{\pi_{2,\mathbf{x}}^2}{a^3}\right]\,,
\end{aligned} \tag{9.42}$$

with the rest unchanged. Finally, the action of $\exp[K_3\Delta\tau]$ yields

$$\begin{aligned}
\pi_{1,\mathbf{x}} &\to \pi_{1,\mathbf{x}} + \Delta\tau\Bigg\{ - a^4\frac{\partial V_{\mathbf{x}}}{\partial\varphi_{1,\mathbf{x}}} - \frac{6a^2\varphi_{1,\mathbf{x}}}{b^2} + \frac{a^2}{2b^2}\sum_j^{1,2,3}\Bigg[U^q_{j,\mathbf{x}}(\varphi_{1,\mathbf{x}+\mathbf{n}_j b} + i\varphi_{2,\mathbf{x}+\mathbf{n}_j b}) \\
&\qquad + (\varphi_{1,\mathbf{x}-\mathbf{n}_j b} - i\varphi_{2,\mathbf{x}-\mathbf{n}_j b})U^q_{j,\mathbf{x}-\mathbf{n}_j b} + c.c.\Bigg]\Bigg\}\,, \\
\pi_{2,\mathbf{x}} &\to \pi_{2,\mathbf{x}} + \Delta\tau\Bigg\{ - a^4\frac{\partial V_{\mathbf{x}}}{\partial\varphi_{2,\mathbf{x}}} - \frac{6a^2\varphi_{2,\mathbf{x}}}{b^2} + \frac{a^2}{2b^2}\sum_j^{1,2,3}\Bigg[- iU^q_{j,\mathbf{x}}(\varphi_{1,\mathbf{x}+\mathbf{n}_j b} + i\varphi_{2,\mathbf{x}+\mathbf{n}_j b}) \\
&\qquad + i(\varphi_{1,\mathbf{x}-\mathbf{n}_j b} - i\varphi_{2,\mathbf{x}-\mathbf{n}_j b})U^q_{j,\mathbf{x}-\mathbf{n}_j b} + c.c.\Bigg]\Bigg\}\,, \\
\pi_{Aj,\mathbf{x}} &\to \pi_{Aj,\mathbf{x}} + \Delta\tau\Bigg\{\frac{a^2 q}{2b}\Big[i(\varphi_{1,\mathbf{x}} - i\varphi_{2,\mathbf{x}})U^q_{j,\mathbf{x}}(\varphi_{1,\mathbf{x}+\mathbf{n}_j b} + i\varphi_{2,\mathbf{x}+\mathbf{n}_j b}) + c.c.\Big] \\
&\qquad + \frac{1}{2e^2b^3}\sum_l^{1,2,3}\left[iP_{jl,\mathbf{x}} + iP_{lj,\mathbf{x}-\mathbf{n}_l b} + c.c.\right]\Bigg\}\,, \\
\pi_a &\to \pi_a + \Delta\tau\sum_{\mathbf{x}}^{N^3}\Bigg\{ - 4a^3V_{\mathbf{x}} - \frac{a}{b^2}\sum_j^{1,2,3}\Bigg[(\varphi^2_{1,\mathbf{x}+\mathbf{n}_j b} + \varphi^2_{2,\mathbf{x}+\mathbf{n}_j b}) + (\varphi^2_{1,\mathbf{x}} + \varphi^2_{2,\mathbf{x}}) \\
&\qquad - \Big((\varphi_{1,\mathbf{x}} - i\varphi_{2,\mathbf{x}})U^q_{j,\mathbf{x}}(\varphi_{1,\mathbf{x}+\mathbf{n}_j b} + i\varphi_{2,\mathbf{x}+\mathbf{n}_j b}) + c.c.\Big)\Bigg]\Bigg\}\,.
\end{aligned} \tag{9.43}$$

One can check that after each individual step, eq. (9.41) and/or eq. (9.42) and/or (9.43), the lattice version of the Gauss constraint, eq. (9.33), is satisfied exactly. Hence, no matter the order of the time integrator,

k, the Gauss constraint is always met to machine precision everywhere on the lattice[5]. To be physically consistent, we need to make sure that the constant on the right hand side in eq. (9.33) is set to zero initially. Initial conditions from inflation for reheating lattice simulations are discussed in the next section.

9.5 Initial conditions in $A_0 = 0$ gauge

In the standard lore the Universe is dominated by the homogeneous inflaton field during and shortly after the end of inflation. All existing particles can be viewed as small fluctuations on top of this background. If we assume that the inflaton is the real part of the Higgs field in the Abelian-Higgs model (i.e., slow-roll inflation happens along the real axis in field space, towards the minimum of the Higgs potential), then at the beginning of our simulations of preheating, the initial form of the 'fields' on the lattice should be

$$\begin{aligned} &\varphi_{1,\mathbf{x}} = \bar{\varphi}_1 + \delta\varphi_{1,\mathbf{x}}\,, \quad \varphi_{2,\mathbf{x}} = \delta\varphi_{2,\mathbf{x}}\,, \quad \pi_{1,\mathbf{x}} = \bar{\pi}_1 + \delta\pi_{1,\mathbf{x}}\,, \\ &\pi_{2,\mathbf{x}} = \delta\pi_{2,\mathbf{x}}\,, \quad a = 1\,, \quad \pi_a = -2\sqrt{3} m_{\rm Pl} N^3 \sqrt{\frac{H_2 + H_3}{N^3}}\,, \end{aligned} \tag{9.44}$$

where the choice for the initial value of the scale factor is arbitrary, whereas the expression for π_a is just the Friedmann equation relating the Hubble parameter and the mean energy density, rewritten in terms of our generalized coordinates. In fact, we use this expression to check the 'energy conservation' of our integrators; we observe deviations that scale correctly with the size of the time step – $\mathcal{O}(\Delta\tau^k)$ for k-th order integrators, in agreement with eq. (9.40).

The Fourier conventions we are going to use on the lattice are

$$f_{i,\mathbf{x}} = \sum_{\mathbf{k}} e^{i\mathbf{k}\cdot\mathbf{x}} \tilde{f}_{i,\mathbf{k}}\,, \quad \tilde{f}_{i,\mathbf{k}} = \frac{1}{N^3} \sum_{\mathbf{x}} e^{-i\mathbf{k}\cdot\mathbf{x}} f_{i,\mathbf{x}}\,, \tag{9.45}$$

implying $\tilde{f}_{i,\mathbf{k}} = \tilde{f}^*_{i,-\mathbf{k}}$ if $f_{i,\mathbf{x}}$ is real. The initial fluctuations for each lattice field can be expanded in terms of Fourier modes, which in turn can be written in terms of mode functions and 'stochastic' complex numbers to account for the quantum nature of the fluctuations (cf., e.g., Section 8.5 for the specific forms of the Fourier

[5]We stress that this is true only for Abelian fields. If one repeats the same analysis for a charged scalar field coupled to a non-Abelian gauge field, the lattice version of the Gauss constraint is not respected by the symplectic integrator.

modes)

$$
\begin{aligned}
\delta\varphi_{1,\mathbf{x}} &= \frac{(2\pi)^{3/2}}{L_{\rm lat}^{3/2}}\sum_{\mathbf{k}} e^{i\mathbf{k}\cdot\mathbf{x}}\delta\varphi_{1,\mathbf{k}} = \frac{(2\pi)^{3/2}}{L_{\rm lat}^{3/2}}\sum_{\mathbf{k}} e^{i\mathbf{k}\cdot\mathbf{x}}\Big[a^1_{\mathbf{k}}u^1_k + a^{1*}_{-\mathbf{k}}u^{1*}_k\Big]\,, \qquad \delta\varphi_{2,\mathbf{x}} = 0\,,\\
\delta\pi_{1,\mathbf{x}} &= \frac{(2\pi)^{3/2}}{L_{\rm lat}^{3/2}}\sum_{\mathbf{k}} e^{i\mathbf{k}\cdot\mathbf{x}}\delta\pi_{1,\mathbf{k}} = \frac{(2\pi)^{3/2}}{L_{\rm lat}^{3/2}}\sum_{\mathbf{k}} e^{i\mathbf{k}\cdot\mathbf{x}}\Big[a^1_{\mathbf{k}}u^{1\prime}_k + a^{1*}_{-\mathbf{k}}u^{1*\prime}_k\Big]\,,\\
\delta\pi_{2,\mathbf{x}} &= q\bar\varphi_1 G_{0,\mathbf{x}} = \frac{(2\pi)^{3/2}}{L_{\rm lat}^{3/2}}\sum_{\mathbf{k}} e^{i\mathbf{k}\cdot\mathbf{x}}\delta\pi_{2,\mathbf{k}} = q\bar\varphi_1\frac{(2\pi)^{3/2}}{L_{\rm lat}^{3/2}}\sum_{\mathbf{k}} e^{i\mathbf{k}\cdot\mathbf{x}}\Big[a^L_{\mathbf{k}}G_{0\mathbf{k}} + a^{L*}_{-\mathbf{k}}G^*_{0-\mathbf{k}}\Big]\,,\\
A_{j,\mathbf{x}} &= \frac{(2\pi)^{3/2}}{L_{\rm lat}^{3/2}}\sum_{\mathbf{k}} e^{i\mathbf{k}\cdot\mathbf{x}}\sum_{\lambda}^{L,T\pm}\epsilon^\lambda_{j\mathbf{k}}A^\lambda_{\mathbf{k}} = \frac{(2\pi)^{3/2}}{L_{\rm lat}^{3/2}}\sum_{\mathbf{k}} e^{i\mathbf{k}\cdot\mathbf{x}}\sum_{\lambda}^{L,T\pm}\epsilon^\lambda_{j\mathbf{k}}\Big[a^\lambda_{\mathbf{k}}G^\lambda_k + a^{\lambda*}_{-\mathbf{k}}G^{\lambda*}_k\Big]\,,\\
\pi_{Aj,\mathbf{x}} &= \frac{(2\pi)^{3/2}}{L_{\rm lat}^{3/2}}\sum_{\mathbf{k}} e^{i\mathbf{k}\cdot\mathbf{x}}\sum_{\lambda}^{L,T\pm}\epsilon^\lambda_{j\mathbf{k}}\pi^\lambda_{A\mathbf{k}} = \frac{(2\pi)^{3/2}}{L_{\rm lat}^{3/2}}\frac{1}{e^2}\sum_{\mathbf{k}} e^{i\mathbf{k}\cdot\mathbf{x}}\Bigg\{\sum_{\lambda}^{T\pm}\epsilon^\lambda_{j\mathbf{k}}\Big[a^\lambda_{\mathbf{k}}G^{\lambda\prime}_k + a^{\lambda*}_{-\mathbf{k}}G^{\lambda*\prime}_k\Big]\\
&\quad + \epsilon^L_{j\mathbf{k}}\Big[a^L_{\mathbf{k}}\left(G^{L,\rm corr\prime}_{\mathbf{k}} + \frac{\boldsymbol{\kappa}_{\mathbf{k}}\cdot\boldsymbol{\kappa}_{\mathbf{k}}}{\sqrt{\boldsymbol{\kappa}_{\mathbf{k}}\cdot\boldsymbol{\kappa}^*_{\mathbf{k}}}}G_{0\mathbf{k}}\right) + a^{L*}_{-\mathbf{k}}\left(G^{L,\rm corr\prime *}_{-\mathbf{k}} + \frac{\boldsymbol{\kappa}^*_{-\mathbf{k}}\cdot\boldsymbol{\kappa}^*_{-\mathbf{k}}}{\sqrt{\boldsymbol{\kappa}^*_{-\mathbf{k}}\cdot\boldsymbol{\kappa}_{-\mathbf{k}}}}G^*_{0-\mathbf{k}}\right)\Big]\Bigg\}\,,\\
G^{L,\rm corr\prime}_{\mathbf{k}} &= -\frac{\boldsymbol{\kappa}_{\mathbf{k}}\cdot\boldsymbol{\kappa}_{\mathbf{k}}}{\sqrt{\boldsymbol{\kappa}_{\mathbf{k}}\cdot\boldsymbol{\kappa}^*_{\mathbf{k}}}}G_{0\mathbf{k}} - \frac{\frac{L_{\rm lat}^{3/2}}{(2\pi)^{3/2}}}{2a^L_{\mathbf{k}}}\frac{\tilde j_{0\mathbf{k}}}{\frac{\boldsymbol{\kappa}_{\mathbf{k}}\cdot\boldsymbol{\kappa}_{\mathbf{k}}}{\sqrt{\boldsymbol{\kappa}_{\mathbf{k}}\cdot\boldsymbol{\kappa}^*_{\mathbf{k}}}}}\,, \quad \tilde j_{0\mathbf{k}} = \frac{1}{N^3}\sum_{\mathbf{x}} e^{-i\mathbf{k}\cdot\mathbf{x}}(\bar\varphi_1 + \delta\varphi_{1,\mathbf{x}})\bar\varphi_1 q^2e^2G_{0,\mathbf{x}}\,.
\end{aligned}
\tag{9.46}
$$

The 'stochastic' complex numbers which are the classical counterpart of the quantum creation and annihilation operators take the following values

$$
|a_{i,\mathbf{k}}| = \sqrt{-\ln\left(X_{i,\mathbf{k}}\right)/2}\,, \quad \arg\left(a_{i,\mathbf{k}}\right) = 2\pi Y_{i,\mathbf{k}}\,,
\tag{9.47}
$$

where $X_{i,\mathbf{k}}$ is a uniform deviate on $(0,1)$ and $Y_{i,\mathbf{k}}$ is a uniform deviate on $[0,1)$. For the mode functions, we use the analytic expressions, cf., e.g., Section 8.3.2,

$$
\begin{gathered}
G^{T\pm}_k = \frac{1}{\sqrt{2}(k^2+k_C^2)^{1/4}}\exp\left(-i\sqrt{k^2+k_C^2}\tau\right)\,, \quad G^L_k = \frac{(k^2+k_C^2)^{1/4}}{\sqrt{2}k_C}\exp\left(-i\sqrt{k^2+k_C^2}\tau\right)\,,\\
u^1_k = \frac{\exp\left(-i\sqrt{k^2+(\partial^2/\partial\varphi_1^2)V}\tau\right)}{\sqrt{2}\left(k^2+(\partial^2/\partial\varphi_1^2)V\right)^{1/4}}\,,
\end{gathered}
\tag{9.48}
$$

which describe well the modes of interest, i.e., subhorizon modes, $k \gg \mathcal{H}$, at the end of inflation, irrespective of the coupling strength, or in other words the value of the Compton wavenumber, $k_C = qe\bar\varphi_1$. The normalization factor of $(2\pi)^{3/2}/L_{\rm lat}^{3/2}$ in eq. (9.46) is necessary to make the initial two-point function, averaged over the lattice, independent of the lattice size, $L_{\rm lat} = Nb$, and equal to the continuous one, cf.,

e.g., [74]. Finally, the transverse and longitudinal polarization vectors on the lattice[6] are

$$\boldsymbol{\epsilon}^{T\pm}_{\mathbf{k}} = \frac{[-(\boldsymbol{\kappa}_{\mathbf{k}})^*_x(\boldsymbol{\kappa}_{\mathbf{k}})_z \pm i(\boldsymbol{\kappa}_{\mathbf{k}})_y\sqrt{\boldsymbol{\kappa}_{\mathbf{k}}\cdot\boldsymbol{\kappa}^*_{\mathbf{k}}},\ -(\boldsymbol{\kappa}_{\mathbf{k}})^*_y(\boldsymbol{\kappa}_{\mathbf{k}})_z \mp i(\boldsymbol{\kappa}_{\mathbf{k}})_x\sqrt{\boldsymbol{\kappa}_{\mathbf{k}}\cdot\boldsymbol{\kappa}^*_{\mathbf{k}}},\ \boldsymbol{\kappa}_{\mathbf{k}}\cdot\boldsymbol{\kappa}^*_{\mathbf{k}} - (\boldsymbol{\kappa}_{\mathbf{k}})_z(\boldsymbol{\kappa}_{\mathbf{k}})^*_z]^T}{\sqrt{2\boldsymbol{\kappa}_{\mathbf{k}}\cdot\boldsymbol{\kappa}^*_{\mathbf{k}}(\boldsymbol{\kappa}_{\mathbf{k}}\cdot\boldsymbol{\kappa}^*_{\mathbf{k}} - (\boldsymbol{\kappa}_{\mathbf{k}})_z(\boldsymbol{\kappa}_{\mathbf{k}})^*_z)}}\,,$$
$$\boldsymbol{\epsilon}^{L}_{\mathbf{k}} = \frac{-i\boldsymbol{\kappa}_{\mathbf{k}}}{\sqrt{\boldsymbol{\kappa}_{\mathbf{k}}\cdot\boldsymbol{\kappa}^*_{\mathbf{k}}}}\,, \tag{9.50}$$

where

$$\boldsymbol{\kappa}_{\mathbf{k}} = e^{-i\mathbf{k}b/2}\frac{\sin(\mathbf{k}b/2)}{b/2}\,. \tag{9.51}$$

The last expression comes from our choice of forward finite differencing of the spatial derivatives. For instance, with central finite differencing, eq. (8.104), we do not have the complex exponent. The polarization vectors obey the usual identities

$$\begin{gathered}\boldsymbol{\epsilon}^{L}_{\mathbf{k}} = \boldsymbol{\epsilon}^{*L}_{-\mathbf{k}}\,,\quad \boldsymbol{\epsilon}^{*L}_{\mathbf{k}}\cdot\boldsymbol{\epsilon}^{L}_{\mathbf{k}} = 1\,,\quad i\boldsymbol{\kappa}_{\mathbf{k}}\cdot\boldsymbol{\epsilon}^{L}_{\mathbf{k}} = \frac{\boldsymbol{\kappa}_{\mathbf{k}}\cdot\boldsymbol{\kappa}_{\mathbf{k}}}{\sqrt{\boldsymbol{\kappa}_{\mathbf{k}}\cdot\boldsymbol{\kappa}^*_{\mathbf{k}}}}\,,\quad i\boldsymbol{\kappa}_{\mathbf{k}}\times\boldsymbol{\epsilon}^{L}_{\mathbf{k}} = \mathbf{0}\,,\\ \boldsymbol{\epsilon}^{T\pm}_{\mathbf{k}} = \boldsymbol{\epsilon}^{*T\pm}_{-\mathbf{k}},\quad \boldsymbol{\epsilon}^{*T\lambda'}_{\mathbf{k}}\cdot\boldsymbol{\epsilon}^{T\lambda}_{\mathbf{k}} = \delta^{\lambda'\lambda}\,,\quad i\boldsymbol{\kappa}_{\mathbf{k}}\cdot\boldsymbol{\epsilon}^{T\pm}_{\mathbf{k}} = 0\,,\quad \boldsymbol{\kappa}^*_{-\mathbf{k}} = -\boldsymbol{\kappa}_{\mathbf{k}}\,,\end{gathered} \tag{9.52}$$

which reduce to

$$\begin{gathered}\boldsymbol{\epsilon}^{L}_{\mathbf{k}} = \boldsymbol{\epsilon}^{*L}_{-\mathbf{k}}\,,\qquad \boldsymbol{\epsilon}^{*L}_{\mathbf{k}}\cdot\boldsymbol{\epsilon}^{L}_{\mathbf{k}} = 1\,,\qquad i\mathbf{k}\cdot\boldsymbol{\epsilon}^{L}_{\mathbf{k}} = k\,,\qquad i\mathbf{k}\times\boldsymbol{\epsilon}^{L}_{\mathbf{k}} = \mathbf{0}\,,\\ \boldsymbol{\epsilon}^{T\pm}_{\mathbf{k}} = \boldsymbol{\epsilon}^{*T\pm}_{-\mathbf{k}},\qquad \boldsymbol{\epsilon}^{*T\lambda'}_{\mathbf{k}}\cdot\boldsymbol{\epsilon}^{T\lambda}_{\mathbf{k}} = \delta^{\lambda'\lambda}\,,\qquad i\mathbf{k}\cdot\boldsymbol{\epsilon}^{T\pm}_{\mathbf{k}} = 0,\end{gathered} \tag{9.53}$$

in the continuous limit $\lim_{b\to 0}\boldsymbol{\kappa}_{\mathbf{k}} = \mathbf{k}$. These expressions can be quite useful when switching from the continuum description to the lattice description, e.g., the familiar result from Section 8.2.3, $G_{0k} = -k(G^L_k)'/(k^2+k_C^2)$, becomes

$$G_{0\mathbf{k}} = \frac{-\frac{\boldsymbol{\kappa}_{\mathbf{k}}\cdot\boldsymbol{\kappa}_{\mathbf{k}}}{\sqrt{\boldsymbol{\kappa}_{\mathbf{k}}\cdot\boldsymbol{\kappa}^*_{\mathbf{k}}}}(G^L_k)'}{\left(\frac{\boldsymbol{\kappa}_{\mathbf{k}}\cdot\boldsymbol{\kappa}_{\mathbf{k}}}{\sqrt{\boldsymbol{\kappa}_{\mathbf{k}}\cdot\boldsymbol{\kappa}^*_{\mathbf{k}}}}\right)^2 + k_C^2}\,, \tag{9.54}$$

on the grid. This accounts for the form of the $\boldsymbol{\kappa}_{\mathbf{k}}$ terms in the last two lines in eq. (9.46).

The 'z-helicity' polarization vectors from eqs. (9.49,9.50) are singular when $k^2 = k_z^2$. In this case, the simple solution is to use 'x-helicity' and/or 'y-helicity' basis instead[7]. We should also point out that the transverse polarization vectors on the lattice, eq. (9.50), are not actually of definite helicity[8], i.e.,

$$i\boldsymbol{\kappa}_{\mathbf{k}}\times\boldsymbol{\epsilon}^{T\pm}_{\mathbf{k}} \neq \pm\sqrt{\boldsymbol{\kappa}_{\mathbf{k}}\cdot\boldsymbol{\kappa}^*_{\mathbf{k}}}\boldsymbol{\epsilon}^{T\pm}_{\mathbf{k}}\,,\quad \boldsymbol{\epsilon}^{T\pm}_{\mathbf{k}} \neq \boldsymbol{\epsilon}^{T\mp *}_{\mathbf{k}}\,. \tag{9.55}$$

However,

$$i\boldsymbol{\kappa}_{\mathbf{k}}\times\boldsymbol{\epsilon}^{T\pm *}_{\mathbf{k}} = \mp\sqrt{\boldsymbol{\kappa}_{\mathbf{k}}\cdot\boldsymbol{\kappa}^*_{\mathbf{k}}}\boldsymbol{\epsilon}^{T\mp}_{\mathbf{k}}\,, \tag{9.56}$$

[6] Their continuous counterparts are

$$\boldsymbol{\epsilon}^{T\pm}_{\mathbf{k}} = \frac{[-k_xk_z \pm ik_yk\,,\ -k_yk_z \mp ik_xk\,,\ k^2-k_z^2]^T}{\sqrt{2k^2(k^2-k_z^2)}}\,,\quad \boldsymbol{\epsilon}^{L}_{\mathbf{k}} = -i\frac{\mathbf{k}}{k}\,. \tag{9.49}$$

[7] If $k=0$, the concept of helicity breaks down, but the homogeneous vector fields are still well-defined.

[8] In the continuum, $b\to 0$ or eq. (9.49), there are no such problems, $i\mathbf{k}\times\boldsymbol{\epsilon}^{T\pm}_{\mathbf{k}} = \pm k\boldsymbol{\epsilon}^{T\pm}_{\mathbf{k}}$, $\boldsymbol{\epsilon}^{T\pm}_{\mathbf{k}} = \boldsymbol{\epsilon}^{T\mp *}_{\mathbf{k}}$.

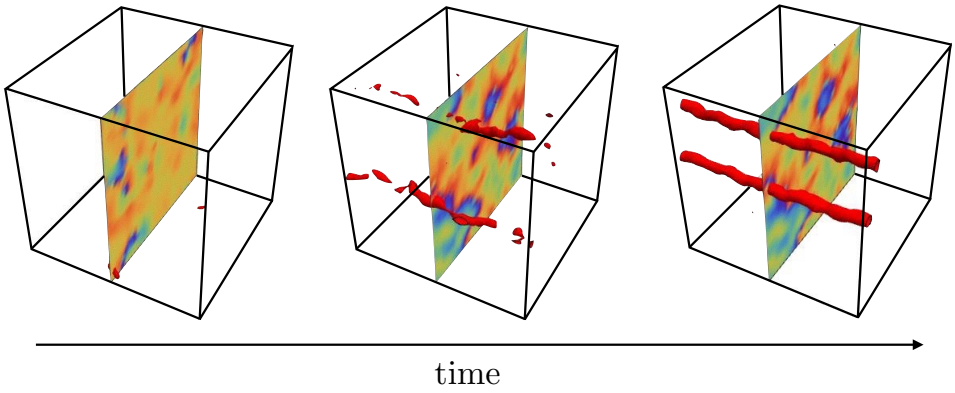

Figure 9.1: Formation of cosmic strings after a non-thermal phase transition during preheating. The boxes are from a representative simulation, using our new algorithm, accounting for the expansion of the Universe self-consistently. In each panel, we plot the complex phase of the Higgs field on a vertical slice through the box (from 0 (blue) to 2π (red)). The red contours are drawn around regions of magnetic field energy density $\geq 7\times$ the mean. During inflation, we assume the inflaton rolls slowly down the real axis of a symmetry breaking potential of the form $V = \lambda(|\varphi|^2 - v^2)^2/4$, near the origin and flatter away from it. We choose the symmetry breaking scale to be much smaller than the value of the inflaton at the end of inflation, $v \ll |\varphi_{\text{end}}|$. Thereby, the initial oscillations of the condensate lead to resonant particle production, cf. Section 8.4, whose back-reaction temporarily restores the symmetry [20, 21]. As the Universe expands, the energy in the excited particles is redshifted and eventually (within about 1 e-fold of expansion for $v \sim 10^{-2}|\varphi_{\text{end}}|$) the symmetry is spontaneously broken, and cosmic strings form. The out-of-equilibrium phase transition happens at some point between the first and the second panel. At that time, the physical size of the box is about half of the Hubble radius. We observe the formation of a pair of strings of opposite topological charge (this is due to our choice of initial conditions) which stretch across the box for the remainder of the simulation, cf. third panel. In fact, plotting the regions of non-zero winding number, instead of magnetic field over-densities, reveals many more open strings and loops in the second panel, which rapidly disappear due to gauge and Higgs radiation [298].

holds, just like $i\mathbf{k} \times \boldsymbol{\epsilon}_{\mathbf{k}}^{T\pm *} = \mp k \boldsymbol{\epsilon}_{\mathbf{k}}^{T\mp}$, for eq. (9.49). Hence, even though $\boldsymbol{\epsilon}_{\mathbf{k}}^{T\pm}$ on the lattice are not of definite helicity, they still describe hermitian, mutually orthogonal, transverse modes and can be used in the Fourier mode expansion of the gauge fields. To make them of definite helicity, we need to use central finite differencing, rather than forward which is possible and can be done if needed, but leads to more cumbersome expressions in general.

The initial conditions presented here, make the constant in the right hand side in eq. (9.33) vanish everywhere on the lattice, which is necessary for our algorithm to yield physically consistent results.

9.6 Conclusions

We have derived a novel algorithm for the computation of the non-linear classical dynamics in the Abelain-Higgs system in FRW spacetime. The symplectic integrator satisfies the consistency relations (Gauss constraint) to machine precision, while the expansion of the Universe is included self-consistently. Furthermore, the order of the integrator can be arbitrarily high.

We have carried out a number of small scale simulations, $N^3 = 128^3$, to test the robustness of our scheme. For instance, we have observed the formation of cosmic strings from non-thermal phase transitions at the end of inflation, cf. Fig. 9.1. The Gauss constraint is violated at levels less than $\mathcal{O}(10^{-10})$ at each

point on the lattice, whereas the violation of the Friedmann equation, $\mathcal{H} = a\bar{\rho}/\sqrt{3m_{\rm Pl}}$, scales as expected, cf. eq. (9.40), with the order of the integrator and the time step, $\mathcal{O}(\Delta\tau^k)$.

The algorithm we have presented can be readily generalized to a system of multiple charged scalar fields interacting with each other and with multiple gauge fields through the covariant derivative coupling. Although, not shown here, the series of Gauss constraints are still satisfied exactly. The scheme performs equally well in the cases of a fixed FRW background, i.e., when the evolution of the scale factor is set to some constant power-law, e.g., $a \propto \tau^2$ for a matter dominated Universe, $a \propto \tau$ for a radiation dominated Universe, or simply $a =$ const if we wish to ignore expansion[9].

Thanks to the self-consistent computation of the expansion history, we can now study how the formation of various non-linear objects affects the post-inflationary equation of state parameter and thereby the interpretation of inflationary observables, cf. Chapter 6. For reliable results, we shall need to carry out simulations with sufficiently large dynamical range. E.g., to study the formation and evolution of cosmic string networks and their effect on the expansion history, we need to consider much bigger boxes, $N^3 = 1024^3$, to capture at least five Hubble radii at the time of the phase transition – the box size in Fig. 9.1 is $N^3 = 128^3$ and corresponds to only half of the Hubble radius at the phase transition. Formation of oscillons coupled to gauge fields is also particularly interesting in the context of the post-inflationary expansion history. Oscillons behave as pressureless dust and can lead to long periods of matter dominated expansion [36]. However, if there is a decay channel to gauge fields, e.g., through the covariant derivative coupling in the Abelian-Higgs system, oscillons could transfer their energy rapidly into radiation. It is not clear, if the transition to radiation domination is faster or slower than in the case of a homogeneously oscillating condensate, resonantly amplifying gauge fields. To address the physical question of whether charged oscillons speed-up or slow-down the approach to a radiation-dominated Universe, we again need large simulation boxes. The IR cut-off is set by the copious production of low-momentum inflatons due to self-resonance which eventually leads to the fragmentation of the condensate into oscillons [36]. The subsequent oscillon decays produce high-momentum gauge fields, making us reach the resolution threshold quickly for $N^3 = 128^3$, 256^3. To improve the resolution, while keeping the IR-cut off fixed, we again need to go to at least $N^3 = 1024^3$. Simulations of this size and reasonable energy conservation for both cosmic strings and oscillons cost at least about 5000 CPU hours and need to be run on large clusters. We are currently working towards achieving this goal. The current version of the code can be used to study the details of the non-linear dynamics in the simpler scenario in which the inflaton does not form any non-linear long-lived objects, but resonantly decays into gauge fields which eventually backreact, leading to the complete fragmentation of the condensate. This will be a natural continuation of the linear analysis in Chapter 8 and it will be interesting to test the usual approximation of a gauge field by three massless scalar fields during preheating, especially given the difference in the initial conditions from inflation, as well as in the non-adiabatic production rate, of the longitudinal and transverse modes.

Possible extensions to the algorithm, which should not affect its performance, include the addition of terms like $f(|\varphi|)R$ and $f(|\varphi|)F^2$ to the Lagrangian. The latter are known for successful magnetogenesis scenarios from reheating [95, 96], but no one has predicted the effect of non-linear dynamics in them. The link variables we are using, allow us to add fermions as well [299]. This opens up a whole new series of models that can be studied. A very intriguing one is reheating after Higgs-inflation [23, 24] for which we know all relevant parameters. One should be in principle able to compute the expansion

[9] In the case of Minkowski spacetime, the relevant consistency relation whose violation scales as $\mathcal{O}(\Delta\tau^k)$ is the conservation of the total energy in the box.

history of the early Universe without any assumptions. However, the complicated particle production after Higgs-inflation (known as *combined preheating* [25]) is strongly affected by the expansion of the Universe – this is the main reason why all analyses deal with the linear regime only and stop short of seeing the full fragmentation of the system. The non-linear dynamics can be calculated with our algorithm, since it is well-suited for self-consistent expansion computations. In principle the non-Abelian terms do not allow us to apply our algorithm and maintain the Gauss constraint to machine precision for arbitrary order of the symplectic time integrator. Nevertheless, there is an indication that non-Abelian non-linear terms might become subdominant [26] and hence, it might be possible that our algorithm still gives reliable results even in this case. At the very least, we can reduce the leading order of the time integrator and in the same time reduce the order of the time step to get reasonable answers. This needs to be tested in detail.

Part IV

Conclusions

Chapter 10

Retrospect

This thesis is a collection of works on the period of reheating after inflation motivated by both cosmological observations and theoretical considerations. In the thesis, we focused on different aspects of reheating including how long it took the universe to reach a radiation-dominated state of expansion, an investigation into a mechanism of generating the matter-antimatter asymmetry and the non-perturbative production of gauge fields sourced by an inflaton charged under global and local symmetries.

We began this thesis with a brief introduction to cosmic inflation (Chapter 1), including a discussion of the problems it resolves and the predictions it makes for the observable universe. We then concentrated on the end of inflation with a review of our current understanding of reheating, beginning with an outline of the different stages of the process, followed by a survey of the different mechanisms for particle production (Chapters 2 & 3) and finally covering the challenges we face in trying to constrain reheating experimentally and observationally (Chapters 4 & 5).

We then considered the effects of non-linear dynamics on the post-inflationary expansion history in a broad class of observationally-favoured single-field models of inflation (Chapter 6). All models with an inflaton potential that is shallower than quadratic away from its minimum fall into this class. If the inflaton's effective mass remains much smaller than the Hubble scale for sufficiently long times after the end of infation, non-perturbative particle production can become effective and non-linear effects important. If the inflaton potential has a quadratic minimum, the inflaton can fragment into long-lived non-linear structures known as oscillons which behave as pressureless dust. For steeper minima, non-perturbative particle production always becomes important eventually because the Hubble scale decays faster than the effective mass. In these cases, non-linear dynamics drives the equation of state of the universe to $1/3$ even in the absence of couplings to other fields. We estimated the duration to radiation domination analytically and confirmed the estimate with detailed numerical simulations. In the non-quadratic minima case, couplings to additional light-enough fields can only decrease the duration to radiation domination. Under the stated assumptions, the results from our work reduce the uncertainties in the expansion history of reheating and thus reduce the theoretical uncertainties in predictions for inflationary observables such as the spectral index, $n_{\rm s}$, and the tensor-to-scalar ratio, r (see Fig. 6.17). We also discussed other observational aspects of the non-linear dynamics such as the generation of stochastic gravitational wave backgrounds, the formation of primordial black holes and bounds on the reheating temperature.

In the remainder of this thesis we investigated the non-perturbative particle production after inflation in models with physically-motivated inflaton interactions. We began with a study of the effects of the

non-linear dynamics after inflation in a model with a charged inflaton under a global $U(1)$ symmetry, weakly broken by a small, technically-natural, term (Chapter 7). Previous studies of this model [38, 41], ignoring non-linear effects, have shown that the dynamics at the end of inflation can generate an asymmetry between the number of inflatons and anti-inflatons which can be then transferred into the observed matter-antimatter asymmetry in our universe if we allow for the inflatons to decay into baryons. We showed that including non-linear dynamics changes the prediction for the inflaton number asymmetry, but that there still exists a parameter range in which the model successfully accommodates the observed baryon-to-photon ratio, η (see eq. (7.58)).

In Chapter 8, we considered the particle production during and after inflation, until non-linear effects become relevant, in models with a charged inflaton under Abelian, $U(1)$, and non-Abelian, $SU(2)$ and $U(1) \times SU(2)$, gauge symmetries. We showed that the transverse and longitudinal gauge modes can be resonantly amplified, at similar rates (see Fig. 8.2), resolving minor points of confusion in the literature [28, 93]. We also found that the magnitude of the generated magnetic fields and charge perturbations on large scales to be below the current observational bounds. The results for the linearized evolution of the fields can be then used as initial conditions for lattice studies of the subsequent non-linear dynamics. In the last chapter in this part of the thesis (Chapter 9), we presented a novel algorithm for evolving the full set of coupled non-linear equations of motion on an expanding lattice, with gravity included at the background level in models with a charged inflaton under a local $U(1)$ symmetry. The main benefit of the algorithm is that the appropriately discretized gauge constraints are satisfied to machine-precision even as the the time-integrator can be of arbitrary high order. We presented a preliminary study of the formation of Abelian cosmic strings after inflation.

Chapter 11

Prospect

The work presented in this dissertation has many possible extensions, some of which we hope to address in the future. The generalized results for the post-inflationary expansion history and the duration to radiation domination from Chapter 6 hold for the broad class of observationally-favoured models. This study should be followed by an investigation in a different direction. For example, in the case where the inflaton is massive and fragments into oscillons (or other localized structures), there is a need to include perturbative and non-perturbative decay to other fields to ensure completion of reheating. In the case where the decay is to gauge fields, we can use the numerical method from Chapter 9. Another important result from Chapter 6 for the massless inflaton models is the unexpected emergence of transient objects, similar to oscillons in energy, but much less stable. It will be interesting to see if they have any consequences for the prediction of the matter-antimatter asymmetry in models, like the one with oscillons described in Chapter 7, or if during their decay they can form primordial black holes, or give rise to an interesting gravitational wave signature.

A natural continuation to the linear analyses of gauge field production during preheating (Chapter 8) will be the employment of the novel numerical technique, presented in Chapter 9, to study the ensuing non-linear dynamics. The algorithm can be also used to examine the effects of not only oscillons coupled to gauge fields, but also of other solitonic objects such as cosmic strings and Q-balls, on the expansion history of the Universe and therefore on the uncertainty in inflationary observables. Among the many other possible applications of the code is the investigation of the non-linear dynamics after Higgs-inflation where the inflaton is played by a non-minimally coupled Standard Model Higgs field and the reheating of the Universe happens directly without the need for any additional physics in the form of intermediaries.

By examining the dynamics in realistic models of reheating, we can tie together the well-understood and well-tested high-energy physics from laboratory experiments and the more speculative physics of inflation. We can determine not only how the Universe was populated with ordinary matter, but also the origin (and perhaps the nature and the fundamental properties of) cosmic relics such as dark matter, the baryon asymmetry, stochastic gravitational wave backgrounds, etc. The study of ever-more realistic models of reheating has been successful in recent years, and this looks set to continue. With the upcoming Stage-4 CMB experiments set to provide superb data to constrain further inflationary observables [117], understanding reheating-related uncertainties will become increasingly important for narrowing the range of viable models of inflation. We hope and expect that reheating will continue to be at the forefront of research in theoretical cosmology in the coming years.

Appendices

Appendix A

"Linearized" asymmetry calculation

We can use the linearized equations of motion for $u_n^J(t,k)$ to calculate the inflaton asymmetry (see Chapter 7) up to the point where the nonlinearities become important. Recall that

$$A_\phi(t) = i\frac{m}{\bar{\rho}_\phi(t)a^3(t)V_{\rm com}}\int d^3\mathbf{x}a^3\left[\phi^*\dot{\phi}-\phi\dot{\phi}^*\right]. \tag{A.1}$$

We can also write these expressions in terms of the real and imaginary parts of the field (see eq. (7.18)):

$$A_\phi(t) = \frac{m}{a^3(t)\bar{\rho}_\phi(t)V_{\rm com}}\int d^3\mathbf{x}a^3\left[\dot{\varphi}^1\varphi^2-\dot{\varphi}^2\varphi^1\right]. \tag{A.2}$$

Dividing the field into a homogeneous background and perturbations $\varphi^J(t,\mathbf{x}) = \bar{\varphi}^J(t)+\delta\varphi^J(t,\mathbf{x})$, the asymmetry can then be written as

$$A_\phi(t) = \bar{A}_\phi(t)+\delta A_\phi(t), \tag{A.3}$$

where

$$\begin{aligned}
\bar{A}_\phi(t) &= \frac{m}{\bar{\rho}_\phi(t)}\left[\dot{\bar{\varphi}}^1(t)\bar{\varphi}^2(t)-\dot{\bar{\varphi}}^2(t)\bar{\varphi}^1(t)\right],\\
\delta A_\phi(t) &= \frac{m}{\bar{\rho}_\phi(t)V_{\rm com}}\int d^3\mathbf{x}\left[\delta\dot{\varphi}^1(\mathbf{x},t)\delta\varphi^2(\mathbf{x},t)-\delta\dot{\varphi}^2(\mathbf{x},t)\delta\varphi^1(\mathbf{x},t)\right],\\
&= \frac{m}{2\bar{\rho}_\phi(t)V_{\rm com}}\int d^3\mathbf{x}d^3\mathbf{k}d^3\mathbf{q}e^{-i(\mathbf{k}-\mathbf{q})\cdot\mathbf{x}}\left[\delta\dot{\varphi}^{1*}_{\mathbf{k}}(t)\delta\varphi^2_{\mathbf{q}}(t)-\delta\dot{\varphi}^{2*}_{\mathbf{k}}(t)\delta\varphi^1_{\mathbf{q}}(t)+\text{c.c}\right].
\end{aligned} \tag{A.4}$$

In the second line, there are no terms linear in $\delta\varphi$, since we assume that $\int d^3\mathbf{x}\delta\varphi = 0$. In the last step by adding the complex conjugate we make the "reality" of $A_\phi(t)$, which follows from the reality of φ^J, manifest.

Using the correlator in eq. (7.36), as well as

$$\langle\delta\dot{\hat{\varphi}}^I_{\mathbf{k}}(t)\delta\hat{\varphi}^{J\dagger}_{\mathbf{q}}(t)\rangle = \delta(\mathbf{k}-\mathbf{q})\sum_{n=1}^{2}\dot{u}^I_n(t,k)u^{J*}_n(t,k). \tag{A.5}$$

the expectation value of the asymmetry operator $\delta\hat{A}_\phi$ is given by

$$\begin{aligned}\langle\delta\hat{A}_\phi(t)\rangle &= (2\pi)^3\frac{m}{\bar{\rho}_\phi(t)}\sum_{n=1}^{2}\int d\ln k\frac{k^3}{2\pi^2}\left[\dot{u}_n^1(t,k)u_n^{2*}(t,k)-\dot{u}_n^2(t,k)u_n^{1*}(t,k)+\text{c.c}\right],\\ &= \frac{m}{2\bar{\rho}_\phi(t)}\sum_{n=1}^{2}\int\frac{d\ln k}{2\pi^2}\frac{k^2}{a(t_{\text{in}})^2}\Big[\{\dot{f}_n^1(t,k)-H(t_{\text{in}})\dot{g}_n^1(t,k)\}\{f_n^2(t,k)-H(t_{\text{in}})g_n^2(t,k)\}\\ &\quad+\frac{k^2}{a^2(t_{\text{in}})}\dot{g}_n^1(t,k)g_n^2(t,k)-1\leftrightarrow 2\Big],\end{aligned} \tag{A.6}$$

where in the second line we used our decomposition of u_n^J described in eq. (7.34). This expression is now well-suited for calculating the asymmetry parameter using the linearized equations of motion.

Appendix B

Gauge field perturbations in de Sitter space

Let us try to understand the electric and magnetic field power-spectra at the end of inflation in the model presented in Chapter 8 using some simplified semi-analytic analysis. For this purpose, we approximate the space-time to be de Sitter, $H = \text{const}$, and the inflaton to roll slow enough (so that $d\ln\rho/d\ln a \ll 1$), or more precisely, $\rho \to \text{const}$. The equations governing the evolution of the mode functions are then given by

$$\begin{aligned} \partial_\tau^2 u_k^{T\pm} + \left(k^2 + k_{_C}^2\right) u_k^{T\pm} &= 0\,, \\ \partial_\tau^2 u_k^{L} - \frac{2}{\tau}\frac{\partial_\tau u_k^L}{1+(k_{_C}/k)^2} + \left(k^2 + k_{_C}^2\right) u_k^{L} &= 0\,, \end{aligned} \tag{B.1}$$

where $k_{_C} = a g_{_A} \bar{\rho}/2 = -g_{_A}\bar{\rho}/2H\tau$. Note that $k_{_C}$ depends on τ and that τ is negative during inflation.[1]

The analytic solutions for the transverse modes of constant mass in de Sitter space-time are known, e.g., cf. [284]. Using the WKB initial conditions, (8.62), we have

$$u_k^{T\pm}(\tau) = \frac{\sqrt{-k\tau}}{(2\pi)^{3/2}}\sqrt{\frac{\pi}{4k}} H_z^{(1)}(-k\tau)\exp\left(iz\frac{\pi}{2} + i\frac{\pi}{4}\right)\,, \tag{B.2}$$

where $H_z^{(1)}(-k\tau)$ is the Hankel function of first kind, of order $z = \sqrt{(1/4) - (k_{_C}/\mathcal{H})^2}$. Now the distinction between the $k_{_C} \ll \mathcal{H}$ and $k_{_C} \gg \mathcal{H}$ regimes discussed in Section 8.3.2 becomes a bit more evident. For $k_{_C}/\mathcal{H} > 1/2$, z is purely imaginary. For $k_{_C}/\mathcal{H} < 1/2$, z is purely real, and cannot exceed $(1/2)$. The asymptotes of the Hankel functions depend on z and its complex phase.

We shall now explain the double power-laws observed in the magnetic and transverse electric fields. We will first focus on the $k_{_C}/\mathcal{H} > \frac{1}{2}$, i.e., $z^2 < 0$ regime. At early enough times $k \gg k_{_C}$ (recall that $k_{_C}$ gets smaller at earlier times), the transverse mode functions $u_k^{T\pm} \sim e^{-ik\tau}/\sqrt{k}$ and $\partial_\tau u_k^{T\pm} \sim \sqrt{k}e^{-ik\tau}$. This can be verified analytically or just by solving the equations of motion, see Fig. B.1. Similarly at late enough times when $k \ll k_{_C}$ it is easy to verify from the analytic solution in eq. (B.2) and Fig. B.1 that $u_k^{T\pm} \sim 1/\sqrt{k_{_C}}$ and $\partial_\tau u_k^{T\pm} \sim \sqrt{k_{_C}}$. Recalling that $a^4\Delta^2_{B^{T\pm}} \sim k^5|u_k^{T\pm}|^2$ and $a^4\Delta^2_{E^{T\pm}} \sim k^3|\partial_\tau u_k^{T\pm}|^2$ one

[1]The equations look a lot simpler, and are easier to analyze by doing the following change of variables: $x = -k\tau$ and $\alpha = k_{_C}/\mathcal{H}$. Doing this makes $x = -k\tau$ the only independent variable, with α acting as a time and scale independent parameter. We do not use x and α in the presentation to avoid introducing too many new variables.

finds the familiar scalings

$$\begin{aligned}\Delta^2_{B^{T\pm}} &\approx \frac{H^4}{4\pi^2} \times \begin{cases} (k/\mathcal{H})^4 \, (k/k_{_C}) \,, & \text{if } k \ll k_{_C} \,, \\ (k/\mathcal{H})^4 \,, & \text{if } k \gg k_{_C} \,, \end{cases} \\ \Delta^2_{E^{T\pm}} &\approx \frac{H^4}{4\pi^2} \times \begin{cases} (k/\mathcal{H})^3 \, (k_{_C}/\mathcal{H}) \,, & \text{if } k \ll k_{_C} \,, \\ (k/\mathcal{H})^4 \,, & \text{if } k \gg k_{_C} \,. \end{cases} \end{aligned} \tag{B.3}$$

We note two things. Firstly, the break in the double power-laws occurs where it did in the plots based on the numerical calculation for $V(\rho) = m^2\rho^2/2$ evaluated at the end of inflation provided in Fig. 8.1 (cf. eq. (8.68)). Secondly, the difference in the $k_{_C}$ dependence implies that at late times ($k \ll k_{_C}$) there will be more power stored in the form of transverse electric field and less in the form of magnetic field. The product of the transverse electric and magnetic power-spectra, however, is unchanged.

We repeat the same procedure for the magnetic and transverse electric fields in the weak coupling regime, $k_{_C}/\mathcal{H} < \frac{1}{2}$, i.e., $\frac{1}{4} > z^2 > 0$. Initially, when $k \gg k_{_C}$, $u_k^{T\pm} \sim e^{-ik\tau}/\sqrt{k}$ and $\partial_\tau u_k^{T\pm} \sim \sqrt{k} e^{-ik\tau}$. Later on, $k \ll k_{_C}$, $u_k^{T\pm} \sim 1/\sqrt{k}$. That is why in this coupling regime the magnetic power-spectrum is described by a single power-law. The late time behaviour of the $\partial_\tau u_k^{T\pm}$ is slightly more intriguing. For $k_{_C}^2/\mathcal{H} \ll k \ll k_{_C}$, $\partial_\tau u_k^{T\pm} \sim \sqrt{k}$. However, when $k \ll k_{_C}^2/\mathcal{H}$, $\partial_\tau u_k^{T\pm} \sim k_{_C}/\sqrt{k}$, implying a double power-law for the transverse electric field, at a scale defined by the square of $k_{_C}$. The actual power-spectra again agree with what we found in Section 8.3.2 for the $m^2\rho^2/2$ inflation (cf. eq. (8.69))

$$\begin{aligned}\Delta^2_{B^{T\pm}} &\approx \frac{H^4}{4\pi^2} \left(\frac{k}{\mathcal{H}}\right)^4 \,, \\ \Delta^2_{E^{T\pm}} &\approx \frac{H^4}{4\pi^2} \times \begin{cases} (k/\mathcal{H})^2 \, (k_{_C}/\mathcal{H})^2 \,, & \text{if } k \ll k_{_C}^2/\mathcal{H} \,, \\ (k/\mathcal{H})^4 \,, & \text{if } k \gg k_{_C}^2/\mathcal{H} \,. \end{cases} \end{aligned} \tag{B.4}$$

The longitudinal mode is harder to approach analytically. It can be solved analytically only for $k \gg k_{_C}$ and $k \ll k_{_C}$. In the former (subhorison) limit the equation of motion reduces to

$$\partial_\tau^2 u_k^L - \frac{2}{\tau} \partial_\tau u_k^L + k^2 u_k^L = 0 \,. \tag{B.5}$$

The exact solution is given by

$$\begin{aligned} u_k^L(\tau) &= \frac{1}{(2\pi)^{3/2}\sqrt{2k}} \left(\frac{k}{k_{_C}} - \frac{i}{k_{_C}\tau}\right) \exp(-ik\tau) \,, \\ \partial_\tau u_k^L(\tau) &= \frac{1}{(2\pi)^{3/2}\sqrt{2k}} \left(-\frac{ik^2}{k_{_C}}\right) \exp(-ik\tau) \,, \end{aligned} \tag{B.6}$$

where we have used the WKB initial conditions, cf. eq. (8.62). Note u_k^L has two sorts of harmonic terms: ones of constant amplitude and ones that are linear in $-k\tau$ (recall $k_{_C} = -g_{_A}\bar{\rho}/2H\tau$ in de Sitter space-time). However, $\partial_\tau u_k^L$ has only terms of the latter kind[2] - this will be important when discussing the weak coupling power-spectrum of $\Delta^2_{E^L}$ on super-Hubble scales.

[2]This is independent on the initial conditions and holds for the general solution of eq. (B.5).

In the superhorison limit, $k \ll k_{_C}$, the longitudinal mode is governed by

$$\partial_\tau^2 u_k^L - \frac{2k^2}{\tau k_{_C}^2}\partial_\tau u_k^L + k_{_C}^2 u_k^L = 0\,. \tag{B.7}$$

This equation has a general solution in terms of hypergeometric functions which is not very illuminative and we shall not give here. It is more straightforward just to solve the full equation of motion eq. (B.1) for u_k^L and from its evolution to infer $\Delta^2_{E^L}$. We did the same thing with the transverse modes.

We again start with the strong coupling limit, $k_{_C}/\mathcal{H} \gg \frac{1}{2}$. At early times, $k \gg k_{_C}$, $u_k^L \sim e^{-ik\tau}\sqrt{k}/k_{_C}$ and $\partial_\tau u_k^L \sim e^{-ik\tau}k^{3/2}/k_{_C}$, as shown in Fig. B.1. See why the two are similar in eq. (B.6). At late times, $k \ll k_{_C}$, $u_k^L \sim 1/\sqrt{k_{_C}}$ and $\partial_\tau u_k^L \sim \sqrt{k_{_C}}$. Rewriting the longitudinal electric field power-spectrum as $\Delta^2_{E^L} \sim k^3|\partial_\tau u_k^L|^2/[1+(k/k_{_C})^2]^2$, we recover the familiar *k*-scalings (cf. eq. (8.68))

$$\Delta^2_{E^L} \approx \frac{H^4}{4\pi^2} \times \begin{cases} (k/\mathcal{H})^3\, k_{_C}/\mathcal{H}\,, & \text{if } k \ll k_{_C}\,, \\ (k/\mathcal{H})^2\, (k_{_C}/\mathcal{H})^2\,, & \text{if } k \gg k_{_C}\,. \end{cases} \tag{B.8}$$

The final case we consider is the weak coupling regime of the longitudinal modes, $k_{_C}/\mathcal{H} \ll \frac{1}{2}$. At the beginning, when $k \gg \mathcal{H}$, $u_k^L \sim e^{-ik\tau}\sqrt{k}/k_{_C}$. However, after the *k*-mode crosses out the Hubble horizon, but is still shorter than the Compton wavelength, i.e., $k_{_C} \ll k \ll \mathcal{H}$, $u_k^L \sim 1/\sqrt{k}$. This transition upon Hubble horizon exit for sub-Compton modes is not observed for $\partial_\tau u_k^L$. Instead for all $k \gg k_{_C}$, $\partial_\tau u_k^L \sim e^{-ik\tau}k^{3/2}/k_{_C}$, cf. eq. (B.6). Later on when $k \ll k_{_C}$, $u_k^L \sim 1/\sqrt{k}$ and $\partial_\tau u_k^L \sim k_{_C}/\sqrt{k}$. The power-spectrum of the longitudinal electric field than becomes

$$\Delta^2_{E^L} \approx \frac{H^4}{4\pi^2} \times \begin{cases} (k/\mathcal{H})^2\, (k_{_C}/\mathcal{H})^2\,, & \text{if } k \ll k_{_C}\,, \\ (k/\mathcal{H})^2\, (k_{_C}/\mathcal{H})^2\,, & \text{if } k \gg k_{_C}\,. \end{cases} \tag{B.9}$$

Although, the *k*-scaling of $\Delta^2_{E^L}$ in the weak coupling regime (cf. eq. (8.69)) is accounted for by our calculations in de Sitter space-time, the power excess on super-Hubble scales seen in Fig. 8.1 is not. This requires a more general consideration in which the time-dependences of *H* and ρ are included.

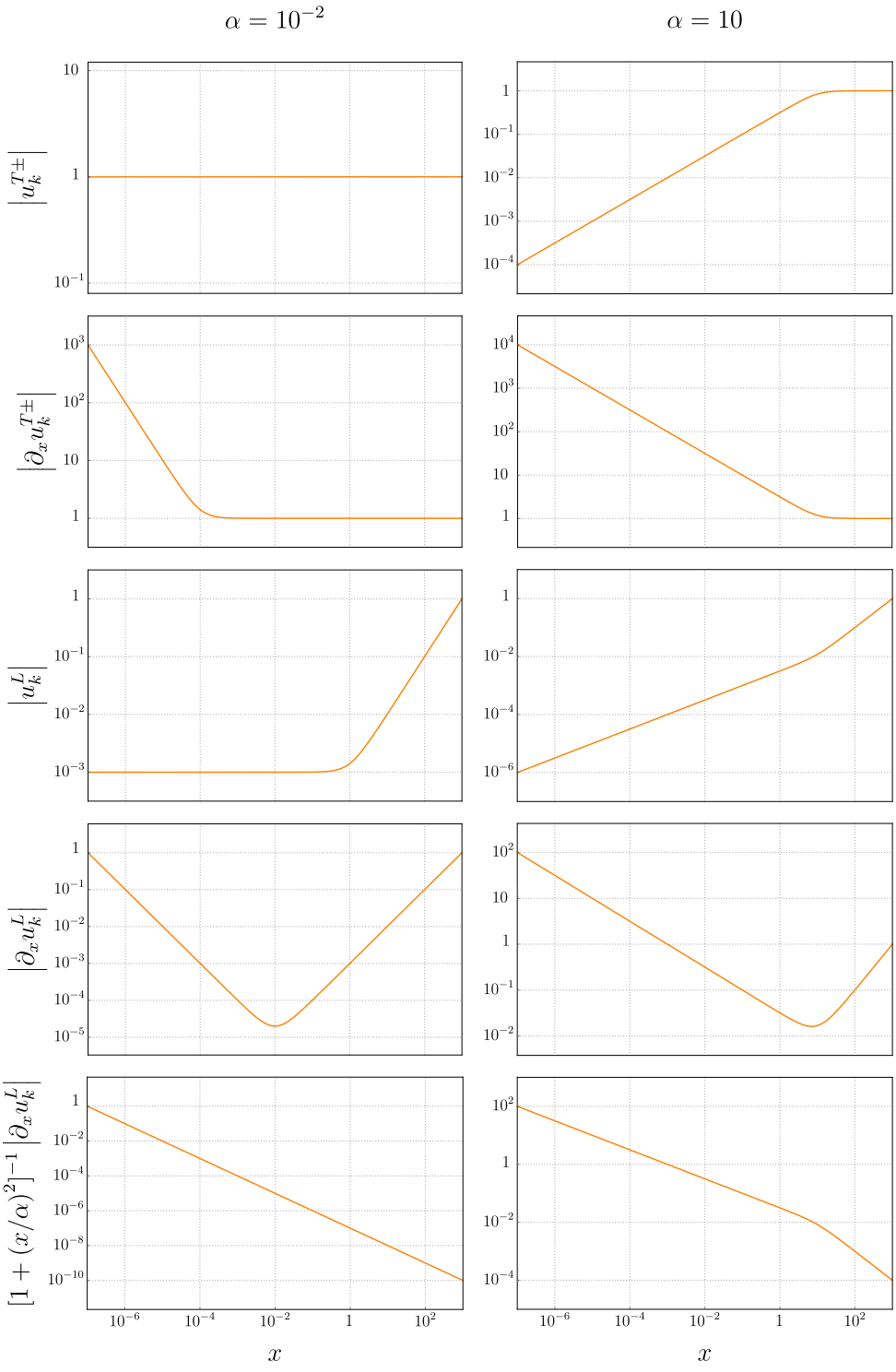

Figure B.1: Numerical solutions to eq. (B.1), i.e., the field modes in de Sitter space-time with the inflaton assumed to be constant. Fields are evolved backwards in x, from $x_{\rm in} = (-k\tau)_{\rm in} \gg \alpha = k_{_C}/\mathcal{H} = g_{_A}\bar{\rho}/(2H)$.

Appendix C

The Abelian model in Coulomb gauge

In Coulomb gauge $\partial_i A^i = 0$, for the models in Chapter 8 the background variables we consider are $(\bar{\varphi}^0, \bar{\varphi}^1) = (\bar{\varphi}^0(\tau), 0)$ (using the $U(1)$ gauge symmetry). The linearised perturbations in Fourier space are $\delta\tilde{\varphi}^0_{\mathbf{k}}, \delta\varphi^1_{\mathbf{k}}, A_{0\mathbf{k}}, A^{T\pm}_{\mathbf{k}}$. Note that we have not chosen a particular space-time slicing, i.e., we are working in diffeomorphism invariant variables. E.g., $\delta\tilde{\varphi}^0$ is given by $\delta\tilde{\rho}$ from eq. (8.12), with $\bar{\rho} \to \bar{\varphi}^0$. The corresponding equations of motion are as follows.

For the background dynamics, the equations of motion are

$$\partial_\tau^2\bar{\varphi}^0 + 2\mathcal{H}\partial_\tau\bar{\varphi}^0 + a^2\partial_{\bar{\varphi}^0}V(\bar{\varphi}^0) = 0\,, \tag{C.1}$$

and equations of motion for the perturbations in real and imaginary parts of φ are given by:

$$\begin{aligned}
&\partial_\tau^2\delta\tilde{\varphi}^0_{\mathbf{k}} + 2\mathcal{H}\partial_\tau\delta\tilde{\varphi}^0_{\mathbf{k}} + k^2\delta\tilde{\varphi}^0_{\mathbf{k}} + a^2\partial^2_{\bar{\varphi}^0}V(\bar{\varphi}^0)\delta\tilde{\varphi}^0_{\mathbf{k}} \\
&\quad + \frac{2}{m_{\rm Pl}^2}\left[\left(\mathcal{H}\partial_\tau\bar{\varphi}^0 + \frac{a^2}{2}\partial_{\bar{\varphi}^0}V(\bar{\varphi}^0)\right)\frac{\delta\tilde{\varphi}^0_{\mathbf{k}}\partial_\tau^2\bar{\varphi}^0 - \partial_\tau\bar{\varphi}^0\left(\partial_\tau\delta\tilde{\varphi}^0_{\mathbf{k}} + \mathcal{H}\delta\tilde{\varphi}^0_{\mathbf{k}}\right)}{\partial_\tau\mathcal{H} - \mathcal{H}^2 + k^2} - \left(\partial_\tau\bar{\varphi}^0\right)^2\delta\tilde{\varphi}^0_{\mathbf{k}}\right] = 0\,, \\
&\partial_\tau^2\delta\varphi^1_{\mathbf{k}} + 2\left[\frac{\mathcal{H} - \frac{\partial_\tau\bar{\varphi}^0}{\bar{\varphi}^0}\left(\frac{g_A\bar{\varphi}^0 a}{2k}\right)^2}{1 + \left(\frac{g_A\bar{\varphi}^0 a}{2k}\right)^2}\right]\partial_\tau\delta\varphi^1_{\mathbf{k}} \\
&\quad + \left\{\frac{a^2}{\bar{\varphi}^0}\partial_{\bar{\varphi}^0}V(\bar{\varphi}^0) + 2\frac{\left(\frac{g_A\partial_\tau\bar{\varphi}^0 a}{2k}\right)^2 + \mathcal{H}\left(\frac{g_A a}{2k}\right)^2\bar{\varphi}^0\partial_\tau\bar{\varphi}^0}{1 + \left(\frac{g_A\bar{\varphi}^0 a}{2k}\right)^2} + k^2 + \left(\frac{g_A\bar{\varphi}^0 a}{2}\right)^2\right\}\delta\varphi^1_{\mathbf{k}} = 0\,.
\end{aligned} \tag{C.2}$$

The equation of motion for the transverse modes in the gauge field are

$$\partial_\tau^2 A^{T\pm}_{\mathbf{k}} + \left[k^2 + \left(\frac{g_A\bar{\varphi}^0 a}{2}\right)^2\right]A^{T\pm}_{\mathbf{k}} = 0\,, \tag{C.3}$$

and finally, the constraint equation yields

$$A_{0\mathbf{k}} = \frac{g_A}{2}\frac{\left[\delta\varphi^1_{\mathbf{k}}\partial_\tau\bar{\varphi}^0 - \bar{\varphi}^0\partial_\tau\delta\varphi^1_{\mathbf{k}}\right]}{\left(\frac{k}{a}\right)^2 + \left(\frac{g_A\bar{\varphi}^0}{2}\right)^2}\,. \tag{C.4}$$

Bibliography

[1] **Planck** Collaboration, P. A. R. Ade *et al.*, "Planck 2015 results. XIII. Cosmological parameters," *Astron. Astrophys.* **594** (2016) A13, arXiv:1502.01589 [astro-ph.CO].

[2] **Planck** Collaboration, P. A. R. Ade *et al.*, "Planck 2015 results. XX. Constraints on inflation," *Astron. Astrophys.* **594** (2016) A20, arXiv:1502.02114 [astro-ph.CO].

[3] A. H. Guth, "Inflationary universe: A possible solution to the horizon and flatness problems," *Phys. Rev. D* **23** (Jan, 1981) 347–356.

[4] A. Linde, "A new inflationary universe scenario: A possible solution of the horizon, flatness, homogeneity, isotropy and primordial monopole problems," *Physics Letters B* **108** no. 6, (1982) 389 – 393.

[5] A. Albrecht and P. J. Steinhardt, "Cosmology for grand unified theories with radiatively induced symmetry breaking," *Phys. Rev. Lett.* **48** (Apr, 1982) 1220–1223.

[6] A. A. Starobinsky, "A New Type of Isotropic Cosmological Models Without Singularity," *Phys. Lett.* **B91** (1980) 99–102.

[7] V. F. Mukhanov and G. V. Chibisov, "Quantum Fluctuations and a Nonsingular Universe," *JETP Lett.* **33** (1981) 532–535. [Pisma Zh. Eksp. Teor. Fiz.33,549(1981)].

[8] L. Senatore, "Lectures on Inflation," arXiv:1609.00716 [hep-th].

[9] G. Steigman, "Primordial Nucleosynthesis in the Precision Cosmology Era," *Ann. Rev. Nucl. Part. Sci.* **57** (2007) 463–491, arXiv:0712.1100 [astro-ph].

[10] A. D. Dolgov and D. P. Kirilova, "On particle creation by a time dependent scalar field," *Sov. J. Nucl. Phys.* **51** (1990) 172–177. [Yad. Fiz.51,273(1990)].

[11] J. H. Traschen and R. H. Brandenberger, "Particle Production During Out-of-equilibrium Phase Transitions," *Phys. Rev.* **D42** (1990) 2491–2504.

[12] L. Kofman, A. D. Linde, and A. A. Starobinsky, "Reheating after inflation," *Phys. Rev. Lett.* **73** (1994) 3195–3198, arXiv:hep-th/9405187 [hep-th].

[13] L. A. Kofman, "The Origin of matter in the universe: Reheating after inflation," 1996. arXiv:astro-ph/9605155 [astro-ph]. http://alice.cern.ch/format/showfull?sysnb=0225922.

[14] L. Kofman, A. D. Linde, and A. A. Starobinsky, "Towards the theory of reheating after inflation," *Phys.Rev.* **D56** (1997) 3258–3295, arXiv:hep-ph/9704452 [hep-ph].

[15] B. A. Bassett, S. Tsujikawa, and D. Wands, "Inflation dynamics and reheating," *Rev. Mod. Phys.* **78** (2006) 537–589, arXiv:astro-ph/0507632 [astro-ph].

[16] R. Allahverdi, R. Brandenberger, F.-Y. Cyr-Racine, and A. Mazumdar, "Reheating in Inflationary Cosmology: Theory and Applications," *Ann. Rev. Nucl. Part. Sci.* **60** (2010) 27–51, arXiv:1001.2600 [hep-th].

[17] M. A. Amin, M. P. Hertzberg, D. I. Kaiser, and J. Karouby, "Nonperturbative Dynamics Of Reheating After Inflation: A Review," *Int.J.Mod.Phys.* **D24** no. 01, (2014) 1530003, arXiv:1410.3808 [hep-ph].

[18] R. Micha and I. I. Tkachev, "Relativistic turbulence: A Long way from preheating to equilibrium," *Phys. Rev. Lett.* **90** (2003) 121301, arXiv:hep-ph/0210202 [hep-ph].

[19] R. Micha and I. I. Tkachev, "Turbulent thermalization," *Phys. Rev.* **D70** (2004) 043538, arXiv:hep-ph/0403101 [hep-ph].

[20] I. Tkachev, S. Khlebnikov, L. Kofman, and A. D. Linde, "Cosmic strings from preheating," *Phys. Lett.* **B440** (1998) 262–268, arXiv:hep-ph/9805209 [hep-ph].

[21] A. Rajantie and E. J. Copeland, "Phase transitions from preheating in gauge theories," *Phys. Rev. Lett.* **85** (2000) 916, arXiv:hep-ph/0003025 [hep-ph].

[22] J.-F. Dufaux, D. G. Figueroa, and J. Garcia-Bellido, "Gravitational Waves from Abelian Gauge Fields and Cosmic Strings at Preheating," *Phys.Rev.* **D82** (2010) 083518, arXiv:1006.0217 [astro-ph.CO].

[23] J. Garcia-Bellido, D. G. Figueroa, and J. Rubio, "Preheating in the Standard Model with the Higgs-Inflaton coupled to gravity," *Phys. Rev.* **D79** (2009) 063531, arXiv:0812.4624 [hep-ph].

[24] F. Bezrukov, D. Gorbunov, and M. Shaposhnikov, "On initial conditions for the Hot Big Bang," *JCAP* **0906** (2009) 029, arXiv:0812.3622 [hep-ph].

[25] J. Repond and J. Rubio, "Combined Preheating on the lattice with applications to Higgs inflation," *JCAP* **1607** no. 07, (2016) 043, arXiv:1604.08238 [astro-ph.CO].

[26] D. G. Figueroa, J. Garcia-Bellido, and F. Torrenti, "Decay of the standard model Higgs field after inflation," *Phys. Rev.* **D92** no. 8, (2015) 083511, arXiv:1504.04600 [astro-ph.CO].

[27] D. G. Figueroa, J. Garca-Bellido, and F. Torrent, "Gravitational wave production from the decay of the standard model Higgs field after inflation," *Phys. Rev.* **D93** no. 10, (2016) 103521, arXiv:1602.03085 [astro-ph.CO].

[28] K. Enqvist, S. Nurmi, and S. Rusak, "Non-Abelian dynamics in the resonant decay of the Higgs after inflation," *JCAP* **1410** no. 10, (2014) 064, arXiv:1404.3631 [astro-ph.CO].

[29] K. Enqvist, S. Nurmi, S. Rusak, and D. Weir, "Lattice Calculation of the Decay of Primordial Higgs Condensate," arXiv:1506.06895 [astro-ph.CO].

[30] P. Adshead and E. I. Sfakianakis, "Fermion production during and after axion inflation," *JCAP* **1511** no. 11, (2015) 021, arXiv:1508.00891 [hep-ph].

[31] P. Adshead, J. T. Giblin, T. R. Scully, and E. I. Sfakianakis, "Gauge-preheating and the end of axion inflation," *JCAP* **1512** no. 12, (2015) 034, arXiv:1502.06506 [astro-ph.CO].

[32] K. D. Lozanov and M. A. Amin, "The charged inflaton and its gauge fields: preheating and initial conditions for reheating," *JCAP* **1606** no. 06, (2016) 032, arXiv:1603.05663 [hep-ph].

[33] D. G. Figueroa and F. Torrenti, "Parametric Resonance in the Early Universe - A Fitting Analysis," arXiv:1609.05197 [astro-ph.CO].

[34] K. D. Lozanov and M. A. Amin, "The Equation of State and Duration to Radiation Domination After Inflation," arXiv:1608.01213 [astro-ph.CO].

[35] D. I. Podolsky, G. N. Felder, L. Kofman, and M. Peloso, "Equation of state and beginning of thermalization after preheating," *Phys. Rev.* **D73** (2006) 023501, arXiv:hep-ph/0507096 [hep-ph].

[36] M. A. Amin, R. Easther, H. Finkel, R. Flauger, and M. P. Hertzberg, "Oscillons After Inflation," *Phys. Rev. Lett.* **108** (2012) 241302, arXiv:1106.3335 [astro-ph.CO].

[37] J. T. Deskins, J. T. Giblin, and R. R. Caldwell, "Gauge Field Preheating at the End of Inflation," *Phys.Rev.* **D88** no. 6, (2013) 063530, arXiv:1305.7226 [astro-ph.CO].

[38] M. P. Hertzberg and J. Karouby, "Baryogenesis from the Inflaton Field," *Phys. Lett.* **B737** (2014) 34–38, arXiv:1309.0007 [hep-ph].

[39] M. P. Hertzberg and J. Karouby, "Generating the Observed Baryon Asymmetry from the Inflaton Field," *Phys.Rev.* **D89** no. 6, (2014) 063523, arXiv:1309.0010 [hep-ph].

[40] M. P. Hertzberg, J. Karouby, W. G. Spitzer, J. C. Becerra, and L. Li, "Theory of self-resonance after inflation. II. Quantum mechanics and particle-antiparticle asymmetry," *Phys. Rev.* **D90** (2014) 123529, arXiv:1408.1398 [hep-th].

[41] M. P. Hertzberg, J. Karouby, W. G. Spitzer, J. C. Becerra, and L. Li, "Theory of self-resonance after inflation. I. Adiabatic and isocurvature Goldstone modes," *Phys. Rev.* **D90** (2014) 123528, arXiv:1408.1396 [hep-th].

[42] J. T. Giblin and E. Thrane, "Estimates of maximum energy density of cosmological gravitational-wave backgrounds," *Phys. Rev.* **D90** no. 10, (2014) 107502, arXiv:1410.4779 [gr-qc].

[43] J. R. Bond, A. V. Frolov, Z. Huang, and L. Kofman, "Non-Gaussian Spikes from Chaotic Billiards in Inflation Preheating," *Phys. Rev. Lett.* **103** (2009) 071301, arXiv:0903.3407 [astro-ph.CO].

[44] S. Antusch, F. Cefala, and S. Orani, "Gravitational waves from oscillons after inflation," arXiv:1607.01314 [astro-ph.CO].

[45] J. B. Munoz and M. Kamionkowski, "Equation-of-State Parameter for Reheating," *Phys. Rev.* **D91** no. 4, (2015) 043521, arXiv:1412.0656 [astro-ph.CO].

[46] L. Dai, M. Kamionkowski, and J. Wang, "Reheating constraints to inflationary models," *Phys. Rev. Lett.* **113** (2014) 041302, arXiv:1404.6704 [astro-ph.CO].

[47] J. Martin, C. Ringeval, and V. Vennin, "Observing Inflationary Reheating," *Phys. Rev. Lett.* **114** no. 8, (2015) 081303, arXiv:1410.7958 [astro-ph.CO].

[48] J. Martin, C. Ringeval, and V. Vennin, "Information Gain on Reheating: the One Bit Milestone," *Phys. Rev.* **D93** no. 10, (2016) 103532, arXiv:1603.02606 [astro-ph.CO].

[49] R. J. Hardwick, V. Vennin, K. Koyama, and D. Wands, "Constraining Curvatonic Reheating," *JCAP* **1608** no. 08, (2016) 042, arXiv:1606.01223 [astro-ph.CO].

[50] J. Martin, C. Ringeval, and V. Vennin, "Encyclopedia Inflationaris," *Phys. Dark Univ.* **5-6** (2014) 75–235, arXiv:1303.3787 [astro-ph.CO].

[51] A. R. Liddle and S. M. Leach, "How long before the end of inflation were observable perturbations produced?," *Phys. Rev.* **D68** (2003) 103503, arXiv:astro-ph/0305263 [astro-ph].

[52] K. D. Lozanov and M. A. Amin, "End of inflation, oscillons, and matter-antimatter asymmetry," *Phys.Rev.* **D90** no. 8, (2014) 083528, arXiv:1408.1811 [hep-ph].

[53] A. Kandus, K. E. Kunze, and C. G. Tsagas, "Primordial magnetogenesis," *Phys. Rept.* **505** (2011) 1–58, arXiv:1007.3891 [astro-ph.CO].

[54] J. Smit, *Introduction to Quantum Fields on a Lattice*. Cambridge Lecture Notes in Physics. Cambridge University Press, 2002. https://books.google.co.uk/books?id=KIHHW9NtbuAC.

[55] S. Weinberg, *Cosmology*. Oxford Univ. Pr., 2008. http://www.oup.com/uk/catalogue/?ci=9780198526827.

[56] A. Linde, "Chaotic inflation," *Physics Letters B* **129** no. 3, (1983) 177 – 181. http://www.sciencedirect.com/science/article/pii/0370269383908377.

[57] A. D. Linde, "Particle physics and inflationary cosmology," *Contemp. Concepts Phys.* **5** (1990) 1–362, arXiv:hep-th/0503203 [hep-th].

[58] D. S. Goldwirth and T. Piran, "Initial conditions for inflation," *Physics Reports* **214** no. 4, (1992) 223 – 292. http://www.sciencedirect.com/science/article/pii/0370157392900739.

[59] W. J. Handley, S. D. Brechet, A. N. Lasenby, and M. P. Hobson, "Kinetic Initial Conditions for Inflation," *Phys. Rev.* **D89** no. 6, (2014) 063505, arXiv:1401.2253 [astro-ph.CO].

[60] R. PENROSE, "Difficulties with inflationary cosmology," *Annals of the New York Academy of Sciences* **571** no. 1, (1989) 249–264. http://dx.doi.org/10.1111/j.1749-6632.1989.tb50513.x.

[61] S. M. Carroll and J. Chen, "Does inflation provide natural initial conditions for the universe?," *Gen. Rel. Grav.* **37** (2005) 1671–1674, arXiv:gr-qc/0505037 [gr-qc]. [Int. J. Mod. Phys.D14,2335(2005)].

[62] M. S. Turner, "Coherent Scalar Field Oscillations in an Expanding Universe," *Phys. Rev.* **D28** (1983) 1243.

[63] J. M. Bardeen, "Gauge-invariant cosmological perturbations," *Phys. Rev. D* **22** (Oct, 1980) 1882–1905. https://link.aps.org/doi/10.1103/PhysRevD.22.1882.

[64] L. Abbott, E. Farhi, and M. B. Wise, "Particle production in the new inflationary cosmology," *Physics Letters B* **117** no. 1, (1982) 29 – 33. http://www.sciencedirect.com/science/article/pii/037026938290867X.

[65] M. E. Peskin and D. V. Schroeder, *An Introduction to Quantum Field Theory; 1995 ed.* Westview, Boulder, CO, 1995. https://cds.cern.ch/record/257493. Includes exercises.

[66] W. Magnus and S. Winkler, *Hill's Equation*. Dover Books on Mathematics Series. Dover Publications, 2004. https://books.google.co.uk/books?id=ML5wm-T4RVQC.

[67] G. Teschl, "Ordinary differential equations and dynamical systems," 2012.

[68] L. Landau and E. Lifshits, *Mechanics*. Butterworth-Heinemann, 1976. https://books.google.co.uk/books?id=e-xASAehg1sC.

[69] A. V. Frolov, "Non-linear Dynamics and Primordial Curvature Perturbations from Preheating," *Class. Quant. Grav.* **27** (2010) 124006, arXiv:1004.3559 [gr-qc].

[70] V. Mukhanov and S. Winitzki, *Introduction to quantum effects in gravity*. Cambridge University Press, 2007. http://www.cambridge.org/us/catalogue/catalogue.asp?isbn=0521868343.

[71] L. Landau and E. Lifshits, *Quantum Mechanics: Non-relativistic Theory*. Butterworth-Heinemann. Butterworth-Heinemann, 1977. https://books.google.co.uk/books?id=J9ui6KwC4mMC.

[72] M. A. Amin and D. Baumann, "From Wires to Cosmology," *JCAP* **1602** no. 02, (2016) 045, arXiv:1512.02637 [astro-ph.CO].

[73] A. D. Linde, "Hybrid inflation," *Phys. Rev.* **D49** (1994) 748–754, arXiv:astro-ph/9307002 [astro-ph].

[74] G. N. Felder and I. Tkachev, "LATTICEEASY: A Program for lattice simulations of scalar fields in an expanding universe," *Comput. Phys. Commun.* **178** (2008) 929–932, arXiv:hep-ph/0011159 [hep-ph].

[75] A. V. Frolov, "DEFROST: A New Code for Simulating Preheating after Inflation," *JCAP* **0811** (2008) 009, arXiv:0809.4904 [hep-ph].

[76] Z. Huang, "The Art of Lattice and Gravity Waves from Preheating," *Phys. Rev.* **D83** (2011) 123509, arXiv:1102.0227 [astro-ph.CO].

[77] H. L. Child, J. T. Giblin, Jr, R. H. Ribeiro, and D. Seery, "Preheating with Non-Minimal Kinetic Terms," *Phys. Rev. Lett.* **111** (2013) 051301, arXiv:1305.0561 [astro-ph.CO].

[78] J. Sainio, "CUDAEASY - a GPU Accelerated Cosmological Lattice Program," *Comput. Phys. Commun.* **181** (2010) 906–912, arXiv:0911.5692 [astro-ph.IM].

[79] J. Sainio, "PyCOOL - a Cosmological Object-Oriented Lattice code written in Python," *JCAP* **1204** (2012) 038, arXiv:1201.5029 [astro-ph.IM].

[80] R. Easther, H. Finkel, and N. Roth, "PSpectRe: A Pseudo-Spectral Code for (P)reheating," *JCAP* **1010** (2010) 025, arXiv:1005.1921 [astro-ph.CO].

[81] A. Kusenko and A. Mazumdar, "Gravitational waves from fragmentation of a primordial scalar condensate into Q-balls," *Phys. Rev. Lett.* **101** (2008) 211301, arXiv:0807.4554 [astro-ph].

[82] S.-Y. Zhou, E. J. Copeland, R. Easther, H. Finkel, Z.-G. Mou, and P. M. Saffin, "Gravitational Waves from Oscillon Preheating," *JHEP* **10** (2013) 026, arXiv:1304.6094 [astro-ph.CO].

[83] R. Easther, R. Flauger, and J. B. Gilmore, "Delayed Reheating and the Breakdown of Coherent Oscillations," *JCAP* **1104** (2011) 027, arXiv:1003.3011 [astro-ph.CO].

[84] G. N. Felder and L. Kofman, "Nonlinear inflaton fragmentation after preheating," *Phys. Rev.* **D75** (2007) 043518, arXiv:hep-ph/0606256 [hep-ph].

[85] A. Rajantie, P. M. Saffin, and E. J. Copeland, "Electroweak preheating on a lattice," *Phys. Rev.* **D63** (2001) 123512, arXiv:hep-ph/0012097 [hep-ph].

[86] E. J. Copeland, S. Pascoli, and A. Rajantie, "Dynamics of tachyonic preheating after hybrid inflation," *Phys. Rev.* **D65** (2002) 103517, arXiv:hep-ph/0202031 [hep-ph].

[87] F. L. Bezrukov and M. Shaposhnikov, "The Standard Model Higgs boson as the inflaton," *Phys. Lett.* **B659** (2008) 703–706, arXiv:0710.3755 [hep-th].

[88] P. B. Greene, L. Kofman, A. D. Linde, and A. A. Starobinsky, "Structure of resonance in preheating after inflation," *Phys. Rev.* **D56** (1997) 6175–6192, arXiv:hep-ph/9705347 [hep-ph].

[89] P. B. Greene and L. Kofman, "Preheating of fermions," *Physics Letters B* **448** no. 12, (1999) 6 – 12. http://www.sciencedirect.com/science/article/pii/S0370269399000209.

[90] E. J. Copeland and O. Seto, "Reheating and gravitino production in braneworld inflation," *Phys. Rev.* **D72** (2005) 023506, arXiv:hep-ph/0505149 [hep-ph].

[91] J. L. Cook and L. Sorbo, "Particle production during inflation and gravitational waves detectable by ground-based interferometers," *Phys. Rev.* **D85** (2012) 023534, arXiv:1109.0022 [astro-ph.CO]. [Erratum: Phys. Rev.D86,069901(2012)].

[92] F. Finelli and A. Gruppuso, "Resonant amplification of gauge fields in expanding universe," *Phys. Lett.* **B502** (2001) 216–222, arXiv:hep-ph/0001231 [hep-ph].

[93] K. Dimopoulos, T. Prokopec, O. Tornkvist, and A. C. Davis, "Natural magnetogenesis from inflation," *Phys. Rev.* **D65** (2002) 063505, arXiv:astro-ph/0108093 [astro-ph].

[94] B. A. Bassett, G. Pollifrone, S. Tsujikawa, and F. Viniegra, "Preheating¯cosmic magnetic dynamo?," *Phys. Rev. D* **63** (Apr, 2001) 103515.

[95] T. Fujita and R. Namba, "Pre-reheating Magnetogenesis in the Kinetic Coupling Model," arXiv:1602.05673 [astro-ph.CO].

[96] T. Kobayashi, "Primordial Magnetic Fields from the Post-Inflationary Universe," *JCAP* **1405** (2014) 040, arXiv:1403.5168 [astro-ph.CO].

[97] M. P. DeCross, D. I. Kaiser, A. Prabhu, C. Prescod-Weinstein, and E. I. Sfakianakis, "Preheating after Multifield Inflation with Nonminimal Couplings, I: Covariant Formalism and Attractor Behavior," arXiv:1510.08553 [astro-ph.CO].

[98] M. P. DeCross, D. I. Kaiser, A. Prabhu, C. Prescod-Weinstein, and E. I. Sfakianakis, "Preheating after multifield inflation with nonminimal couplings, II: Resonance Structure," arXiv:1610.08868 [astro-ph.CO].

[99] M. P. DeCross, D. I. Kaiser, A. Prabhu, C. Prescod-Weinstein, and E. I. Sfakianakis, "Preheating after multifield inflation with nonminimal couplings, III: Dynamical spacetime results," arXiv:1610.08916 [astro-ph.CO].

[100] Y. Ema, R. Jinno, K. Mukaida, and K. Nakayama, "Violent Preheating in Inflation with Nonminimal Coupling," *JCAP* **1702** no. 02, (2017) 045, arXiv:1609.05209 [hep-ph].

[101] M. Alishahiha, E. Silverstein, and D. Tong, "DBI in the sky," *Phys. Rev.* **D70** (2004) 123505, arXiv:hep-th/0404084 [hep-th].

[102] D. G. Figueroa and T. Meriniemi, "Stochastic Background of Gravitational Waves from Fermions – Theory and Applications," *JHEP* **10** (2013) 101, arXiv:1306.6911 [astro-ph.CO].

[103] I. Affleck and M. Dine, "A New Mechanism for Baryogenesis," *Nucl. Phys.* **B249** (1985) 361–380.

[104] K. Enqvist and J. McDonald, "Q balls and baryogenesis in the MSSM," *Phys. Lett.* **B425** (1998) 309–321, arXiv:hep-ph/9711514 [hep-ph].

[105] K. Enqvist and J. McDonald, "The dynamics of Affleck-Dine condensate collapse," *Nucl. Phys.* **B570** (2000) 407–422, arXiv:hep-ph/9908316 [hep-ph]. [Erratum: Nucl. Phys.B582,763(2000)].

[106] S. Mollerach, "Isocurvature baryon perturbations and inflation," *Phys. Rev. D* **42** (Jul, 1990) 313–325. https://link.aps.org/doi/10.1103/PhysRevD.42.313.

[107] A. D. Linde and V. F. Mukhanov, "Nongaussian isocurvature perturbations from inflation," *Phys. Rev.* **D56** (1997) R535–R539, arXiv:astro-ph/9610219 [astro-ph].

[108] D. H. Lyth and D. Wands, "Generating the curvature perturbation without an inflaton," *Physics Letters B* **524** no. 12, (2002) 5 – 14. http://www.sciencedirect.com/science/article/pii/S0370269301013661.

[109] L. Kofman, "Probing string theory with modulated cosmological fluctuations," arXiv:astro-ph/0303614 [astro-ph].

[110] A. D. Sakharov, "Violation of CP Invariance, c Asymmetry, and Baryon Asymmetry of the Universe," *Pisma Zh. Eksp. Teor. Fiz.* **5** (1967) 32–35. [Usp. Fiz. Nauk161,61(1991)].

[111] R. Durrer and A. Neronov, "Cosmological Magnetic Fields: Their Generation, Evolution and Observation," *Astron. Astrophys. Rev.* **21** (2013) 62, arXiv:1303.7121 [astro-ph.CO].

[112] **Planck** Collaboration, P. A. R. Ade *et al.*, "Planck 2015 results. XIX. Constraints on primordial magnetic fields," *Astron. Astrophys.* **594** (2016) A19, arXiv:1502.01594 [astro-ph.CO].

[113] P. Adshead, J. T. Giblin, T. R. Scully, and E. I. Sfakianakis, "Magnetogenesis from axion inflation," *JCAP* **1610** (2016) 039, arXiv:1606.08474 [astro-ph.CO].

[114] T. Markkanen, S. Nurmi, S. Rasanen, and V. Vennin, "Narrowing the window of inflationary magnetogenesis," arXiv:1704.01343 [astro-ph.CO].

[115] E. Hardy and J. Unwin, "Symmetric and Asymmetric Reheating," arXiv:1703.07642 [hep-ph].

[116] P. Adshead, Y. Cui, and J. Shelton, "Chilly Dark Sectors and Asymmetric Reheating," *JHEP* **06** (2016) 016, arXiv:1604.02458 [hep-ph].

[117] **CMB-S4** Collaboration, K. N. Abazajian *et al.*, "CMB-S4 Science Book, First Edition," arXiv:1610.02743 [astro-ph.CO].

[118] S. Y. Khlebnikov and I. I. Tkachev, "Relic gravitational waves produced after preheating," *Phys. Rev.* **D56** (1997) 653–660, arXiv:hep-ph/9701423 [hep-ph].

[119] C. Guzzetti, M., N. Bartolo, M. Liguori, and S. Matarrese, "Gravitational waves from inflation," *Riv. Nuovo Cim.* **39** no. 9, (2016) 399–495, arXiv:1605.01615 [astro-ph.CO].

[120] C. J. Moore, R. H. Cole, and C. P. L. Berry, "Gravitational-wave sensitivity curves," *Class. Quant. Grav.* **32** no. 1, (2015) 015014, arXiv:1408.0740 [gr-qc].

[121] L. Bethke, D. G. Figueroa, and A. Rajantie, "On the Anisotropy of the Gravitational Wave Background from Massless Preheating," *JCAP* **1406** (2014) 047, arXiv:1309.1148 [astro-ph.CO].

[122] L. Bethke, D. G. Figueroa, and A. Rajantie, "Anisotropies in the Gravitational Wave Background from Preheating," *Phys. Rev. Lett.* **111** no. 1, (2013) 011301, arXiv:1304.2657 [astro-ph.CO].

[123] D. G. Figueroa, M. Hindmarsh, and J. Urrestilla, "Exact Scale-Invariant Background of Gravitational Waves from Cosmic Defects," *Phys. Rev. Lett.* **110** no. 10, (2013) 101302, arXiv:1212.5458 [astro-ph.CO].

[124] Y. Watanabe and E. Komatsu, "Improved Calculation of the Primordial Gravitational Wave Spectrum in the Standard Model," *Phys. Rev.* **D73** (2006) 123515, arXiv:astro-ph/0604176 [astro-ph].

[125] A. Chambers and A. Rajantie, "Lattice calculation of non-Gaussianity from preheating," *Phys. Rev. Lett.* **100** (2008) 041302, arXiv:0710.4133 [astro-ph]. [Erratum: Phys. Rev. Lett.101,149903(2008)].

[126] A. Chambers and A. Rajantie, "Non-Gaussianity from massless preheating," *JCAP* **0808** (2008) 002, arXiv:0805.4795 [astro-ph].

[127] **Planck** Collaboration, P. A. R. Ade *et al.*, "Planck 2015 results. XVII. Constraints on primordial non-Gaussianity," *Astron. Astrophys.* **594** (2016) A17, arXiv:1502.01592 [astro-ph.CO].

[128] G. Leung, E. R. M. Tarrant, C. T. Byrnes, and E. J. Copeland, "Reheating, Multifield Inflation and the Fate of the Primordial Observables," *JCAP* **1209** (2012) 008, arXiv:1206.5196 [astro-ph.CO].

[129] G. Leung, E. R. M. Tarrant, C. T. Byrnes, and E. J. Copeland, "Influence of Reheating on the Trispectrum and its Scale Dependence," *JCAP* **1308** (2013) 006, arXiv:1303.4678 [astro-ph.CO].

[130] J. M. Maldacena, "Non-Gaussian features of primordial fluctuations in single field inflationary models," *JHEP* **05** (2003) 013, arXiv:astro-ph/0210603 [astro-ph].

[131] A. Linde, "Inflationary Cosmology after Planck 2013," in *100e Ecole d'Ete de Physique: Post-Planck Cosmology Les Houches, France, July 8-August 2, 2013*, pp. 231–316. 2015. arXiv:1402.0526 [hep-th]. https://inspirehep.net/record/1280019/files/arXiv:1402.0526.pdf.

[132] S. Dodelson and L. Hui, "A Horizon ratio bound for inflationary fluctuations," *Phys. Rev. Lett.* **91** (2003) 131301, arXiv:astro-ph/0305113 [astro-ph].

[133] P. Adshead, R. Easther, J. Pritchard, and A. Loeb, "Inflation and the Scale Dependent Spectral Index: Prospects and Strategies," *JCAP* **1102** (2011) 021, arXiv:1007.3748 [astro-ph.CO].

[134] P. Creminelli, D. Lpez Nacir, M. Simonovi, G. Trevisan, and M. Zaldarriaga, "ϕ^2 or Not ϕ^2: Testing the Simplest Inflationary Potential," *Phys. Rev. Lett.* **112** no. 24, (2014) 241303, arXiv:1404.1065 [astro-ph.CO].

[135] J. L. Cook, E. Dimastrogiovanni, D. A. Easson, and L. M. Krauss, "Reheating predictions in single field inflation," *JCAP* **1504** (2015) 047, arXiv:1502.04673 [astro-ph.CO].

[136] J. Ellis, M. A. G. Garcia, D. V. Nanopoulos, and K. A. Olive, "Calculations of Inflaton Decays and Reheating: with Applications to No-Scale Inflation Models," *JCAP* **1507** no. 07, (2015) 050, arXiv:1505.06986 [hep-ph].

[137] Y. Ueno and K. Yamamoto, "Constraints on α-attractor inflation and reheating," arXiv:1602.07427 [astro-ph.CO].

[138] M. Eshaghi, M. Zarei, N. Riazi, and A. Kiasatpour, "CMB and reheating constraints to α-attractor inflationary models," arXiv:1602.07914 [astro-ph.CO].

[139] J. Martin and C. Ringeval, "First CMB Constraints on the Inflationary Reheating Temperature," *Phys. Rev.* **D82** (2010) 023511, arXiv:1004.5525 [astro-ph.CO].

[140] J. Mielczarek, "Reheating temperature from the CMB," *Phys. Rev.* **D83** (2011) 023502, arXiv:1009.2359 [astro-ph.CO].

[141] P. Creminelli, D. L. Nacir, M. Simonovi, G. Trevisan, and M. Zaldarriaga, "ϕ^2 Inflation at its Endpoint," *Phys. Rev.* **D90** no. 8, (2014) 083513, arXiv:1405.6264 [astro-ph.CO].

[142] R.-G. Cai, Z.-K. Guo, and S.-J. Wang, "Reheating phase diagram for single-field slow-roll inflationary models," *Phys. Rev.* **D92** (2015) 063506, arXiv:1501.07743 [gr-qc].

[143] G. F. Giudice, I. Tkachev, and A. Riotto, "Nonthermal production of dangerous relics in the early universe," *JHEP* **08** (1999) 009, arXiv:hep-ph/9907510 [hep-ph].

[144] G. Kane, K. Sinha, and S. Watson, "Cosmological Moduli and the Post-Inflationary Universe: A Critical Review," *Int. J. Mod. Phys.* **D24** no. 08, (2015) 1530022, arXiv:1502.07746 [hep-th].

[145] S. Yu. Khlebnikov and I. I. Tkachev, "Classical decay of inflaton," *Phys. Rev. Lett.* **77** (1996) 219–222, arXiv:hep-ph/9603378 [hep-ph].

[146] M. A. Amin, "Inflaton fragmentation: Emergence of pseudo-stable inflaton lumps (oscillons) after inflation," arXiv:1006.3075 [astro-ph.CO].

[147] M. A. Amin, R. Easther, and H. Finkel, "Inflaton Fragmentation and Oscillon Formation in Three Dimensions," *JCAP* **1012** (2010) 001, arXiv:1009.2505 [astro-ph.CO].

[148] R. V. Konoplich, S. G. Rubin, A. S. Sakharov, and M. Yu. Khlopov, "Formation of black holes in first-order phase transitions as a cosmological test of symmetry-breaking mechanisms," *Phys. Atom. Nucl.* **62** (1999) 1593–1600. [Yad. Fiz.62,1705(1999)].

[149] M. Yu. Khlopov, R. V. Konoplich, S. G. Rubin, and A. S. Sakharov, "First order phase transitions as a source of black holes in the early universe," *Grav. Cosmol.* **2** (1999) S1, arXiv:hep-ph/9912422 [hep-ph].

[150] S. G. Rubin, M. Yu. Khlopov, and A. S. Sakharov, "Primordial black holes from nonequilibrium second order phase transition," *Grav. Cosmol.* **S6** (2000) 51–58, arXiv:hep-ph/0005271 [hep-ph].

[151] B. J. Carr, K. Kohri, Y. Sendouda, and J. Yokoyama, "New cosmological constraints on primordial black holes," *Phys. Rev.* **D81** (2010) 104019, arXiv:0912.5297 [astro-ph.CO].

[152] J. Garcia-Bellido, A. D. Linde, and D. Wands, "Density perturbations and black hole formation in hybrid inflation," *Phys. Rev.* **D54** (1996) 6040–6058, arXiv:astro-ph/9605094 [astro-ph].

[153] A. M. Green and K. A. Malik, "Primordial black hole production due to preheating," *Phys. Rev.* **D64** (2001) 021301, arXiv:hep-ph/0008113 [hep-ph].

[154] B. A. Bassett and S. Tsujikawa, "Inflationary preheating and primordial black holes," *Phys. Rev.* **D63** (2001) 123503, arXiv:hep-ph/0008328 [hep-ph].

[155] J. C. Hidalgo, L. A. Urena-Lopez, and A. R. Liddle, "Unification models with reheating via Primordial Black Holes," *Phys. Rev.* **D85** (2012) 044055, arXiv:1107.5669 [astro-ph.CO].

[156] E. Torres-Lomas, J. C. Hidalgo, K. A. Malik, and L. A. Urea-Lpez, "Formation of subhorizon black holes from preheating," *Phys. Rev.* **D89** no. 8, (2014) 083008, arXiv:1401.6960 [astro-ph.CO].

[157] T. Suyama, T. Tanaka, B. Bassett, and H. Kudoh, "Are black holes over-produced during preheating?," *Phys. Rev.* **D71** (2005) 063507, arXiv:hep-ph/0410247 [hep-ph].

[158] T. Suyama, T. Tanaka, B. Bassett, and H. Kudoh, "Black hole production in tachyonic preheating," *JCAP* **0604** (2006) 001, arXiv:hep-ph/0601108 [hep-ph].

[159] J. J. M. Carrasco, R. Kallosh, and A. Linde, "α-Attractors: Planck, LHC and Dark Energy," *JHEP* **10** (2015) 147, arXiv:1506.01708 [hep-th].

[160] J. J. M. Carrasco, R. Kallosh, and A. Linde, "Cosmological Attractors and Initial Conditions for Inflation," *Phys. Rev.* **D92** no. 6, (2015) 063519, arXiv:1506.00936 [hep-th].

[161] E. Silverstein and A. Westphal, "Monodromy in the CMB: Gravity Waves and String Inflation," *Phys. Rev.* **D78** (2008) 106003, arXiv:0803.3085 [hep-th].

[162] L. McAllister, E. Silverstein, A. Westphal, and T. Wrase, "The Powers of Monodromy," *JHEP* **09** (2014) 123, arXiv:1405.3652 [hep-th].

[163] M. C. Johnson and M. Kamionkowski, "Dynamical and Gravitational Instability of Oscillating-Field Dark Energy and Dark Matter," *Phys. Rev.* **D78** (2008) 063010, arXiv:0805.1748 [astro-ph].

[164] R. Kallosh and A. Linde, "Superconformal generalizations of the Starobinsky model," *JCAP* **1306** (2013) 028, arXiv:1306.3214 [hep-th].

[165] R. Kallosh and A. Linde, "Universality Class in Conformal Inflation," *JCAP* **1307** (2013) 002, arXiv:1306.5220 [hep-th].

[166] R. Kallosh, A. Linde, and D. Roest, "Superconformal Inflationary α-Attractors," *JHEP* **11** (2013) 198, arXiv:1311.0472 [hep-th].

[167] R. Kallosh and A. Linde, "Superconformal generalization of the chaotic inflation model $\frac{\lambda}{4}\phi^4 - \frac{\xi}{2}\phi^2 R$," *JCAP* **1306** (2013) 027, arXiv:1306.3211 [hep-th].

[168] R. Kallosh and A. Linde, "Non-minimal Inflationary Attractors," *JCAP* **1310** (2013) 033, arXiv:1307.7938 [hep-th].

[169] M. Galante, R. Kallosh, A. Linde, and D. Roest, "Unity of Cosmological Inflation Attractors," *Phys. Rev. Lett.* **114** no. 14, (2015) 141302, arXiv:1412.3797 [hep-th].

[170] A. Linde, "Single-field α-attractors," *JCAP* **1505** (2015) 003, arXiv:1504.00663 [hep-th].

[171] D. Roest and M. Scalisi, "Cosmological attractors from -scale supergravity," *Phys. Rev.* **D92** (2015) 043525, arXiv:1503.07909 [hep-th].

[172] M. Scalisi, "Cosmological α-attractors and de Sitter landscape," *JHEP* **12** (2015) 134, arXiv:1506.01368 [hep-th].

[173] R. Kallosh and A. Linde, "Cosmological Attractors and Asymptotic Freedom of the Inflaton Field," arXiv:1604.00444 [hep-th].

[174] H. Segur and M. D. Kruskal, "Nonexistence of Small Amplitude Breather Solutions in ϕ^4 Theory," *Phys. Rev. Lett.* **58** (1987) 747–750.

[175] M. P. Hertzberg, "Quantum Radiation of Oscillons," *Phys. Rev.* **D82** (2010) 045022, arXiv:1003.3459 [hep-th].

[176] D. Boyanovsky, C. Destri, and H. J. de Vega, "The Approach to thermalization in the classical phi**4 theory in (1+1)-dimensions: Energy cascades and universal scaling," *Phys. Rev.* **D69** (2004) 045003, arXiv:hep-ph/0306124 [hep-ph].

[177] M. A. Amin and D. Shirokoff, "Flat-top oscillons in an expanding universe," *Phys. Rev.* **D81** (2010) 085045, arXiv:1002.3380 [astro-ph.CO].

[178] R. Easther and E. A. Lim, "Stochastic gravitational wave production after inflation," *JCAP* **0604** (2006) 010, arXiv:astro-ph/0601617 [astro-ph].

[179] R. Easther, J. T. Giblin, Jr., and E. A. Lim, "Gravitational Wave Production At The End Of Inflation," *Phys. Rev. Lett.* **99** (2007) 221301, arXiv:astro-ph/0612294 [astro-ph].

[180] J.-F. Dufaux, G. Felder, L. Kofman, and O. Navros, "Gravity Waves from Tachyonic Preheating after Hybrid Inflation," *JCAP* **0903** (2009) 001, arXiv:0812.2917 [astro-ph].

[181] **Virgo, LIGO Scientific** Collaboration, B. P. Abbott *et al.*, "GW150914: Implications for the stochastic gravitational wave background from binary black holes," *Phys. Rev. Lett.* **116** no. 13, (2016) 131102, arXiv:1602.03847 [gr-qc].

[182] M. Gleiser, N. Graham, and N. Stamatopoulos, "Generation of Coherent Structures After Cosmic Inflation," *Phys. Rev.* **D83** (2011) 096010, arXiv:1103.1911 [hep-th].

[183] M. Khlopov, B. A. Malomed, and I. B. Zeldovich, "Gravitational instability of scalar fields and formation of primordial black holes," *Mon. Not. Roy. Astron. Soc.* **215** (1985) 575–589.

[184] J. Berges, "Nonequilibrium Quantum Fields: From Cold Atoms to Cosmology," arXiv:1503.02907 [hep-ph].

[185] P. Coppi, "How Do We know Antimater is Absent?," *eConf* **C040802** (2004) L017.

[186] V. A. Kuzmin, V. A. Rubakov, and M. E. Shaposhnikov, "On the Anomalous Electroweak Baryon Number Nonconservation in the Early Universe," *Phys. Lett.* **B155** (1985) 36.

[187] M. Dine and A. Kusenko, "The Origin of the matter - antimatter asymmetry," *Rev. Mod. Phys.* **76** (2003) 1, arXiv:hep-ph/0303065 [hep-ph].

[188] J. M. Cline, "Baryogenesis," in *Les Houches Summer School - Session 86: Particle Physics and Cosmology: The Fabric of Spacetime Les Houches, France, July 31-August 25, 2006*. 2006. arXiv:hep-ph/0609145 [hep-ph].

[189] M. P. Hertzberg and J. Karouby, "Generating the Observed Baryon Asymmetry from the Inflaton Field," *Phys. Rev.* **D89** no. 6, (2014) 063523, arXiv:1309.0010 [hep-ph].

[190] R. Rangarajan and D. V. Nanopoulos, "Inflationary baryogenesis," *Phys. Rev.* **D64** (2001) 063511, arXiv:hep-ph/0103348 [hep-ph].

[191] I. L. Bogolyubsky and V. G. Makhankov, "Lifetime of Pulsating Solitons in Some Classical Models," *Pisma Zh. Eksp. Teor. Fiz.* **24** (1976) 15–18.

[192] M. Gleiser, "Pseudostable bubbles," *Phys. Rev.* **D49** (1994) 2978–2981, arXiv:hep-ph/9308279 [hep-ph].

[193] E. J. Copeland, M. Gleiser, and H. R. Muller, "Oscillons: Resonant configurations during bubble collapse," *Phys. Rev.* **D52** (1995) 1920–1933, arXiv:hep-ph/9503217 [hep-ph].

[194] M. A. Amin, "K-oscillons: Oscillons with noncanonical kinetic terms," *Phys. Rev.* **D87** no. 12, (2013) 123505, arXiv:1303.1102 [astro-ph.CO].

[195] L. McAllister, E. Silverstein, and A. Westphal, "Gravity Waves and Linear Inflation from Axion Monodromy," *Phys. Rev.* **D82** (2010) 046003, arXiv:0808.0706 [hep-th].

[196] R. Flauger, L. McAllister, E. Pajer, A. Westphal, and G. Xu, "Oscillations in the CMB from Axion Monodromy Inflation," *JCAP* **1006** (2010) 009, arXiv:0907.2916 [hep-th].

[197] X. Dong, B. Horn, E. Silverstein, and A. Westphal, "Simple exercises to flatten your potential," *Phys. Rev.* **D84** (2011) 026011, arXiv:1011.4521 [hep-th].

[198] K. Enqvist, S. Kasuya, and A. Mazumdar, "Inflatonic solitons in running mass inflation," *Phys. Rev.* **D66** (2002) 043505, arXiv:hep-ph/0206272 [hep-ph].

[199] M. Gleiser, N. Graham, and N. Stamatopoulos, "Long-Lived Time-Dependent Remnants During Cosmological Symmetry Breaking: From Inflation to the Electroweak Scale," *Phys. Rev.* **D82** (2010) 043517, arXiv:1004.4658 [astro-ph.CO].

[200] S. R. Coleman, "Q Balls," *Nucl. Phys.* **B262** (1985) 263. [Erratum: Nucl. Phys.B269,744(1986)].

[201] T. D. Lee and Y. Pang, "Nontopological solitons," *Phys. Rept.* **221** (1992) 251–350.

[202] M. Gleiser and N. Graham, "Transition To Order After Hilltop Inflation," *Phys. Rev.* **D89** no. 8, (2014) 083502, arXiv:1401.6225 [astro-ph.CO].

[203] C. Cheung, A. Dahlen, and G. Elor, "Bubble Baryogenesis," *JHEP* **09** (2012) 073, arXiv:1205.3501 [hep-ph].

[204] A. Mazumdar, "The origin of dark matter, matter-anti-matter asymmetry, and inflation," arXiv:1106.5408 [hep-ph].

[205] D. S. Salopek, J. R. Bond, and J. M. Bardeen, "Designing Density Fluctuation Spectra in Inflation," *Phys. Rev.* **D40** (1989) 1753.

[206] L. McAllister, S. Renaux-Petel, and G. Xu, "A Statistical Approach to Multifield Inflation: Many-field Perturbations Beyond Slow Roll," *JCAP* **1210** (2012) 046, arXiv:1207.0317 [astro-ph.CO].

[207] V. Assassi, D. Baumann, D. Green, and L. McAllister, "Planck-Suppressed Operators," *JCAP* **1401** (2014) 033, arXiv:1304.5226 [hep-th].

[208] R. Easther, J. Frazer, H. V. Peiris, and L. C. Price, "Simple predictions from multifield inflationary models," *Phys. Rev. Lett.* **112** (2014) 161302, arXiv:1312.4035 [astro-ph.CO].

[209] M. A. Amin, P. Zukin, and E. Bertschinger, "Scale-Dependent Growth from a Transition in Dark Energy Dynamics," *Phys. Rev.* **D85** (2012) 103510, arXiv:1108.1793 [astro-ph.CO].

[210] M. Gleiser and D. Sicilia, "A General Theory of Oscillon Dynamics," *Phys. Rev.* **D80** (2009) 125037, arXiv:0910.5922 [hep-th].

[211] P. Salmi and M. Hindmarsh, "Radiation and Relaxation of Oscillons," *Phys. Rev.* **D85** (2012) 085033, arXiv:1201.1934 [hep-th].

[212] M. Hindmarsh and P. Salmi, "Oscillons and domain walls," *Phys. Rev.* **D77** (2008) 105025, arXiv:0712.0614 [hep-th].

[213] M. A. Amin, E. A. Lim, and I.-S. Yang, "A scattering theory of ultrarelativistic solitons," *Phys. Rev.* **D88** no. 10, (2013) 105024, arXiv:1308.0606 [hep-th].

[214] A. Mazumdar, "Inflatonic Q ball evaporation: A New paradigm for reheating the universe," in *Supersymmetry and unification of fundamental interactions. Proceedings, 10th International Conference, SUSY'02, Hamburg, Germany, June 17-23, 2002*, pp. 1204–1208. 2002. arXiv:hep-ph/0211233 [hep-ph]. http://www-library.desy.de/preparch/desy/proc/proc02-02/Proceedings/pa.4/mazumdar_pr.pdf.

[215] M. Kawasaki and M. Yamada, "Q ball Decay Rates into Gravitinos and Quarks," *Phys. Rev.* **D87** no. 2, (2013) 023517, arXiv:1209.5781 [hep-ph].

[216] K. Harigaya, A. Kamada, M. Kawasaki, K. Mukaida, and M. Yamada, "Affleck-Dine Baryogenesis and Dark Matter Production after High-scale Inflation," *Phys. Rev.* **D90** no. 4, (2014) 043510, arXiv:1404.3138 [hep-ph].

[217] M. Bastero-Gil, A. Berera, R. O. Ramos, and J. G. Rosa, "Warm baryogenesis," *Phys. Lett.* **B712** (2012) 425–429, arXiv:1110.3971 [hep-ph].

[218] M. Bastero-Gil, A. Berera, R. O. Ramos, and J. G. Rosa, "Observational implications of mattergenesis during inflation," *JCAP* **1410** no. 10, (2014) 053, arXiv:1404.4976 [astro-ph.CO].

[219] T. Chiba, K. Kamada, and M. Yamaguchi, "Gravitational Waves from Q-ball Formation," *Phys. Rev.* **D81** (2010) 083503, arXiv:0912.3585 [astro-ph.CO].

[220] R. Easther, R. Galvez, O. Ozsoy, and S. Watson, "Supersymmetry, Nonthermal Dark Matter and Precision Cosmology," *Phys. Rev.* **D89** no. 2, (2014) 023522, arXiv:1307.2453 [hep-ph].

[221] A. Kusenko, L. Loveridge, and M. Shaposhnikov, "Supersymmetric dark matter Q-balls and their interactions in matter," *Phys. Rev.* **D72** (2005) 025015, arXiv:hep-ph/0405044 [hep-ph].

[222] I. M. Shoemaker and A. Kusenko, "Gravitino dark matter from Q-ball decays," *Phys. Rev.* **D80** (2009) 075021, arXiv:0909.3334 [hep-ph].

[223] M. Yu. Khlopov and S. G. Rubin, *Cosmological pattern of microphysics in the inflationary universe*. 2004.

[224] Y. Shtanov, J. H. Traschen, and R. H. Brandenberger, "Universe reheating after inflation," *Phys. Rev.* **D51** (1995) 5438–5455, arXiv:hep-ph/9407247 [hep-ph].

[225] S. Yokoyama and J. Soda, "Primordial statistical anisotropy generated at the end of inflation," *JCAP* **0808** (2008) 005, arXiv:0805.4265 [astro-ph].

[226] K. Dimopoulos, M. Karciauskas, D. H. Lyth, and Y. Rodriguez, "Statistical anisotropy of the curvature perturbation from vector field perturbations," *JCAP* **0905** (2009) 013, arXiv:0809.1055 [astro-ph].

[227] C. A. Valenzuela-Toledo, Y. Rodriguez, and D. H. Lyth, "Non-gaussianity at tree- and one-loop levels from vector field perturbations," *Phys. Rev.* **D80** (2009) 103519, arXiv:0909.4064 [astro-ph.CO].

[228] C. A. Valenzuela-Toledo and Y. Rodriguez, "Non-gaussianity from the trispectrum and vector field perturbations," *Phys. Lett.* **B685** (2010) 120–127, arXiv:0910.4208 [astro-ph.CO].

[229] N. Bartolo, E. Dimastrogiovanni, S. Matarrese, and A. Riotto, "Anisotropic bispectrum of curvature perturbations from primordial non-Abelian vector fields," *JCAP* **0910** (2009) 015, arXiv:0906.4944 [astro-ph.CO].

[230] N. Bartolo, E. Dimastrogiovanni, S. Matarrese, and A. Riotto, "Anisotropic Trispectrum of Curvature Perturbations Induced by Primordial Non-Abelian Vector Fields," *JCAP* **0911** (2009) 028, arXiv:0909.5621 [astro-ph.CO].

[231] M. Karciauskas, "The Primordial Curvature Perturbation from Vector Fields of General non-Abelian Groups," *JCAP* **1201** (2012) 014, arXiv:1104.3629 [astro-ph.CO].

[232] K. Dimopoulos, "Statistical Anisotropy and the Vector Curvaton Paradigm," *Int. J. Mod. Phys.* **D21** (2012) 1250023, arXiv:1107.2779 [hep-ph]. [Erratum: Int. J. Mod. Phys.D21,1292003(2012)].

[233] K. Dimopoulos, D. Wills, and I. Zavala, "Statistical Anisotropy from Vector Curvaton in D-brane Inflation," *Nucl. Phys.* **B868** (2013) 120–155, arXiv:1108.4424 [hep-th].

[234] C. A. Valenzuela-Toledo, Y. Rodriguez, and J. P. Beltran Almeida, "Feynman-like Rules for Calculating n-Point Correlators of the Primordial Curvature Perturbation," *JCAP* **1110** (2011) 020, arXiv:1107.3186 [astro-ph.CO].

[235] J. P. Beltran Almeida, Y. Rodriguez, and C. A. Valenzuela-Toledo, "The Suyama-Yamaguchi consistency relation in the presence of vector fields," *Mod. Phys. Lett.* **A28** (2013) 1350012, arXiv:1112.6149 [astro-ph.CO].

[236] R. Emami and H. Firouzjahi, "Issues on Generating Primordial Anisotropies at the End of Inflation," *JCAP* **1201** (2012) 022, arXiv:1111.1919 [astro-ph.CO].

[237] K. Dimopoulos and M. Karciauskas, "Parity Violating Statistical Anisotropy," *JHEP* **06** (2012) 040, arXiv:1203.0230 [hep-ph].

[238] D. H. Lyth and M. Karciauskas, "Statistically anisotropic curvature perturbation generated during the waterfall," arXiv:1204.6619 [astro-ph.CO].

[239] D. H. Lyth and M. Karciauskas, "Modulation of the waterfall by a gauge field," *JCAP* **1301** (2013) 031, arXiv:1209.4266 [astro-ph.CO].

[240] R. K. Jain and M. S. Sloth, "On the non-Gaussian correlation of the primordial curvature perturbation with vector fields," *JCAP* **1302** (2013) 003, arXiv:1210.3461 [astro-ph.CO].

[241] S. Nurmi and M. S. Sloth, "Constraints on Gauge Field Production during Inflation," *JCAP* **1407** (2014) 012, arXiv:1312.4946 [astro-ph.CO].

[242] N. Barnaby and M. Peloso, "Large Nongaussianity in Axion Inflation," *Phys. Rev. Lett.* **106** (2011) 181301, arXiv:1011.1500 [hep-ph].

[243] N. Barnaby, R. Namba, and M. Peloso, "Phenomenology of a Pseudo-Scalar Inflaton: Naturally Large Nongaussianity," *JCAP* **1104** (2011) 009, arXiv:1102.4333 [astro-ph.CO].

[244] M. M. Anber and L. Sorbo, "Non-Gaussianities and chiral gravitational waves in natural steep inflation," *Phys. Rev.* **D85** (2012) 123537, arXiv:1203.5849 [astro-ph.CO].

[245] N. Barnaby, R. Namba, and M. Peloso, "Observable non-gaussianity from gauge field production in slow roll inflation, and a challenging connection with magnetogenesis," *Phys. Rev.* **D85** (2012) 123523, arXiv:1202.1469 [astro-ph.CO].

[246] R. Namba, "Curvature Perturbations from a Massive Vector Curvaton," *Phys. Rev.* **D86** (2012) 083518, arXiv:1207.5547 [astro-ph.CO].

[247] M. D'Onofrio, R. N. Lerner, and A. Rajantie, "Electrically charged curvaton," *JCAP* **1210** (2012) 004, arXiv:1207.1063 [astro-ph.CO].

[248] C. M. Nieto and Y. Rodriguez, "Massive Gauge-flation," arXiv:1602.07197 [gr-qc].

[249] J. P. Beltran Almeida, Y. Rodriguez, and C. A. Valenzuela-Toledo, "Scale and shape dependent non-Gaussianity in the presence of inflationary vector fields," *Phys. Rev.* **D90** (2014) 103511, arXiv:1405.7374 [astro-ph.CO].

[250] Y. Rodriguez, J. P. Beltran Almeida, and C. A. Valenzuela-Toledo, "The different varieties of the Suyama-Yamaguchi consistency relation and its violation as a signal of statistical inhomogeneity," *JCAP* **1304** (2013) 039, arXiv:1301.5843 [astro-ph.CO].

[251] V.-M. Enckell, K. Enqvist, and S. Nurmi, "Observational signatures of Higgs inflation," arXiv:1603.07572 [astro-ph.CO].

[252] C. Goolsby-Cole and L. Sorbo, "On the electric charge of the observable Universe," arXiv:1511.07465 [hep-ph].

[253] M. Giovannini and M. E. Shaposhnikov, "Primordial magnetic fields from inflation?," *Phys. Rev.* **D62** (2000) 103512, arXiv:hep-ph/0004269 [hep-ph].

[254] A. Dolgov and D. N. Pelliccia, "Photon mass and electrogenesis," *Phys. Lett.* **B650** (2007) 97–102, arXiv:hep-ph/0610421 [hep-ph].

[255] L. Sorbo, "Parity violation in the Cosmic Microwave Background from a pseudoscalar inflaton," *JCAP* **1106** (2011) 003, arXiv:1101.1525 [astro-ph.CO].

[256] N. Barnaby, E. Pajer, and M. Peloso, "Gauge Field Production in Axion Inflation: Consequences for Monodromy, non-Gaussianity in the CMB, and Gravitational Waves at Interferometers," *Phys. Rev.* **D85** (2012) 023525, arXiv:1110.3327 [astro-ph.CO].

[257] N. Barnaby, J. Moxon, R. Namba, M. Peloso, G. Shiu, and P. Zhou, "Gravity waves and non-Gaussian features from particle production in a sector gravitationally coupled to the inflaton," *Phys. Rev.* **D86** (2012) 103508, arXiv:1206.6117 [astro-ph.CO].

[258] R. Z. Ferreira and M. S. Sloth, "Universal Constraints on Axions from Inflation," *JHEP* **12** (2014) 139, arXiv:1409.5799 [hep-ph].

[259] R. Z. Ferreira, J. Ganc, J. Norea, and M. S. Sloth, "On the validity of the perturbative description of axions during inflation," arXiv:1512.06116 [astro-ph.CO].

[260] V. Domcke, M. Pieroni, and P. Bintruy, "Primordial gravitational waves for universality classes of pseudoscalar inflation," arXiv:1603.01287 [astro-ph.CO].

[261] R. Namba, M. Peloso, M. Shiraishi, L. Sorbo, and C. Unal, "Scale-dependent gravitational waves from a rolling axion," *JCAP* **1601** no. 01, (2016) 041, arXiv:1509.07521 [astro-ph.CO].

[262] M. S. Turner and L. M. Widrow, "Inflation-produced, large-scale magnetic fields," *Phys. Rev. D* **37** (May, 1988) 2743–2754.

[263] B. Ratra, "Cosmological 'seed' magnetic field from inflation," *Astrophys. J.* **391** (1992) L1–L4.

[264] K. Bamba and J. Yokoyama, "Large-scale magnetic fields from inflation in dilaton electromagnetism," *Phys. Rev. D* **69** (Feb, 2004) 043507.

[265] K. Bamba and M. Sasaki, "Large-scale magnetic fields in the inflationary universe," *JCAP* **0702** (2007) 030, arXiv:astro-ph/0611701 [astro-ph].

[266] J. Martin and J. Yokoyama, "Generation of Large-Scale Magnetic Fields in Single-Field Inflation," *JCAP* **0801** (2008) 025, arXiv:0711.4307 [astro-ph].

[267] M. M. Anber and L. Sorbo, "N-flationary magnetic fields," *JCAP* **0610** (2006) 018, arXiv:astro-ph/0606534 [astro-ph].

[268] K. Dimopoulos, "Correlated curvature perturbations and magnetogenesis from the GUT gauge bosons," *Astropart. Phys.* **42** (2013) 86–89, arXiv:0806.4680 [hep-ph].

[269] R. Emami, H. Firouzjahi, and M. S. Movahed, "Inflation from Charged Scalar and Primordial Magnetic Fields?," *Phys.Rev.* **D81** (2010) 083526, arXiv:0908.4161 [hep-th].

[270] C. T. Byrnes, L. Hollenstein, R. K. Jain, and F. R. Urban, "Resonant magnetic fields from inflation," *JCAP* **1203** (2012) 009, arXiv:1111.2030 [astro-ph.CO].

[271] V. Demozzi, V. Mukhanov, and H. Rubinstein, "Magnetic fields from inflation?," *JCAP* **0908** (2009) 025, arXiv:0907.1030 [astro-ph.CO].

[272] T. Suyama and J. Yokoyama, "Metric perturbation from inflationary magnetic field and generic bound on inflation models," *Phys. Rev.* **D86** (2012) 023512, arXiv:1204.3976 [astro-ph.CO].

[273] T. Fujita and S. Mukohyama, "Universal upper limit on inflation energy scale from cosmic magnetic field," *JCAP* **1210** (2012) 034, arXiv:1205.5031 [astro-ph.CO].

[274] R. J. Z. Ferreira, R. K. Jain, and M. S. Sloth, "Inflationary Magnetogenesis without the Strong Coupling Problem II: Constraints from CMB anisotropies and B-modes," *JCAP* **1406** (2014) 053, arXiv:1403.5516 [astro-ph.CO].

[275] R. J. Z. Ferreira, R. K. Jain, and M. S. Sloth, "Inflationary magnetogenesis without the strong coupling problem," *JCAP* **1310** (2013) 004, arXiv:1305.7151 [astro-ph.CO].

[276] P. Adshead, J. T. Giblin, T. R. Scully, and E. I. Sfakianakis, "Gauge-preheating and the end of axion inflation," *JCAP* **1512** no. 12, (2015) 034, arXiv:1502.06506 [astro-ph.CO].

[277] J. Garcia-Bellido, M. Garcia-Perez, and A. Gonzalez-Arroyo, "Chern-Simons production during preheating in hybrid inflation models," *Phys.Rev.* **D69** (2004) 023504, arXiv:hep-ph/0304285 [hep-ph].

[278] N. Graham, "An Electroweak oscillon," *Phys.Rev.Lett.* **98** (2007) 101801, arXiv:hep-th/0610267 [hep-th].

[279] A. Diaz-Gil, J. Garcia-Bellido, M. Garcia Perez, and A. Gonzalez-Arroyo, "Magnetic field production during preheating at the electroweak scale," *Phys.Rev.Lett.* **100** (2008) 241301, arXiv:0712.4263 [hep-ph].

[280] N. Graham, "Numerical Simulation of an Electroweak Oscillon," *Phys.Rev.* **D76** (2007) 085017, arXiv:0706.4125 [hep-th].

[281] A. Diaz-Gil, J. Garcia-Bellido, M. G. Perez, and A. Gonzalez-Arroyo, "Primordial magnetic fields from preheating at the electroweak scale," *JHEP* **0807** (2008) 043, arXiv:0805.4159 [hep-ph].

[282] L. Yang, L. Pearce, and A. Kusenko, "Leptogenesis via Higgs Relaxation," arXiv:1505.07912 [hep-ph].

[283] A. Maleknejad, M. M. Sheikh-Jabbari, and J. Soda, "Gauge Fields and Inflation," *Phys. Rept.* **528** (2013) 161–261, arXiv:1212.2921 [hep-th].

[284] A.-C. Davis, K. Dimopoulos, T. Prokopec, and O. Tornkvist, "Primordial spectrum of gauge fields from inflation," *Phys. Lett.* **B501** (2001) 165–172, arXiv:astro-ph/0007214 [astro-ph].

[285] E. McDonough, H. B. Moghaddam, and R. H. Brandenberger, "Preheating and Entropy Perturbations in Axion Monodromy Inflation," arXiv:1601.07749 [hep-th].

[286] J. Garcia-Bellido, D. G. Figueroa, and J. Rubio, "Preheating in the Standard Model with the Higgs-Inflaton coupled to gravity," *Phys.Rev.* **D79** (2009) 063531, arXiv:0812.4624 [hep-ph].

[287] P. W. Graham, J. Mardon, and S. Rajendran, "Vector Dark Matter from Inflationary Fluctuations," *Phys. Rev.* **D92** (2015) 075012, arXiv:1504.02102 [hep-ph].

[288] T. Fujita, R. Namba, Y. Tada, N. Takeda, and H. Tashiro, "Consistent generation of magnetic fields in axion inflation models," *JCAP* **1505** no. 05, (2015) 054, arXiv:1503.05802 [astro-ph.CO].

[289] S.-L. Cheng, W. Lee, and K.-W. Ng, "Numerical study of pseudoscalar inflation with an axion-gauge field coupling," *Phys. Rev.* **D93** no. 6, (2016) 063510, arXiv:1508.00251 [astro-ph.CO].

[290] C. W. Misner, K. S. Thorne, and J. A. Wheeler, *Gravitation*. W. H. Freeman, San Francisco, 1973.

[291] R. Emami, H. Firouzjahi, S. Sadegh Movahed, and M. Zarei, "Anisotropic Inflation from Charged Scalar Fields," *JCAP* **1102** (2011) 005, arXiv:1010.5495 [astro-ph.CO].

[292] V. Mukhanov, *Physical Foundations of Cosmology*. Cambridge University Press, 2005.

[293] D. Polarski and A. A. Starobinsky, "Semiclassicality and decoherence of cosmological perturbations," *Class.Quant.Grav.* **13** (1996) 377–392, arXiv:gr-qc/9504030 [gr-qc].

[294] C. Caprini, S. Biller, and P. G. Ferreira, "Constraints on the electrical charge asymmetry of the universe," *JCAP* **0502** (2005) 006, arXiv:hep-ph/0310066 [hep-ph].

[295] H. Yoshida, "Construction of higher order symplectic integrators," *Physics Letters A* **150** no. 5, (1990) 262 – 268. http://www.sciencedirect.com/science/article/pii/0375960190900923.

[296] A. V. Frolov, *Private communication,* 2014.

[297] E. J. Weinberg, *Classical solutions in quantum field theory*. Cambridge Monographs on Mathematical Physics. Cambridge University Press, 2015. http://www.cambridge.org/us/knowledge/isbn/item6813336/.

[298] M. Hindmarsh, S. Stuckey, and N. Bevis, "Abelian Higgs Cosmic Strings: Small Scale Structure and Loops," *Phys. Rev.* **D79** (2009) 123504, arXiv:0812.1929 [hep-th].

[299] P. M. Saffin and A. Tranberg, "Dynamical simulations of electroweak baryogenesis with fermions," *JHEP* **02** (2012) 102, arXiv:1111.7136 [hep-ph].